High-Resolution Stratigraphy, Biostratigraphy, and Diagenesis of Upper Khartam Member, Khuff Formation: Implication on Reservoir Quality and Architecture. Outcrop Analog from Central Saudi Arabia

BY

Ammar Mohammed Adam Mohammed

A Dissertation Presented to the

DEANSHIP OF GRADUATE STUDIES

KING FAHD UNIVERSITY OF PETROLEUM & MINERALS

DHAHRAN, SAUDI ARABIA

In Partial Fulfillment of the
Requirements for the Degree of

DOCTOR OF PHILOSOPHY

In

Geology

DECEMBER 2016

KING FAHD UNIVERSITY OF PETROLEUM & MINERALS

DHAHRAN- 31261, SAUDI ARABIA

DEANSHIP OF GRADUATE STUDIES

This thesis, written by **Ammar Mohammed Adam Mohammed** under the direction his thesis advisor and approved by his thesis committee, has been presented and accepted by the Dean of Graduate Studies, in partial fulfillment of the requirements for the degree of **DOCTOR OF PHILOSOPHY IN GEOLOGY**.

Dr. Michael Kaminski
(Advisor)

Dr. Abdulaziz Al-Shaibani
Department Chairman

Dr. Osman Abdullatif
(Co-Advisor)

Dr. Salam A. Zummo
Dean of Graduate Studies

Dr. Mustafa Hariri
(Member)

18/4/17

Date

Dr. Abdulazeez Abdulraheem
(Member)

Dr. Mohamed Mahmoud
(Member)

To my mother and father, to my wife, to my kids, Mohammed and Yusra

ACKNOWLEDGMENTS

Praise is only for Allah, Lord of the Universe. The most Kind, the most Merciful. The master of the Day of Judgement.

In my soul and heart, I am very gratitude to King Fahd University of Petroleum & Minerals for giving me the opportunity to complete my PhD. Also I would like to express my gratefulness to the Geosciences Department for the unlimited support through providing the facility and administrative support.

My sincere gratitude to my PhD committee Professor Michael Kaminski, Dr Osman Abdullatif, Dr Mustafa Hariri, Dr Abdulazeez Abdulraheem, and Dr Mohamed Mahmoud, for their insightful comments and encouragement.

Extremely critical and valuable comments were kindly received from Professor Rudy Swennen, KU Leuven. Dear Professor Rudy, from my heart, I thank you so much and I strongly appreciate your help. Thanks also due to Professor Gabor Korvin for his kind technical supports and concerns.

My dear mother and my dear father, your supplications and prayers are the ultimate success and the unique strength of mine, may Allah bless you.

My dear wife and my kids, Mohammed and Yusra, without your supports and smiles I would not be able to complete this milestone achievement.

Sincere thanks are due to Shaikh warg Ammar, Al-halfawi Mo'az, Al-shaigi Mazin, Mohammed Ali Jongor, Elhibir Al-Kabashi, Al-Hager Abdullah, and Alfaki Jarrah, guys, without your helps it would be difficult to complete my field works.

Special thanks to the generous Gadoora Mohammed Yassin and ammo Amir and to the Sudanese community at KFUPM.

TABLE OF CONTENT

LIST OF TABLES

LIST OF FIGURES

LIST OF PLATES

ABSTRACT

Full Name : [Ammar Mohammed Adam Mohammed]

Thesis Title : [High-Resolution Stratigraphy, Biostratigraphy, and Diagenesis of Upper Khartam Member, Khuff Formation: Implication on Reservoir Quality and Architecture. Outcrop Analog from Central Saudi Arabia]

Major Field : [Geology]

Date of Degree : [December, 2016]

The Khuff reservoirs are known for having complex heterogeneities and these were described to occur at inter-well and sub-seismic scale. I therefore studied the high-resolution stratigraphic framework of the Upper Khartam Member of the Khuff reservoirs in outcrop analogues. Four outcrop localities were logged and about 100 representative samples were collected for microfacies, micropaleontology, and porosity and permeability analyses. Furthermore high-resolution photo-mosaics of the outcrops were made. The latter cover an extension of about 7 kms, mostly along dip direction. Centimetre-thick beds are followed laterally and logged for detailed sedimentology and sequence stratigraphy. Seventeen lithofacies were defined, with coarse-grained oolitic grainstone, interlaminated quartz-bearing recrystallized limestone, recrystallized limestone, interlaminated quartz-bearing fine-grained oolitic grainstone, bioclastic grainstone/packstone, and marlstone making up the bulk of the successions. These lithofacies are occurring as sheet-like and channelized bodies. The former range in thicknesses from 5 to 40 cm and possess a lateral extension varying between 5 and 300 m, while channelized bodies have two anatomies, i.e., small tidal creeks (1 m in width by 30 cm in height) and large tidal channels (3 m in width by 50 cm in height). Accordingly, seven depositional settings were distinguished, including

intertidal-subtidal flats, supratidal settings, intertidal channels and creeks, shoal ridges, reef complex, and outer ramp settings.

Four stratigraphic identities were defined, these include; beds, bedset, high-frequency fifth-order sequences, and fourth-order sequences. About 20,000 beds are defined and traced laterally, ranging in thickness from 5 to 40 cm and extending between 5 and 300 m. The beds are stacked into well-developed bedsets composed of a complex internal amalgamation with relatively large lateral extension of several thousand of metre and thickness ranging between 1 and 5 m. These are genetically stacked into six high-frequency sequences with prominent flooding surfaces linked to shifts in shoreline position. The high-frequency sequences likely represent fifth-order cycles and possibly relate to Milankovitch cycles (i.e., eccentricity cycles of 100,000 year).

Six major diagenetic processes could be differentiated in the studied outcrops, namely: dissolution, pore lining and pore blocking calcite cementation, dolomitization, fracturing, and stylolitization. Ten porosity types could be differentiated in the studied outcrops, namely: intergranular, intragranular, shelter, dissolution-enlarged, moldic, vuggy, micro-porosity, and porosity in relation to dolomite–dedolomite, dolomite-leaching, and fracture development. The oolitic grainstones of the intertidal sheets, intertidal creeks, and intertidal channels are dominated by dissolution, moldic, and vuggy porosity, whereas intercrystalline and fracture porosity prevails in the recrystallized limestone. The interplayed diagenetic processes have impacted the ultimate reservoir quality. Most critically, the reservoir quality of the studied reservoir units along their lateral extension, as defined in their sequence stratigraphic framework, was influenced differentially by diagenesis, which resulted in a lateral segmentation of single bodies into different hydraulic units. XRD data show a control of certain mineralogical associations (such as SiO_2 and $SrSO_4$) on the lateral

intermittence of the intra-reservoir body. SEM observations reveal a textural control on porosity and permeability. The differential mold-filling calcite cements of the oolitic grainstones of the intertidal sheets and channels have significantly reduced porosity and permeability. Generally, the mineral content has little impact on reservoir quality, although clay minerals have played a central role in lining the pore space and affecting reservoir quality. Overall, the lateral segmentation was most likely caused by differential diagenetic evolution, and most critically, this evolution seems to have been controlled by fractures and stylolites which respectively acted as conduits to, and barriers for, vertical fluid flow, and hence controlled the differential cementation and dissolution processes.

The lithofacies models are critically valid and consistent with the detailed sedimentological and sequence stratigraphic data. The short-scale property heterogeneity models were established. Porosity of intertidal sheets has relatively great horizontal ranges (300 m) compared with the intertidal channels and creeks (150 m).

A high degree of similarity is expected between the studied outcrops and the Khuff reservoirs, as inferred from the nature of high-resolution sequence stratigraphy. Therefore, the studied succession of the Upper Khartam Member in central Saudi Arabia possibly represents an excellent analogue for the Khuff reservoirs in Eastern Arabia. And thus, the results of this study could enhance the quantitative and the qualitative assessment of the Khuff reservoirs heterogeneities.

ملخص الرسالة

الاسم الكامل: عمار محمد آدم محمد

عنوان الرسالة: دراسة جيولوجية تفصيلية لمكن الخف بإستخدام مماثل سطحي في وسط المملكة العربية السعودية

التخصص: جيولوجيا الدكتوراة

تاريخ الدرجة العلمية: يانير 2017

تعرف مكامن الخف في حقول النفط في شرق شبه الجزيرة العربية بعدم التجانس من ناحية التتابع الطبقي وجودة المكمن. عضو الخرطم التابع لتكوين الخف في وسط المملكة العربية السعودية يتيح فرصة جيدة لدراسة عدم التجانس الهندسي وجودة مكامن الخف. تمت دراسة أربعة مواقع بصورة تفصيلية من ناحية الخصائص الرسوبية والطبقية كما تم تحليل المسامية والنفاذية لحوالي 1000 عينة. تم تحديد سبعة عشر سحنة صخرية، يشكل حجر الأوليت الحبيبي, والحجر الجيري المتبلور وحجر الدولوميت النسبة الأكبر من هذه السحنات. هذه السحنات ترسبت في سبع بيئات مختلفة أدت إلى تكوين مكمن معقد من ناحية التتابع الطبقي والشكل الهندسي. من ناحية أخري, عمليات مابعد الترسيب أثرت وبشكل كبير على مسامية ونفاذية هذا المكمن. هذه العمليات تشمل وبصورة كبير عمليات الإذابة والسمنتة والدلمتة والكسور والإستيلوليتس. والأهم من ذلك، أن مسامية ونفاذية طبقات المكمن وعلى امتدادات صغير تتغير وبشكل كبير. هذا التغير عزي لعمليات مابعد الترسيب والتي بدورها أثرت وبشكل تفاضلي على جودة طبقات المكمن. من المعتقد أن الكسور والإستالوليتس هي المتحكم الرئيسي في عمليات التغيير التفاصلي لعمليات مابعد الترسيب حيث أنها لعبت دور القنوات والحواجز لسوائل عمليات التغير.

من المتوقع وجود درجة عالية من التشابه بين المماثل السطحي ومكامن الخف، هذا مستدل من طبيعة التتابع والترتيب الطباقي. ولذلك، فإن عضو الخرتم العلوي في وسط المملكة العربية السعودية ربما يمثل تماثلا ممتازاً لمكامن الخف في شرق شبه الجزيرة العربية. وبالتالي، فإن نتائج هذه الدراسة يمكن أن تعزز المعرفه النوعية والتقييمية لمكامن الخف.

CHAPTER 1

INTRODUCTION

1.1. Introduction

The increasing demands to maximize recovery from oil and gas fields have led to an increase of more advanced techniques of reservoir characterization and modeling. The limitation of techniques and difficulty to determine the detailed reservoir heterogeneity in subsurface encourage the use of surface outcrop analogs. Outcrop analogs provide valuable insight towards understanding the internal high-resolution architectural and reservoir quality distribution. As a matter of fact, outcrop analogs can provide information about rock body dimension, size, orientation in 2D and 3D, and details about diagenetic overprint which are difficult to obtain from the subsurface. Consequently, this provides insight for high-resolution geological modeling and heterogeneity characterization. It has been indicated that development of geologically constrained reservoir model and subsequent upscaling of the model for reservoir simulation depend on critical parameters related to geometrical attributes and distribution of targeted reservoir facies (Grammer et al., 2004). Well-exposed Phanerozoic outcrops in Saudi Arabia provide good outcrop analogs to subsurface formations and reservoirs. These outcrops allow close description and evaluation of rock heterogeneity and its effect on reservoir quality and architecture. Quantitative modeling of the outcrop is needed to recognize the scales and types of heterogeneity. Results obtained from such a model can be beneficial for the understanding of the influence of heterogeneity on fluid flow. The constructed geological model will be of

great value for reservoir fluid simulation and reservoir development and management. Recently, terrestrial scanning LIDAR (light detection and ranging) technique has been widely used in outcrop stratigraphic imaging and mapping. When combined with directly sampled data, digital mapping generates high-precision facies models and helps in constructing 3D outcrop-based geological models. Digital outcrop models can improve geologic and flow simulation. Many previous studies (Grammer et al., 2004; Homewood et al., 2008; Adam and Abdullatif, 2013; Eltom et al., 2013; Adam et al., 2014) have indicated that the utilization of outcrop studies for aquifer and reservoir characterization is useful in several aspects such as:

1. Provide better understanding of facies architecture and environments.
2. Determine geometry of reservoir/non-reservoir bodies within the reservoir.
3. Describe the reservoir's macro- and meso- heterogeneities.
4. Provides correlation guidelines and maximum correlation length.
5. Help to interpret the controls on sediment architecture.
6. Place constraints on input variables to stratigraphic and fluid flow units.
7. The obtained model is critical to understanding reservoir behavior and development strategies.

Therefore, the facies and porosity-permeability and stratigraphic hierarchy models from outcrop analogs may provide invaluable reference and input that may allow refinement of reservoir characterization models based on subsurface data. The direct benefit of such input is to improve reservoir characterization and fluid simulation models that will allow capturing different scales of sedimentological heterogeneity and their impacts on reservoir quality and architecture. Consequently, this will help to achieve better reservoir characterization and to take sound decisions related to development and management of oil and gas reservoirs.

The Khuff formation is hosting important carbonate reservoirs in the Eastern Saudi Arabian fields; these are estimated to contain about 15 to 20% of the world's gas reserve, Figure 1.1 (Al-Jallal, 1987, 1995; Al-Aswad, 1997; Vaslet et al., 2005; Koehrer et al., 2010).

During the late Early Permian, a major continental rifting and crustal stretching and thinning took place in west Pangaea, this rifting phase has separated the so-called Cimmerian continent from Gondwana and has resulted in the formation of Neo-Tethys Ocean at the expense of the Paleo-Tethys (Alsharhan and Kendall, 1986; Al-Jallal, 1995; Sengör and Natalin, 1996; Alsharhan and Nairn, 1997; Ziegler, 2001). The opening of the Neo-Tethys Ocean resulted in the first regional marine transgressive event on the Arabian Plate, this was associated with the establishment of the first Plate-wide carbonate succession of Khuff formation (Alsharhan and Kendall, 1986; Al-Jallal, 1995). The Khuff formation was deposited over a large epeiric ramp platform that assumed to build large facies belts (Al-Jallal, 1995; Alsharhan, 2006).

Well-exposed Permian-Triassic Khuff outcropping strata in central Saudi Arabia provide good outcrop analogs to the subsurface Khuff reservoir, Figure 1.2. The subsurface Khuff reservoirs are known for their complex vertical and lateral sub-seismic heterogeneity (Janson et al., 2013). The approach and methods to be followed in this study consist of integrated detailed sedimentological, sequence stratigraphical, diagenetic analysis and petrophysical measurements from the upper Khartam member of the Khuff formation on at least three quadrangles to investigate the sedimentological, architectural, and petrophysical heterogeneities. Digital outcrop modeling will be used to establish the high-resolution stratigraphic framework on which all data will be visualized and interpreted. Geostatistical approach will be used

as a tool box for analyzing and integrating the results to build 3D computer-based geological and petrophysical models.

The Khuff formation was subdivided into five members, from bottom to top, Ash Shiqqah, Huqayl, Duhaysan, Midhnab and Khartam, Figure 1.3 and Figure 1.4 (Powers, 1962; Al-Aswad, 1997; Vaslet et al., 2005). The lowermost, Ash Shiqqah member was deposited in a transitional coastal to lagoonal setting and is dominated by siliciclastic deposits, the overlying members are dominated by shallow subtidal to intertidal carbonate lithofacies interbedded with lagoonal evaporites. (Vaslet et al., 2005) subdivided the Khuff formation into four depositional sequences each of which is bounded by two sequence boundaries and contains a lower transgressive system tract and an upper highstand system tract.

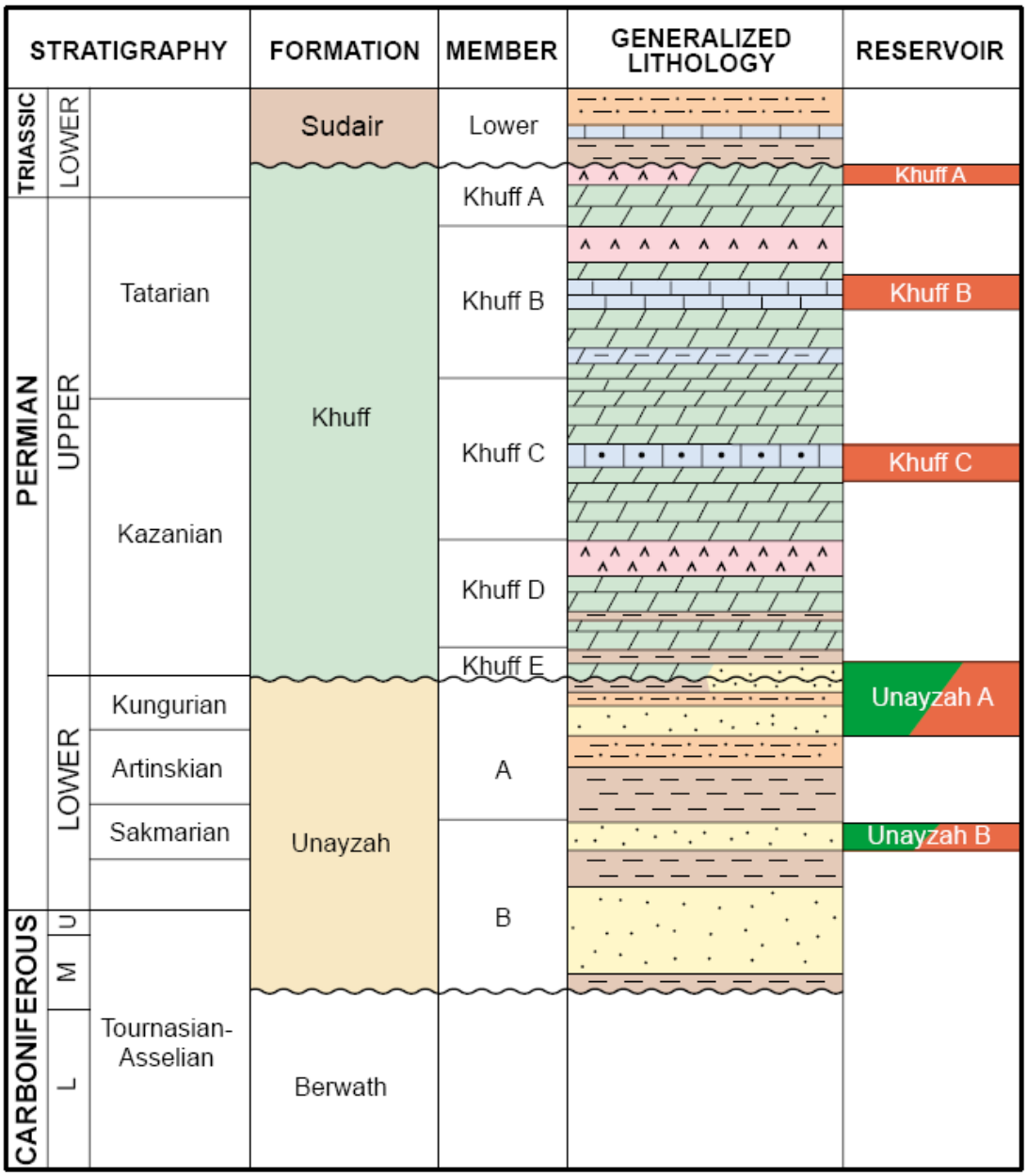

Figure 1.1 The stratigraphic position of Permo-Triassic Khuff Formation in Saudi Arabia stratigraphy (Dasgupta et al., 2002).

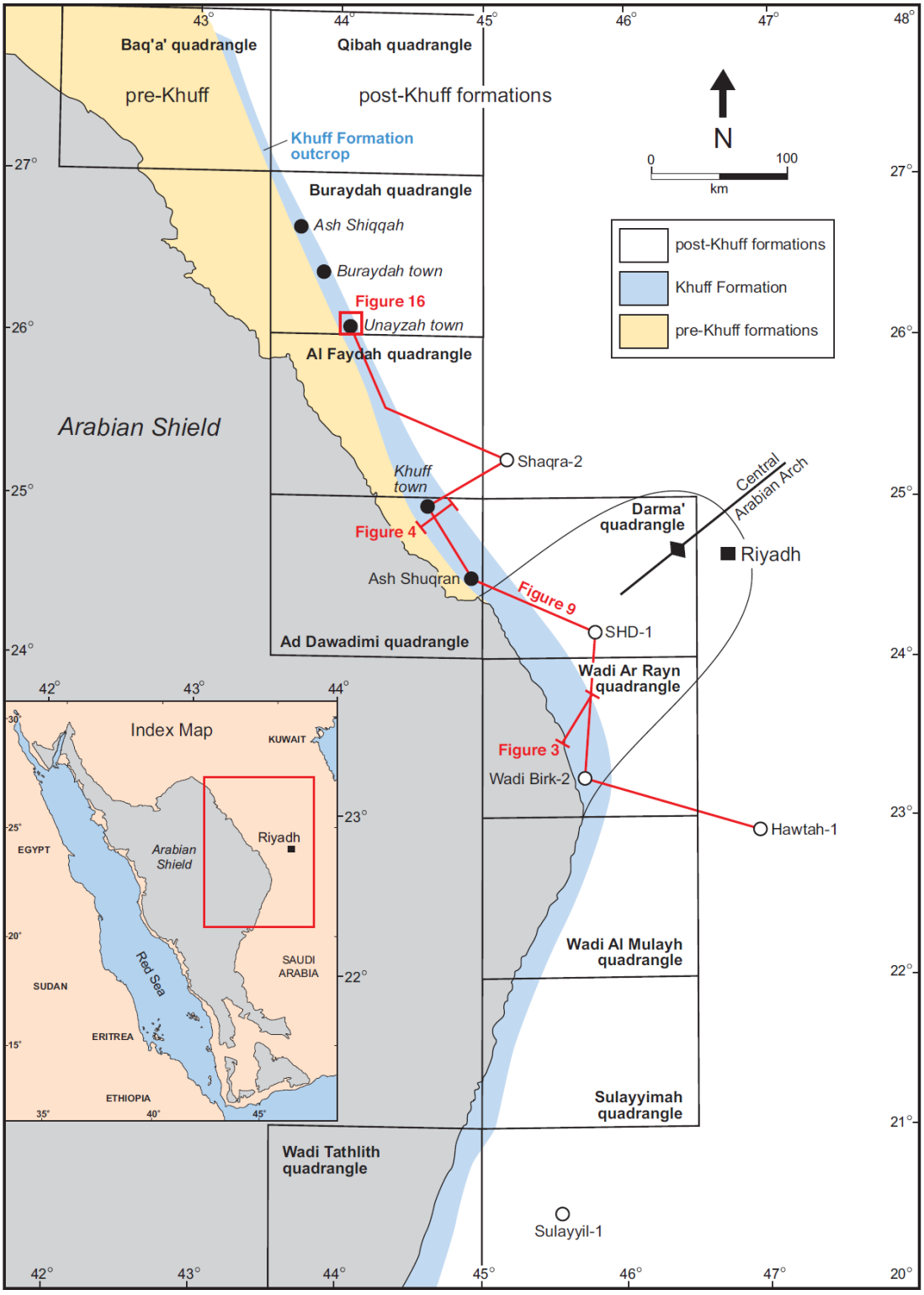

Figure 1.2 The Khuff Formation outcrop in central Saudi Arabia (Vaslet et al., 2005).

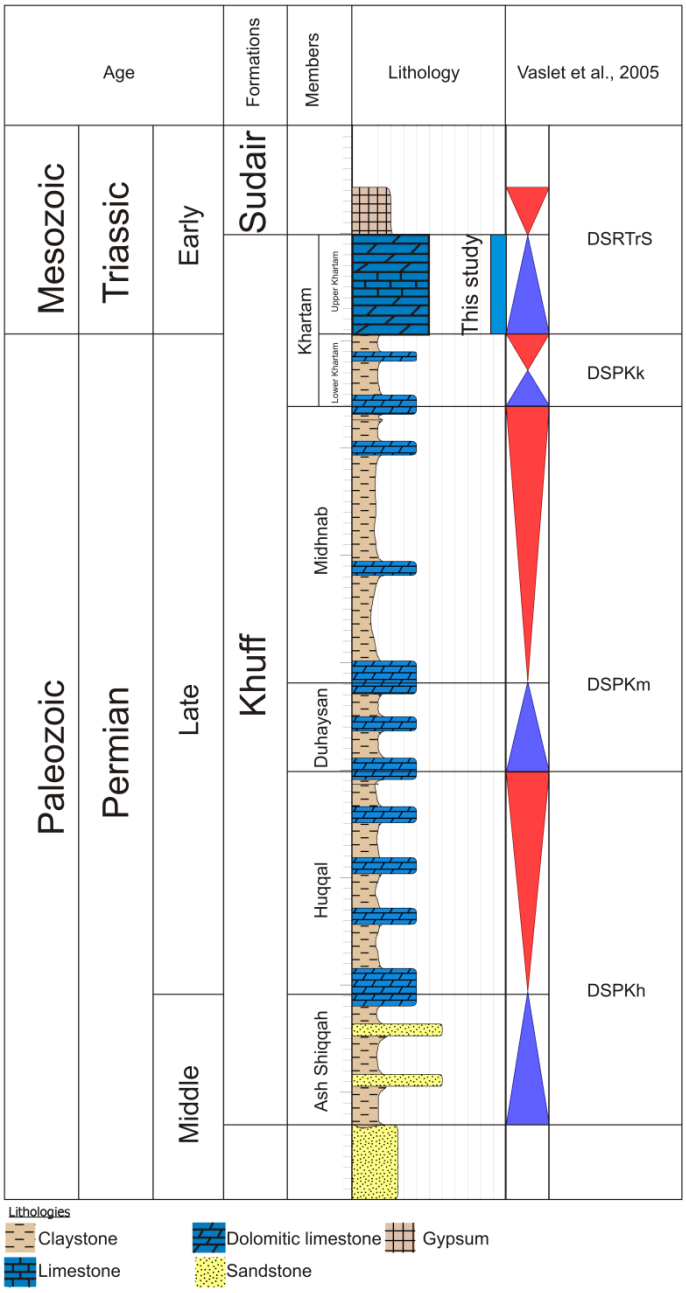

Figure 1.3. The composite section of the Khuff Formation in the Ad Dawadimi quadrangle (modified after Vaslet et al., 2005). In this quadrangle, Delfour et al. (1982) recognized five members of the Khuff Formation, from bottom to top Ash Shiqqah, Huqayl, Duhaysan, Midhnab and Khartam members. Vaslet et al. (2005) subdivided the succession into four depositional sequences DSPKh, DSPKm, DSPKk, and DSTrS, the studied interval is located at the topmost of the Khuff Formation (blue rectangular).

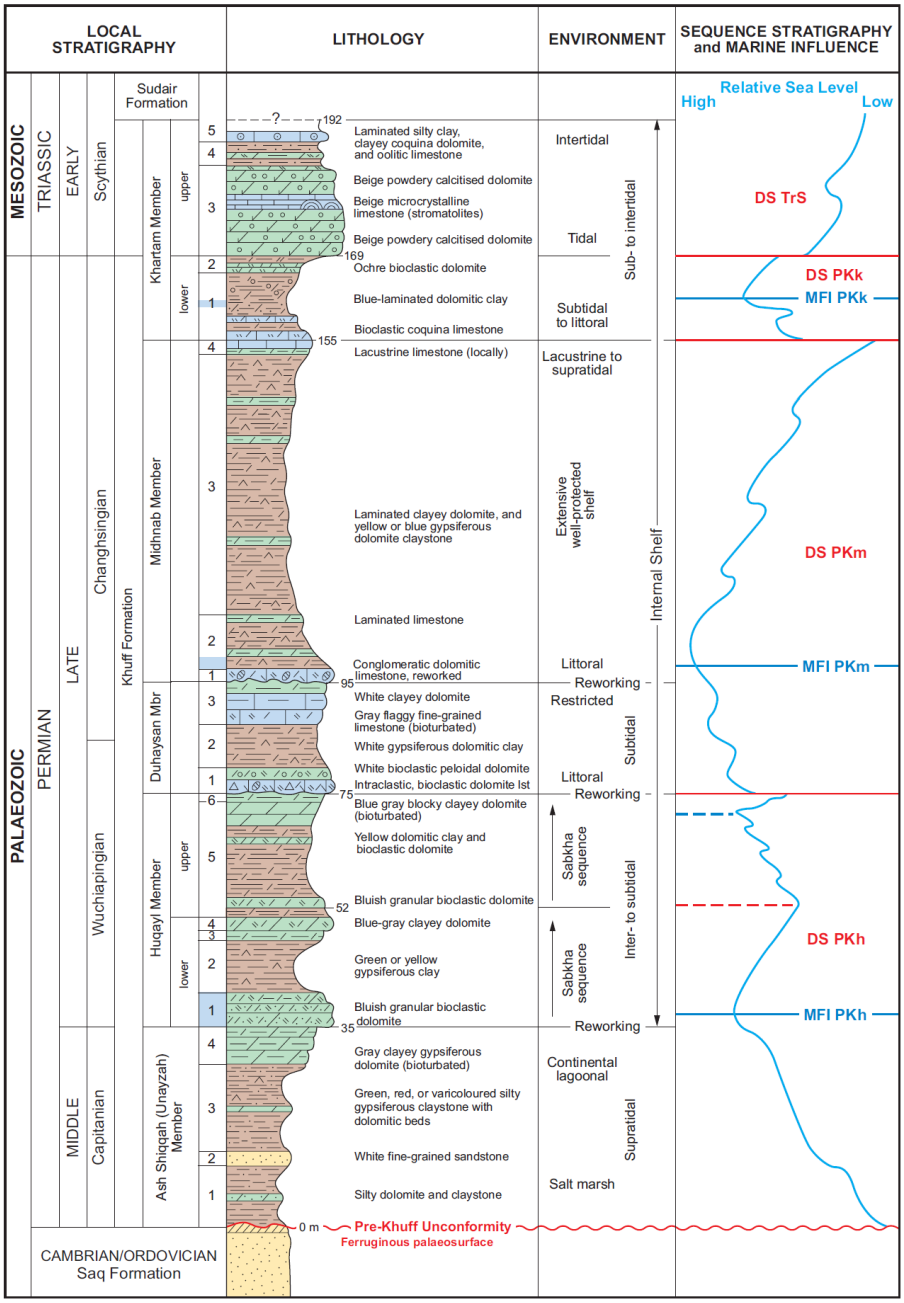

Figure 1.4 The type section of the Khuff Formation in the Ad Dawadimi quadrangle, note the lithological character, depositional settings, and sequence stratigraphy of the Khuff members (Delfour et al., 1982).

1.2. Justification

Micro and macro reservoir heterogeneity is difficult to assess or predict accurately from subsurface data, core information, logs, and seismic data. Coring density from the eastern reservoirs are about one core per five square kilometers at best, it is often more, one core per hundred square kilometers. Within this range a wide scale of heterogeneities may be encountered and in many cases their evaluation may be impossible from the subsurface. Excellently exposed outcrops of the Lower Triassic upper Khartam Member in central Saudi Arabia provide a good opportunity to observe and measure different scales of heterogeneities at the facies, grain/mud geometry and their vertical and lateral stacking patterns, the types and arrangement of architectural elements and their spatial distribution. From the previous review of the Permian-Triassic outcrop equivalents of Khuff Formation in central Arabia, different scales of observation and measurements could be made to assess the heterogeneity of these rocks in relation to reservoir quality. For example, observation and measurements can be made at the microscopic texture and composition scales, at mesoscopic facies scale and at the macroscopic sequences and cycle stratigraphic hierarchy scale. Outcrops also provide an opportunity to measure the porosity and permeability in relation to different facies. Therefore, facies and porosity-permeability and stratigraphic hierarchy models from outcrop analogs may provide invaluable reference and input that may allow refinement of reservoir characterization models based on subsurface data. The direct benefit of such input is to improve reservoir characterization and fluid simulation models that will allow capturing different scales of sedimentological heterogeneity and its impacts on reservoir quality and architecture. Consequently, this will help to achieve better reservoir characterization and allow taking sound decision related to development and management of oil and gas reservoirs. The approach and

methods to be followed in this study are to combine both field and laboratory sedimentological, micropaleontological, and stratigraphic facies and architectural, petrophysical, statistical and geostatistical analysis (Grammer et al., 2004).

The uniqueness and novelty of the proposed research is that

- It provides integrated approach for observation which is not available from subsurface data.
- The results may be integrated and upscaled to actual subsurface reservoir scale.
- It reveals the control of sedimentary and stratigraphic heterogeneity on reservoir quality at different scales (micro to macro scales) that is difficult hard to assess from subsurface geological or geophysical data. All above elements will have direct impacts on hydrocarbon reservoir characterization, development and management.

1.3. Motivations

Beside my strong interest in working on high-resolution reservoir characterization, the following points have motivated me to select this topic;

- The Khuff formation holds five important gas reservoirs in the Middle East; these are estimated to contain about 30 % of the world's gas reserve.
- The complexity of carbonate reservoirs both depositional and diagenetic needs to be understood.
- The outcrop approach allows looking at different scales of observation, which overcomes subsurface limitation to achieve better reservoir prediction.
- To refine the chronostratigraphy of the formation by examining the micropaleontology.

- Industrial implication in term of reservoir development, recovery, and production.
- To meet one of the main strategic objectives of Saudi Arabia related to hydrocarbon energy resources.

1.4. Problem statement

The increasing demands to maximize recovery from oil and gas fields have led to wide technical innovations in the oil and gas industry. Most of these are focused on exploration and reservoir characterization. Reservoir characterization aims to assess architectural and quality elements of the reservoir rocks. The Khuff reservoirs are known for having complex heterogeneities at the well-scale (Janson et al., 2013). These are sub-seismic heterogeneities. Therefore, optimum exploitation of these reservoirs is highly dependent upon understanding the intra-reservoir layering architecture and quality that are mostly controlled by syn-depositional processes and subsequent diagenetic evolution.

Outcrop analogs provide valuable insight into understanding ancient sedimentation processes and products (Grammer et al., 2004; Pringle et al., 2006). Importantly, outcrop studies have been utilized widely to understand critical quality and architectural elements (Calvo et al., 1983; Aigner et al., 1995; Olsen, 1995; Meyer et al., 1996; Jennings et al., 2000; Frykman, 2001; Mattner and Al-husseini, 2002; Philip et al., 2002; Lüning et al., 2003; Eschard et al., 2003; Gardner et al., 2003; Weidlich and Bernecker, 2004; Schwab et al., 2005; Homewood et al., 2008; Nindre et al., 2008; Maurer et al., 2009; Wilson et al., 2009; Koehrer et al., 2010; Mukti and Ito, 2010; Mulder et al., 2010; Pöppelreiter et al., 2011; Pyles et al., 2011; Tuuling and Flodén, 2011; Iñigo et al., 2012; Retallack and Dilcher, 2012; Adam et al., 2013, 2014; Bruna et al., 2013; Cogné et al., 2013; Eltom et al., 2013).

The Khuff Formation out crops extensively within central Saudi Arabia and is, therefore, readily available for analysis. However, there is a lack of detailed information concerning its intra-reservoir quality and architectural distributional patterns. The Khuff outcrops provide a complete stratigraphic context, where the individual beds can be traced laterally for a great distance. Therefore, if the sequence boundaries and system tracts could be determined in the outcrop analogue, a much better understanding of the Khuff reservoirs could be obtained. Therefore, the sequence analysis of the outcrops would then have a direct application to reservoir studies. Likewise, studying diagenetic evolution and the subsequent implication on porosity and permeability could assist in understanding and predicting subsurface reservoir qualities. Generally, the study of outcrops of the Khuff Formation can contribute significantly to a better understanding of reservoir characteristics which will eventually facilitate the reservoir development and management.

1.5. Quantitative and qualitative characterization of reservoir heterogeneity

Carbonate reservoir rocks are known for their heterogeneity in sedimentological and petrophysical properties, these are mostly controlled by depositional and post-depositional processes (Tiab and Donaldson, 2012). “In spite of all the advances in core analysis, well logging, geostatistic, and in particular well testing, petroleum engineers are still unable to specify the nature and extent of heterogeneities at every point in the formation” (Tiab and Donaldson, 2012). (Warren and Price, 1961) stated that “In many cases, the predicted performance of a reservoir is so completely dominated by irregularities in the physical properties of the formation that the

gratuitous assumption of a particular form for the variation can reduce the solution of the problem to a mere tautological exercise". On the other hand, the outcrop provides complete stratigraphic context, where the individual beds can be traced laterally for a great distance. Therefore, the intra-reservoir beds could be characterized individually for optimal reservoir heterogeneity characterization. Qualitative and quantitative approaches will be followed to characterize the reservoir heterogeneity; these will include measurements at meter scale to cover inter-well scale, field scale, and basin-wide scale. For example sorting coefficient will be used for quantitative characterization of grains and pores attributes at the studied outcrops, whereas porosity and permeability will be quantitatively characterized by using core plugs measurements. On the other hand, intra-reservoir layering, porosity, and permeability will be qualitatively characterized. A number of outcrops in at least three quadrangles will be selected for the meter scale heterogeneity characterization. The selection will be made to answer critical questions related to inter-well scale, filed scale, and basin scale heterogeneities. Table 1.1 illustrates the types of the reservoir heterogeneity and the methodology that will be used for their qualitative and quantitative characterization.

1.6. Objectives

The study intends to investigate, describe, and characterize the upper Khartam member of the Khuff formation in central Saudi Arabia in at least three quadrangles. The main objective is to examine the reservoir heterogeneity at scales varying from centimeter to hundreds of kilometers along the outcrop belts. Integrated detailed sedimentological, micropaleontological, stratigraphical, diagenetic, and petrophysical investigations will be conducted to achieve the objectives of this study. This study is

expected to provide better understanding and prediction of the high-resolution Khuff reservoir heterogeneity. Scope, methods, and techniques used in this research are illustrated in Figure 1.5 and 6. Approach utilized for achieving the objectives of this research is summarized in Table 1.2. The following objectives represent the framework of this study

1.6.1. Main objective:

- To investigate the detailed sedimentological and diagenetic controls on reservoir quality and heterogeneity at scale ranging from pore-geometry to inter-well spacing

1.6.2. Sub-objectives:

- To determine the lithofacies and lithofacies associations
- To construct a high-resolution stratigraphic scheme using sequence stratigraphic concept
- To analyze the diagenetic evolution and to construct a diagenetic model
- To investigate the impact of the high-resolution stratigraphy and diagenesis on reservoir quality and heterogeneity
- To analyze the diagenetic evolution of the reservoir and to construct qualitative diagenetic models, the models will provide better understanding and prediction of reservoir architecture and quality.

Table 1.1. Illustrates the types of the reservoir heterogeneity and the methodology that will be used for their qualitative and quantitative characterization.

Scale	**Level**	**Reservoir parameters**	**Techniques and methods**	**Heterogeneity characterization**
Meter scale, inter-well, and field scale	Microscopic	− Grains character (size, shape, sorting, packing, and distribution) − Pores characters (size, shape, connectivity, roughness and distribution) − Pore throat character (type, size, and distribution) − Pore and pore throat lining (e.g., clay)	− Scanning Electron Microscopy (SEM) − EDS − XRD − Pore Image Analysis (PIA)	Mostly quantitative characterization
	Macroscopic	− Porosity − Permeability	− Core − CT scan	
	Mesoscopic	− Average bed properties	− Well logging signature	
	Megascopic	− Lateral and vertical intra-reservoir continuity − Vertical and lateral porosity and permeability pinch-out − Mud/grain intercalation − Reservoir compartmentalization	− Semivariogram − DP coefficient − Lorenz coefficient − Lidar − Image analysis − GR on outcrop − Well logging correlation	Mostly qualitative characterization
Basin scale	Gigascopic	− Flow units characteristics − Thickness, shape, size and vertical and lateral connectivity of reservoir units − Spatial distribution of lithofacies − Depositional and lithological relationship	− Quadrangles − Lidar − Image analysis	

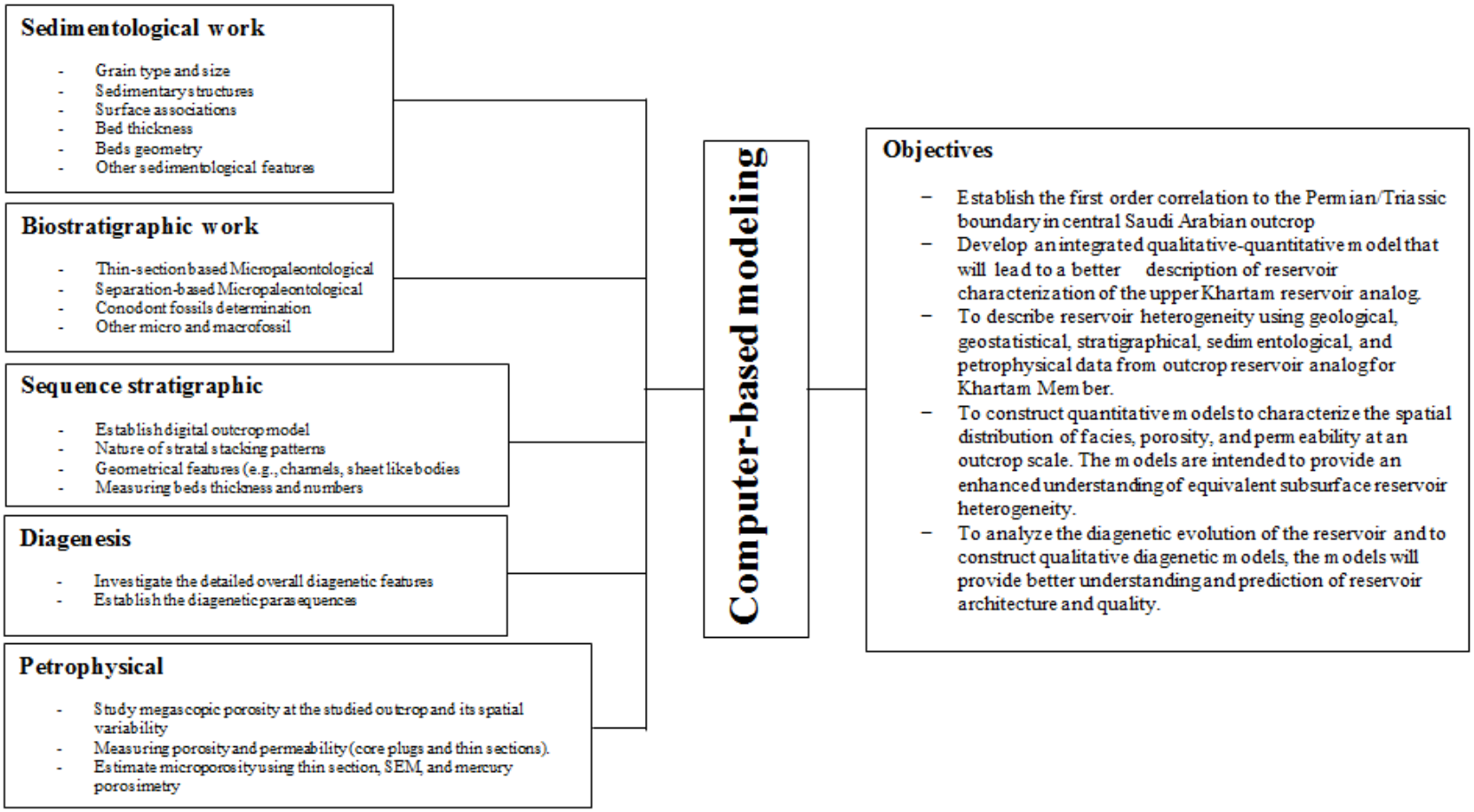

Figure 1.5. Scope and methodology he following methods and concepts will be followed to accomplish the objectives of this study

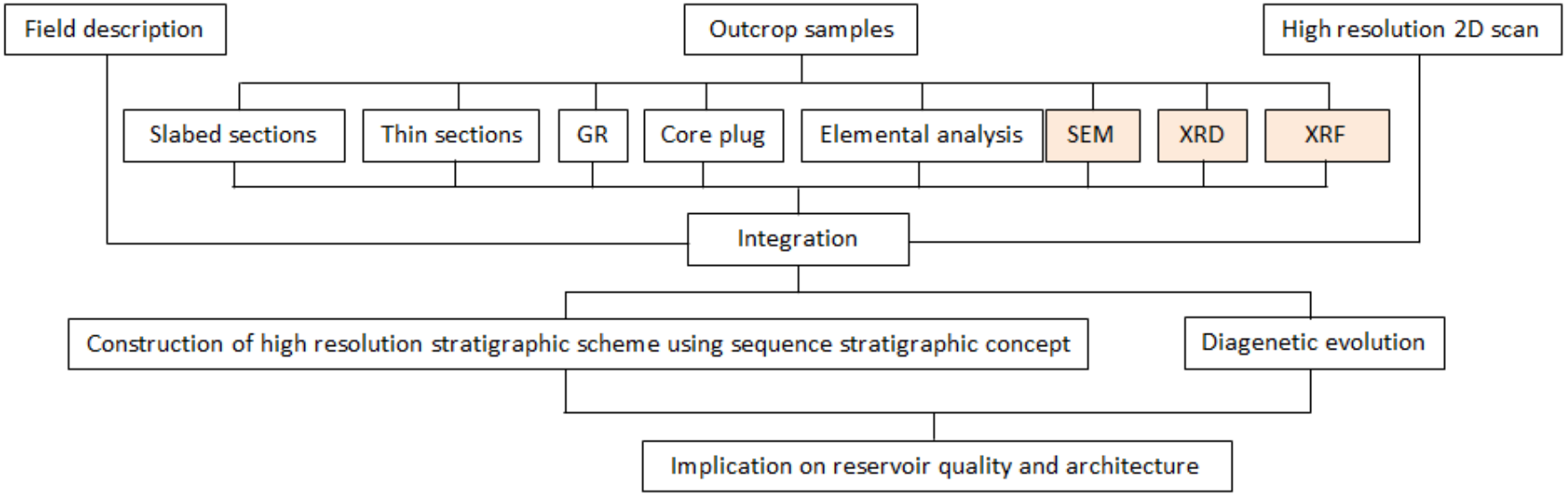

Figure 1.6. Techniques and methods will be used (upon availability) to accomplish the objectives of this study

Table 1.2. Approach utilized for achieving the objectives

Objective	**Approach of achieving the objective**
To develop an integrated qualitative-quantitative model that will lead to a better description of reservoir characterization of upper Khartam reservoir analog	Conduct field study at selected outcrops in at least three quadrangles, and then describe the sedimentology, stratigraphic hierarchies, stratal stacking patterns, and field outcrop measurements and sampling that will be supported by further laboratory analysis and measurements.
To describe reservoir heterogeneity using geological, stratigraphical, sedimentological, and petrophysical data from outcrop reservoir analog for Khartam Member	To identify lithofacies, cyclicity and sequence stratigraphic hierarchies and heterogeneities at microscopic, macroscopic, mesoscopic, megascopic, and gigascopic scales, supported by Gamma Ray, porosity, permeability and geochemistry using portable equipments in the outcrop. This will be supported by further lab petrographic, XRD, SEM, and porosity and permeability measurements.
To construct quantitative models to characterize the spatial distribution of facies, porosity, and permeability at outcrop scale. The model is intended to provide an enhanced understanding of equivalent subsurface reservoir heterogeneity	Using geological and geostatistical techniques to establish high resolution models for facies, porosity and permeability spatial distribution at the outcrop scale. The geostatistical models will be generated to evaluate the spatial heterogeneity of the variables. Models will be constructed by Kriging procedures. The spatial distribution of facies at different locations will be utilized to explain porosity and permeability spatial variability.
To analyze the diagenetic evolution of the reservoir and to construct qualitative diagenetic models, the models will provide better understanding and prediction of reservoir architecture and quality	Thin-section petrography, SEM, XRD, isotopes, and elemental analysis will all be utilized to establish a diagenetic model that will enhance understanding and prediction of reservoir quality and architecture.

CHAPTER 2

LITERATURE REVIEW

2.1. Geological setting

The ongoing tectonic evolution of the Arabian Plate had a significant control on the Phanerozoic depositional setting, sediment types, and sediment distributional patterns throughout the Arabian Plate (Konert et al., 2001; Bell, 2004). In addition to the tectonic evolution, eustatic sea level changes and climatic changes were also believed to have an important control on the Phanerozoic sedimentary record.

The present-day boundaries of the Arabian Plate display three tectonic regimes, Figure 2.1. Extension and sea-floor spreading are taking place along the axis of the Red Sea, Gulf of Aden, and Arabian Sea. Convergent-collisional regime is occurring along the Zagros fold belt, and a convergent-subductional regime is going on along the Makran zone in south Oman. Transform movement is taking place along the Dead Sea and Owen-Sheba fault (Ziegler, 2001).

Three stress regimes are considered to control the structural evolution, intra-continental basin development, and the depositional patterns and style of the Arabian Platform (Edgell, 1992). These evolved during the mid-Proterozoic, Proterozoic-Mesozoic, and Cenozoic, Figure 2.2. The Mid Proterozoic stress regime resulted in the formation of three structural trends; 1) north-trending structures, 2) northwest-trending structures, 3) northeast-trending structures. The north-trending structures are located in the eastern Arabian Plate and they have regular spacing. They include

Summan Platform, Dibdibah Trough, Ghawar Anticline, and Qatar Arch (Figure 2.1), and they formed during Amar Collision (640 – 620 Ma). The Amar collision occurred Amar suture, and has reoriented most of the Proterozoic structures of the Arabian Platform, Figure 2.3 (Al-Husseini, 2000). Between 620 and 530 Ma, a widespread extensional collapse took place in the Arabian-Nubian Shield, this has resulted in the formation of major horst and grabens (Al-Husseini, 2000). The northwest-trending structures are located in the Arabian Shield, and include the Najd fault system, Figure 2.4 (Al-Husseini 2000). During the final extensional stage (570 – 530 Ma), the NW Najd fault system dislocated the Arabian Shield left-laterally by about 250 – 300 Km, this dislocation appears to complement the NE oriented intra-continental rift basins in Oman, the Zagros Mountains, and Arabian Gulf (Al-Husseini 2000). The northeast-trending structures located around the Arabian Gulf and include the NE-oriented intra-continental rift basins of Oman, Zagros Mountains, and Arabian Gulf, these were described as pull-apart basins and they associated with the left-lateral dislocation induced by the Najd fault systems, Figure 2.4 (Al-Husseini 2000). Later these basins were filled by evaporite sediments (Gorin et al., 1982; Hughes Clarke, 1988; Husseini, 1988; Al-Husseini, 2000; Al-Husseini et al., 2003). The Proterozoic – Mesozoic stress regime intermittently activated the pre-existing structures as defined in the Ghawar Anticline, Dibdibah Trough, and Qatar Arch. This reactivation probably persisted until the end of the Pliocene (Edgell, 1992). During the Cenozoic, a new set of stress conditions prevailed in the basement and has resulted in the formation of two major vertical shear regimes at about N36^{o}E and N20^{o}W (Edgell, 1992). The N20^{o}W shear produced right-lateral, strike slip fault in the basement (Agar, 1985; Edgell, 1992). The N36^{o}E has produced a series of left-lateral strike slip faults in the basement, these are located in northeast Arabia and they are critical for

hydrocarbon (Powers et al., 1966; Al-Husseini, 2000; Brew and Barazangi, 2001; Ziegler, 2001).

During the Late Devonian, and as Gondwana and Laurasia collided to form Pangaea, a major tectonic event affected the entire Arabian Plate. This event is called “the Hercynian Orogeny”. The Hercynian Orogeny lasted for about 25 Ma and resulted in the removal of several kilometers of sediment over uplifted areas, Figure 2.5 (Alsharhan and Nairn, 1997; Konert et al., 2001; Sharland et al., 2001). The stratigraphic hiatus produced by the Hercynian Orogeny is referred to as the Pre-Unayzah Unconformity (PUU) (Wender et al., 1998; Konert et al., 2001).

During the late Early Permian, a major continental rifting and crustal stretching and thinning took place in west Pangaea. This rifting phase separated what is so-called Cimmerian continent from Gondwana and resulted in the formation of Neo-Tethys Ocean at the expense of the Paleo-Tethys (Sengör and Natalin, 1996; Alsharhan and Nairn, 1997). The opening of the Neo-Tethys Ocean was associated with regional uplift in the Arabian Plate and hence resulted in the formation of a Plate-wide unconformity which is the so-called Pre-Khuff unconformity. Besides the continental uplifting, this opening was associated with the first critical regional marine transgressive event on the Arabian Plate, which has established the first Plate-wide carbonate succession (Khuff formation) (Alsharhan and Kendall, 1986; Al-Jallal, 1995).

Following the Late Permian opening of the Neo-Tethys, came the formation of series of intra-shelf basins (e.g., Arabian and Gotnia Basins), these were most probably of tectonic and/or eustatic origin with the later sediment load playing a role in increasing subsidence rate (Alsharhan and Kendall, 1986; Al-Husseini, 1997; Alsharhan and

Nairn, 1997; Sharland et al., 2001; Ziegler, 2001; Hughes, 2004; Haq and Al-qahtani, 2005; Hughes et al., 2008). The Jurassic intra-shelf basins were associated with reservoir and source rocks. The reservoir rocks were measured at the basin margins, whereas source rocks were most probably associated with the deep intra-shelf areas (Sharland et al., 2001; Ziegler, 2001; Hughes et al., 2008).

In early Late Cretaceous, the closing onset of the Neo-Tethys Ocean was associated with the formation of a significant and widely spread unconformity, which is the so-called Pre-Aruma Unconformity (Sharland et al., 2001).

Following the subduction of the Afro-Arabian Plate beneath Eurasia (consumption of the Neo-Tethys Ocean), continental collision took place along the present-day Zagros fold belt (Alsharhan and Nairn, 1997; Sharland et al., 2001). Simultaneous to Zagros Orogeny, the Red Sea Basin was formed; however, the compressional phase associated with Zagros Orogeny was responsible for removing most of the Turonian-Santonian successions from the high areas. This compressional event has also reactivated the Najd Fault System and changed the pre-existing NW-SE trending normal faults that are located in the northeast of the Plate to reverse faults (Konyuhov and Maleki, 2000; Montenat et al., 2003).

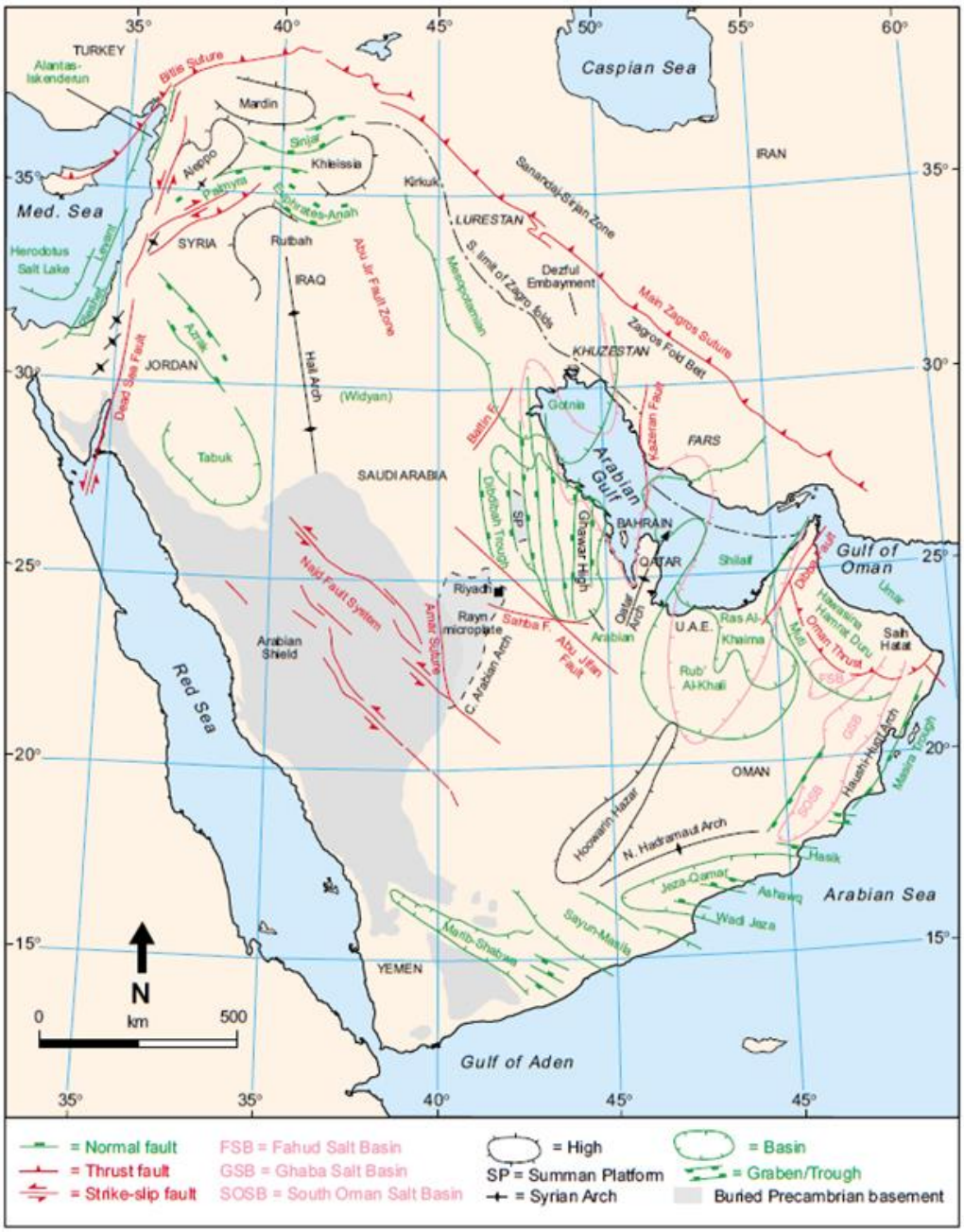

Figure 2.1 Tectonic and structural settings of the Arabian Plate (Ziegler, 2001).

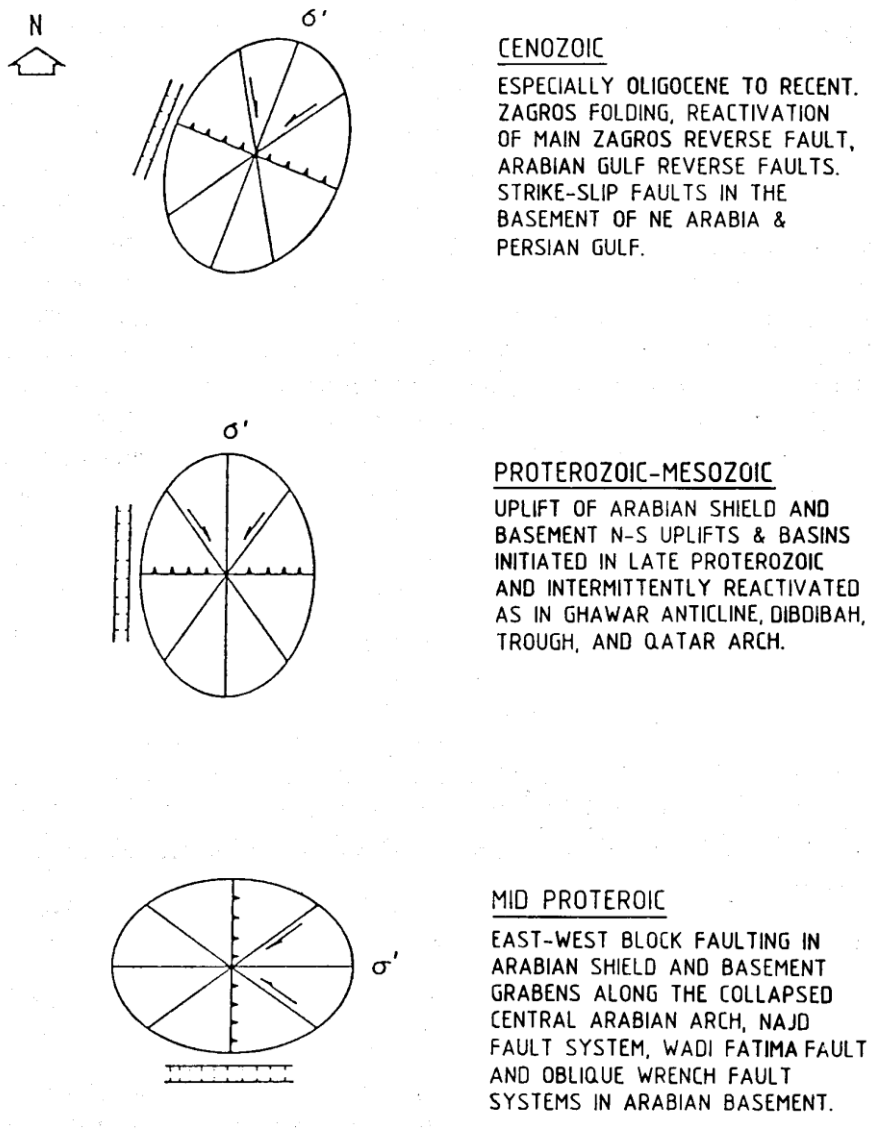

Figure 2.2 Stress evolution of Arabian Plate as indicated by the Stress Ellipse (Edgell, 1992).

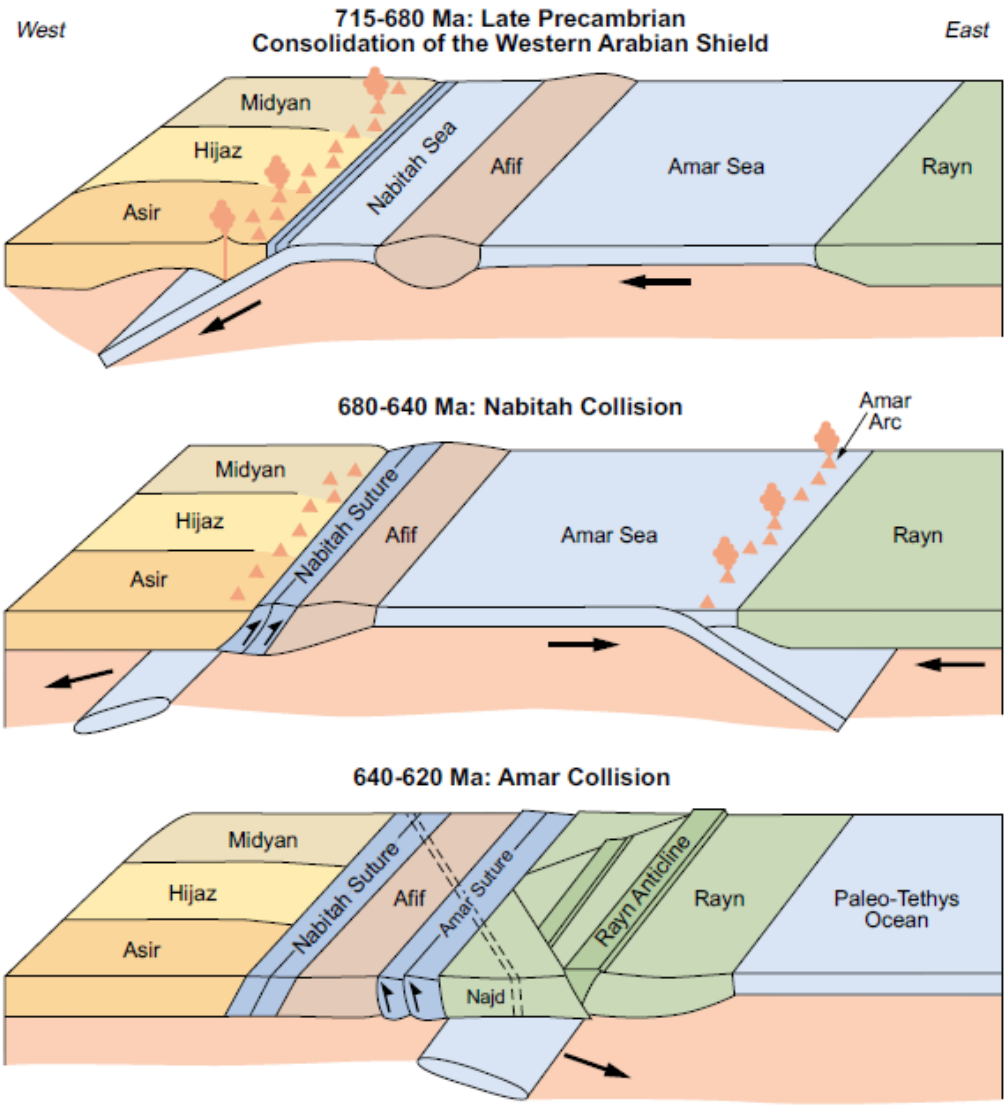

Figure 2.3 Tectonic evolution of the Arabian Plate basement (Al-Husseini, 2000).

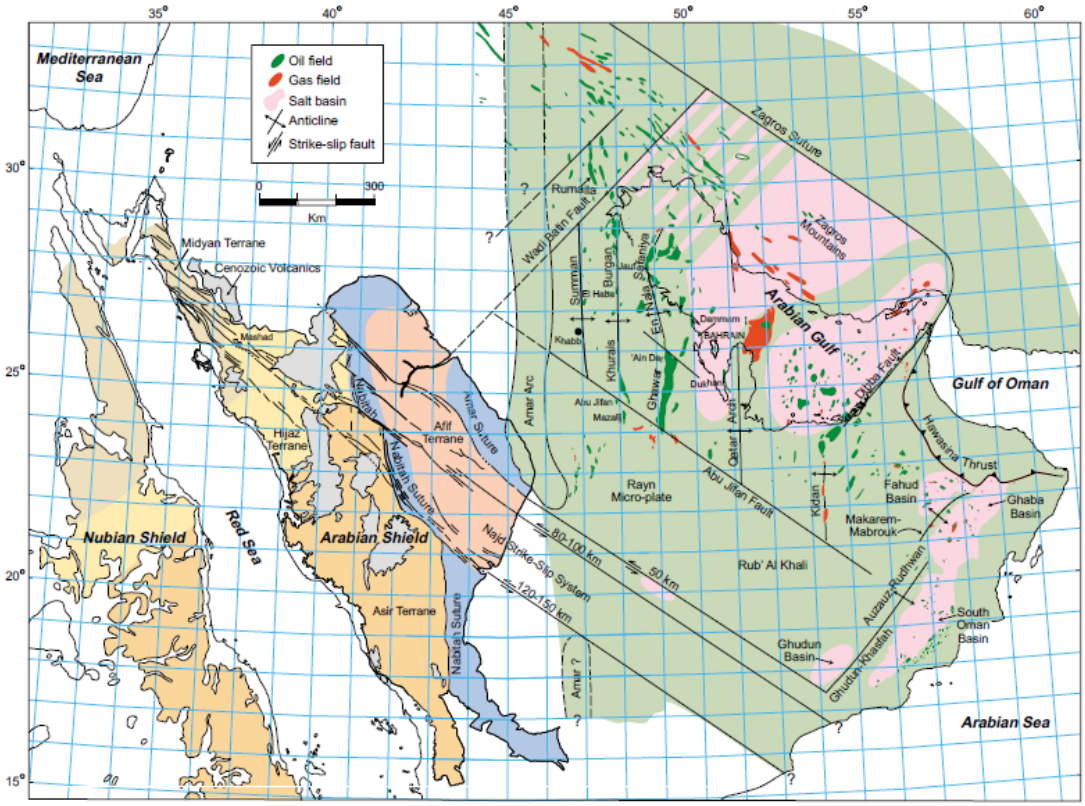

Figure 2.4 Major structures of the Arabian Plate as a result of the unique tectonic evolution, these structures have a significant control on hydrocarbon distribution (Al-Husseini, 2000).

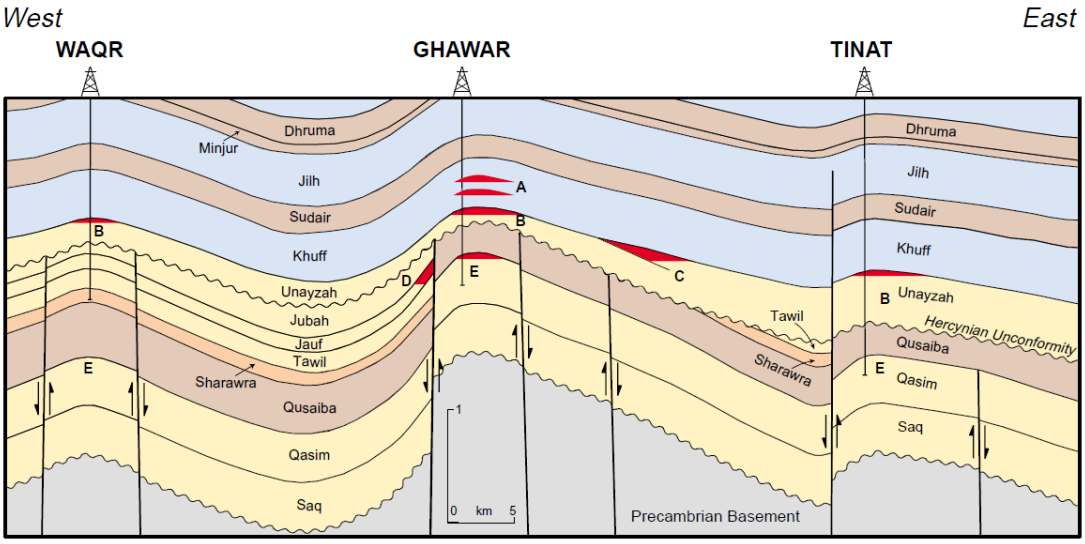

Figure 2.5 Schematic structural cross-section showing the prominent Hercynian Unconformity which is so called Pre-Unayzah Unconformity (Konert et al., 2001).

2.2. Paleo-Plate position

In addition to the tectonic evolution, climatically-controlled eustatic sea level changes and climatic changes were also believed to have significant control on the Phanerozoic sedimentary records of the Arabian Plate. These were extensively controlled by the paleo-Plate positions.

During the Late Precambrian, the Arabian Plate was attached to the African continent located close to the equator with East-West orientation, Figure 2.6 (Konert et al., 2001). In the Early Paleozoic, the plate moved into the southern latitudes, and rotated anti-clockwise, and a major glacial pulse covered western Arabia (Konert et al., 2001). By the Silurian to late Carboniferous time, a major clockwise rotation of about 100 degree without significant latitudinal translation took place. During the Late Carboniferous, a second glacial phase affected Oman, Yemen, Southern Arabia (Konert et al., 2001; Sharland et al., 2001). By the Permian time, the plate moved rapidly to the north from 25^{o} south to 5^{o} north. During the Early Jurassic, the Arabian Plate was standstill at an equatorial position (Al-fares et al., 1998). This equatorial position was essential for the intensive carbonate sedimentation during the Jurassic time. During the Cretaceous, the opening of the Atlantic Ocean drifted the African and the Arabian Plate to the north from 5^{o} N to 10^{o} N and the opening of the Red Sea tilted the African and the Arabian Plate to the east (Sharland et al., 2001). The paleogeographic settings of the Arabian plate during the Khuff time is characterized by rapid thermal collapse of the new northeast Arabian passive margin and continues as a northward continental drift which resulted in widespread early Late Permian Khuff transgression and development of a new passive margin with Neo-Tethys which is clearly expressed by very rapid subsidence resulting in a major marine transgression

and deposition of the Khuff formation (Al-Jallal, 1995). Several authors studied the macro- and micropaleontology in the Khuff outcrops in central Arabia, these studies revealed similarities and correlations with associations in the Arabian Platform and the western Tethyan realm. This allows the establish paleoecological and paleobiological relationships between different Palaeo-Tethyan areas (Vachard et al., 2005; Angiolini et al., 2006; Chirat et al., 2006; Crasquin-soleau et al., 2006).

2.3. Lithostratigraphy of Khuff Formation

The Permian-Triassic Khuff formation crops out in central Saudi Arabia along a N-S belt that is some 1200 km in length and 50 km in width (Bramkamp, R.A. and Steineke, 1952; Powers, 1968), Figure 1.2. The Khuff formation was formally defined by (Steineke et al., 1958) near Ayn Khuff (Latitude 245836 N 444148 E and 245312N, 444248 E), however the formation was first recognized in a publication by (Bramkamp, R.A. and Steineke, 1952). In the type section, the formation is 171.4 m thick. The Khuff formation in central Saudi Arabia unconformably overlies the Proterozoic Basement of the Arabian Shield or the lower Paleozoic deposits (Powers et al., 1966; Powers, 1968). This unconformity reflects a period of major continental rifting and crustal stretching and thinning that took place in west Pangaea during the late Early Permian (Powers, 1968; Wender et al., 1998). This surface is associated with lateritic and duricrust layer containing goethite pisoliths or an iron crust. The upper contact is located at the sharp transition from limestone and dolomite below to red and green gypsiferous shale of the Sudair formation. A complete stratigraphic section of the formation was described in Wadi Ar Rayn Quadrangle 23 ^{o} 32’45” N, 45 ^{o} 34’30” E, and 23 ^{o} 43’ N, 45 ^{o} 42’ E. In this quadrangle, the formation directly sits on the Proterozoic rocks of the Arabian Shield. The formation was revised and described

in the Ad Dawadimi quadrangle and was subdivided into five informal members from bottom to top Unayzah, Huqayl, Duhaysan, Midhnab, and Khartam (Delfour et al., 1982). This subdivision was adopted across Central Saudi Arabia by DMMR and BRGM during mineral exploration. (Enay et al., 1987) synthesized the lithostratigraphic, sedimentologic, and biostratigraphic results of the DMMR and BRGM together with analytic data. These syntheses included revisions of the lithostratigraphic, sedimentologic, biostratigraphic, paleoenvironments. The lithostratigraphic nomenclature of the Khuff members varies according to authors and from subsurface to surface (Powers et al., 1966; Powers, 1968; Delfour et al., 1982; Al-Jallal, 1995; Alsharhan and Nairn, 1997; Alsharhan, 2006). (Delfour et al., 1982) named the lower siliciclastic deposits of the Khuff formation as Unayzah member, whereas (Al-Laboun, 1982, 1986, 1987; El-Khayal and Wagner, 1983; Senalp and Al-Duaiji, 1995) named this section as Unayzah formation. (Vaslet et al., 2005) proposed the name Ash Shiqqah member to replace the Unayzah member.

2.3.1. Lithostratigraphy of the Khuff formation; Central Saudi Arabia

The five member s of the Khuff formation were recognized and described along NS trending outcrops in central Saudi Arabia. Following is a generalized lithostratigraphy of the Khuff's members as been described by (Powers et al., 1966; Powers, 1968; Delfour et al., 1982; Vaslet et al., 1983, 2005; Le Nindre et al., 1990a).

2.3.1.1. Ash Shiqqah member

The Ash Shiqqah member in central Saudi Arabia generally consists of fine-grained lithofacies interbedded with sandstone beds; these are overlain by dolomite intervals (Vaslet et al., 2005).

2.3.1.2. The Huqayl member

The Huqayl member displays a homogeneous lithological character to the south and north of the Arabian Arch. The member is dominated by calcarenitic and gypsiferous claystone lithofacies deposited in restricted sabkhah settings. The presence of marine faunas in this member indicates marine transgression (Vaslet et al., 2005).

2.3.1.3. Duhaysan member

The Duhaysan Member contains the first true carbonate lithofacies of the Khuff Formation (Delfour et al., 1982; Vaslet et al., 1983, 2005; Le Nindre et al., 1990a). The base is characterized by the presence of reworked materials and marine faunas indicating marine transgressive phase. The member contains less detrital materials and the thickness decreases to the central Arabian Arch where the clay percentage also decreases.

2.3.1.4. The Midhnab member

The lower part of the Midhnab member is dominated by carbonate lithofacies, whereas the upper part consists of channelized sandstone and claystone facies with abundant fossilized plant (Vaslet et al., 2005).

2.3.1.5. The Khartam member

This member is characterized by uniformably thick oolitic to peloidal to bioclastic lithofacies that extends for about 700 km, Figure 2.7. Part of this member is dominated by detrital to lacustrine claystone and dolomitic sandstone (Vaslet et al., 2005).

2.3.2. Lithostratigraphy of the Khuff formation; Type section

2.3.2.1. The Ash Shiqqah member

In the type section, the Ash Shiqqah member is about 35 m thick. The member has been subdivided into four subunits; from bottom to top: Subunit 1 is 10.5 m thick of silty claystone, with minor gypsum beds in the lower part, this is interbedded with silty dolomite; subunit 2, is about 2.5 m of white, fine-grained sandstone with cross-bedding; subunit 3 consists of 15 m of silty claystone interbedded with dolomitic lithofacies; subunit 4 comprised of 7 m of clayey and finely bioclastic dolomite, Figure 1.4. The Ash Shiqqah member thins toward the southeast in the Ad Dawadimi quadrangle.

2.3.2.2. The Huqayl member

The type section of this member was also defined in the Ad Dawadimi quadrangle at Safra Huqayl (between 24°44’25” and 24°45’37”N, to 44°39’08” and 44°39’15”E) (Delfour et al., 1982; Le Nindre et al., 1990a). At this locality, the member is about 34.2 m thick and was divided into lower and upper units, Figure 1.4. The lower unit consists of three subunits; from bottom to top: 1) 6 m of bioclastic to intraclastic dolomite with localized silty and peloidal dolomite containing oolitized bioclasts, silty, bioclastic dolomite with a clear patina, overlying an intraclastic dolomitic bed; subunit 2 is about 4 m of gypsiferous claystone; subunit 3 is about 2.7 m thick clayey dolomite containing algal and fenestral gypsum and anhydrite. The upper unit was subdivided into three subunits; from bottom to top: 1) 2.9 m of channelized bioclastic dolomite; 2) 17.6 m dominated by clayey dolomites interbedded with thin beds of bioclastic and oolitic dolomite; 3) 1.0 m of clayey dolomite with distributed cherty and gypsum and anhydrites nodules.

2.3.2.3. The Duhaysan member

At Jabal Duhaysan, the type section of this member was defined where it is 13.4 m thick, Figure 2.7 (Delfour et al., 1982; Le Nindre et al., 1990a). The Duhaysan member consists of three units; from bottom to top; 1) 3.7 m of dolomitic calcarenite, with coarse materials, overlain by white bioclastic dolomite; 2) 5.6 m gypsiferous, dolomitic clay; 3) 4.1 m of peloidal limestone overlaid by clayey dolomite.

2.3.2.4. The Midhnab member

Along Wadi Maghib, near Khuff town (Le Nindre et al., 1990a) measured the type section of the Midhnab member, Figure 1.4. At this locality, the Midhnab member is about 57.9 m thick and has been subdivided into four subunits; from bottom to top; 1) 2 m of conglomeritic limestone; 2) 9 m of interbedded gypsiferous dolomite and bioclastic limestone and dolomite; 3) 46 m dominated by claystone facies; 4) 3 m of lacustrine limestone.

2.3.2.5. The Khartam member

This member represents the Khartam limestone or Unit 4 of (Powers, 1968). (Delfour et al., 1982) adopted the name Khartam member. The type section of this member was described near Khuff town in Ad Dawadimi quadrangle (Le Nindre et al., 1990a). At this locality, the member is about 37 m thick, Figure 1.4. The lower Khartam member is about 14 m thick and is subdivided into two subunits; from bottom to top; 1) 10.9 m of bioclastic and peloidal limestone overlain by dolomitic claystone; 2) 3.1 m thick dominated by bioclastic dolomite and a claystone facies. The upper Khartam member is about 23 m thick and comprises three subunits from bottom to top; 1) 15 m of channelized oolitic and peloidal limestone. This subunit has stromatolitic buildups in

the middle part; 2) 6.5 m of interbeds of dolomitic coquina and clayey dolomite; 3) 1.5 m of massive oolitic limestone. A clayey soft bed of 10 m thick, probably overlain this subunit, is however hidden by Quaternary sediments. The boundary between the Khuff and Sudair formation is not well-defined in the type section (Delfour et al., 1982).

2.3.3. Lateral variations within the Khartam member

2.3.3.1. The Khartam member: northwards the type section

Northwards, in Al Faydah quadrangle, the Khartam member becomes increasingly thicker. At Khashm Khartam, the member has a thickness of about 50 m (Denis. Vaslet et al., 1985). At this locality, the lower Khartam consists of two units, from bottom to top; unit 1 consists of 10.5 m of dolomite overlain by gypsiferous claystone; unit 2 consists of 3 m of microcrystalline limestone and claystone facies, Figure 2.7. The upper Khartam consists of three units; from bottom to top; unit 1 is about 14 m thick and consists of massive oolitic and peloidal limestone; unit 2 has a thickness of 13 m and consists of bivalve clasts (bioclastic) interbedded with dolomitic limestone; unit 3 is a 9.5 m thick of oolitic and bioclastic limestone interbeded with clayey dolomite (Denis. Vaslet et al., 1985). In Buraydah quadrangle, the Khartam member has a uniform thickness; however, in Wadi ar Rimah (Jal Al Aswad) the member thins to 36 m.

2.3.3.2. The Khartam member: northwards the type section

In the Darma quadrangle the member increases somewhat in thickness to about 60 m (Manivit, Pellaton, Vaslet, Nindre, et al., 1985). At Jabal Sufan (2420), although the upper Khartam member is thicker (about 52 m), however, the facies is similar to those

in the type section. The upper part of the lower Khartam consists of a claystone facies with abundant ammonoids. In the SHD-1 well, the Khartam member is about 61 m and dominated by carbonate facies (Manivit et al., 1983; Manivit, Pellaton, Vaslet, Nindre, et al., 1985; Nindre et al., 1990). At this locality, the lower Khartam consists of 14 m of bioclastic arenitic calcarenite. The upper Khartam is about 46 m thick and consists of 30 m clayey dolomite overlain by an oolitic dolomite followed by 16 m of bioclastic dolomite. At Wadi Ar Rayn (2340), the Khartam member progressively decreases in thickness to about 58 m. At this locality, the lower Khartam is about 20 m thick and is dominated by a clayey facies of 20 m thickness. Further south, the member becomes enriched with detrital material such as claystone and mica sandstone. In the Al Huwwah area, the upper Khartam is about 20 m thick and consists of cross-bedded oolitic limestone overlain by coquina, peloidal limestone, claystone, and bioclastic interbeds. In Jabal Umm Mus'ham (2474), at Wadi Al Mulayh quadrangle, the member is about 37 m thick. At this locality, the lower Khartam is about 15 m thick and consists entirely of dolomitic claystone and bioclastic, and is rich in algae. The upper Khartam is 22 m thick and dominated by oolitic facies. The best outcrops of the Khuff Formation were described in Sulayyimah quadrangle (22 N and 21 N), however, this outcrop has limited extent (D. Vaslet et al., 1985). Towards 2155 N, the member contains oolitic and skeletal materials. Towards 2125 N, the member has reworked materials at the base overlain the gypsiferous materials of the Midhnab member.

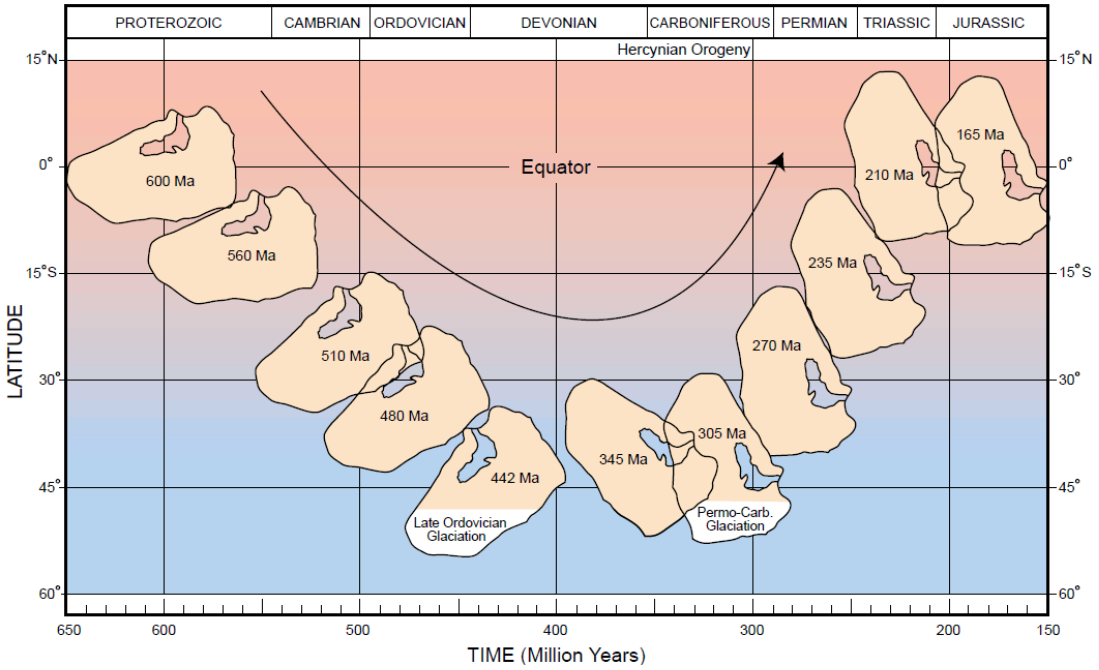

Figure 2.6 Paleo-Plate positions of the Arabian Plate during the Paleozoic (Konert et al., 2001).

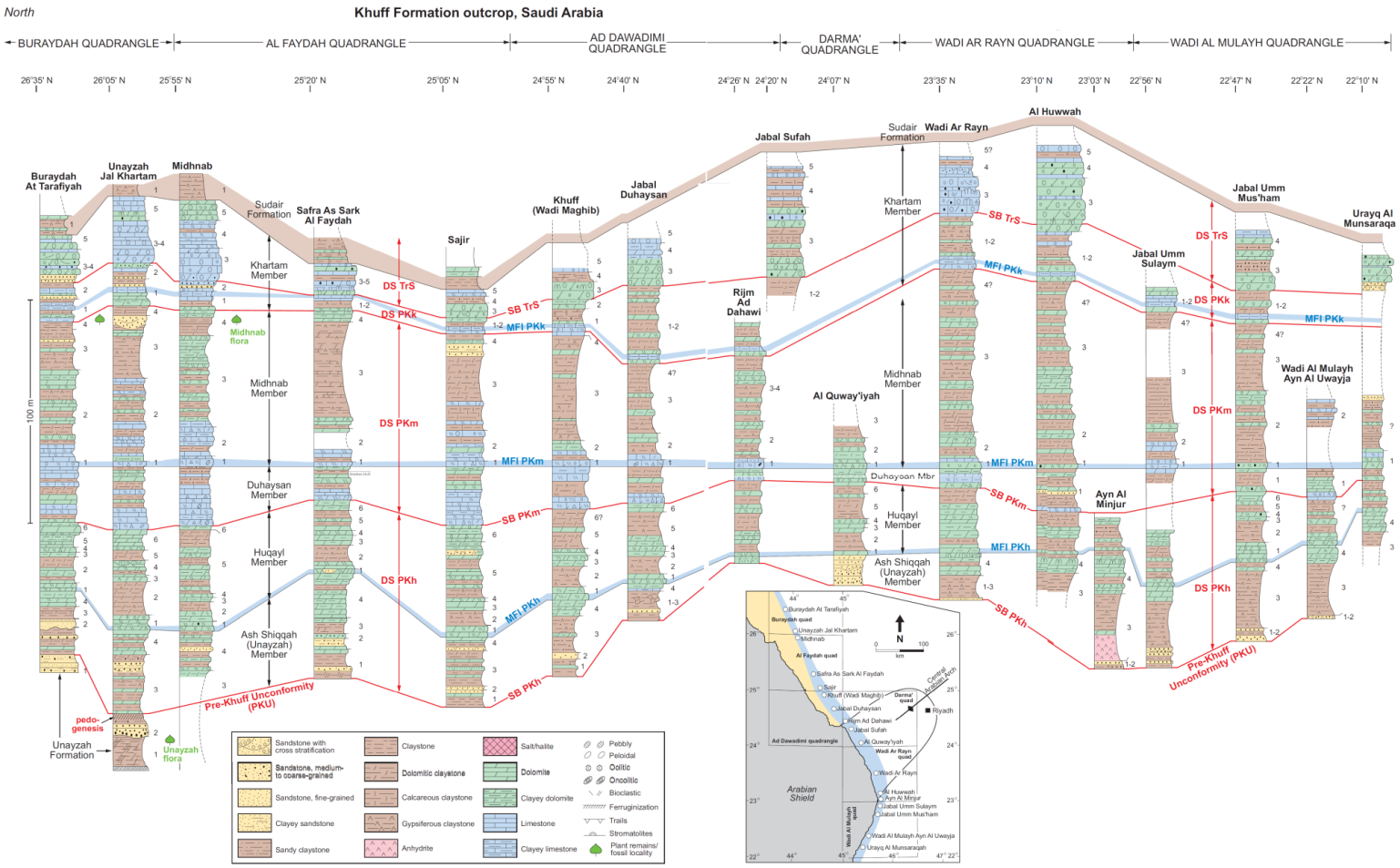

Figure 2.7 Regional correlation of the Khuff Formation in central Saudi Arabia (Vaslet et al., 2005).

2.4. Sequence stratigraphy and depositional settings

The Khuff Formation predominantly contains low-energy carbonate facies and evaporite facies deposited in a relatively confined environmental setting, Figure 2.8 and Figure 2.9 (Vaslet et al., 2005). In outcrops, in central Saudi Arabia, (Vaslet et al., 2005) subdivided the formation into four depositional sequences, from bottom to top; DSPKh, DSPKm, DSPKk, DSTrS. Each of these sequences is characterized by a basal sequence boundary (SB), transgressive system tract (TST), maximum flooding interval (MFI), and highstand system tract (HST), (Vaslet et al., 2005).

2.4.1. The DSPKh (named after Depositional Sequence Permian Khuff Huqayl)

This sequence includes the lower two members of the Khuff formation (Ash Shiqqah and Huqayl). The basal sequence boundary corresponds to the Pre-Khuff unconformity (PKU). The basal Khuff clastics of the Ash Shiqqah member corresponds to the TST of DSPKh, while the upper and lower Huqayl member is represented by two sabkha sequences that have been deposited in intertidal to subtidal environments during a period of HST, Figure 2.8. The Ash Shiqqah member exhibits very different facies and hence depositional settings north and south of the Central Arabian Arch. The MFI PKh of this sequence represents the first flooding event over central Saudi Arabia (Vaslet et al., 2005). This surface is located at the base of Huqayl member, Figure 1.4, where it is associated with a marine bioclastic facies. The MFI PKh is followed by the two higher-order regressive sabkha sequences of the Huqayl member (Le Nindre et al., 1990a). The basal Huqayl sequence contains abundant microfauna. The DSPKh is superimposed on Khuff cycle 1 of (Al-Aswad, 1997) and the MFS P30 of (Sharland et al., 2001).

2.4.2. The DSPKm (named after Depositional Sequence Permian Khuff Midhnab)

This sequence comprises the Duhaysan and Midhnab member. The Duhaysan member is interpreted to be deposited in subtidal to littoral environment during a transgression period (TST PKm), this transgression phase has eroded and reworked the underlying carbonate mud of the upper Huqayl member. The Midhnab member comprises regressive supratidal to continental deposits that evolved during the HST. The DSPKm SB is marked by reworked deposits. The DSPKm MFI is located at the base of Midhnab member and contain abundant marine fauna (Le Nindre et al., 1990a). This surface represents the maximum extent of the marine domain in central Saudi Arabia, Figure 2.8 and Figure 2.9 (Vaslet et al., 2005). The DSPKm corresponds to Khuff cycle 2 and 3 of (Al-Aswad, 1997), and may contain the MFS P40 of (Sharland et al., 2001) (Vaslet et al., 2005).

2.4.3. The DSPKk (named after Depositional Sequence Permian Khuff Khartam)

The lower Khartam member represents the depositional domain of this sequence. The basal sequence boundary represents a return to marine condition following the continental settings at the upper DSPKm, Figure 2.7, Figure 2.8, and Figure 2.9. The reworked materials at basal Khartam member represent the transgressive system tract and the maximum flooding interval of the PKk, this interval contains abundant ostracods, bactritids, and local cephalopods (Crasquin-Soleau et al., 2005; Chirat et al., 2006). The dolomitic sandstone at the base of the upper Khartam member is probably the eroded part of the HST PKk (Vaslet et al., 2005). The DSPKk corresponds to Khuff cycle 4 of (Al-Aswad, 1997). The MFI has the same position as MFS Tr10 of (Sharland et al., 2001).

2.4.4. The DS TrS (named after Depositional Sequence Triassic Sudair Shale)

The DS TrS comprises the early Triassic upper Khartam member and the early Triassic Sudair formation. The upper Khartam member was deposited during the TST of the DS TrS and it consists of littoral, tidal, to intertidal deposits, whereas, the Sudair Formation consists of closed-basin, clayey to evaporitic rocks that evolved during the HST, Figure 2.7, Figure 2.8, and Figure 2.9 (Le Nindre et al., 1990a). The TrS SB is marked by an abrupt change in facies from subtidal and intertidal to beach deposits (Vaslet et al., 2005). This erosional boundary could represents the Permian/Triassic boundary in central Saudi Arabia (Vaslet et al., 2005), but the index species for the boundary has not yet been found. The MFS Tr10 represents an early Triassic flooding event (Stephenson et al., 2003; Sharland et al., 2004), this should be placed at the top of Khartam Member or in the lower Sudair Formation (Vaslet et al., 2005).

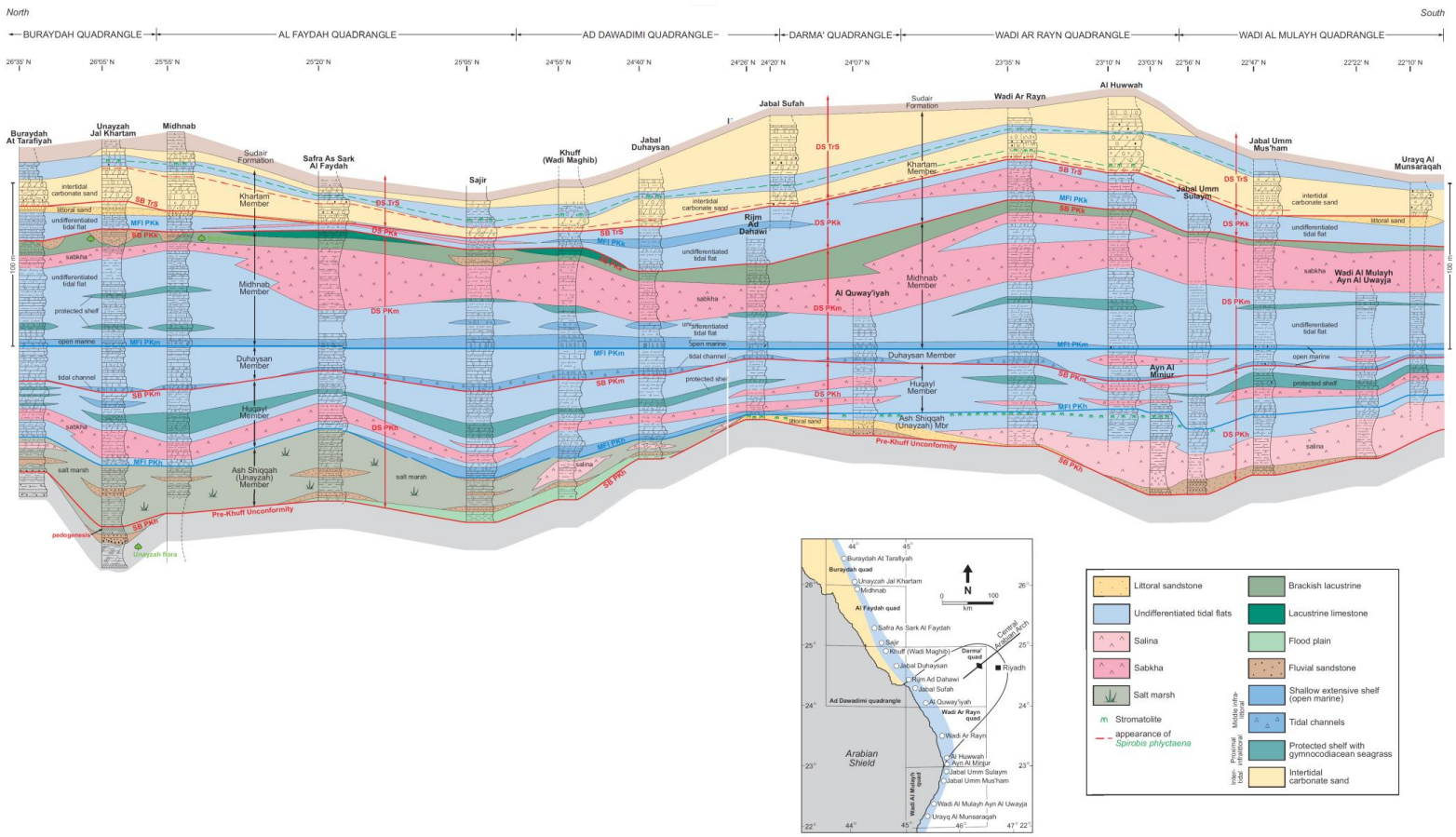

Figure 2.8 Paleoenvironmental interpretation of the Khuff Formation from central Saudi Arabian outcrops (Vaslet et al., 2005).

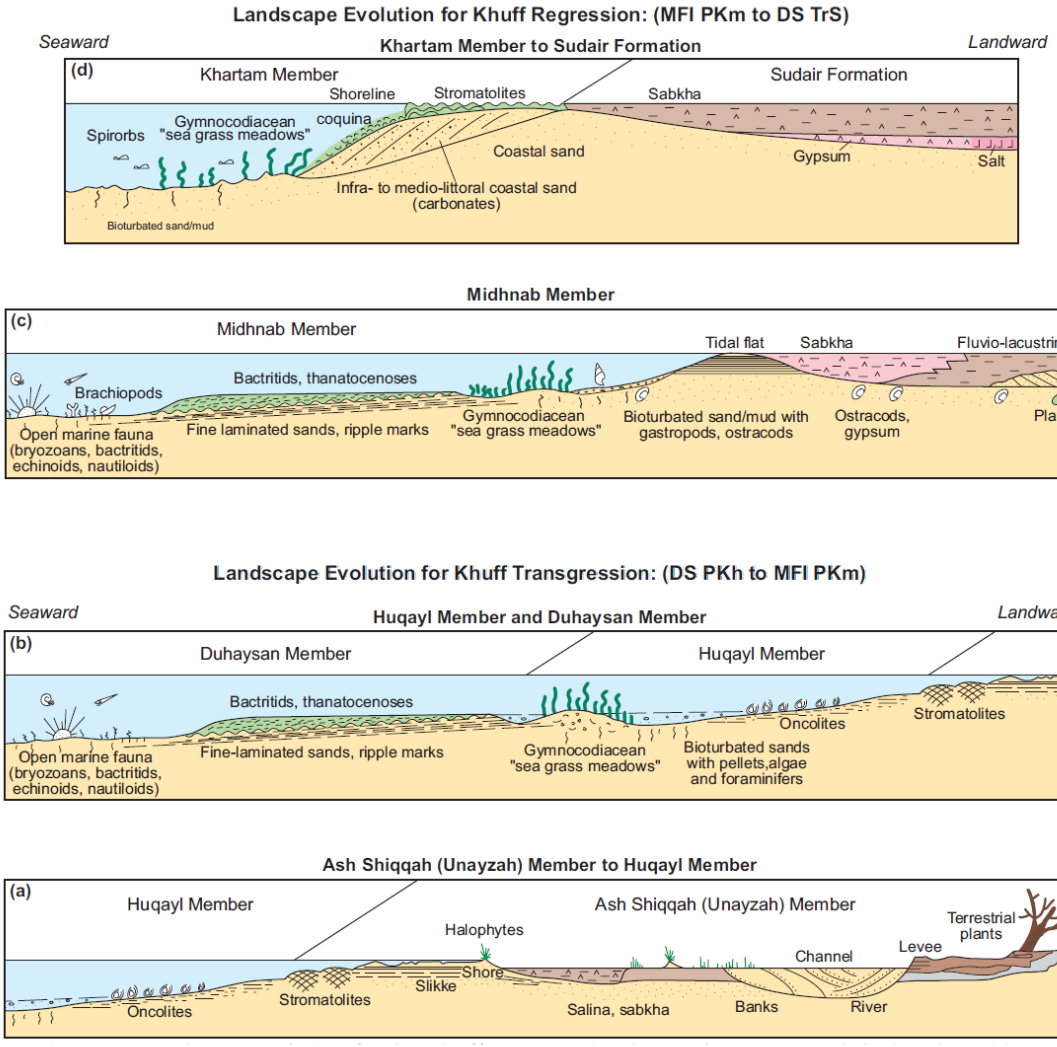

Figure 2.9 Paleoenvironmental models of the five Khuff members (Vaslet et al., 2005).

2.5. Reservoir outcrop analog

The increasing demands to maximize recovery from oil and gas fields have led to many new innovative methods in the oil and gas industry. Most of these focus on exploration and reservoir characterization. Reservoir characterization deals with assessing architectural and quality elements of the reservoir rocks. Optimum exploitation of hydrocarbon reservoirs is highly dependent upon understanding the intra-reservoir flow unit architecture and quality that are mostly controlled by syn-depositional processes and subsequent diagenetic evolution. Obviously, conventional subsurface data are not sufficiently detailed to reveal critical high-resolution architectural and reservoir quality elements. This is related to three main reasons, the lower three-dimensional coverage and vertical resolution of the conventional 2D and 3D seismic data, the large inter-well spacing, and the small number of cores. The high cost associated with acquisition, processing, and interpreting the subsurface data is also a prime factor. Outcrop analogs provide valuable insight into understanding ancient sedimentation processes and products (Grammer et al., 2004; Pringle et al., 2006). Importantly, the outcrop analogs have been utilized widely to understand critical quality and architectural elements (Calvo et al., 1983; Aigner et al., 1995; Olsen, 1995; Meyer et al., 1996; Jennings et al., 2000; Frykman, 2001; Mattner and Al-husseini, 2002; Philip et al., 2002; Lüning et al., 2003; Eschard et al., 2003; Gardner et al., 2003; Weidlich and Bernecker, 2004; Schwab et al., 2005; Homewood et al., 2008; Nindre et al., 2008; Maurer et al., 2009; Wilson et al., 2009; Koehrer et al., 2010; Mukti and Ito, 2010; Mulder et al., 2010; Pöppelreiter et al., 2011; Pyles et al., 2011; Tuuling and Flodén, 2011; Iñigo et al., 2012; Retallack and Dilcher, 2012;

Adam et al., 2013, 2014; Bruna et al., 2013; Cogné et al., 2013; Eltom et al., 2013). Most of the published sedimentologic, stratigraphic, biostratigraphic, and chronostratigraphic researches on the Phanerozoic stratigraphic succession of Saudi Arabia were based partially of completely on outcrops (Examples; Bramkamp, R.A. and Steineke 1952; Powers et al. 1966; Powers 1962; Powers 1968; Imlay 1970; Manivit, Pellaton, et al. 1985; Manivit, Vaslet, et al. 1985; Fischer et al. 2001; Vaslet et al. 2005; Enay et al. 1987; Le Nindre et al. 1990). Excellently exposed Khuff outcrops in Central Saudi Arabia provide complete stratigraphic context, where the individual beds can be traced laterally for a great distance (Hughes, 2004, 2005; Hughes et al., 2008; Lindsay and Hughes, 2010). Therefore, if the sequence boundaries and system tracts could be determined in the outcropping analogue, a much better understanding of the Khuff reservoirs would be obtained. Therefore, the sequence analysis at the outcrops would then have a direct application to reservoir studies. Likewise, studying diagenetic evolution and the subsequent implication on porosity and permeability could assist in understanding the subsurface reservoir. Generally, the use of outcrop analog from the Khuff formation is valuable tool that can contribute significantly to better understanding of reservoir characteristics which will eventually facilitate the reservoir development and management (Grammer et al., 2004).

This study intends to determine the sedimentological heterogeneity, architecture, chronostratigraphy, and reservoir quality, at outcrop scale, of the upper Khartam member of the Khuff formation in Central Saudi Arabia. The study is expected to

provide better understanding and prediction of the Khuff reservoirs heterogeneity at outcrop scale and of its influence on reservoir quality and architecture.

2.6. Reservoir Heterogeneity

Reservoir rocks are known for their heterogeneities in sedimentological and petrophysical properties, these are mostly controlled by depositional and post-depositional processes (Tiab and Donaldson, 2012). The scale of heterogeneity varies from microscopic level to gigascopic level. Tiab & Donaldson 2012 gives five levels of reservoir heterogeneities (Figure 2.10)

2.6.1. Microscopic Heterogeneity

Represents the variations of porosity and permeability in the pore domain, as determined by

1. Grains character (size, shape, sorting, packing, and distribution)
2. Pores characters (size, shape, connectivity, roughness and distribution)
3. Pore throat character (type, size, and distribution)
4. Pore and pore throat lining (e.g., by clay)

These properties are controlled by

1. Depositional settings and processes
2. Post-depositional processes such as cementation, compaction, and dissolution.

The microscopic heterogeneity is usually studied by the following techniques

1. Scanning Electron Microscopy (SEM)
2. Mercury injection and Pore Image Analysis (PIA)
3. Magnetic Nuclear Resonance (MRI) and (MNR)

2.6.2. Macroscopic Heterogeneity

The macroscopic heterogeneity represents variations in core plug domain and includes laboratory measurements of porosity, permeability, wettability, and capillary pressure.

2.6.3. Mesoscopic Heterogeneity

Well log data represent the characteristic scale of mesoscopic heterogeneity. At this level of heterogeneity, variations in the microscopic and macroscopic geological and petrophysical properties will be assigned a single value (e.g., gamma ray, resistivity, sonic, and density).

2.6.4. Megascopic heterogeneity

Flow units represent the domain scale of megascopic heterogeneity, and usually are investigated by conducting computer-based reservoir simulation. However, outcrop data can provide guidance to characterize flow units size, architecture, and quality. In subsurface studies, high-resolution seismic, well test analysis, and inter-well correlation can provide information about the megascopic heterogeneity. The megascopic heterogeneity includes lateral and vertical stratal stacking, mud and sand intercalation, and vertical and lateral porosity and permeability distributional patterns.

2.6.5. Gigascopic heterogeneity

This represents variations in reservoir properties basin-wide. The gigascopic heterogeneity in reservoir properties is a result of syn-depositional and/or structural settings. Information for this scale of heterogeneity is obtained from structural and tectonic analysis, regional seismic measurements and seismic stratigraphy, and subsurface mapping.

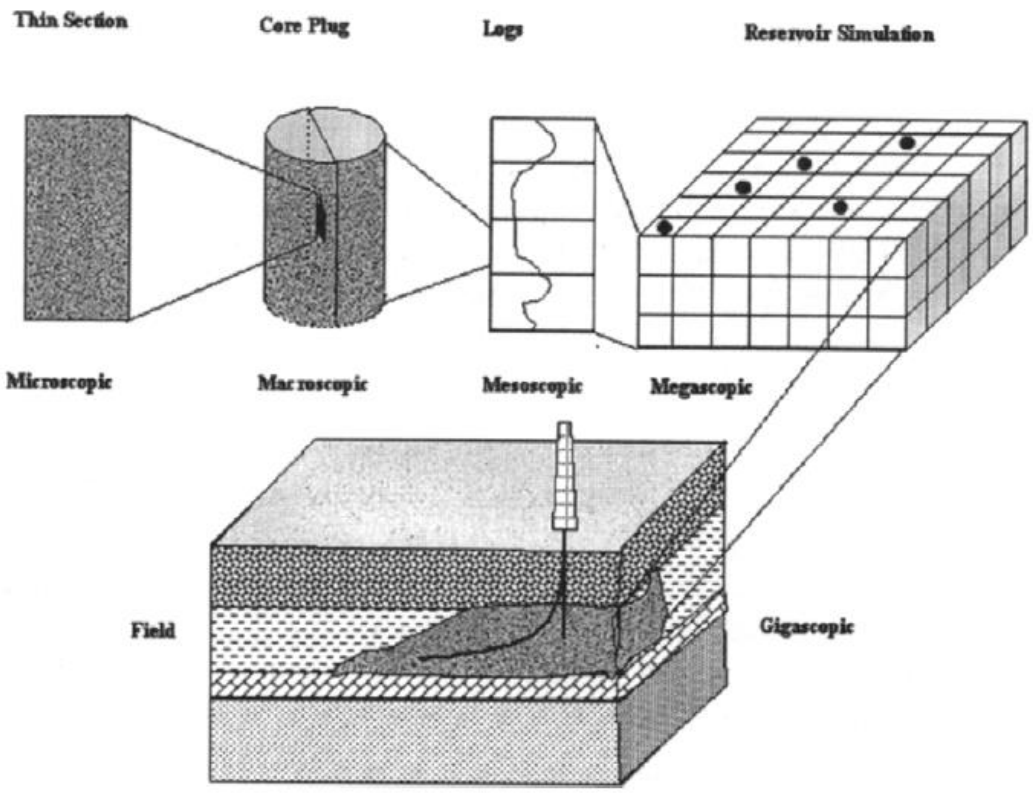

Figure 2.10 Reservoir heterogeneities scales (Tiab and Donaldson, 2012).

CHAPTER 3

HIGH-RESOLUTION SEDIMENTOLOGY AND SEQUENCE STRATIGRAPHY

3.1. Overview

The Khuff reservoirs are known for having complex heterogeneities and these were described to occur at inter-well and sub-seismic scale. We therefore studied the high-resolution stratigraphic framework of the Upper Khartam Member of the Khuff reservoirs in outcrop analogues. Four outcrop localities were logged and about 300 representative samples were collected for microfacies analysis. Furthermore high-resolution photo-mosaics of the outcrops were made. The latter cover an extension of about 7 kms, mostly along dip direction. Centimetre-thick beds are followed laterally and logged for detailed sedimentology and sequence stratigraphy. Seventeen lithofacies were defined, with coarse-grained oolitic grainstone, interlaminated quartz-bearing recrystallized limestone, recrystallized limestone, interlaminated quartz-bearing fine-grained oolitic grainstone, bioclastic grainstone/packstone, and marlstone making up the bulk of the successions. These lithofacies are occurring as sheet-like and channelized bodies. The former range in thicknesses from 5 to 40 cm and possess a lateral extension varying between 5 and 300 m, while channelized bodies have two anatomies, i.e. small tidal creeks (1m in width by 30cm in height) and large tidal channels (3m in width by 50cm in height). Accordingly, seven depositional settings

were distinguished, including intertidal-subtidal flats, supratidal settings, intertidal channels and creeks, shoal ridges, reef complex, and outer ramp settings.

Four stratigraphic identities were defined, these include; beds, bedset, high-frequency fifth-order sequences, and fourth-order sequences. About 20,000 beds are defined and traced laterally, ranging in thickness from 5 to 40 cm and extending between 5 and 300 m. The beds are stacked into well-developed bedsets composed of a complex internal amalgamation with relatively large lateral extension of several thousand of metre and thickness ranging between 1 and 5 m. These are genetically stacked into six high-frequency sequences with prominent flooding surfaces linked to shifts in shoreline position. The high-frequency sequences likely represent fifth-order cycles and possibly relate to Milankovitch cycles (i.e. eccentricity cycles of 100,000 year). Furthermore, and based on the sedimentological characteristics and nature of stacking patterns, the latter could be grouped into two fourth-order sequences, which are separated by major sequence boundaries associated with large intertidal channels and microbialites constructions. Essentially, the high-resolution stratigraphic sequences of the Upper Khartam Member are typified by regressive cycles dominated by regressive deposits. This nature is likely identical for the entire Upper Khartam (mostly third-order sequence) where the nature of the rapid transgression over the Lower Khartam (mostly clayey and evaporitic deposits) is prominent and characterized by thin (20 cm) skeletal accumulations.

Essentially, the presented qualitative and quantitative results of the lithofacies types, beds, bedsets, high-frequency sequences will stand as a unique input for enhanced-geological modelling and fluid flow simulation, and eventually, critical for a better assessment of Khuff reservoirs of Eastern Arabian gas Fields.

3.2. Introduction

Optimal exploitation of hydrocarbon reservoirs depends on the qualitative as well as quantitative geological characterization of these reservoirs. This includes the identification of architectural and quality elements from core plug to inter-well scale. This up-scaling addresses vertical (often at cm-scale) to lateral (regularly at metre-decametre-scale) correlations. Obviously, this scale cannot be covered based on subsurface data. Outcrop analogues provide valuable insight into understanding ancient sedimentation processes and products (Grammer et al., 2004; Pringle et al., 2006; Catuneanu and Zecchin, 2013; Zecchin and Catuneanu, 2013). Generally, resolution of seismic images has been improved significantly, however, the detailed information concerning the physical attributes of surfaces and sediments packages offered by outcrops and cores is irreplaceable and essential (Catuneanu and Zecchin, 2013; Zecchin and Catuneanu, 2013). Outcrop studies have been utilized widely to understand critical quality and architectural elements within reservoir bodies (Zecchin and Catuneanu 2013; Alnazghah et al., 2013; Grammer et al., 2004; Haase and Aigner, 2013; Smith and Read, 1999; Zeller et al., 2011). Application of sequence stratigraphy covers a wide range of scales, including the global geological record and the controls governing sedimentary processes improving the success of petroleum exploration, development, and production (Catuneanu et al., 2009). Sequence stratigraphy focuses on analysing changes in facies and geometric characteristics of strata and identification of key surfaces to determine the chronological order within a stratigraphic succession (Catuneanu et al., 2009). Furthermore, sequence stratigraphy can be an excellent basis for architectural and facies analysis and interpretation of

paleoenvironmental settings (Embry, 2009). Sequences were recently defined as stratigraphic units related to shoreline shifts, whereas cycles unrelated to shoreline shifts are bedsets (i.e. sedimentological cycles), which are bounded by facies contacts (Catuneanu and Zecchin, 2013; Zecchin and Catuneanu, 2013). Stratal stacking patterns encompass signatures of changes in the depositional trends, including progradation, retrogradation, aggradation, and downcutting (Catuneanu et al., 2009). Each stratal stacking pattern defines a particular genetic type of deposit with a distinct geometry style and facies type (Hunt and Tucker, 1992; Posamentier and Morris, 2000). In addition to the biological evolution, tectonic activities, and paleogeographical position, small sea-level fluctuations critically controls the intra-reservoir sedimentary architectural configuration. The latter encompasses high-resolution sequences and they are mostly triggered by orbital forcing known as Milankovitch cycles. High-resolution sequences stratigraphy tackles scale of observation fall below the resolution of seismic data. This scale is essential in solving issues of reservoir characterization and fluid flow at stages of petroleum production and developments (Zecchin and Catuneanu, 2013). Outcrops provide unique opportunity to observe the physical attributes of various types of sediment bodies and bounding surfaces at these scales and allow the identification of a wider array of surfaces and hence units compared to those recognized at the seismic scale or in boreholes. Time- and depositional-equivalent outcrops are key in characterizing sub-surface carbonate reservoirs. Consequently, integrating outcrop-based high-resolution sequence stratigraphy (addressing the three dimensional geometry of thin sedimentary bodies) and sedimentology (including observations ranging from outcrop to thin-section, such as grain-type, grain-size, sedimentary structures, fossil associations,

nature of specific surfaces, etc.) enhances the understanding of the nature of architectural geobody and provides critical quantitative data that can be used to enhance development and production of subsurface hydrocarbon bearing reservoirs. Therefore, data acquired from outcrop analogues are critical since small scale geometrical variations can be observed and accordingly interpreted with more confidence. For example shoals and tidal channels could have similar sedimentological features such as grain type, fossils content, sedimentary structures such as scour base, however, they can only be differentiated on the basis of their geometry, a shoal complex having a convex upper surface with flat lower surface while a tidal channel is characterized by an erosional and concave lower surface and flat upper surface.

The Khuff reservoirs in Eastern Arabia are estimated to contain about 15 to 30% of the world's gas reserves (Al-Jallal, 1995; Al-Aswad, 1997; Koehrer et al., 2010). These reservoirs are known for having complex heterogeneities at the inter-well scale that is beyond seismic resolution (Janson et al., 2013). Therefore, optimum exploitation of these reservoirs is highly dependent upon understanding internal architectural structure that are controlled by syn-depositional processes and diagenetic overprinting. Outcrop equivalents of these reservoirs in central Saudi Arabia provide an interesting stratigraphic context, where thin bodies can be traced laterally over large distances. The latter can genetically be related to vertical stratal stacking patterns.

The main objective of this paper is to examine the high-resolution stratigraphic framework providing quantitative data on the intra-reservoir stratal stacking patterns and lateral amalgamation of the Upper Khartam Member of the Khuff Formation. This member was described to be equivalent to Khuff A and B reservoirs in Eastern Arabian(Al-Dukhayyil and Al Tawil, 2006). The applied workflow allows for the better understanding of the internal facies patterns and provides a new quantitative analysis of architectural elements of Khuff reservoirs. For this purpose, four outcrop sections were logged in detail from sedimentological and high-resolution sequence stratigraphical point of view. The studied outcrops are located along a lateral distance of about 70 km, and they are mostly road-cuts each of which consists of several faces. The latter have an accumulative total length of about 7 km. They are mostly oriented along dip direction. Along bedding, beds were logged and for each locality, a detailed composite section was established and about 600 samples were collected for further analysis.

3.3. Database and methods

Four outcrop localities were logged in detail from sedimentological and sequence stratigraphical point of view. These outcrops are located in the Buraydah and Faydah quadrangles in central Saudi Arabia (Figure **3.1**). Outcrop 1 is located in central Buraydah Quadrangle on Qassim-Riyadh highway (Figure **3.1**). It is a road-cut with four faces. These faces extend along dip direction over a length of respectively 100, 100, 900, and 900 m. Outcrop 2 is located northeast of Buraydah City on the Qassim-

Hail highway about 28 Km to the north from outcrop 1. This outcrop has 7 faces with accumulative total length of about 3 kilometres extending along dip direction (Figure **3.1**). Outcrop 3 is about 5 Km to the north of outcrop 2 and has three faces with total accumulative length of about 1.5 Km. Outcrop 4 is located in the Al Faydah quadrangle in Jal Al Khartam, about 70 km to the south from the most northern outcrop (outcrop 3). Main faces of this outcrop extend in north eastern direction with a total length of about 400m (Figure **3.1**).

The logs are based on a bed-by-bed field description where bed thickness, bed geometry, nature of stratal stacking patterns, grain type and size, sedimentary structures, surface associations, and geometrical characteristics (e.g., channels, sheet-like bodies) are documented in vertical and lateral direction. Approximately 300 samples were collected for detailed petrographic analysis. Accordingly, lithofacies types are defined and described. Lithofacies abundances and quantities are also calculated, these will assist in describing the reservoir heterogeneities. These are calculated based on the following equations: facies abundance (FA) = ((number of beds of the lithofacies/total beds number)*100), facies quantity (FQ) = ((thickness of beds of the lithofacies /total thickness)*100). Most critically, high-resolution photo-mosaics were constructed of the entire faces of the studied outcrops. The photos were taken using a high resolution camera (20 MP), with a single photo covering a lateral width of about 7 m with 60-70% overlap. During field photography, a constant distance to the outcrop was kept. This approach with the large overlap reduced the distortion of the photo-mosaic and allowed thin beds (at centimetre scale) to be traced laterally (Figure **3.2**). In the established photo-mosaic, about 20000 beds are followed laterally and their stratigraphic patterns and relation with underlying and overlying

strata is examined from sequence stratigraphic point of view. The detailed sedimentological and architectural analyses simplify the paleoenvironmental interpretations, allowing grouping the defined lithofacies types into lithofacies associations. Accordingly, local and regional high-frequency sequence stratigraphic schemes for the Upper Khartam Member are constructed.

3.4. Results

3.4.1. Lithofacies and architectural analysis

Seventeen lithofacies types were identified and will be described below along with their architectural occurrences. The lithofacies are described based of their abundances and a summary of main characteristics is given in Table **3.1**.

3.4.1.1. LFT 1: Coarse-grained oolitic grainstone (FA: 25.8% - FQ: 39.5%)

This lithofacies is light beige to light pinkish in color and ooids are well-sorted and well-rounded. They range in size from 100 to 600 µm. Few quartz grains (less than 5%) occur which are sub-angular, moderately-sorted, and about 250µm in size. Bioclastic fragments include bivalves, gastropods, ostracods, brachiopods, and sparse Earlandia foraminifera. Sedimentary structures include dominance of cross-laminations such as cross-herringbone (**Figure 3.3**A), tidal bundle (**Figure 3.3**B), planar (**Figure 3.3**C), hummocky, sigmoidal, trough-cross laminations, and symmetrical ripples (**Figure 3.3**D). Rib-up mud intraclasts, localized imbrication

structures, and reactivation surfaces also exist. This lithofacies is dominant in the Upper Khartam Member and ranges in thickness from 10 to 300 cm (STD=57.4).

Units of this lithofacies occur predominantly as relatively large channel-like bodies of about 3 m in width and 50 cm thick (example, Figure **3.4**A and B and Figure **3.5**B). Even though, condensed small channel-like bodies of less than 1 m in width and 20 cm in thickness also exist. The channel-like bodies are marked by a highly irregular erosional base incising into the underlying units. Locally the channelized bodies are associated with microbialitic structures. Upper surfaces are mostly flat and uniform. Sheet-like bodies of this lithofacies are also observed; these are ranging in their extension between 5 m to several hundreds of metres. The sheet-like bodies occur in thickening-upward sequences separated by uniform flat surfaces. Localized symmetrical wavy and lenticular geometries are also observed. Internally, marlstones that laterally evolve into stylolites crosscut the lithology.

3.4.1.2. LFT 2: Interlaminated quartz-bearing recrystallized limestone *(FA: 11.2% - FQ: 13%)*

This lithology is light beige to dark pinkish in colour and contains ostracods and Earlandia foraminifera. Quartz grains are angular, well-sorted, and range in size from 5 to 20 µm. Quartz abundance ranges from 15 to 40%. Sedimentary structures include horizontal laminations and cross-laminations (sigmoidal **(Figure 3.3E)**, planar, herringbone). Units of this lithofacies range in thickness from 5 to 100 cm (STD=27.6). This lithofacies occurs in association with the marlstone, and it is

vertically stacked in well-developed thickening-upward sequences where the marlstone presents in the base of the succession.

Units of this lithofacies occur predominantly as sheet-like bodies displaying a lateral extent ranging from 5 to 100 m. The sheet-like bodies are laterally pinching and swelling and they locally possess a patchy geometry. Very locally a complex amalgamation of channel-like bodies was also observed, having an average width and thickness of about 1m and 30cm respectively. Lateral bifurcations by stylolites and localized erosional contacts with the oolitic grainstone lithofacies have been observed.

3.4.1.3. LFT 3: Recrystallized limestone (FA: 7.7% - FQ: 8.9%)

The entire succession of the Upper Khartam is strongly affected by meteoric diagenesis. Nevertheless most lithologies preserved their original texture except the herein described facies which is composed of fine-crystalline limestone (with average crystal size of 30 µm). Bioclastic fragments mostly consist of ostracods with presence of Earlandia foraminifera and localized occurrences of mud-intraclasts. Sedimentary structures dominantly consist of thin-horizontal laminations (**Figure 3.3**F) with rare cross-laminations (e.g., hummocky cross-laminations, and few reactivation surfaces. Cross-laminations less frequently occur in comparison to the interlaminated quartz-bearing recrystallized limestone lithofacies. This lithology ranges in thickness from 5 to 100 cm (STD=29.4). This lithofacies occurs in association with marlstone and laterally merges with mudstone.

This lithofacies occurs as a complex amalgamation of sheet-like bodies. Individual sheets have length ranging from 5 m to several hundreds of metres (Figure **3.4**A and

Figure **3.5**A). The sheet-like bodies are described as horizontal, uniform, and continuous. Local swelling and pinching bodies are observed. Complex amalgamations of channelized bodies are described only in outcrop 4, whereby individual channelized bodies are about 1m in width and 30cm in thickness. Sparse symmetrical wavy geometries also exist, these occur as thin interbeds with marlstone and they are stacked in thickening-upward patterns with lateral extensions of about 5m. Lower surfaces of this lithofacies are sharp and are underlain by marlstone. Laterally these surfaces are irregular and regularly evolve into stylolites. They are locally associated with scouring and erosion. The upper surfaces vary from scoured to flat as well as horizontal, depending on the overlying lithofacies. Units of this lithofacies are intensively crosscut by stylolites.

3.4.1.4. LFT 4: Interlaminated quartz-bearing and fine-grained oolitic grainstone (FA: 2.7% - FQ: 7.1%)

This lithofacies is light beige in colour. Quartz grains are concentrated in laminae of about 500 µm and its contents ranges from 1 to 10%. These grains are angular and well-sorted, and grain sizes vary around 50 µm. Bivalve fragments are present as well as localized occurrence of mud-intraclasts. Ooids are well-rounded and well-sorted with average size of 75µm. Sedimentary structures include horizontal laminations and cross-laminations (sigmoidal, planar, herringbone (**Figure 3.6**A)). The thickness of the beds of this lithology varies from 20 to 300 cm (STD=94.6).

Beds of this lithofacies occur as relatively uniform, flat, horizontal, and continuous sheet-like bodies, ranging in extent from 50 to 150 m. The sheets are stacked in thickening-upward patterns and they are internally crosscut by stylolites and fissile marlstone.

3.4.1.5. LFT 5: Fine-grained oolitic grainstone (FA: 4.6 % - FQ: 5.9 %)

This lithofacies is light beige to pinkish in colour and is composed of pure and homogeneous oolitic grains which are well-sorted and well-rounded, ranging in size from 20 to 100 µm. Sparse bivalve fragments also occur. Sedimentary structures include thin laminations and planar cross- as well as sigmoidal cross-laminations. The thickness of the beds varies from 10 to 80 cm (STD=20.2).

This lithofacies occurs predominantly within thickening-upward sheets; individual sheets are laterally uniform, horizontal, and continuous with local swelling and pinching geometry. The latter are amalgamated over a lateral distance of about 100 m. This lithofacies is intensively crosscut by stylolites and marlstone interlayers.

3.4.1.6. LFT 6: Bioclastic grainstone/packstone (FA: 3.1% - FQ: 4.4%)

This lithofacies possesses a dark pinkish to light beige colour. Bioclasts dominantly consist of bivalves with gastropods and presence of Earlandia foraminifera. The bioclastic components are about 2 mm in size and they have no preferred orientation.

This lithology also contains oolites and quartz grains. Ooids are well-rounded and well-sorted, and range in size from 500 to 200µm. Quartz are angular, well-sorted, and ranging in size from 50 to 100 µm. Sedimentary structures include abundant cross-laminations such as herringbone and trough cross-lamination and sparse thin-lamination (>500 µm). This lithofacies type contains abundant mud-intraclasts displaying an imbricated structure. This lithology has a bed thickness varying between 20 to 80 cm (STD=37.5).

Importantly, this lithofacies first appears in the upper half of the studied interval and geographically exists in outcrop 2 where it occurs in association with bioclastic wackestone/mudstone in thickening-upward sequences. The lithofacies occurs as sheet-like bodies, ranging in length from 50 to 200 m.

3.4.1.7. LFT 7: Marlstone (FA: 20.4% - FQ: 3%)

This lithofacies occurs as thin grayish interbeds, and forms important stratigraphic units. The latter are important units in the sequence stratigraphic interpretations of the Upper Khartam Member. Importantly, it has a high facies abundance of 20.4%. The beds thickness of this lithology ranges from 1 to 10 cm (STD=3.2).

3.4.1.8. LFT 8: Bioclastic wackestone/mudstone (FA: 3.1% - FQ: 2.8%)

This lithology is light beige in colour and contains localized mud-intraclasts. Bioclasts consist dominantly of ostracods. Thin (< 1 mm) laminations are a dominant

sedimentary structure. It occurs as thin interbeds ranging in thickness between 5 to 80 cm (STD=29.8). Beds of this lithofacies possess a wavy symmetrical geometry (**Figure 3.6**B) and form uniform, horizontal, and continuous sheet-like as well as lenticular bodies. These range in their lateral extent from 5 m to several hundreds of metres.

3.4.1.9. LFT 9: Non-fabric preserving dolomite (FA: 3.1% - FQ: 2.4%)

This lithology is sometimes reddish, greenish, yellowish, or beige in colour. The dolomite crystals range in their size from 30 to 100 µm. Sedimentary structures includes large imbrication structures (**Figure 3.6**C) as well as horizontal and planar cross-laminations. This lithofacies is restricted to the upper part of the studied interval in outcrop 2. Its thickness ranges from 20 to 50 cm (STD=12.5).

Units of this lithofacies occur as sheet-like bodies with uniform, flat, horizontal, and continuous geometry. Individual sheets range in length from 5 m to several hundreds of metres. The sheets are stacked in thickening-upward patterns.

3.4.1.10. LFT 10: Calcareous sandstone (FA: 3.8% - FQ: 4.2%)

This lithofacies is reddish in colour, and contains a quantity of spicule-like bioclasts and bivalves (5%) as well as mud-intraclasts. It is intensively bioturbated. The quartz grains are angular, well-sorted, and range in size from 75 to 250 µm. Sedimentary structures dominantly consist of thin laminations to fenestral, lenticular, and crinkled

laminations with rare cross-laminations. This lithofacies is present in the lower part near the boundary between the Upper and Lower Khartam Member. Its thickness ranges from 5 to 25 cm (STD=9.1).

3.4.1.11. LFT 11: Microbialites build-ups (FA: 1.5% - FQ: 2.1%)

This lithology is reddish to pinkish in colour and contains ooid grains (up to 20%) and scattered quartz grains as well as bioclastic fragments. The microbialite accumulations have a lateral separation distance of 15m, and they range in size from 20 to 300cm. The domal stromatolites and thrombolitic heads (Figure **3.4** and **Figure 3.6**D) range in height from 20 to 90 cm (STD=39.0).

Importantly, this lithofacies occurs in association with the channelized coarse-grained oolitic grainstone (LFT 1).

3.4.1.12. LFT 12: Oolitic grainstone/grapestone (FA: 0.4% - FQ: 2.1%)

It contains a quantity of large bioclasts grains (occurring as elongated molds of 2 mm in size and making up less than 5% of the lithology). Oolitic grains are well-rounded, moderately sorted, and ranging in size from 1000 to 500µm. Sedimentary structures includes high-angle cross-lamination (**Figure 3.6**E) and imbricated accumulations of mud intraclasts. This lithofacies has been recognised only from a single stratigraphic position in outcrop 2 and 3 where it has a thickness of 174 cm. Units of this lithofacies occur as convex bodies associated with stromatolitic and thrombolitic microbialites.

The channel-like bodies are incising into the underlying units and are internally crosscut by stylolites.

3.4.1.13. LFT 13: Mudstone (FA: 3.5% - FQ: 1.6%)

This lithofacies is beige to yellow in colour and sometimes contains anhydrite crystals. Sedimentary structures dominantly consist of thin (average 500µm) laminations with localized imbrication structures. Its bed thicknesses ranging from 150 to 5 cm (STD= 10.5).

This lithofacies occurs as thin interbeds of sheet-like bodies have lateral extent ranges from 100 to 20m. The sheets are flat, uniform, and continuous.

3.4.1.14. LFT 14: Peloidal grainstone/packstone (FA: 1.5% - FQ: 1.4%)

This lithology is light beige to yellowish in colour. It contains a number of mud-intraclasts, ranging in size from 1 to 2 mm, and it is associated by mud-lenses. Localized concentrations of bioclast fragments, mostly bivalves occur. Sedimentary structures include horizontal to lenticular and crinkled laminations (**Figure 3.6**F). This lithology ranges in thickness from 40 to 20 cm (STD=8.1).

Beds of this lithofacies occur as laterally uniform, horizontal, and continuous sheet-like bodies ranging in length from 200 to 5 m. These bodies are stacked in thickening-upward successions which locally are swelling and pinching out. Lenticular geometries are also observed which are laterally merging and bifurcating. Depending

on their stratigraphic positions, this lithofacies locally displays wavy basal surfaces and erosional features.

3.4.1.15. LFT 15: Skolithos bioclastic oolitic grainstone (FA: 0.4% - FQ: 0.3%)

This lithofacies is red in colour and is intensively bioturbated. It contains a quantity of skolithos, bioclastic fragments, and mud-intraclasts. Existing ooids are poorly-sorted. Sedimentary structures include thin laminations and cross-laminations. This lithofacies is present in one stratigraphic level in outcrop 3, where it has a thickness of 70 cm. Here it occurs in association with domal stromatolites at the top.

3.4.1.16. LFT 16: Gypsum and gypsiferous claystone (FA: 3.5% - FQ: 0.5%)

This lithofacies, which likely has a diagenetic origin, occurs as clean fibrous gypsum. It possibly originally consisted of gypsiferous claystone. It occurs at the top of the studied interval and is only presents in outcrop 2 and 3.

3.4.1.17. LFT 17: Thin-walled bivalve rudstone (FA: 0.8% - FQ: 0.5%)

This lithofacies is pinkish to reddish in colour and it consists predominantly of *placunopsis ostracina* bivalve with sparse ostracods. This lithofacies is similar to that

of the Middle Triassic Muschelkalk sequence of Central and Western Europe. The *placunopsis ostracina* is about 2 mm in size and these fossils are horizontally oriented parallel to bedding. This lithofacies also contains mud-intraclasts. Sedimentary structures consist of crinkled to fenestral laminations. This facies occurs in three stratigraphic positions in the topmost part of outcrop 2, near the boundary between the Khuff and Sudair Formation. Average bed thickness is 20 cm. The latter display a complex convex geometry.

3.4.2. Lithofacies associations

The Khuff carbonates were deposited on a gently sloping homoclinal ramp (Al-Jallal, 1995; Sharland et al., 2001), similar to the modern day Arabian Gulf (Purser, 1973) or Shark Bay (Logan et al., 1974). Based on the sedimentological and architectural analysis (e.g., cross-laminated coarse-grained oolitic grainstone with herringbone structures occurring as channelized bodies incising into the underlying strata are obviously intertidal channels), a paleoenvironmental interpretation is proposed. The defined lithofacies types are arranged into seven environmental settings, i.e. shoal ridge, intertidal channels, intertidal flats, bivalve reef complex, supratidal settings, subtidal settings, and outer ramp settings. The latter will subsequently be described below and illustrated in figure 8.

3.4.2.1. Shoal ridges

The high-angle cross-laminated coarse-grained oolitic grainstone/grapestone make up some shoal deposits, this lithofacies makes up convex bodies, and therefore, the lithofacies characteristics, architectural configuration, and stratigraphic association

(associated with the microbialites lithofacies and intertidal channels) are indicative for shoal settings. The overall architectural configuration of the Upper Khartam Member is predominantly composed of thin intertidal and subtidal sheet-shaped bodies that amalgamated forming a complex pattern with intertidal channels. This nature points to a gently sloping homoclinal ramp with rare occurrences of shoal ridges and hence lagoonal back-shoal. This is likely controlled by auto- and allogenic processes such as sediment productivity (which is considered to be relatively low as inferred from the thin interbedded nature of the strata) and sea-level fluctuations (with agitated tidal currents inferred from the abundancy of erosional surfaces).

3.4.2.2. Intertidal channels

The intertidal channels have two anatomies, i.e. small tidal creeks (1m in width by 30cm in height) and large tidal (based on the abundancy of herringbone structures) channels (3m in width by 50cm in height). The coarse-grained oolitic grainstone lithofacies (LFT 1) makes up the intertidal channels. This interpretation is based on the lithofacies characteristics and very critically on the architectural configuration of this lithofacies, where it occurs predominantly as relatively large channelized bodies incising into the underlying intertidal and subtidal successions. The intertidal creeks include the interlaminated quartz-bearing recrystallized limestone (LFT 2) and the recrystallized limestone (LFT 3). The latter lithofacies types occur as complex amalgamations of small channelized bodies, and accordingly they are interpreted as intertidal creeks that developed in the intertidal zone and likely associated with the channels.

3.4.2.3. Intertidal flats

Intertidal flats occur as sheet-like bodies ranging in their length from 5 to several hundreds of metres and having an average thickness of about 20 cm. The dominant sedimentary structure consists of herringbone cross-laminations indicating bidirectional tidal current activity, and accordingly, most of the grainy lithofacies types of the Upper Khartam Member (i.e. LFT 1, 2, 3, 4, 5, 6, and 14) have been deposited in intertidal settings. This environment occurs in association with the intertidal creeks, intertidal channels, and subtidal environments.

3.4.2.4. Bivalve reef complex

The bivalve reef complex appears in three intervals in the upper part of the Upper Khartam. It is composed of the thin-walled bivalve rudstone, with mostly *Placunopsis Ostracina* (LFT 17). The bioclastic fragments are horizontally oriented indicating autochthonous sedimentation and in-life position as intertidal reef complex.

3.4.2.5. Supratidal settings

The marlstone lithofacies (LFT 7) as very characteristic lithofacies type reflecting low-energy deposition likely formed in supratidal settings. The lithofacies associations (dominated by shallow water intertidal settings occurring as intertidal flats and channels) of the LFT 7 may support the supratidal origin of this lithofacies. This interpretation has significance in the sequence interpretation.

3.4.2.6. Subtidal settings

The relatively long sheet-like bodies and fine-grained lithofacies (in comparison to the intertidal flats), typified by hummocky to sigmoidal cross-laminations are interpreted to be deposited in a subtidal setting. The lithofacies characterising this setting consist of the recrystallized limestone (LFT 3), fine-grained oolitic grainstone (LFT 5), and the peloidal grainstone/packstone (LFT 14).

3.4.2.7. Outer ramp settings

Two lithofacies types make up the outer ramp environment. These include the bioclastic wackestone/mudstone (LFT 8) and the mudstone (LFT 13). These lithofacies are dominated by thin laminations, indicating deposition from suspension in a calm environmental setting below fair weather wave-base.

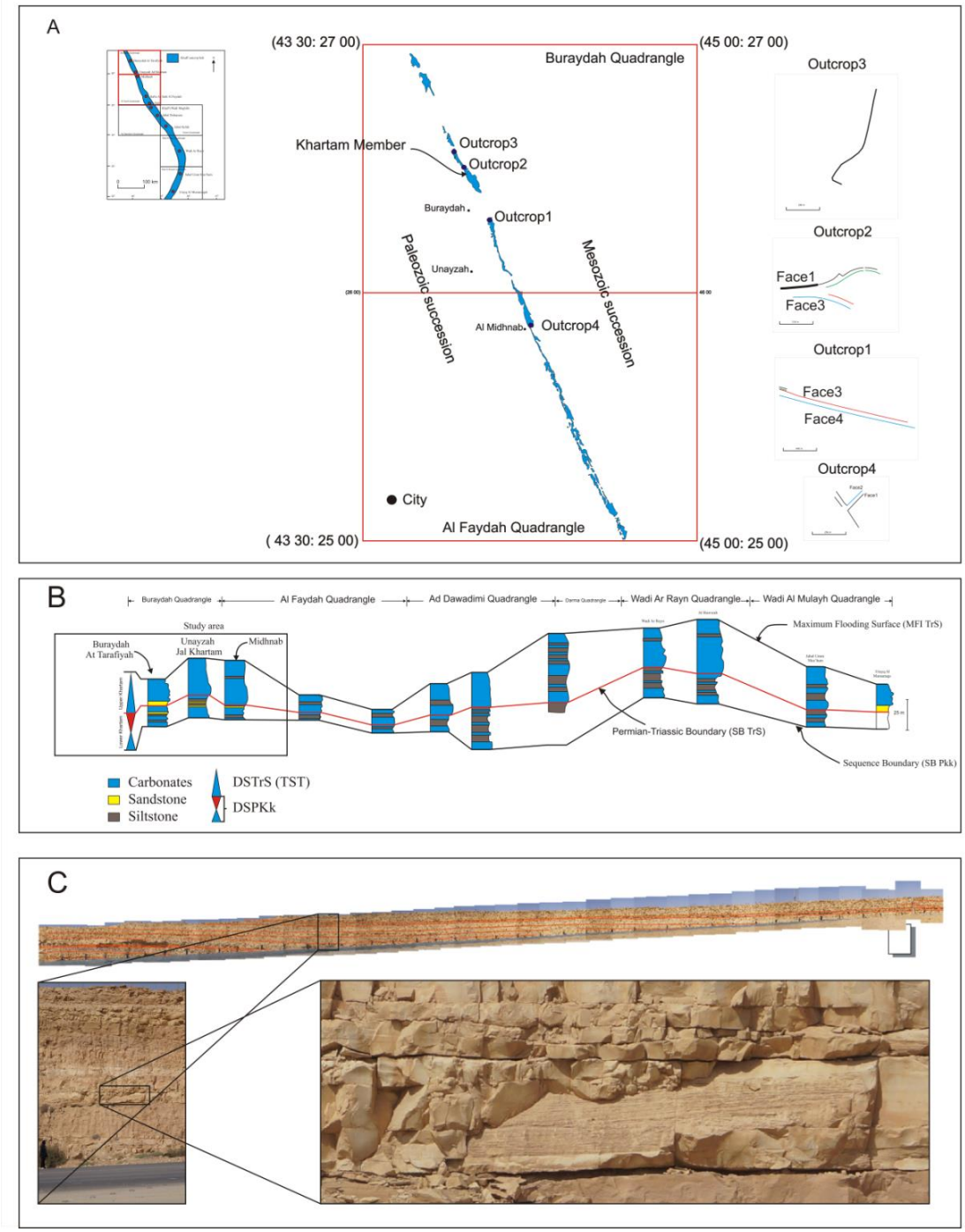

Figure 3.1. A) The Khuff Formation outcrop in central Saudi Arabia and the Khartam Member belt in the Buraydah and Al Faydah quadrangles (red rectangular), three outcrops are located in the Buraydah quadrangle while outcrop 4 is located in the Al Faydah quadrangle (modified after Manivit et al., 1985b; Vaslet et al., 1985, 2005), B) Regional correlation and variations in facies and stratal thicknesses of the Upper Khartam Member (modified after Vaslet et al., 2005), C) Example of studied road-cuts from outcrop 2 (note the location of the photomosaic in A (bold black) and the different zoom in levels.

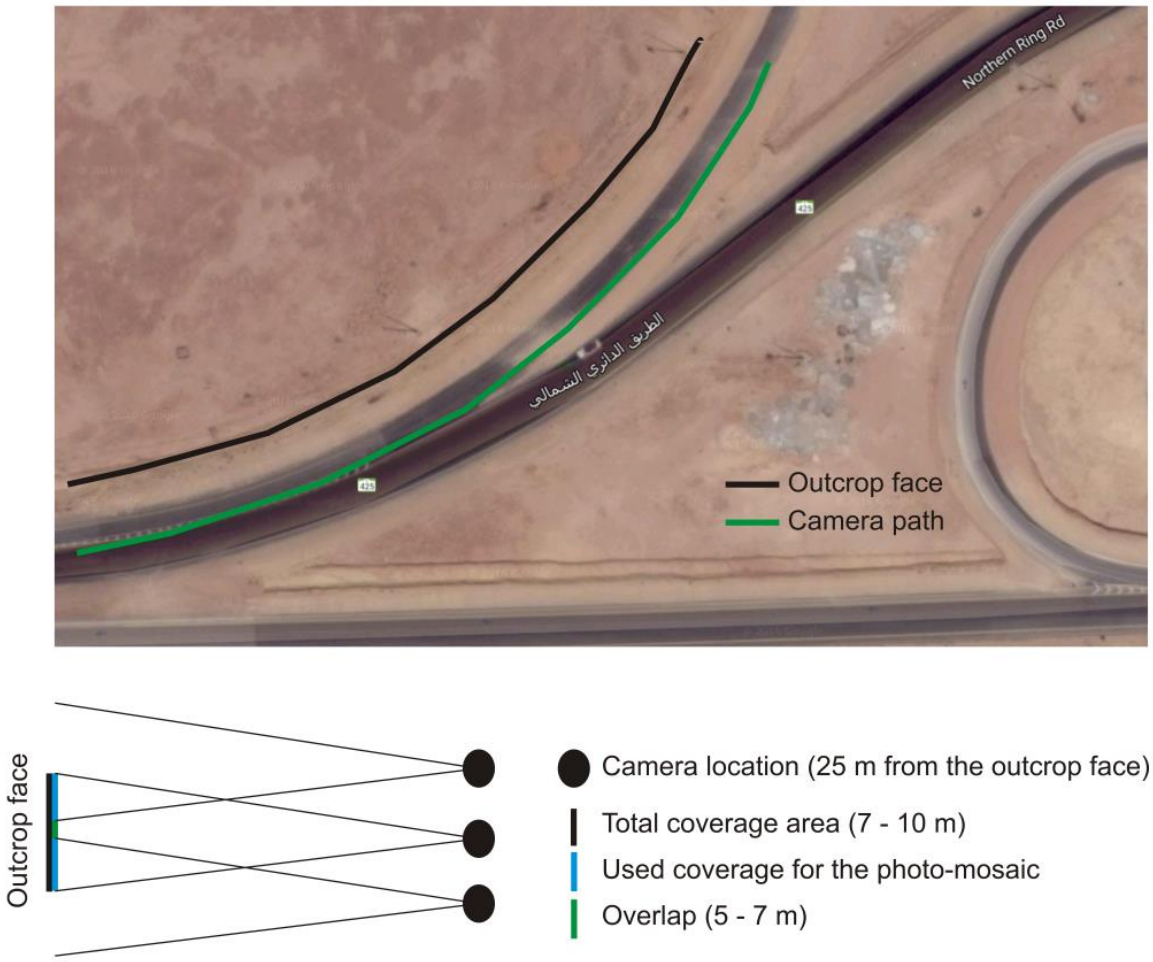

Figure 3.2. The field photograph strategy, to avoid photo distortion and to acquire high resolution images, a high resolution camera (21 MP) was used with photos taken with large overlapping area (60-70%) and close and constant distance to the outcrop faces (about 25 m).

Table 3.1. Summary of the Upper Khartam lithofacies and their deduced environmental settings. Abbreviations: Max, Min, and Average (maximum, minimum, and average thickness measured) and STD (standard deviations of the thickness measurements).

Lithofacies type	**Colours and components**	**Sedimentary structures**	**Facies abundances (FA) and quantities (FQ)**	**Vertical trend**	**Architectural description**	**Depositional environment**
LFT 1: Coarse-grained oolitic grainstone	Light beige and light pinkish, ooids are well-sorted and well-rounded, range in size from 100 to 600 µm, few quartz grains, they are sub-angular, moderate-sorted, and about 250µm in size, bioclastic fragments include bivalves, gastropods, ostracods, brachiopods, and sparse of Earlandia foraminifera	Dominance of cross-laminations such as cross-planar, hummocky, herringbone, sigmoidal, tidal bundle, trough-cross laminations, and symmetrical ripples. Mud intraclasts, localized quantities of imbricating structures	FA:25.8%; FQ:39.5% Max:270cm; Min:5cm, Average:49cm; STD:57.4cm	Thickening-upward trends	1. Predominantly as channel-like bodies of about 3 m width and 50 cm thick 2. Sheet-like bodies, lateral extent vary between 5 m to several hundreds of metres	1. Intertidal channels 2. Intertidal flats
LFT 2: Interlaminated quartz-bearing recrystallized limestone	Light beige to dark pinkish, contains ostracods and Earlandia foraminifera, quartz grains are angular, well-sorted, and range in size from 5 to 20 µm. Their abundance ranges from 15 to 40%, marlstone	Horizontal laminations and cross-laminations (planar, sigmoidal, herringbone)	FA:12.4% ; FQ:13.8% Max:100cm ; Min:4cm ; Average: 37.7cm; STD:27.6cm	well-developed thickening-upward patterns	1. Sheet-like bodies, length ranges from 5 to 100m 2. Sparse of channel-like bodies, width 1m, thickness 20cm	1. Intertidal flats 2. Intertidal creeks
LFT 3: Recrystallized limestone	Beige colour, fine-crystals of limestone (average crystal size is 30 µm), localized occurrences of mud-intraclasts, mostly ostracods with presence of Earlandia foraminifera, marlstone and laterally merges with mudstone	Dominantly thin-horizontal laminations with rare cross-laminations and minor reactivation surfaces	FA:7.7% ; FQ:8.9% Max:110cm ; Min:5cm ; Average: 38.2cm; STD:29.4cm	Well-developed thickening-upward pattern	1. Sheet-like bodies (length 5-100s m), symmetrical wavy geometry 2. Channelized-bodies (15cm thick, 20cm width)	1. Intertidal/subtidal flats 2. Intertidal creeks
LFT4 : Interlaminated quartz-bearing and fine-grained oolitic grainstone	Light beige in colour, quartz grains occur as lamination and ranges in contents from 1 to 10%, they are angular and well-sorted, and their grain sizes varies around 50 µm, bivalve fragments, localized occurrence of mud-intraclasts, ooids are well-rounded and well-sorted with average grain size of 100µm	Horizontal laminations and cross-laminations (sigmoidal to planar)	FA:2.7% ; FQ:7.1% Max:290cm ; Min:18cm ; Average:85.6cm; STD:94.6cm	Stacked in thickening-upward patterns	Relatively uniform, flat, horizontal, and continuous sheet-like bodies, range in their extent from 50 m to 150 m	Intertidal to subtidal flats
LFT 5: Fine-grained oolitic grainstone	Light beige to pinkish in colour, pure and homogeneous oolitic grains which are well-sorted and well-rounded, and range in size from 20 to 100 µm, sparse bivalve fragments	Thin laminations and planar cross- and sigmoidal cross-laminations	FA:4.6% ; FQ:5.9% Max:80cm ; Min:11cm ; Average:41.6cm; STD:20.2cm	thickening-upward patterns	Laterally uniform, horizontal, and continuous sheet-like bodies, local swelling and pinching geometry, lateral amalgamation distance of about 100 m	Intertidal to subtidal flats

LFT6: Bioclastic grainstone/packstone	Dark pinkish to light beige in colour, bioclasts dominantly bivalves with gastropods (2 mm in size) and single presences of Earlandia foraminifera and they have no defined orientation, contains oolitic and quartz grains, ooids are well-rounded and well-sorted, and range in size from 500-200µm, occurs in association with gypsiferous claystone	Abundant of cross-laminations such as herringbone and trough cross-lamination and abundant of mud-intraclast and imbricates and sparse of thin laminations	FA:3.1% ; FQ:4.4% Max:120cm ; Min:12cm ; Average: 52.7cm; STD:37.5cm	thickening-upward patterns	Sheet-like bodies, ranges in length from 50 m to 200 m	Intertidal to subtidal flats
LFT 7: Marlstone	Thin grayish interbeds, important stratigraphic units and has significances in the sequence stratigraphic interpretations since it interbeds with the carbonates of the Upper Khartam Member	Thin-laminations	FA:20.4%; FQ:3.0% Max:20cm; Min:1cm; Average:3.5cm; STD:3.2cm	Stacked in a coarsening-upward patterns with the carbonates	Thin-sheets interbeds with the carbonates all-over the studied interval	Supratidal settings
LFT8: Bioclastic wackestone/mudstone	Light beige in colour, localized mud-intraclasts, and bioclastic grains are ostracods	Dominated by thin laminations	FA:3.1% ; FQ:2.8% Max:83cm ; Min:4cm ; Average:29.9cm; STD:29.8cm	Coarsening-upward	Wavy symmetrical geometry and uniform, horizontal, and continuous sheet-like and lenticular bodies, range in their extent from 5 m to several hundreds of metre	Outer-ramp
LFT 9: Non-fabric preserved dolomite	Reddish, greenish, yellowish, and beige in colour, dolomite crystals range in their size from 30 to 100 µm	Large imbricated structures and horizontal and planar cross-laminations	FA:3.1% ; FQ:2.4% Max:44cm ; Min:8cm ; Average:25.4cm; STD:12.5cm	Stacked in thickening-upward patterns.	Sheet-like bodies of uniform, flat, horizontal, and continuous geometry, ranges in length from 5 m to several hundreds of metres	Intertidal to subtidal setting
LFT 10: Calcareous sandstone	Reddish to grayish and yellowish, quartz grains are angular, moderately sorted, and range in size from 75 to 250 µm, locally contains mud-intraclasts, undefined bioclasts (up to 10%), reddish/grayish claystone, quartzwacke, and quartz arenite	Dominantly thin laminations to fenestral, lenticular, and crinkled laminations with rare cross-lamination, Intensive bioturbation	FA:5.3% ; FQ:2.7% Max:41cm ; Min:10cm ; Average:22.1cm; STD:9.1cm	Coarsening-upward patterns	Sheet-like bodies	Intertidal to subtidal settings
LFT 11: Microbialites build-ups	Reddish to pinkish in colour, contains ooids grains (up to 20%) and scattered quartz grains and bioclastic fragments, occurs in association with thickening- and coarsening-upward strata of marlstone and bioclastic and oolitic grainstone	Crinkled laminations (microbialites films)	FA:1.5% ; FQ:2.1% Max:90cm ; Min:5cm ; Average:44.5cm; STD:39cm		The microbialitic heads have a lateral separation distance of 15m, and they range in size from 300 to 20 cm	Intertidal flats
LFT 12: Oolitic grainstone/grapestone	Beige colour, oolitic grains are well-rounded, moderately sorted, and range in size from 500-1000µm, quantity of bioclasts grains, occurs in association with the microbialite build-ups and mudstone and channel-like bodies	High-angle cross-lamination and imbricates of mud intraclasts, s. It is contains a quantity of bioclasts grains	FA:0.4%; FQ:2.1%		Convex geometry	Shoal ridges
LFT 13: Mudstone	Beige to yellow in colour and sometimes contains anhydrite crystals	Dominantly thin lamination and localized imbricates	FA:3.5% ; FQ:1.6% Max:30cm ; Min:5cm ; Average:14.8cm; STD:10.5cm	Thin-interbeds	Flat, uniform, and continuous sheet-like bodies range in from 20 m to 100 m	Outer-ramp
LFT 14: Peloidal grainstone/packstone	Light beige to yellowish in colour, quantity of mud-intraclasts, range in size from 1 to 2 mm, localized concentrations of bioclast fragments, mostly bivalves	horizontal to lenticular laminations	FA:1.5% ; FQ:1.4% Max:37cm ; Min:20cm ; Average:29.3cm; STD:8.1cm	Thickening-upward patterns	Uniform, horizontal, and continuous sheet-like bodies range in length from 5 to 200 m	Subtidal settings
LFT 15: Skolithos bioclastic oolitic grainstone	Red in colour, bioclastic fragments, and mud-intraclasts, ooids are poorly-sorted, domal stromatolites	Intensively bioturbated and contains a quantity of skolithos, thin laminations	FA:0.4% FQ:0.8%		Limited lateral exposure, horizontal sheet-like bodies	Intertidal flats

		and cross-laminations				
LFT 16: Gypsiferous claystone	Clean white fibrous gypsum, occurs in associations with the marlstone		FA:3.5% ; FQ:0.5% Max:5cm ; Min:2cm ; Average:4.7cm; STD:1cm		Thin-seems	Supratidal flats
LFT 17: Thin-walled bivalval rudstone	Pinkish to reddish in colour, consists predominantly of thin-walled bivalves with ostracods (2 mm size), these are horizontally oriented indicating in-place deposition, mud-intraclasts	Crinkled to fenestrally laminations.	FA:0.8% ; FQ:0.5% Max:28cm ; Min:10cm ; Average:19cm; STD:12.7cm		Occurs as sheet-like bodies range in length from 5 m to several hundreds of metres	Intertidal reef complex

Figure 3.3. Photographs of the sedimentary structures observed in the field. (A) herringbone cross-laminations of the coarse-grained oolitic grainstone (LFT 1), (B) tidal bundle of the coarse-grained oolitic grainstone lithofacies (LFT 1), (C) planar cross-lamination of the coarse-grained oolitic grainstone with stylolite (LFT 1), (D) symmetrical wavy ripples, interbedded coarse-grained oolitic grainstone (LFT 1) and marlstone (LFT 7), (E) hummocky cross-laminations of the interlaminated quartz and recrystallized limestone (LFT 2), (D) horizontal thin laminations of the recrystallized limestone (LFT 3).

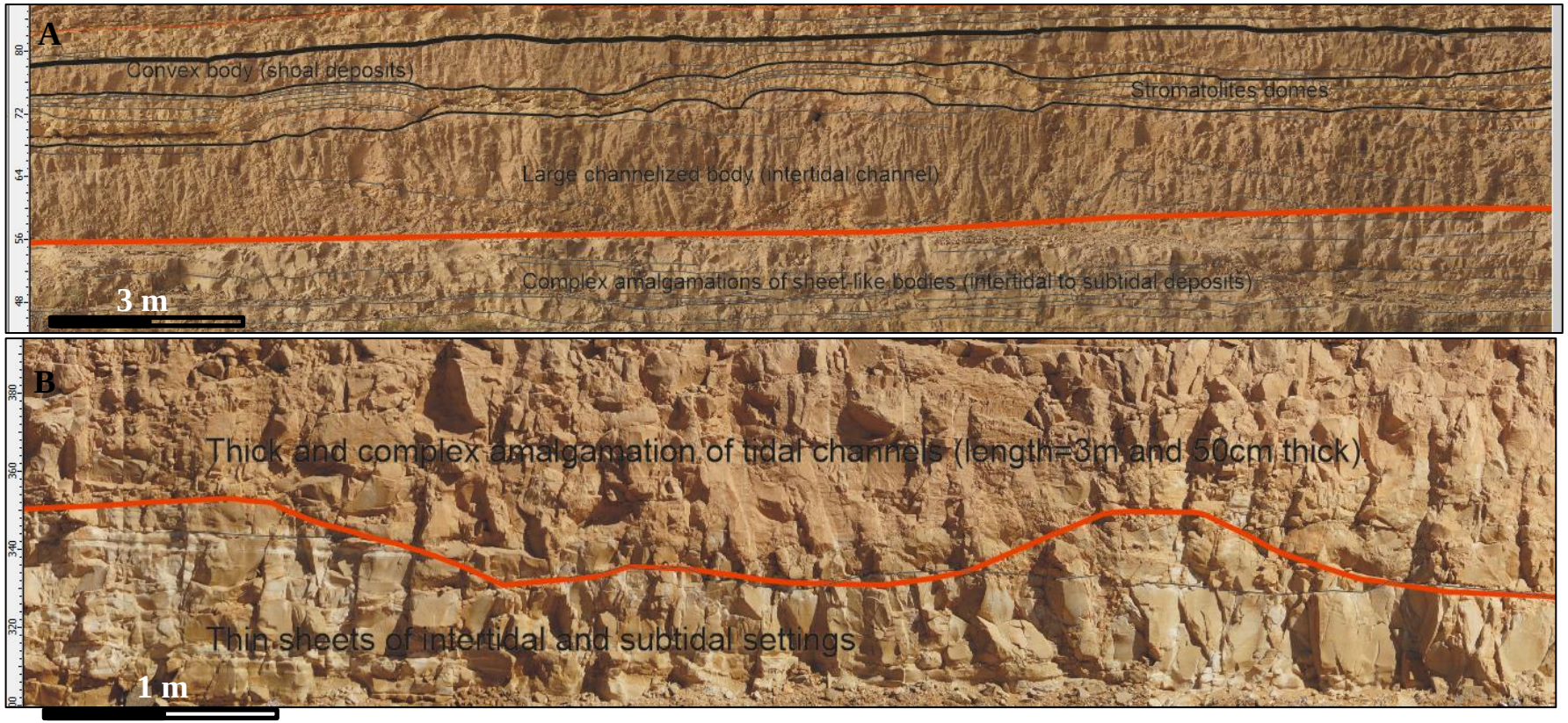

Figure 3.4. Photographs of field-scale features, (A) photograph from outcrop 2, succession of large amalgamated intertidal channels consisting of coarse-grained oolitic grainstone (LFT 1) incising into sheet-like intertidal and subtidal deposits (recrystallized limestone; LFT 3) and overlain by stromatolites domes (microbialites; LFT 11) and capped by convex body of shoal deposits (oolitic grainstone/grapestone; LFT 12), note red lines are erosional surfaces, black lines are lithofacies boundaries, (B) photograph from outcrop 1, intertidal channel (coarse-grained oolitic grainstone; LFT 1) incising into intertidal and subtidal deposits (recrystallized limestone; LFT 3).

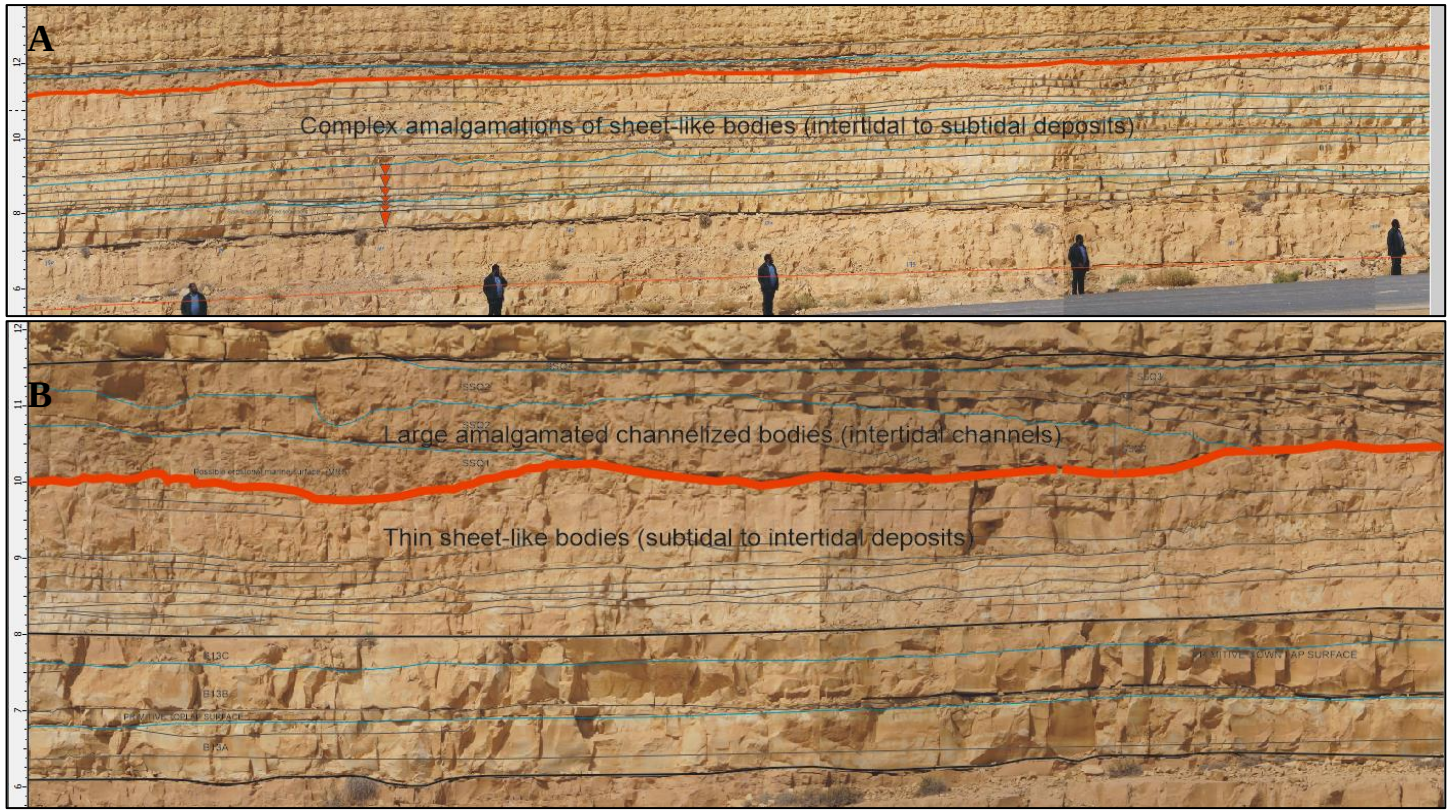

Figure 3.5. Photomosaic from field-scale features (outcrop 2), (A) complex amalgamations of thin (10 – 30 cm thick) and laterally continuous (50 – 300 m in length) sheet-like bodies, consisting of recrystallized limestone (LFT 3) and coarse-grained oolitic grainstone (LFT 1). These are interpreted as intertidal to subtidal deposits, (B) amalgamated intertidal channels (coarse-grained oolitic grainstone (LFT 1); channelized bodies) incised into the intertidal and subtidal sheets (LFT 3 and 5). Red lines are erosional surfaces.

Figure 3.6. Photographs of the sedimentary structures observed in the field. (A) herringbone cross-laminations of interlaminated quartz-bearing fine-grained oolitic grainstone (LFT 4), (B) symmetrical wavy ripples of the interbedded bioclastic wackestone/mudstone (LFT 8), (C) imbrications of the non-fabric preserved dolomite (LFT 9), (D) thrombolitic head (LFT 11) (E) high-angle cross-laminated oolitic grainstone/grapestone (LFT 12), (F) crinkled laminations of the peloidal grainstone/packstone (LFT 14).

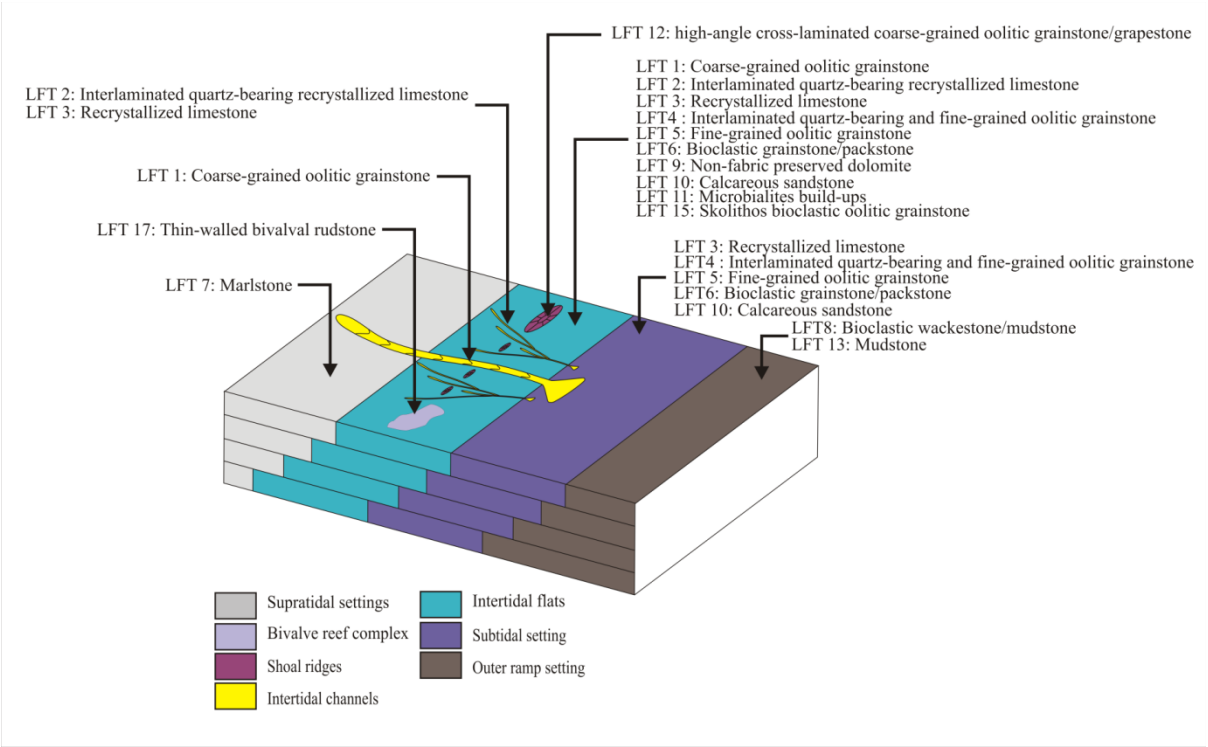

Figure 3.7. Environmental settings of the Upper Khartam Member, these are dominated by prograding intertidal-subtidal flats and important occurrences of intertidal channels and shoal ridges.

3.4.3. Stratigraphic analysis

The stratigraphic succession of the Upper Khartam Member is composed of about 20,000 beds. These are traced laterally in the studied outcrops and they are ranging in thickness from 5 to 40 cm and extend laterally between 5 and 300 m. Following Zecchin and Catuneanu (2013) and the earlier definitions of Van Wagoner et al (1990), these beds are stacked to form about fourteen bedsets. The latter are likely related to sediment supply and accommodation space and slight changes in sea-levels (mostly linked to tidal actions). The bedsets are range in thickness from 1 to 5 m and they are traceable laterally over 1000 m. Outcrop 2 is taken as the reference outcrop where the complete stratigraphic succession of the Upper Khartam is preserved. The bedsets will be subsequently described from bottom to top and illustrated in Figure **3.8** to 3.17.

3.4.3.1. Bedset 1 (BS 1)

This bedset is 20 cm thick and sharply overlays a regionally extended reddish/grayish claystone. The latter is representing the Permian-Triassic boundary. This bedset is predominantly composed of calcareous sandstone (LFT 10) containing localized concentrations of bivalve fragments. The skeletal accumulation could be similar to the condensed Onlap Skeletal Beds (OSBs) of Kidwell (1991) and Zecchin and Catuneanu (2013). Accordingly, the base of this bedset is defined as a major flooding surface (Flooding Surface-S1, FS-S1). Of course, the vertical abrupt change in the lithology (from thick reddish/grayish claystone to thick carbonate) is a strong indicative of the flooding event. The FS-S1 is most likely representing the maximum flooding interval

of the Triassic depositional sequence (DS TrS) of Vaslet et al., 2005. This surface is taken as a datum for the regional correlation.

3.4.3.2. Bedset 2 (BS 2)

This bedset is 50 cm thick and predominantly composed of coarse-grained oolitic grainstone (LFT 1) with the prominent herringbone cross-laminations. The bedset is capped by thin bed of marlstone (LFT 7: about 2 cm thick). Beds of this bedset occur as uniform and horizontal bodies with irregular top and bottom. Accordingly, this bedset is deposited in tidally agitated settings most likely intertidal flats.

3.4.3.3. Bedset 3 (BS 3)

This bedset is about 50 cm thick and composed of coarse-grained oolitic grainstone (LFT 1) and thin interbeds of marlstone (LFT 7: 2 cm). Sigmoidal and wavy cross-lamination and mud-intraclasts are the prominent sedimentary structures observed in this bedset. Beds of this unit are laterally bifurcating, swelling, and pinching.

3.4.3.4. Bedset 4 (BS 4)

This bedset is about 300 cm thick and is composed of a complex amalgamation of landward-stepping (retrograding) and backward-stepping (prograding) beds with thickening-upward patterns. The retrograding beds are thin (10 cm) and located at the bottom of this bedset. They locally are eroded by the overlying prograding sheets. The bedset is composed from bottom to top: bioclastic grainstone/packstone lithofacies (LFT 6), interlaminated quartz-bearing recrystallized limestone (LFT 2), recrystallized

limestone (LFT 3), and fine-grained oolitic grainstone (LFT 5) and coarse-grained oolitic grainstone (LFT 1). Likewise, the succession has intercalations of marlstone (LFT 7). The bedset is deposited in an intertidal flat. The basal interval of this bedset represented by LFT 6 is interpreted as a lag deposits and accordingly a ravinement surface is placed at the base of this bedset (Ravinement Surface-Surface 3, RS-S2). The LFT 6 is likely similar to the condensed Onlap Skeletal Beds (OSBs) of Kidwell (1990) and Zecchin and Catuneanu (2013). This bedset represents a gradual shallowing-upward within the intertidal setting as indicated by the change from interlaminated quartz-bearing limestone (LFT 2) to a thick stack of homogeneous oolitic grainstone (LFT 1 and 5).

3.4.3.5. Bedset 5 (BS 5)

This bedset has a total thickness of about 250 cm and extends laterally for about 250 m before becoming covered; it is bounded at its base by an erosional surface. This surface is incising into the underlying succession of BS 4. The bedset is predominately composed of stacks of condensed and small intertidal channels (about 1 m in width and 30 cm in thickness). These are regionally recognizable and predominantly consist of coarse-grained oolitic grainstone (LFT 1). The bedset is bounded at the top by a regionally extended fissile marlstone (LFT 7) deposited in a supratidal setting.

3.4.3.6. Bedset 6 (BS 6)

This bedset has a total thickness of 213 cm and is composed of about three thickening-upward units and three lithofacies types. The latter consist from bottom to top of

recrystallized limestone (LFT 3), fine-grained oolitic grainstone (LFT 5) and three thin beds (5 cm) of fissile marlstone (LFT 7). The lithofacies are developing thin (about 20 cm), flat, and uniform prograding beds. In comparison with the underlying bedset, this bedset reflects deposition in a relatively quiet intertidal environment during a period of marine transgression. This is inferred from the dominant lithofacies type (LFT 3) and is also supported by the presence of mud-intraclasts at the bottom indicating pulses of reworking. Accordingly, a flooding surface (Flooding Surface-S3, FS-S3) is placed between BS 5 and BS 6.

3.4.3.7. Bedset 7 (BS 7)

This bedset has a total thickness of about 370 cm. The bedset is continuous and has a uniform thickness with complex internal amalgamation and stacking patterns. Generally, the internal architectural makeup is similar to the BS 6; however, LFT 2 in this bedset is sparse. This is interpreted to reflect a gradual shallowing-upward trend from BS 6 towards BS 7. The complex amalgamations are possibly controlled by the nature of tide, most likely, related to a highly agitated tidal action inferred from the dominant cross-laminated sedimentary structures (mostly herringbone-cross laminations). The bedset is deeply incised by overlying intertidal channels.

3.4.3.8. Bedset 8 (BS 8)

This bedset has a total thickness of about 450 cm. The composite section of this bedset is from bottom to top composed of thin symmetrically wavy interbeds consisting of marlstone (LFT 7) alternating with coarse-grained oolitic grainstone (LFT 1), likely

deposited during supratidal and intertidal flats development respectively. They are locally incised by thick intertidal channels consisting predominately of coarse-grained oolitic grainstone (LFT 1). The latter is overlain by regionally extended microbialites (LFT 11: stromatolite domes and thrombolitic heads), which are capped by high-angle cross-laminated oolitic grainstone/grapestone (LFT 12) deposited as shoal ridges. Individual intertidal sheets have a lateral extension of about 100 m and a vertical thickness of about 20 cm. They are laterally pinching and swelling beds and they are associated by intertidal channels (maximum thickness of 30 cm and width of 5m). The microbialites occur in outcrops 2 and 3.

3.4.3.9. Bedset 9 (B 9)

This bedset has a total thickness of 356 cm. The basal succession consists of thinly (5 cm thick) interbedded bioclastic mudstone/wackestone (LFT 6). These occur as wavy symmetrical, lenticular, and swelling sheets (5 m in length) displaying a prograding succession with pinch-out geometry in basin-ward direction. This interval was deposited in an outer ramp setting during a period of major flooding event overlying the shoal ridge of BS 8. And accordingly a flooding surface (Flooding Surface-S4, FS-S4) is positioned between BS8 and BS9. This interpretation is supported by the abundancy of reworked material such as mud-intraclasts and localized accumulation of skeletal fragments on the top of the BS 8. Although they are thin, the basal beds (LFT 8) are traceable along an exposure of 2 km in outcrop 2. This succession is overlain by complex amalgamations of prograding intertidal sheets of coarse-grained

oolitic grainstone (LFT 1). The latter occur as relatively thick sheets of about 20 cm and about 100 m length. The LFT 13 is thinning-upward.

3.4.3.10. Bedset 10 (BS 10)

This bedset is 414 cm thick and consists predominantly of coarse-grained oolitic grainstone (LFT 1) interbedded with mudstone (LFT 13), bioclastic wackestone/mudstone (LFT 8), bioclastic grainstone/packstone (LFT 6), and peloidal grainstone/packstone (LFT 14). The lower stratigraphy of this bedset is composed of interbedded mudstone and grainstone. and extending for about 100 m laterally, this is overlying by several swelling and pinching beds, contains an occasional concentration of bioclastic fragments (bivalves).

3.4.3.11. Bedset 11 (BS 11)

This bedset is 114 cm thick and is characterized by two prominent thickening-upward units, each of which consists of thin sheet-like bodies occurring as flat and horizontal beds characterized by back-stepping patterns. Individual sheets range in lateral length from 5 m to several hundreds of metres. The basal succession of each unit is composed of bioclastic mudstone/wackestone lithofacies (LFT 8), while the grainy beds at the top are composed of coarse-grained oolitic grainstone (LFT 1) and the thin-walled bivalve rudstone (LFT 17) respectively. The units are in part terminated by discontinuous supratidal deposits (LFT 7). The reefal accumulations of the bivalves are described in outcrop 2 and they occur as convex bodies. Similar to the basal surface of BS 9, the basal interval of this bedset is composed of thinly interbedded

bioclastic wackestone/mudstone occurring as symmetrical wavy beds. And accordingly, a flooding surface is placed at the base of this bedset (FS-S5).

3.4.3.12. Bedset 12 (BS 12)

This bedset is 187 cm thick and it has a similar stratigraphic pattern as BS 11, however, the LFT 17 is absent and the beds are composed of bioclastic wackestone/mudstone (LFT 8) at the base capped by coarse-grained oolitic grainstone (LFT 1). This bedset is characterized by two prominent thickening-upward units; each of these units consists of thin sheet-like bodies composed of flat and horizontal beds characterized by back-stepping patterns. Individual sheets range in lateral length from 5 m to several hundreds of metres.

3.4.3.13. Bedset 13 (BS 13)

This bedset is 150 cm thick. It is composed of a well-developed thickening-upward pattern, consisting of dolomitized coarse-grained oolitic grainstone (LFT 1) and non-fabric preserving dolomite (LFT 9). Likewise, the thinly interbedded wavy symmetrical deposits at the base of this bedset is similar to the previously described intervals (for example base of BS 11) and therefore it is possibly represents a flooding event **(FS-S6)** similar to **FS-S4, and FS-S5.** The prominent sedimentary structure of this bedset is the abundancy of large imbrication structures. This association supports the interpretation of the FS-S6.

3.4.3.14. Bedset 14 (BS 14)

This bedset is 169 cm thick. It is composed of several well-developed thickening-upward strata of dolomitized lithofacies (LFT 17, 14, and 6) and non-fabric preserving dolomite (LFT 9) interbedded with marlstone (LFT 7) and gypsum and gypsiferous claystone (LFT 16). Similarly to BS 13, beds of this bedset are laterally flat and uniform. Also it contains an abundancy of large imbrication structures indicating high actions of waves and tides. The topmost part of this sequence is characterized by thin interbeds of dolomitized bioclastic grainstone/packstone and gypsiferous claystone. The upper part of this bedset has been taken as the boundary between the Khuff and Sudair Formations **(Khuff-Sudair boundary-S8, KSB-S8)**.

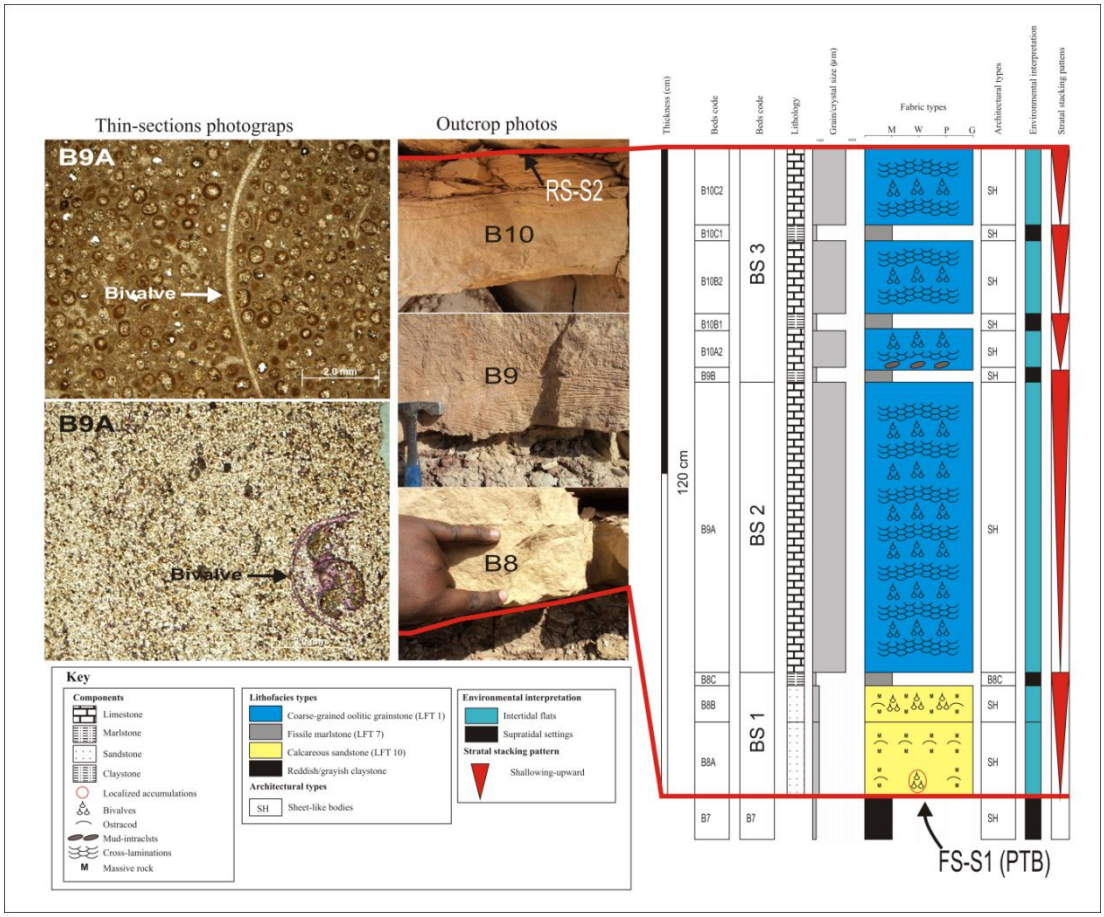

Figure 3.8. Outcrops appearance, thin-section micrograph, and simplified lithofacies log of the bedset 1, 2, and 3 described in the reference outcrop 2.

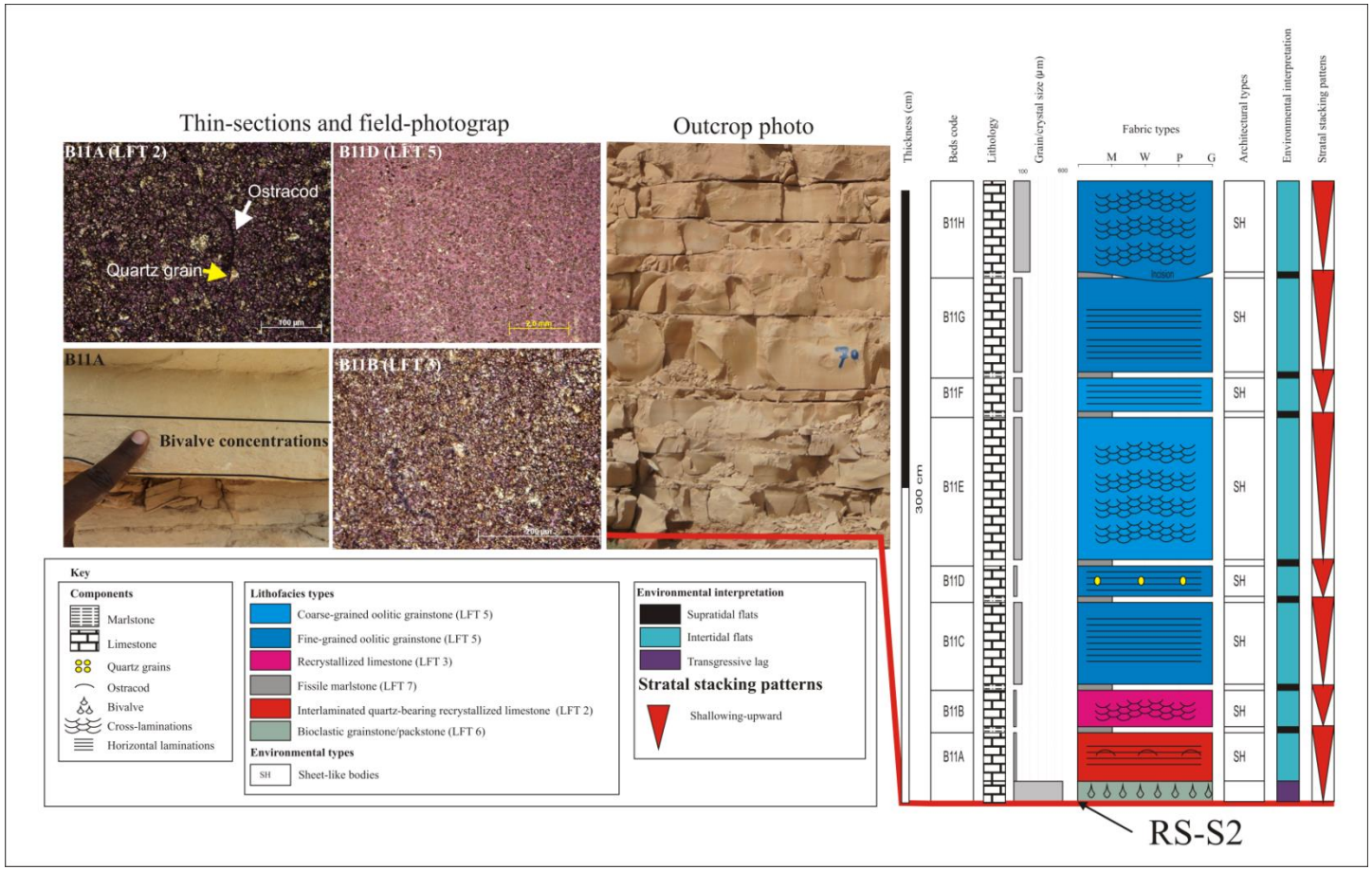

Figure 3.9. Outcrops appearance, thin-section micrograph, and simplified lithofacies log of the bedset 4 described in the reference outcrop 2.

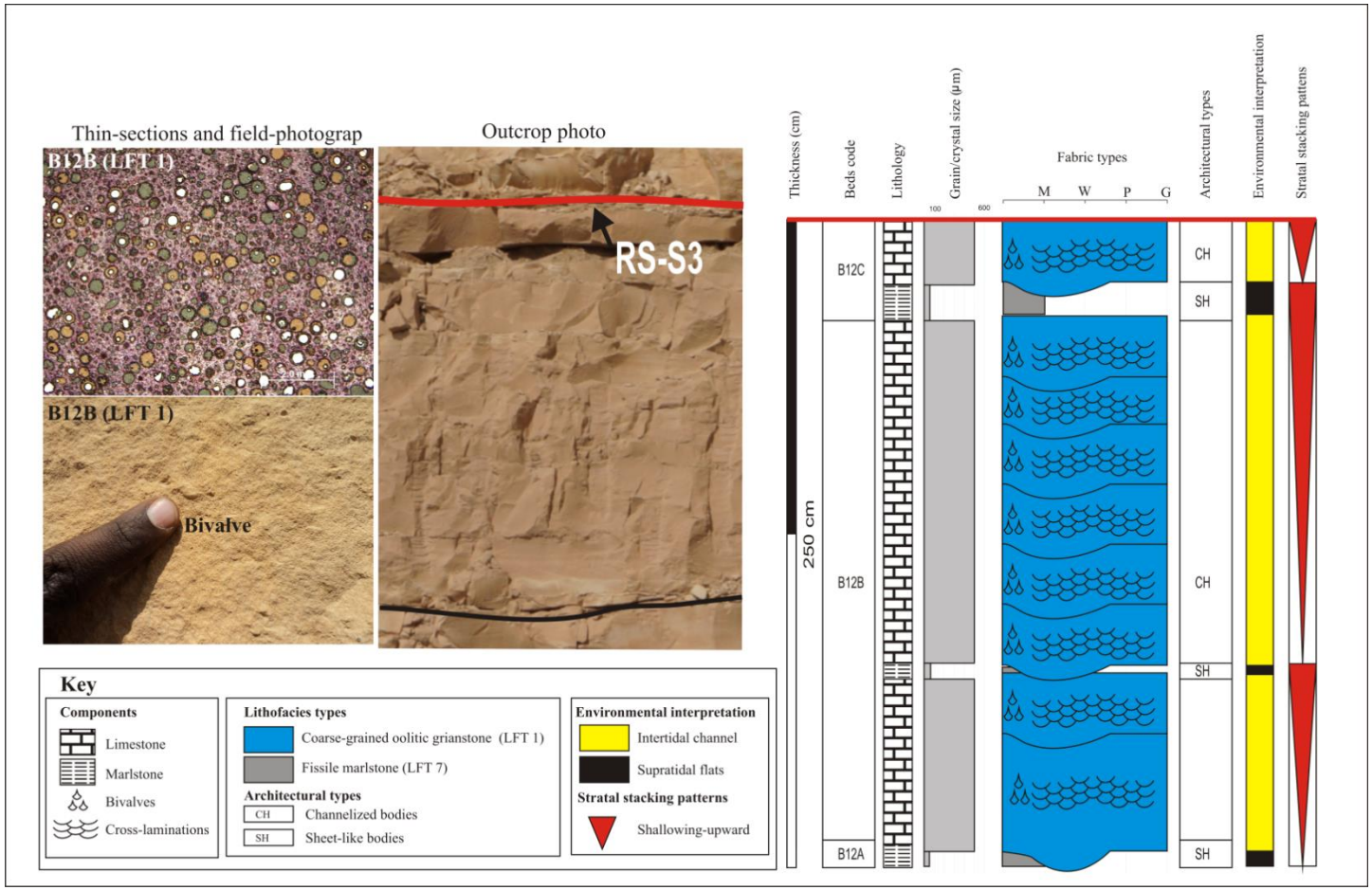

Figure 3.10. Outcrops appearance, thin-section micrograph, and simplified lithofacies log of the bedset 5 described in the reference outcrop 2.

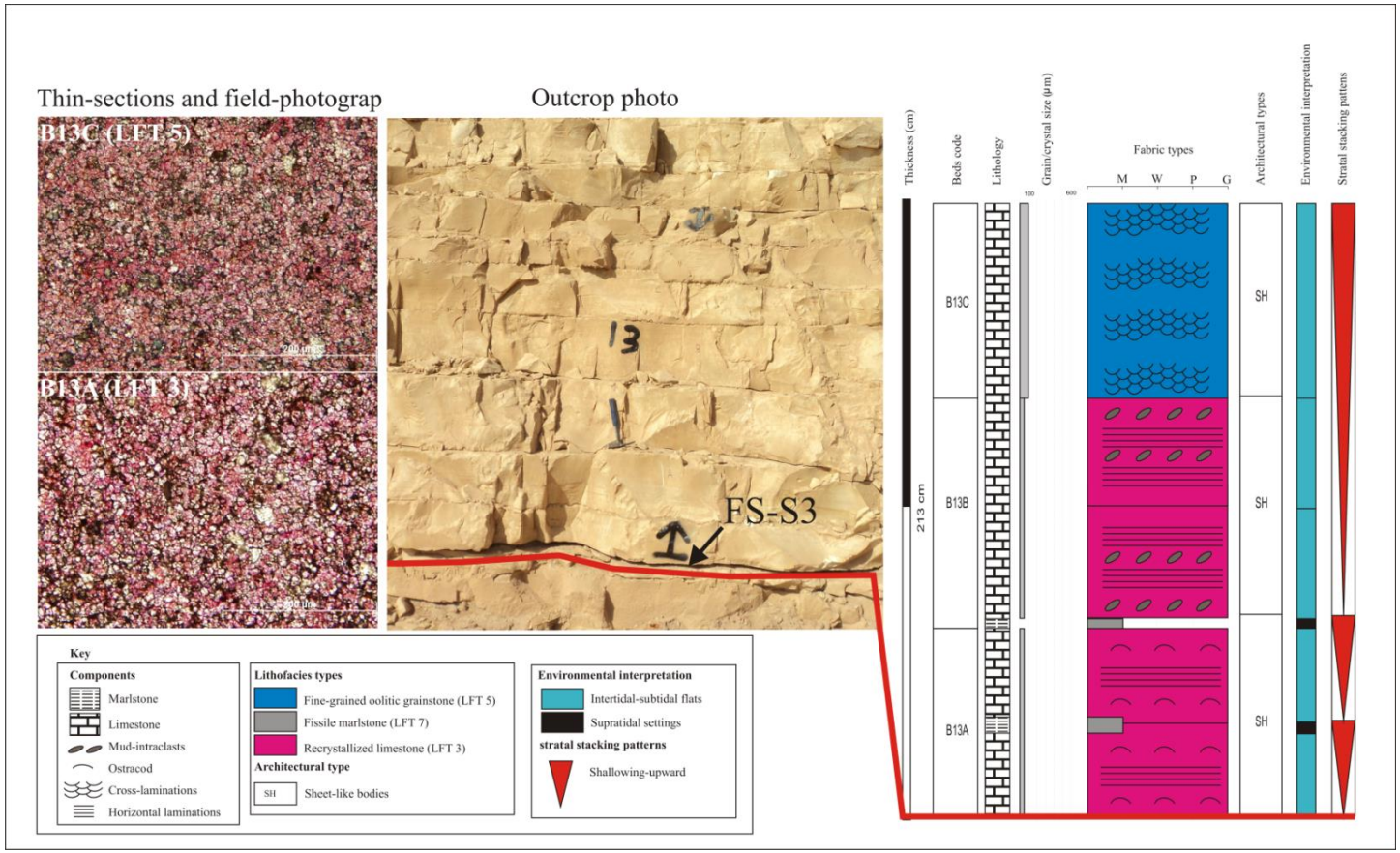

Figure 3.11. Outcrops appearance, thin-section micrograph, and simplified lithofacies log of the bedset 6 described in the reference outcrop 2.

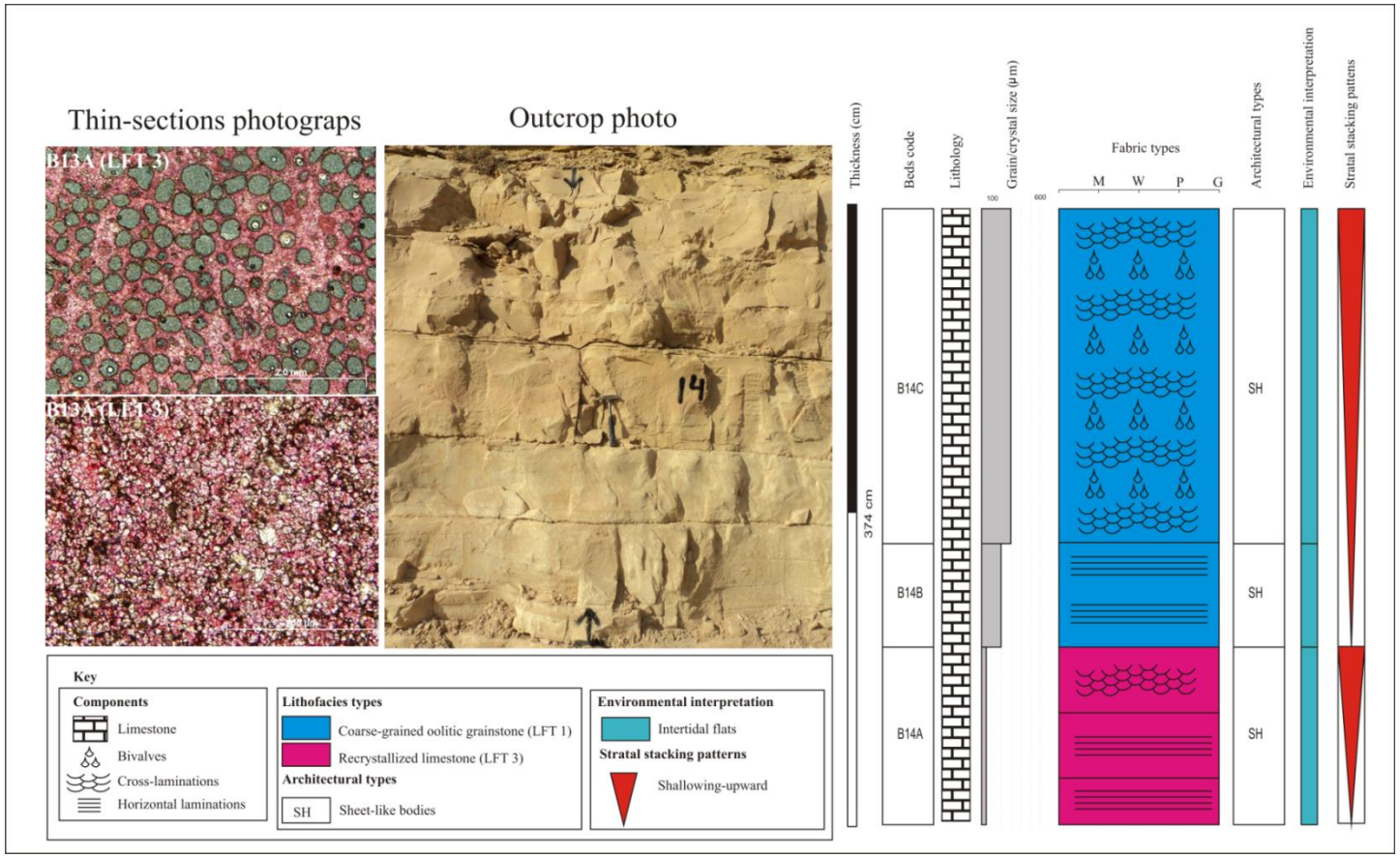

Figure 3.12. Outcrops appearance, thin-section micrograph, and simplified lithofacies log of the bedset 7 described in the reference outcrop 2.

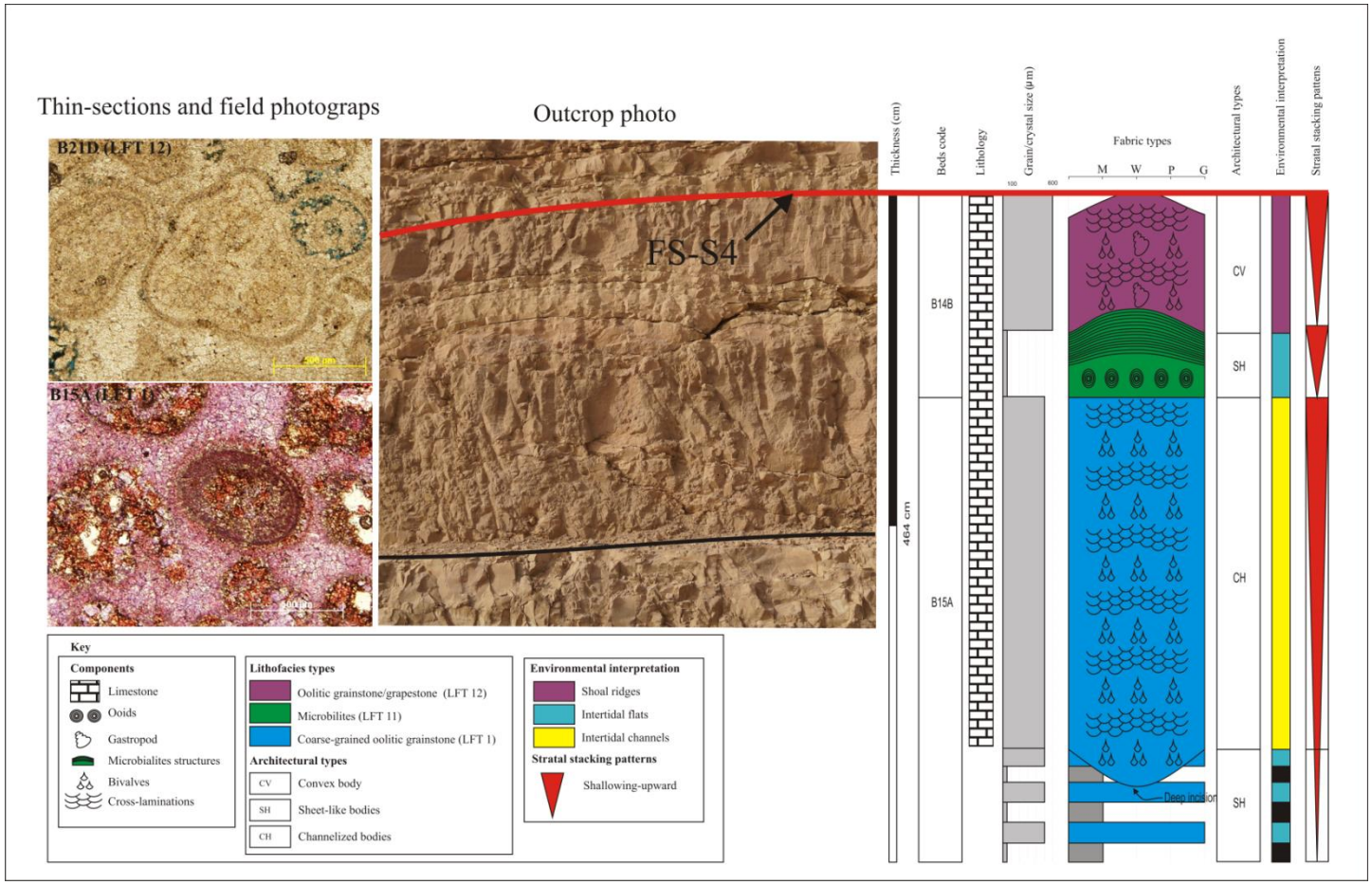

Figure 3.13. Outcrops appearance, thin-section micrograph, and simplified lithofacies log of the bedset 8 described in the reference outcrop 2.

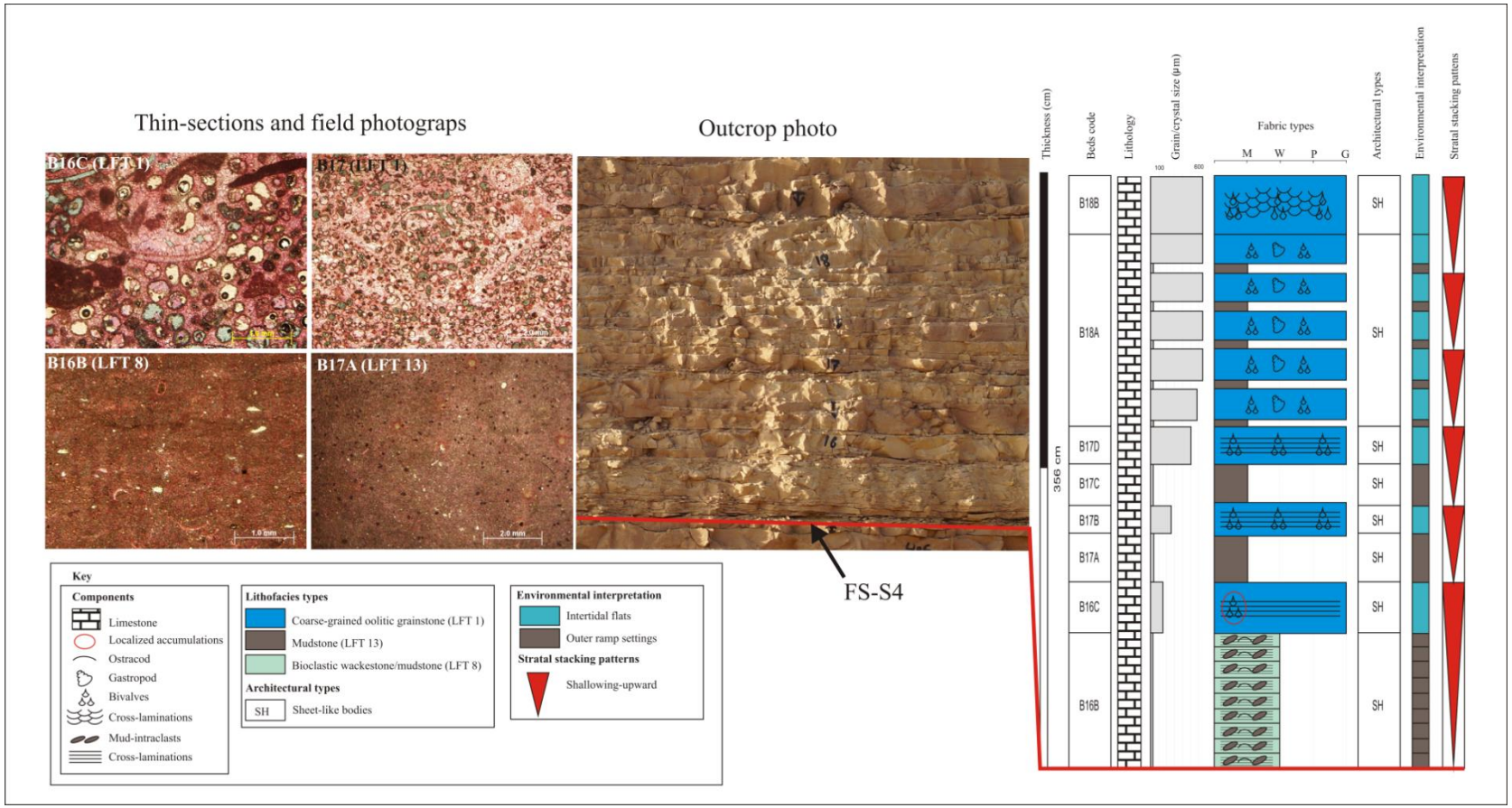

Figure 3.14. Outcrops appearance, thin-section micrograph, and simplified lithofacies log of the bedset 9 described in the reference outcrop 2.

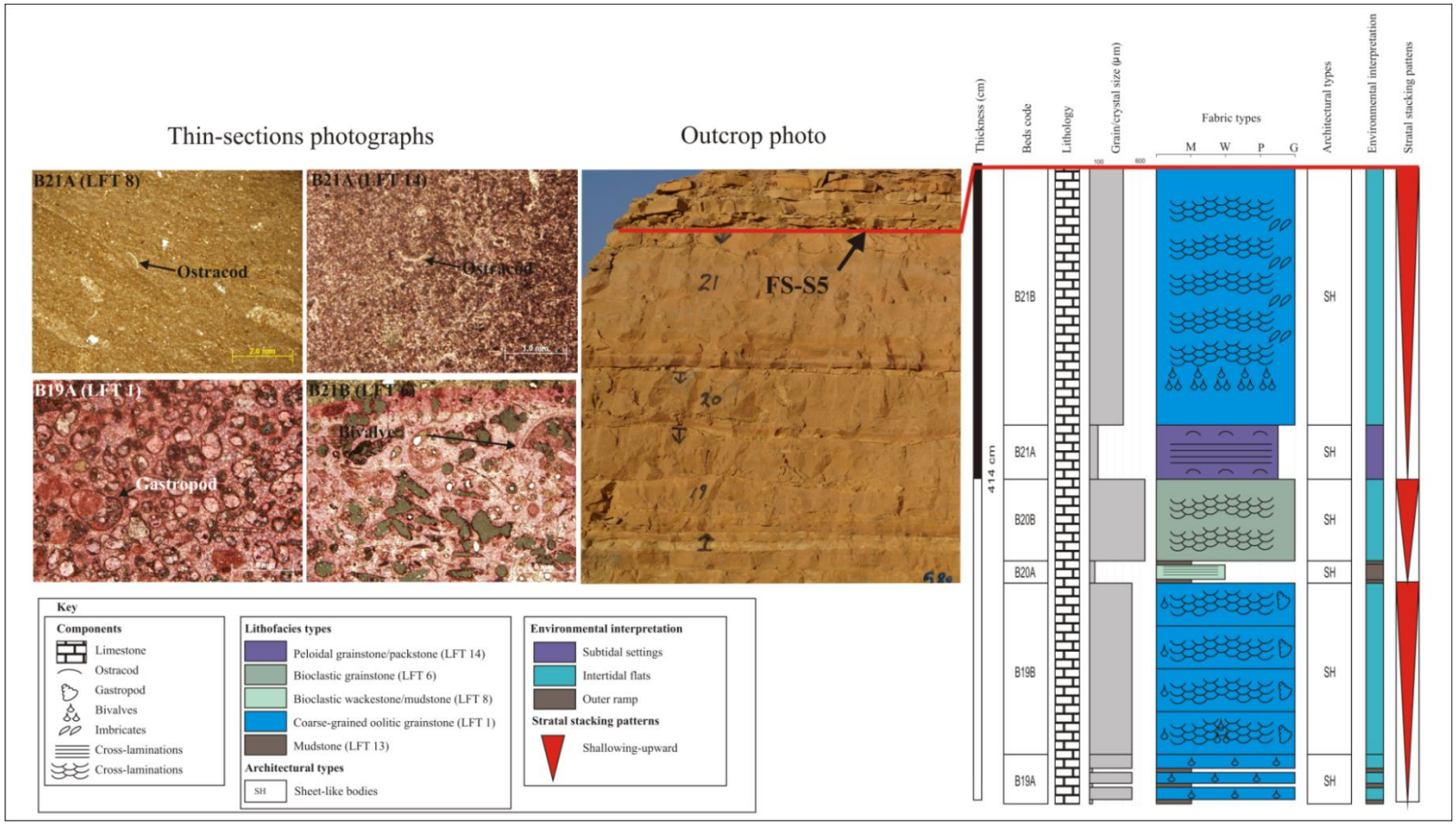

Figure 3.15. Outcrops appearance, thin-section micrograph, and simplified lithofacies log of the bedset 10 described in the reference outcrop 2.

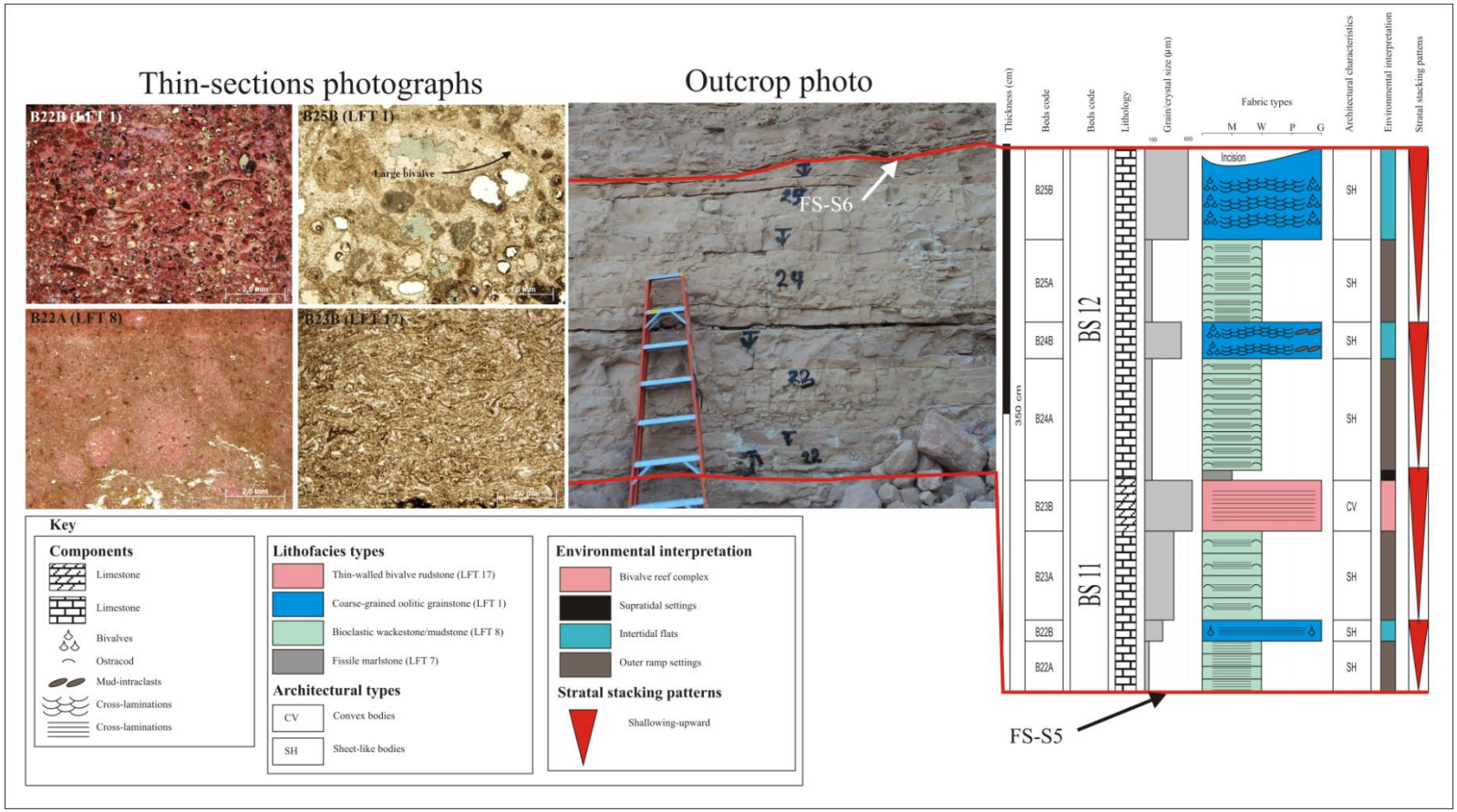

Figure 3.16. Outcrops appearance, thin-section micrograph, and simplified lithofacies log of the bedset 11 and 12 described in the reference outcrop 2.

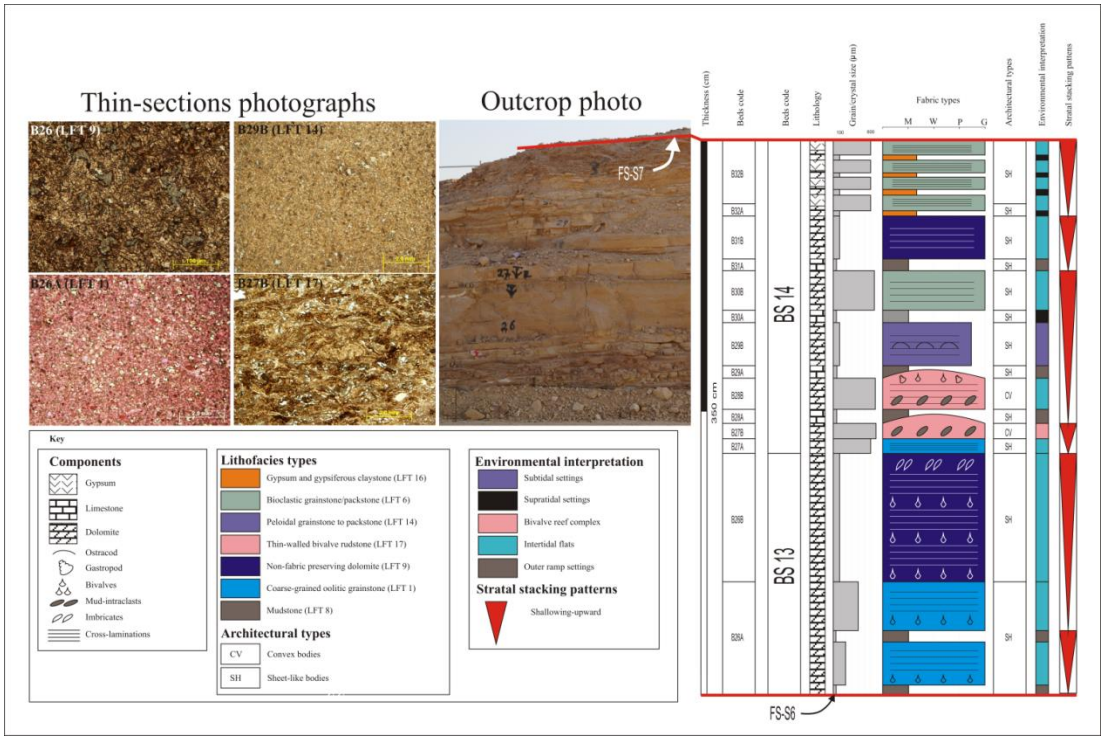

Figure 3.17. Outcrops appearance, thin-section micrograph, and simplified lithofacies log of the bedset 13 and 14 described in the reference outcrop 2.

3.5. Discussion

3.5.1. High-frequency sequences (HFS)

Vaslet et al. (2005) subdivided the Khuff Formation into five depositional sequences, each of which are composed of a transgressive system tract and highstand system tract separated by a flooding interval and bounded by two sequence boundaries. The Upper Khartam Member has been deposited according to these authors as a transgressive system tract package span in age between 250.5 and 251.75 Ma (about 1.25 Ma). Following Zecchin and Catuneanu (2013) and Catuneanu and Zecchin (2013), the bedsets are grouped into six high-frequency sequences (HFS). The defined HFSs are illustrated in Figure 3.18 to 33. Most importantly, these HFSs are bounded by prominent sequence stratigraphic surfaces, mainly transgressive surfaces occurring as shoreline ravinement and flooding surfaces reflecting shoreline trajectory shifts. These are associated with reworking materials and skeletal accumulations (transgressive lag) and mudstone and bioclastic wackestone/mudstone lithofacies types indicating agitated transgression and deep marine setting respectively. The transgressive package is sometimes preserved as a thin (20 cm) lag deposits of shell accumulation. The latter is most probably representing the Onlap Skeletal Beds (OSBs) of Kidwell (1990) and Zecchin and Catuneanu (2013). Therefore, the high-resolution stratigraphic build-ups of the Upper Khartam Member reflect regressive cycles and deposits. These are similar to the defined R cycles of Zecchin (2007) and they are likely representing the fifth-order cycles and possibly related to Milankovitch cycles (eccentricity = 100.000 year). These are comparable to the Middle Triassic Muschelkalk small-scale cycles of

Aigner et al. (1999) and Koehrer et al. (2009). The high-frequency sequences will be described below and illustrated in figure 19 to 34 where outcrop 2 is taken as reference outcrop. It is likely that, the fifth- and higher-order sequences are occurring as amalgamated bodies migrating westward in a genetic pattern where the lateral fragmentation of the depositional environments is following Walther law (Figure **3.34**). This nature is likely typified the upper Khartam member (mostly third-order sequence; 1.25 Ma age) where the nature of the rapid transgressive over the Lower Khartam (mostly clayey and evaporitic deposits) is prominent and characterized by skeletal accumulation. Beside the detailed lithofacies and stratigraphic analysis, regional correlation of the high-frequency sequences is based on the following criteria: 1) the lowermost regionally extended Permian-Triassic Boundary (PTB-S1) is defined as a datum for regional correlation, 2) on the vertical repetition and lateral continuity of the marlstone and carbonate lithofacies, 3) on similarities in the nature of vertical stratal stacking patterns and lateral succession, 4) the regionally extended microbialites and the thick intertidal channels, 5) and the stratigraphic position.

3.5.1.1. High-frequency sequence 1 (HFS 1)

This sequence is about 120 cm thick and encompasses bedset 1, 2 and 3. It is bounded at the bottom by the FS-S1 (coincides with the MFI TrS and Permian-Triassic boundary) and at the top by the TRS-S2. Laterally, from north to south, the lithofacies changes from coarse-grained oolitic grainstone (LFT 1) to calcareous sandstone (LFT 10) and bioclastic grainstone/packstone lithofacies (LFT 6) and from skolithos bioclastic oolitic grainstone (LFT 15) to coarse-grained oolitic grainstone and

bioturbated calcareous sandstone. The upper part of this sequence is composed on microbialites and marlstone defining a shallowing-upward trend. The regional variations in the lithofacies type are most likely controlled by accommodation space and sediment supply, where clastic influxes are common to the south. This interpretation is consistent with the regional variations in Khuff lithology as described by Vaslet et al. (2005).

3.5.1.2. High-frequency sequence 2 (HFS 2)

This sequence is about 550 cm thick and encompasses bedset 4 and 5, to the north, is outcrop 3, the thickness reach 1300 cm. At the reference outcrop, the sequence is pathing vertically from intertidal flats to intertidal channels indicating an overall shallowing-upward pattern. Regionally, bedset 4 varies in the lithofacies types. To the north, in outcrop 3, the BS 4 is defined by complex amalgamation of sheet-like bodies (50 m long and 20 cm thick). This is relatively shorter if compared with the reference outcrop where length ranges between 50 and 300 m). It is composed of interlaminated quartz-bearing recrystallized limestone and coarse-grained oolitic grainstone deposited in intertidal flats. Regional correlation of BS 4 is mainly based on the similarity of the internal accumulations (nature of stratal stacking and amalgamation patterns). In the most southern outcrop 4, the lithofacies types slightly changed to interlaminated quartz-bearing fine-grained oolitic grainstone. The lithofacies and architectural variations of the BS4 are thought to be controlled by sediment supply and accommodation respectively. The quartz-bearing lithofacies types were deposited in distal intertidal settings. Regionally, BS 5 is dominated by coarse-grained oolitic grainstone occurring as complex amalgamations of intertidal creeks less than 1 m in

width and 30 cm in thickness. To the north, in outcrop 3, the lithofacies changes to interlaminated quartz-bearing fine-grained oolitic grainstone, this variation is accompanied by relatively less erosional phenomena of the intertidal channels compared with the other localities where intertidal channels locally removed up to about 5 m thick deposits. Generally, the stratigraphic succession of this sequence is characterized by shallowing-upward pattern corresponding to intertidal flats to intertidal channels capped by thick (20 cm) marlstone of supratidal deposits (LFT 7).

3.5.1.3. High-frequency sequence 3 (HFS 3)

This sequence is about 952 cm thick and encompasses three bedsets, i.e. BS 6, 7 and 8. These are bounded by **FS-S3 and FS-S4** and are build up by intertidal-subtidal flats, intertidal channels, intertidal microbialites, to shoal ridge, which make up a shallowing-upward pattern. This pattern can be followed in the studied outcrops over a lateral distance of 70 km. The basal stratigraphy of this sequence (BS6 and 7) is characterized by a complex amalgamation of intertidal sheet-like bodies. In the north, in outcrop 3, beds are getting shorter (5 m in length). To the south, in outcrop 1, beds are dominantly horizontal, flat, and uniform and extend for a large distance laterally (about 300 m). Further to the south, in outcrop 4, the architectural pattern changed to intertidal channels stacked in a complex pattern; individual channels have a width of 1 m and are each about 30 cm thick. In addition, the lithofacies content varies laterally from interlaminated quartz-bearing recrystallized limestone (LFT 2) and coarse-grained oolitic grainstone (LFT 1) to recrystallized limestone (LFT 3) and fine-grained oolitic grainstone (LFT 5). The architectural and lithofacies variability of the basal succession is most likely controlled by accommodation space and in part by sediment

type where in the south clastic influxes are involved. The upper sequence (BS 8) is dominated by intertidal channels. Regionally, these channels are traceable, even though, the architectural characteristic of these channels changes. A condense small tidal creeks are described in outcrop 4. In outcrop 1 and 2, these channels are well-developed and are deep incised into the underlying units. The intertidal channels are overlain by microbialites; these are consistently traceable over a lateral distance of 5 km. They represent a second growth stage and they are relatively large (3 m wide and 50 cm thick) if compared with the earlier growth of the stromatolites in HFS 1 (20 cm wide and about 10 cm thick). The microbialites are capped by shoal ridge deposits representing the shallowest beds of this sequence.

3.5.1.4. High-frequency sequence 4 (HFS 4)

This sequence encompasses bedset 9 and 10 and described in outcrop 2 and 3 and it is about 770 cm. It is bounded by two flooding surfaces FS-S4 and FS-S5 respectively. In the reference outcrop, the lithofacies type is dominated by coarse-grained oolitic grainstone (LFT 1), interbedded with mudstone (LFT 13). Most importantly, in outcrop 3, the non-fabric preserved dolomite makes up the bulk of the succession, however, the stratigraphic pattern is similar to the references bedsets (BS8 and 9).

3.5.1.5. High-frequency sequence 5 (HFS 5)

This sequence is described in outcrop 2 and 3 where it encompasses BS 11 and 12. The sequence is bounded by two flooding surface the F**S-S5** at the bottom and the F**S-S6** to the top. It is composed of four shallowing-upward units with relatively thick (50 cm) bioclastic wackestone/mudstone lithofacies (LFT 8) at the base. These are most likely related to flooding events associated with the FS-S6 event. The localized

abundances of the mud-intraclasts may support this interpretation. To the north, in outcrop 3, the lithofacies change to non-fabric preserved dolomite (LFT 9), even though the architectural make-up is similar to that of the reference outcrop.

3.5.1.6. High-frequency sequence 6 (HFS 6)

This sequence is described in outcrop 2 and encompasses BS 12 and 13. The sequence is bounded at the base by the F**S-S6.** Vaslet et al., 2005 placed the maximum flooding interval of his sequence DS TrS between the Upper Khartam and Sudair Formation, this surface was not well-described in central Arabia, however it was located between the intertidal carbonates of the Upper Khartam Member and the clayey to evaporitic deposits of Sudair Formation. And accordingly, a flooding surface is placed at the topmost of this sequence and termed **FS-7.**

3.5.2. Fourth-order sequences (FSQ)

On the other hand, and based on the sedimentological characteristics and nature of stacking patterns, the HFSs of the Upper Khartam Member could be grouped into two fourth-order sequences, these are separated by major sequence boundary associated with large intertidal channels, microbialites constructions of the HFS 3. The lower fourth-order sequence (FSQ 1) consists of three high-frequency sequences include HFS 1, 2, and 3 and it is composed of non-skeletal components, dominantly consisting of oolitic grainstones (LFT 1, 4, and 5) and recrystallized limestone (LFT 2 and 3), the microbialites structures (LFT 11) and the high-angle cross-laminated oolitic grainstone (LFT 12) that cap this sequence. The sequence (FSQ 2) is composed of skeletal and non-skeletal components, dominated by bioclastic grainstone/packstone (LFT 6) and coarse-grained oolitic grainstone (LFT 1) with absence of the

recrystallized lithofacies (LFT 2 and 3) and fine-grained oolitic grainstone (LFT 4 and 5). This succession is capped by thin-walled bivalval grainstone (LFT 17) and dolomitized lithofacies types. Beside the prominent shift in the sea-level trajectory, the fourth-order sequences are likely reflecting certain biological conditions may link to sea-water chemistry.

3.5.3. Implication on reservoir architecture and quality

For critical assessment of architectural parameters and reservoir continuity, insight in the high-frequency sequence stratigraphic configuration is needed. There is a need integrating detailed information at bed level from outcrop analogues with sub-surface data which allows investigating the primary nature of the internal geobody architecture. However, most of the existing publications on the Khuff carbonate (Al-Jallal, 1995; Al-Aswad, 1997; Vaslet et al., 2005; Maurer et al., 2009; Koehrer et al., 2011; Zeller et al., 2011; Bendias et al., 2013; Haase and Aigner, 2013; Janson et al., 2013; Walz et al., 2013) did not investigated this architecture at bed-level scale, although this level is eventually critical for assessing reservoir capacity, productivity, and continuity. The studied outcrops have provided a unique opportunity to examine the different heterogeneity levels. While individual outcrop is providing the scale to characterize the interwell heterogeneity (laterally continuous exposure of 2 km), the studied area (70 km) enabled the field-scale heterogeneity to be characterized and assessed. Facies analysis demonstrates a complex cyclic nature of deposition, due to sea level fluctuations, sediment supply, and accommodation space, these resulting into deposition of varying lithofacies types (seventeen lithofacies types) within the studied interval. This variation in lithofacies will influenced reservoir properties and

eventually the capacity and productivity and vertical reservoir continuity. Furthermore, the lithofacies types are laterally amalgamated in complex patterns composed of sheet-like bodies of intertidal-subtidal flats and intertidal channels. These bodies have different anatomies and dimensions (the sheet-like bodies range in length from 5 to 300 m and have thicknesses range between 5 and 40 cm, the channels range in width from 1 m to 5 m, and their thicknesses range between 20 and 50 cm), consequently this will put further complication to the lateral and vertical reservoir continuity and hence productivity. Additionally, regional correlation has shown lateral facies changes within individual high-frequency sequence; this in turn will impact field-scale reservoir heterogeneity and continuity. Therefore, the layer cake definition of the Khuff carbonate (Al-Jallal, 1995; Koehrer et al., 2011) appears to be an adequate description from reservoir assessments (development and production) point of view, since these are apparently relies on quantifying the high-resolutional intra-reservoir frame which seems to be highly heterogeneous for both lithofacies and architectures and at both interwell and field scales. However, the layer cake definition is scale dependant, and most probably refers to the third-order or lower level (member level).

On the other hand, the dip-ward (west-east) amalgamation patterns of the high-frequency sequences is likely indicates a gradual and regional shift (to west) is shoreline (Figure **3.34**), and accordingly, a high degree of similarity is expected between the studied outcrops and the Khuff reservoirs in Eastern Arabia, as inferred from the nature of high-resolution sequence stratigraphy. Therefore, the studied succession of the Upper Khartam Member in central Saudi Arabia is possibly represents an excellent analogue for the Khuff reservoirs in Eastern Arabia.

Fundamentally, the presented qualitative and quantitative results of the lithofacies types, beds, bedsets, high-frequency sequences will stand as a unique input for enhanced-geological modelling and fluid flow simulation, and eventually, critical for better assessment of Khuff reservoirs of Eastern Arabian Fields.

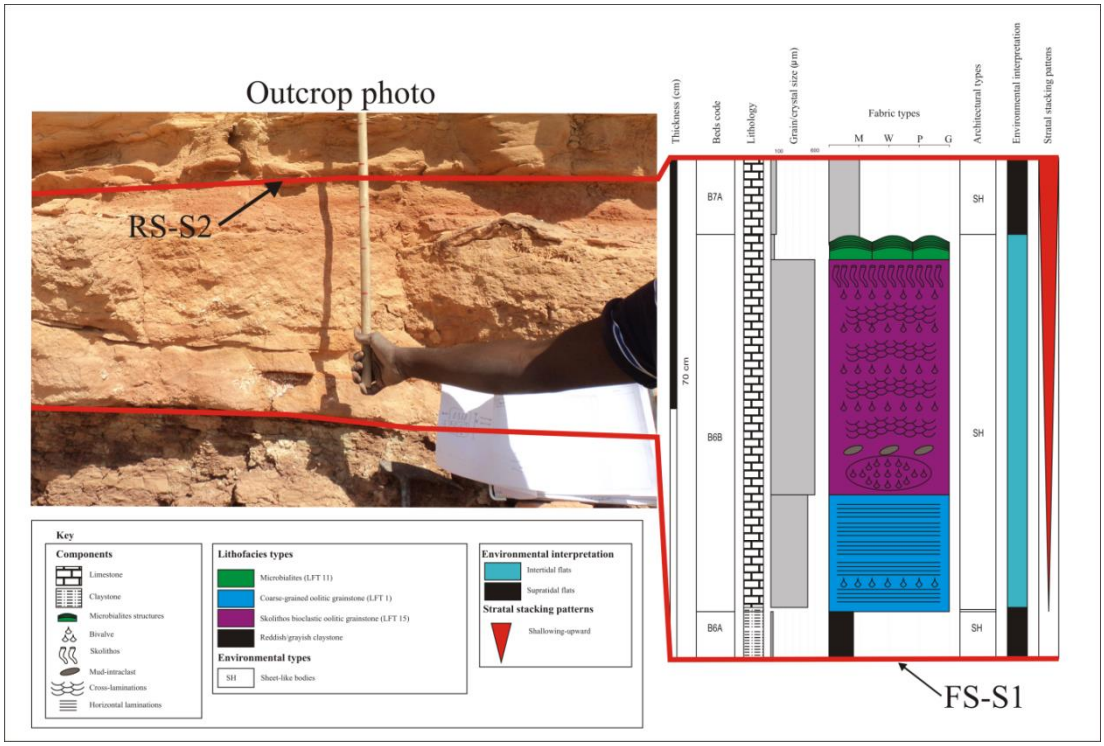

Figure 3.18. Outcrops photo and simplified lithofacies log of the high-frequency sequence 1 described in outcrop 3.

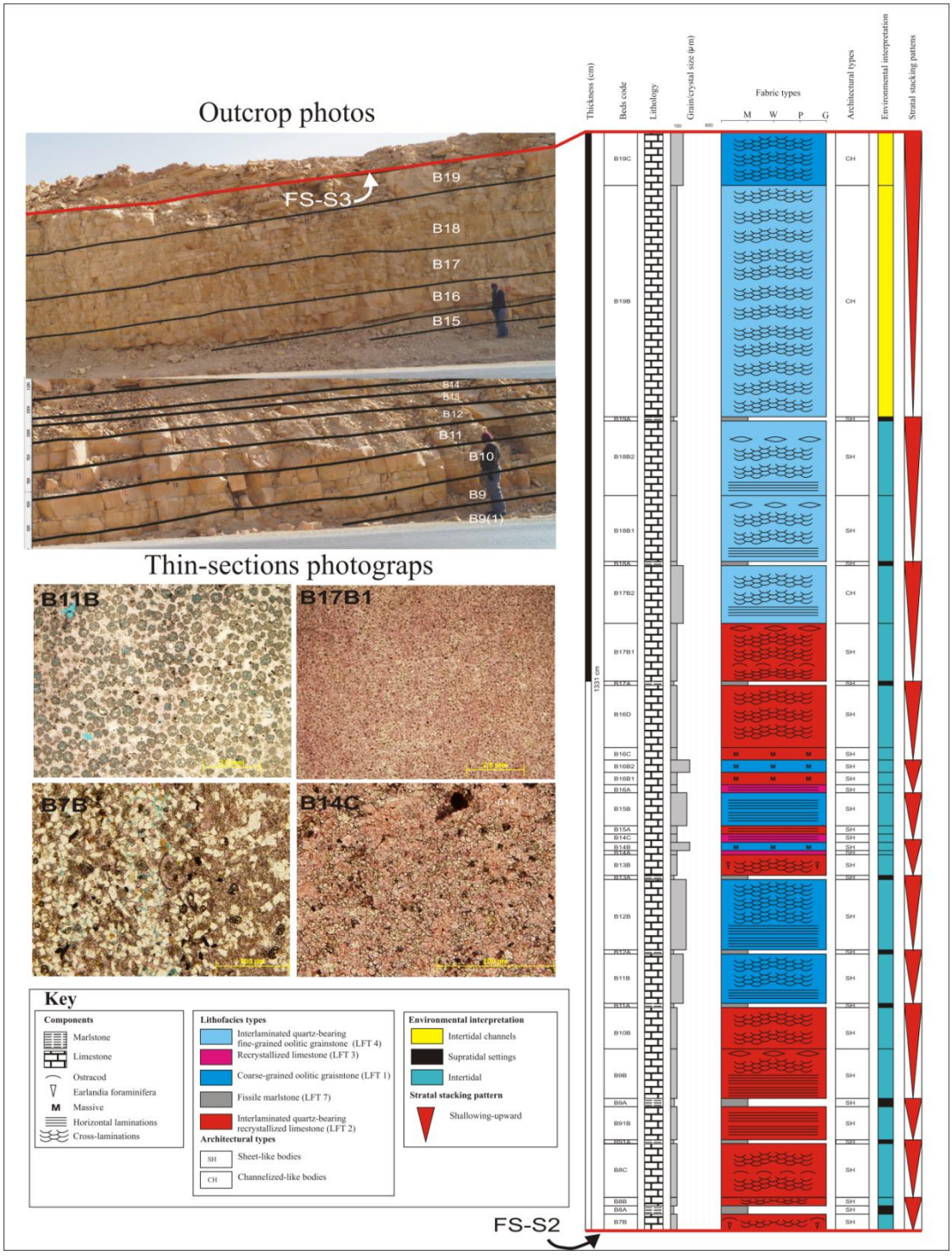

Figure 3.19. Outcrops photo, thin-section micrograph, and simplified lithofacies log of the high-frequency sequence 2 described in outcrop 3.

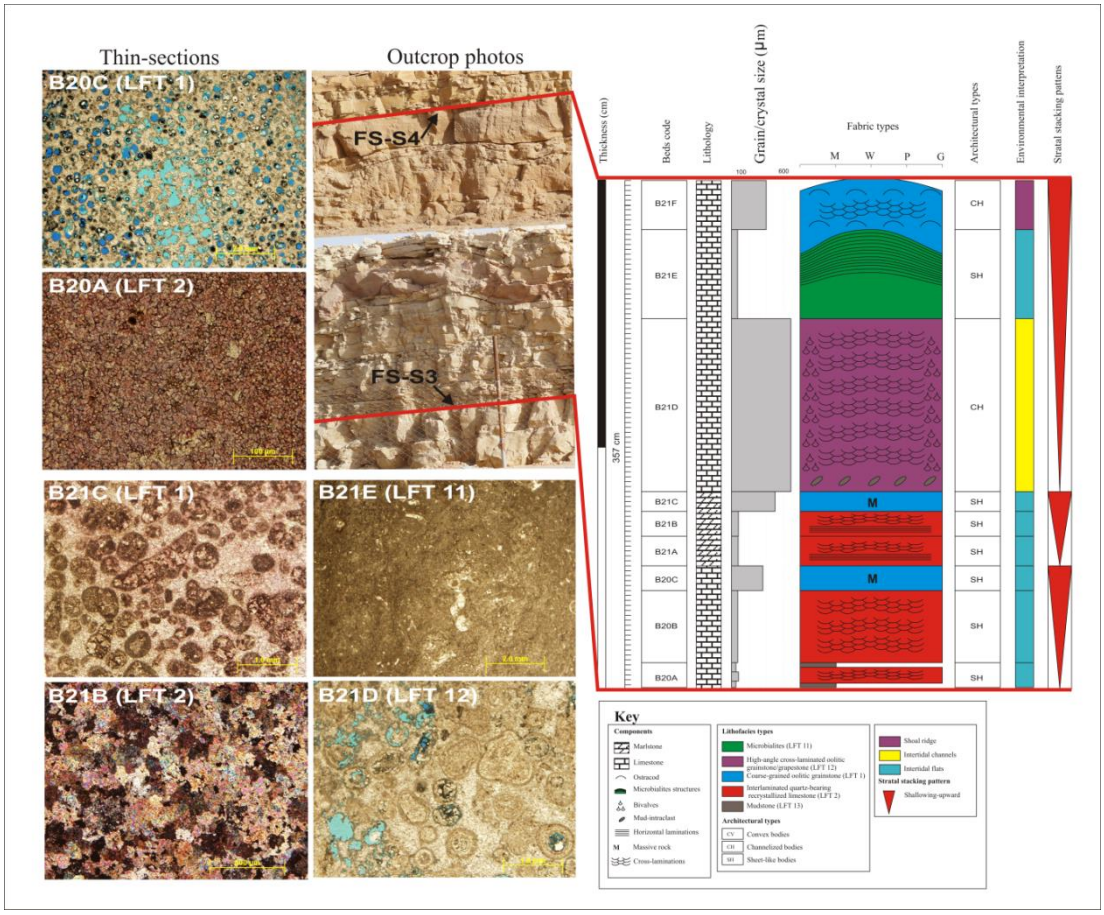

Figure 3.20. Outcrops photo, thin-section micrograph, and simplified lithofacies log of the high-frequency sequence 3 described in outcrop 3.

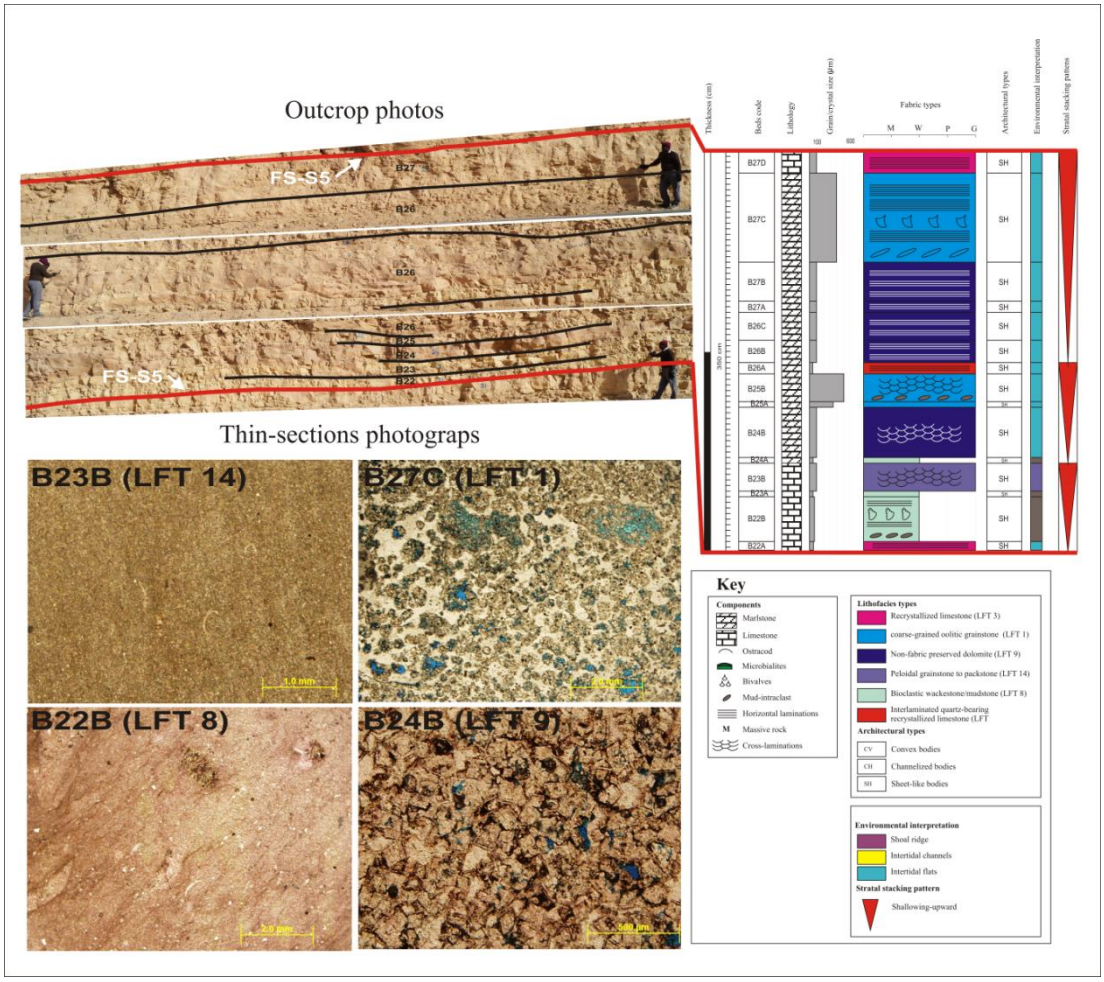

Figure 3.21. Outcrops photo, thin-section micrograph, and simplified lithofacies log of the high-frequency sequence 4 described in outcrop 3.

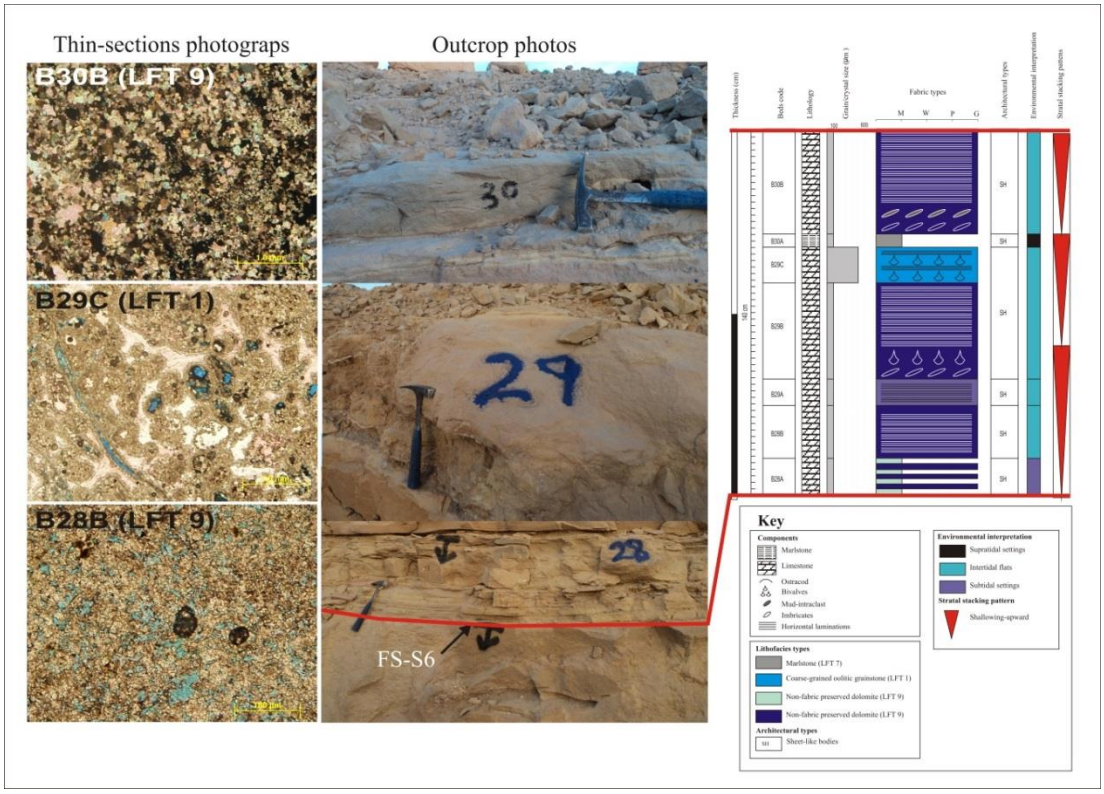

Figure 3.22. Outcrops photo, thin-section micrograph, and simplified lithofacies log of the high-frequency sequence 5 described in outcrop 3.

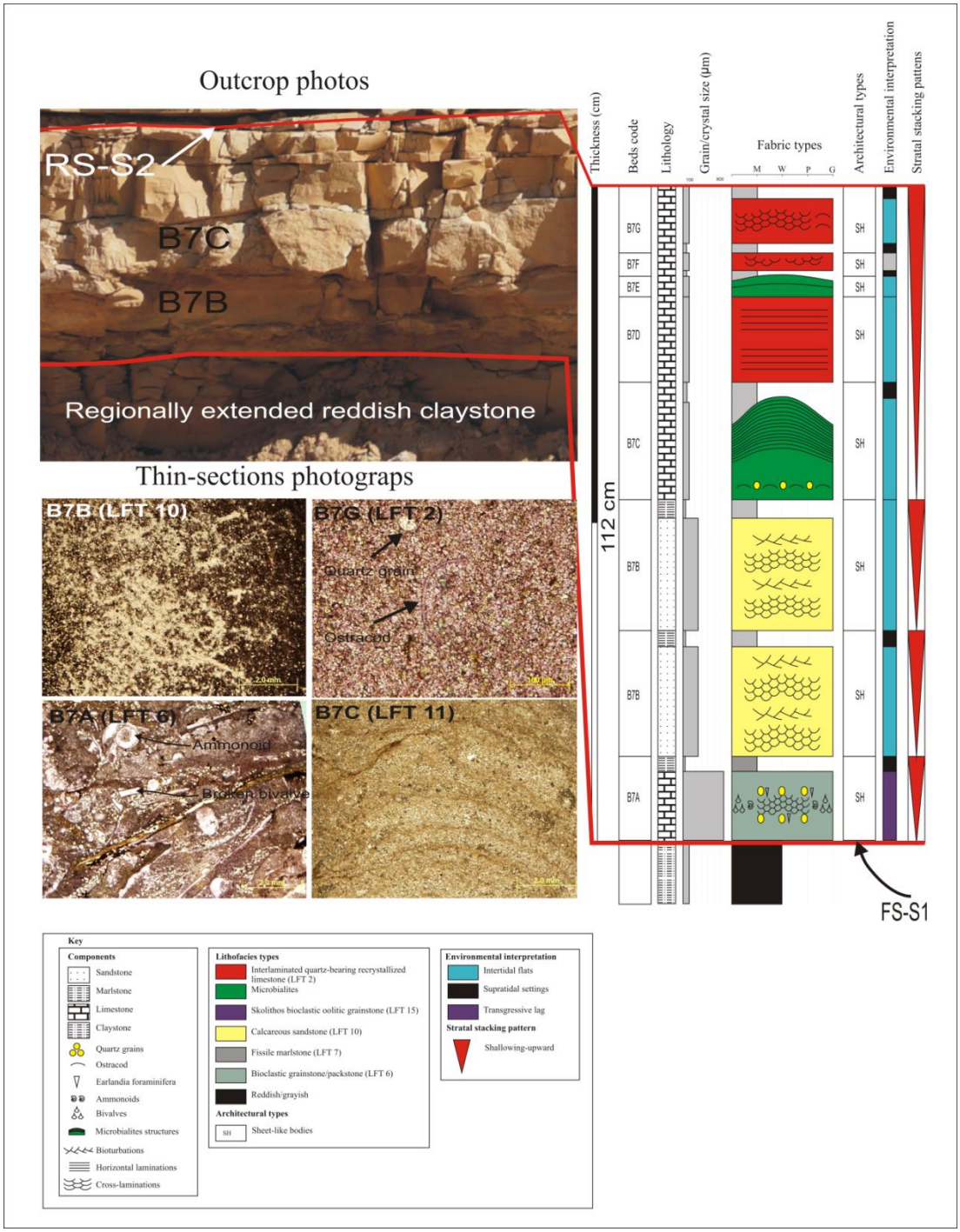

Figure 3.23. Outcrops photo, thin-section micrograph, and simplified lithofacies log of the high-frequency sequence 1 described in outcrop 1.

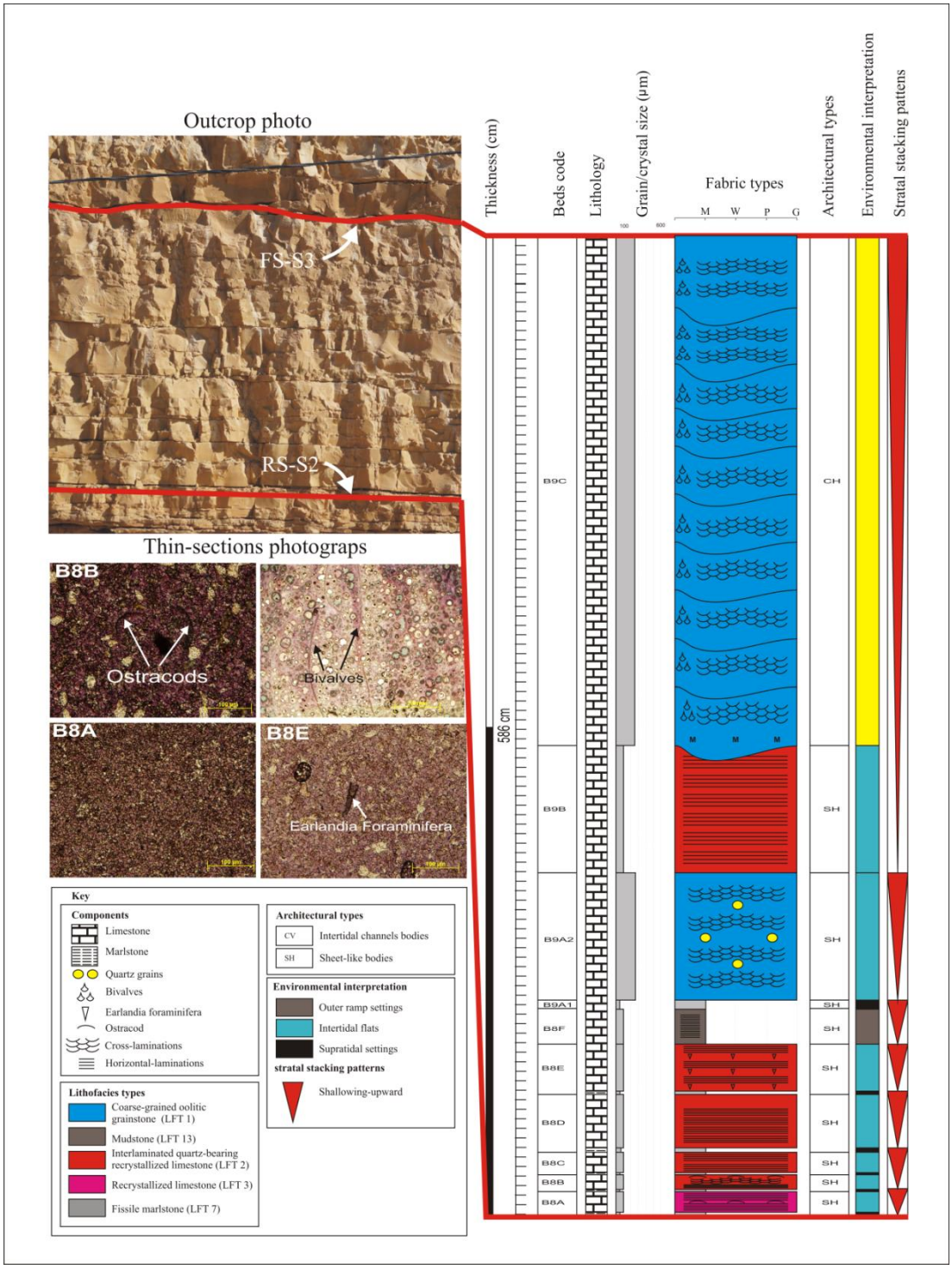

Figure 3.24. Outcrops photo, thin-section micrograph, and simplified lithofacies log of the high-frequency sequence 2 described in outcrop 1.

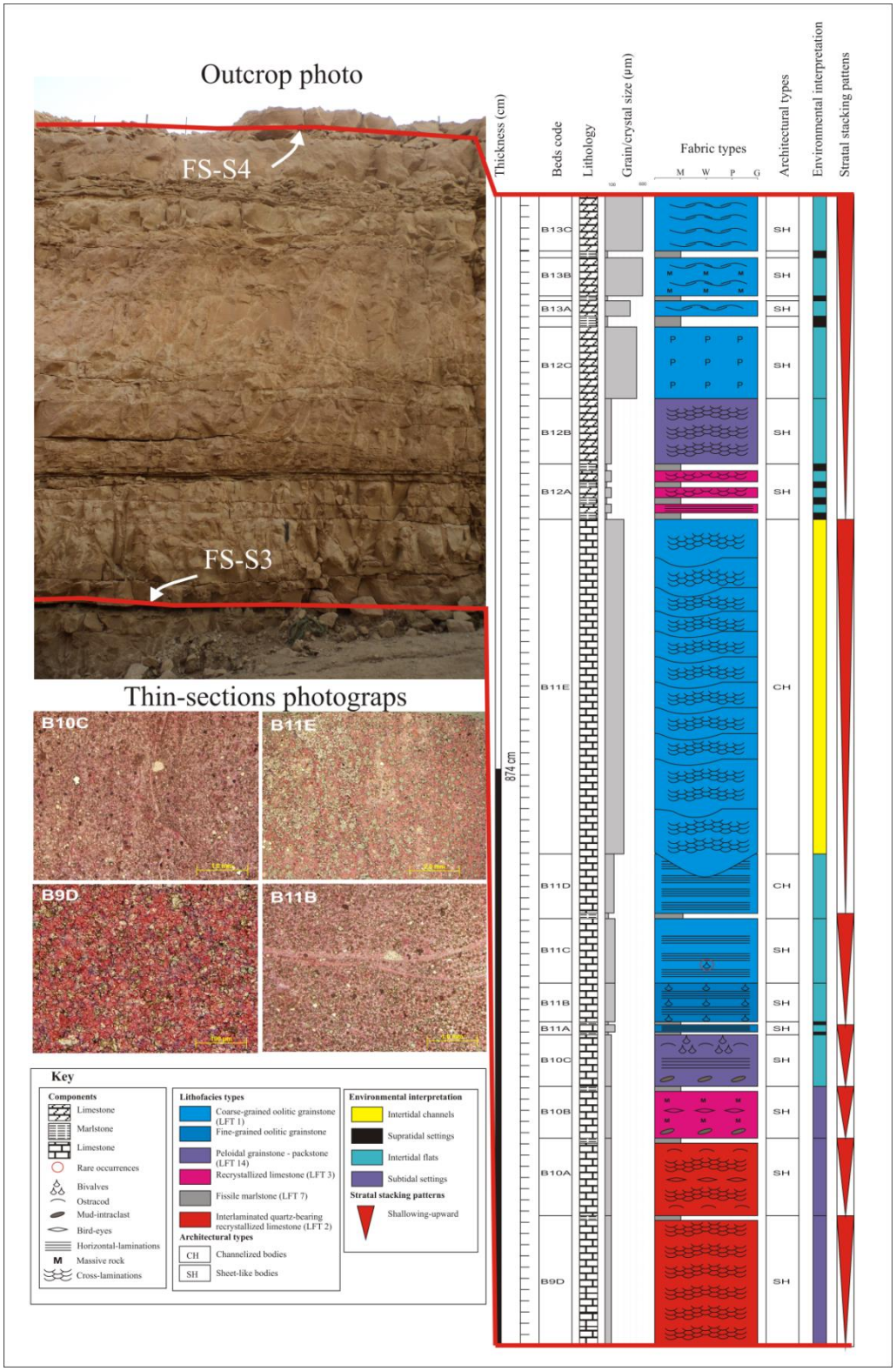

Figure 3.25. Outcrops photo, thin-section micrograph, and simplified lithofacies log of the high-frequency sequence 3 described in outcrop 1.

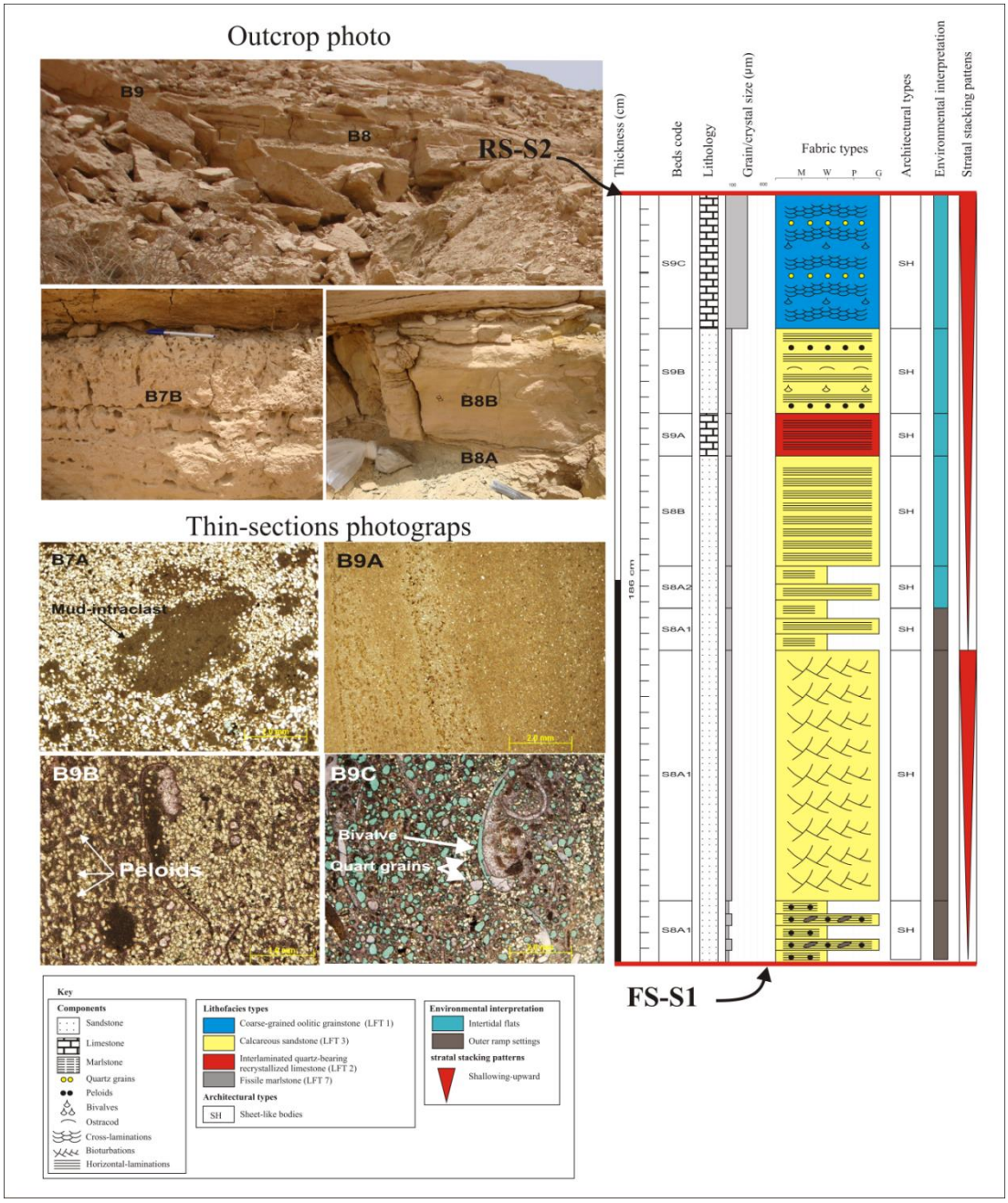

Figure 3.26. Outcrops photo, thin-section micrograph, and simplified lithofacies log of the high-frequency sequence 1 described in outcrop 4.

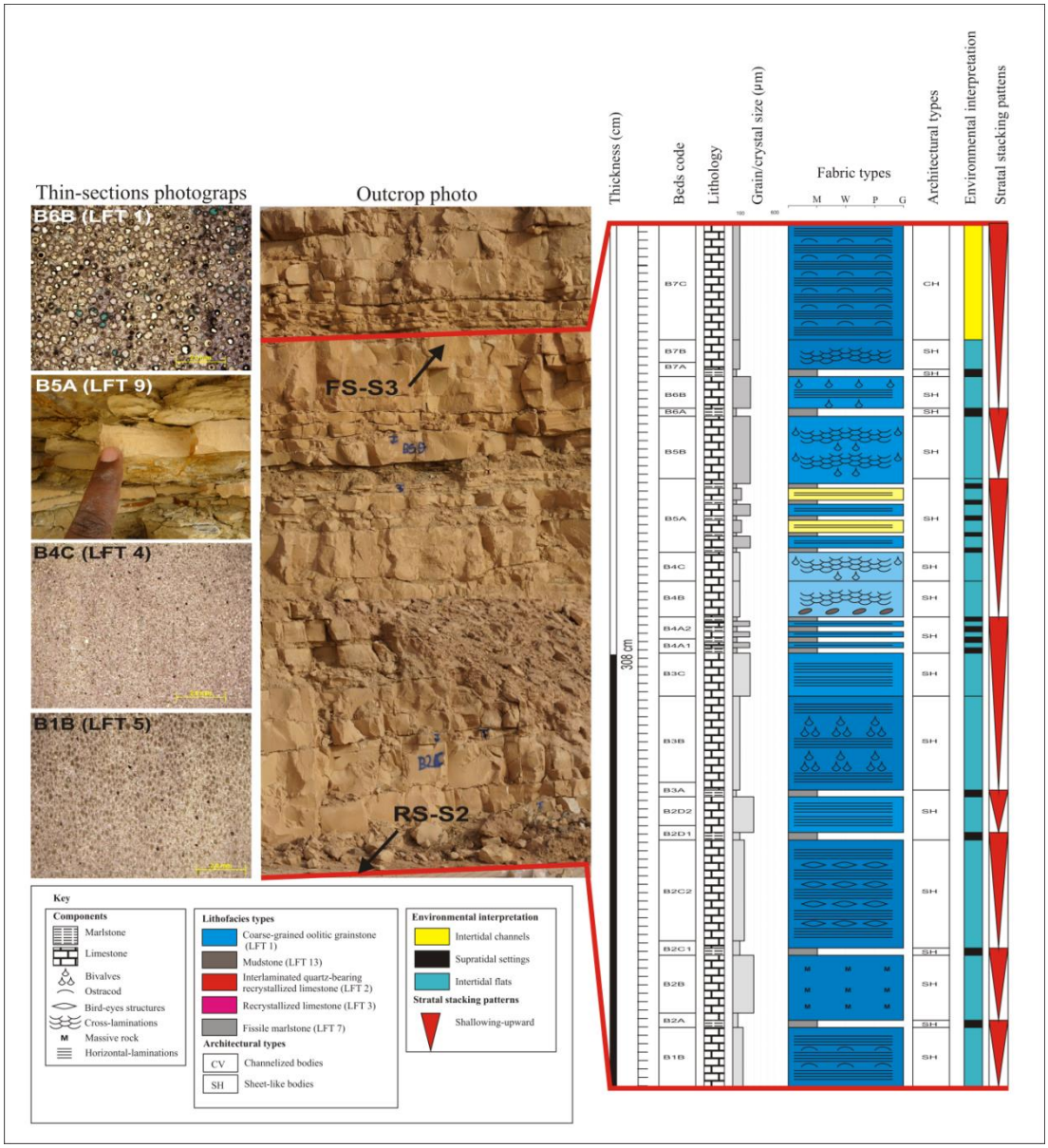

Figure 3.27. Outcrops photo, thin-section micrograph, and simplified lithofacies log of the high-frequency sequence 2 described in outcrop 4.

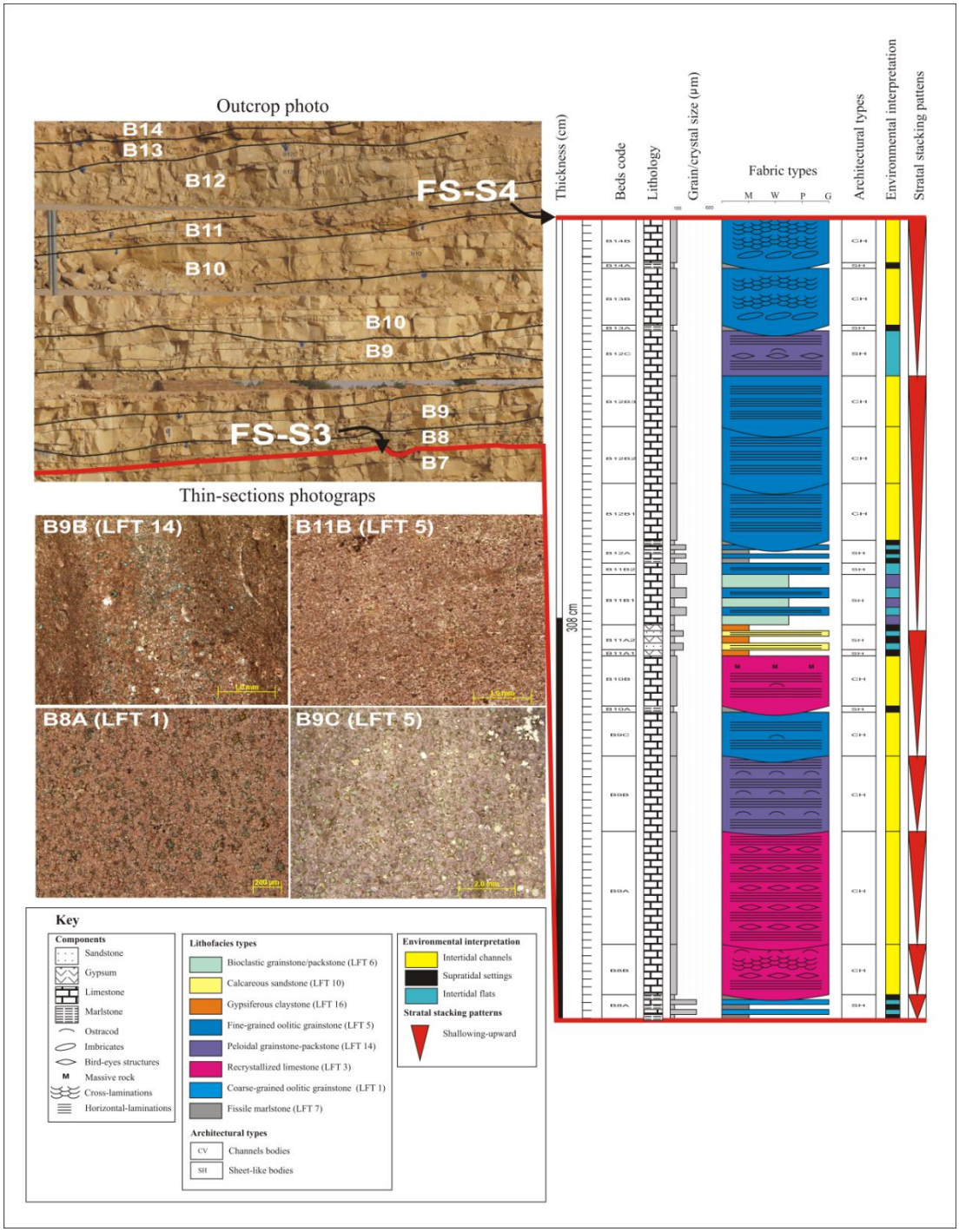

Figure 3.28. Outcrops photo, thin-section micrograph, and simplified lithofacies log of the high-frequency sequence 3 described in outcrop 4.

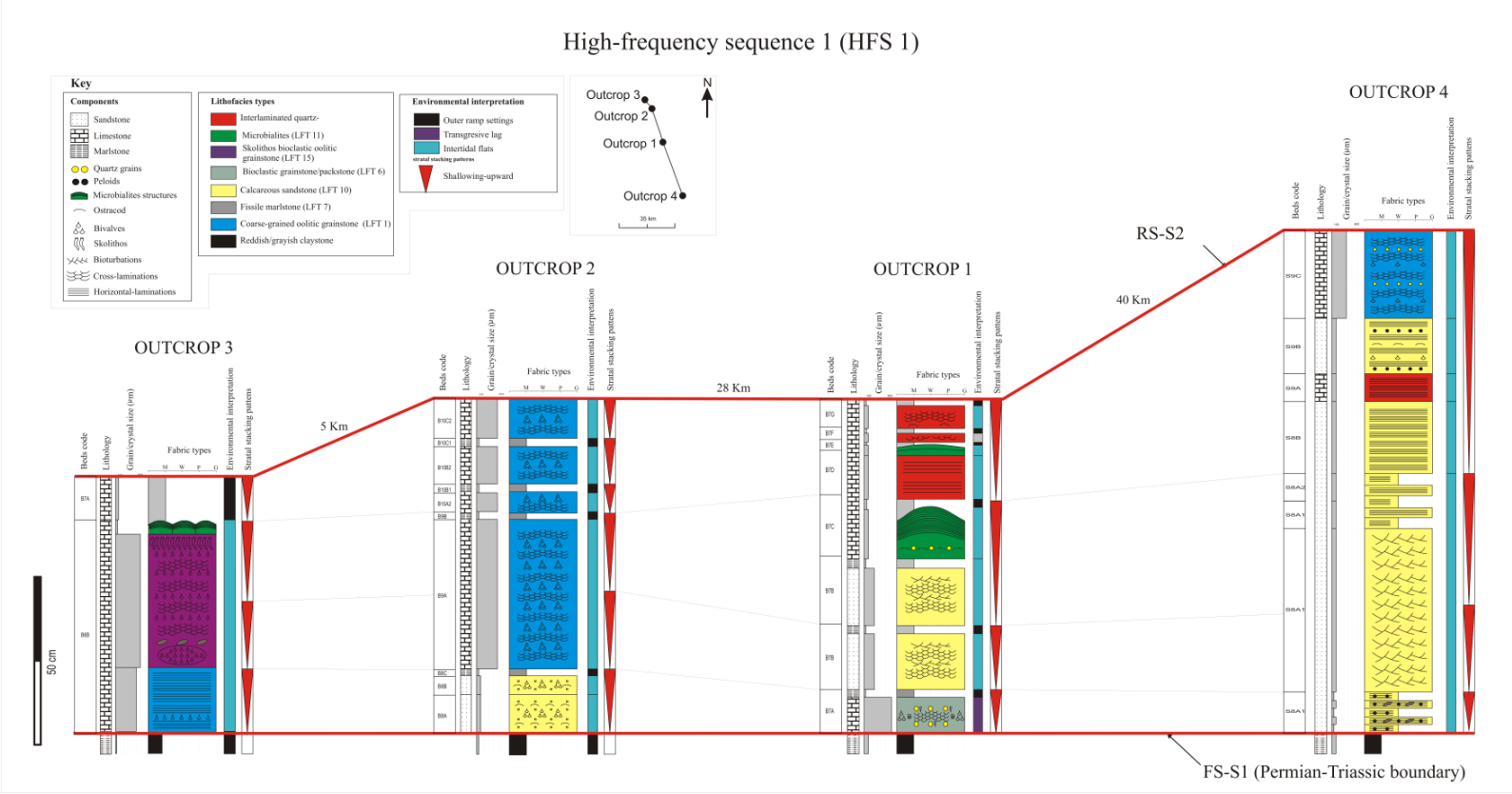

Figure 3.29. Regional correlation of the HFS 1 over the study area (70 km) showing the lateral lithofacies variation in the strike direction.

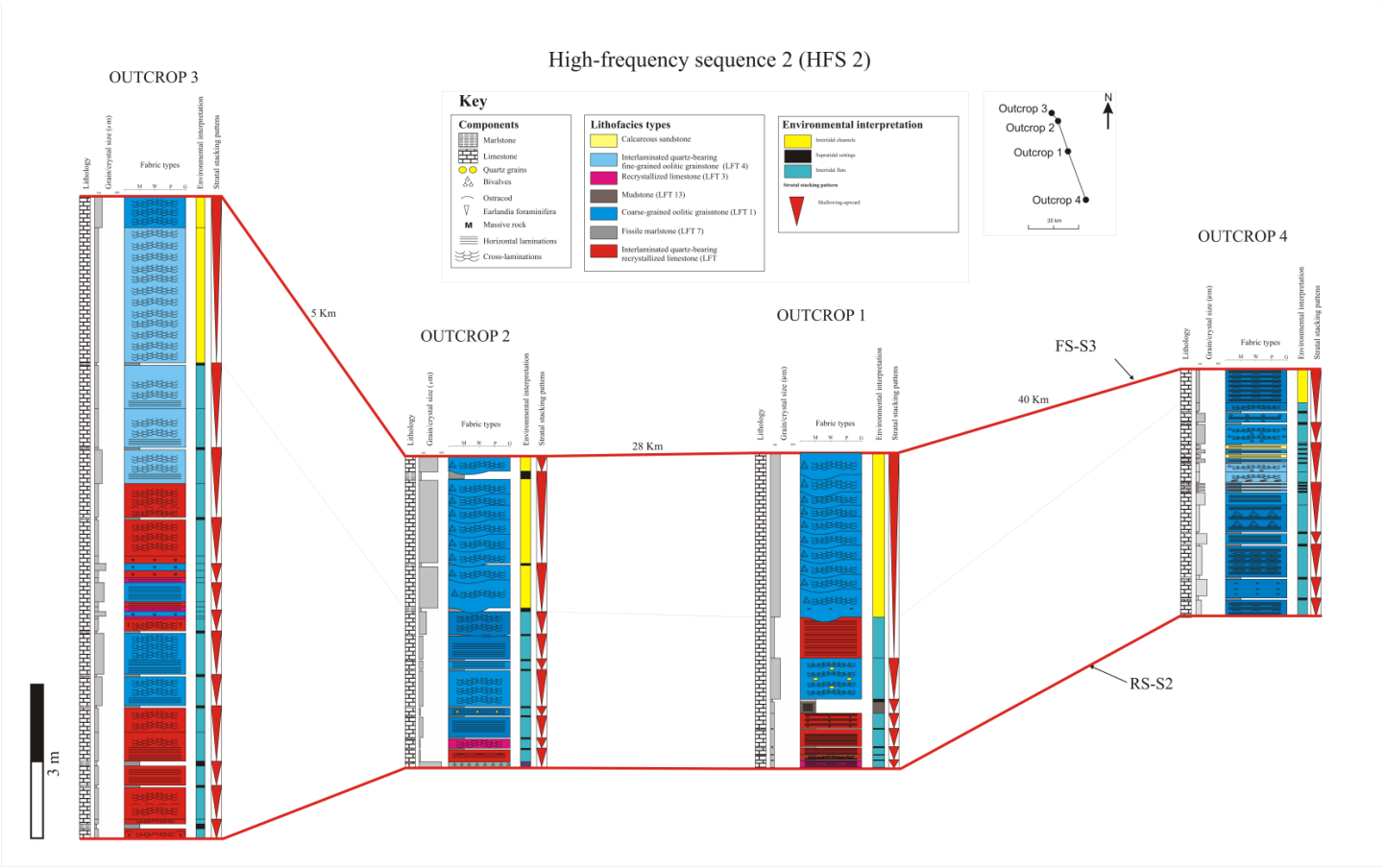

Figure 3.30. Regional correlation of the HFS 1 over the study area (70 km) showing the lateral lithofacies variation in the strike direction.

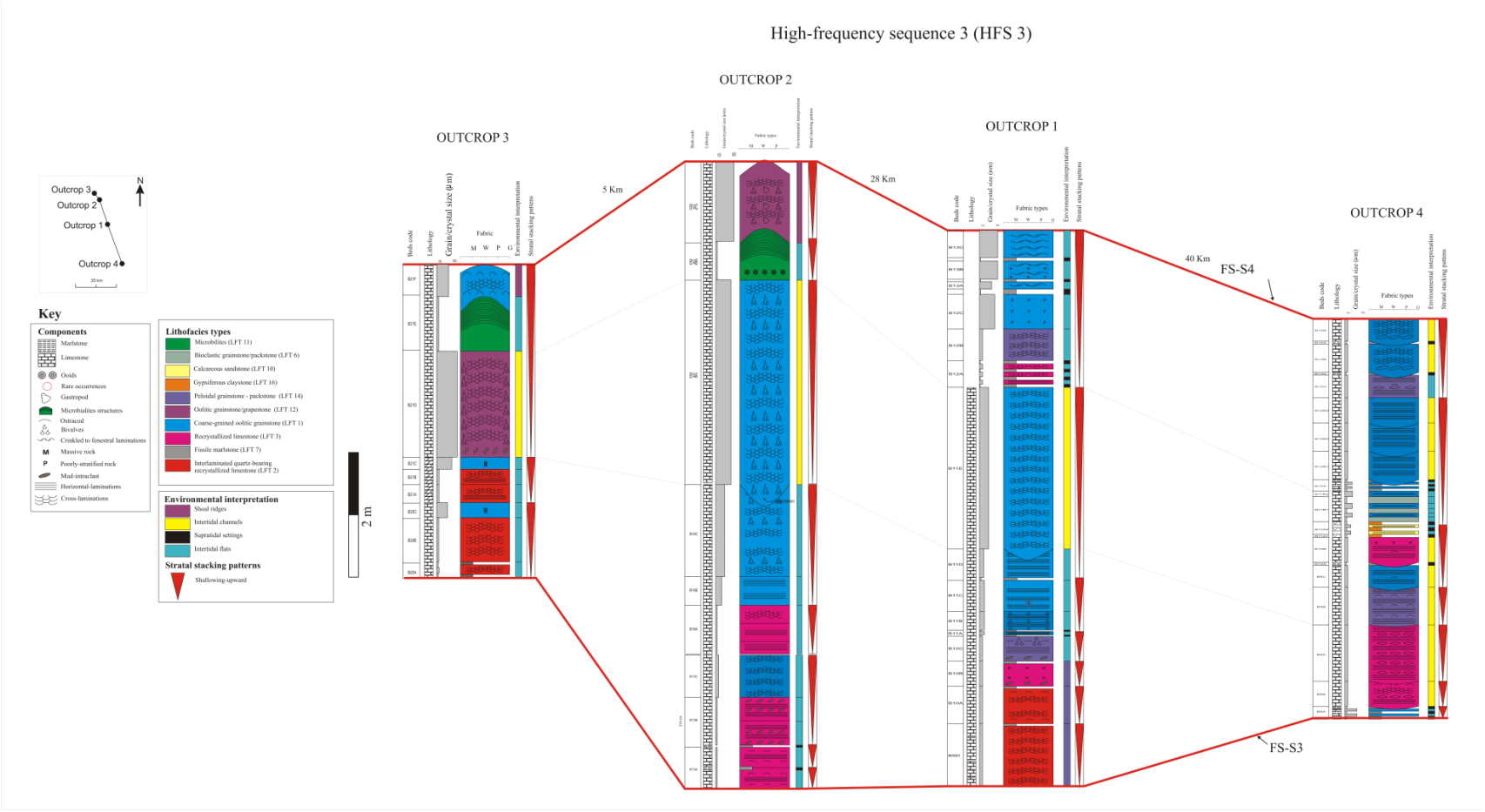

Figure 3.31. Regional correlation of the HFS 1 over the study area (70 km) showing the lateral lithofacies variation in the strike direction.

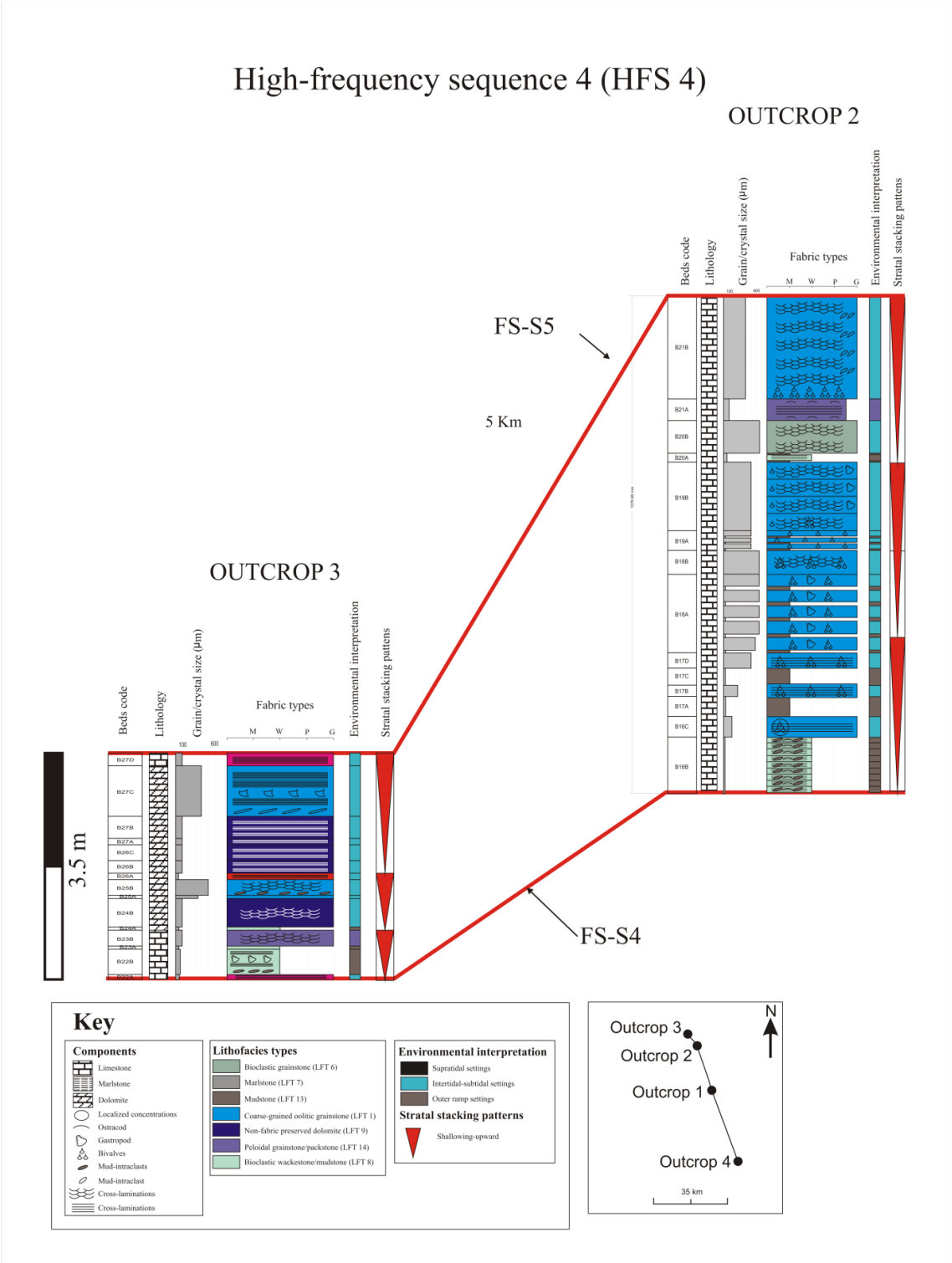

Figure 3.32. Regional correlation of the HFS 1 over the study area (outcrop 2 and 3) showing the lateral lithofacies variation in the strike direction.

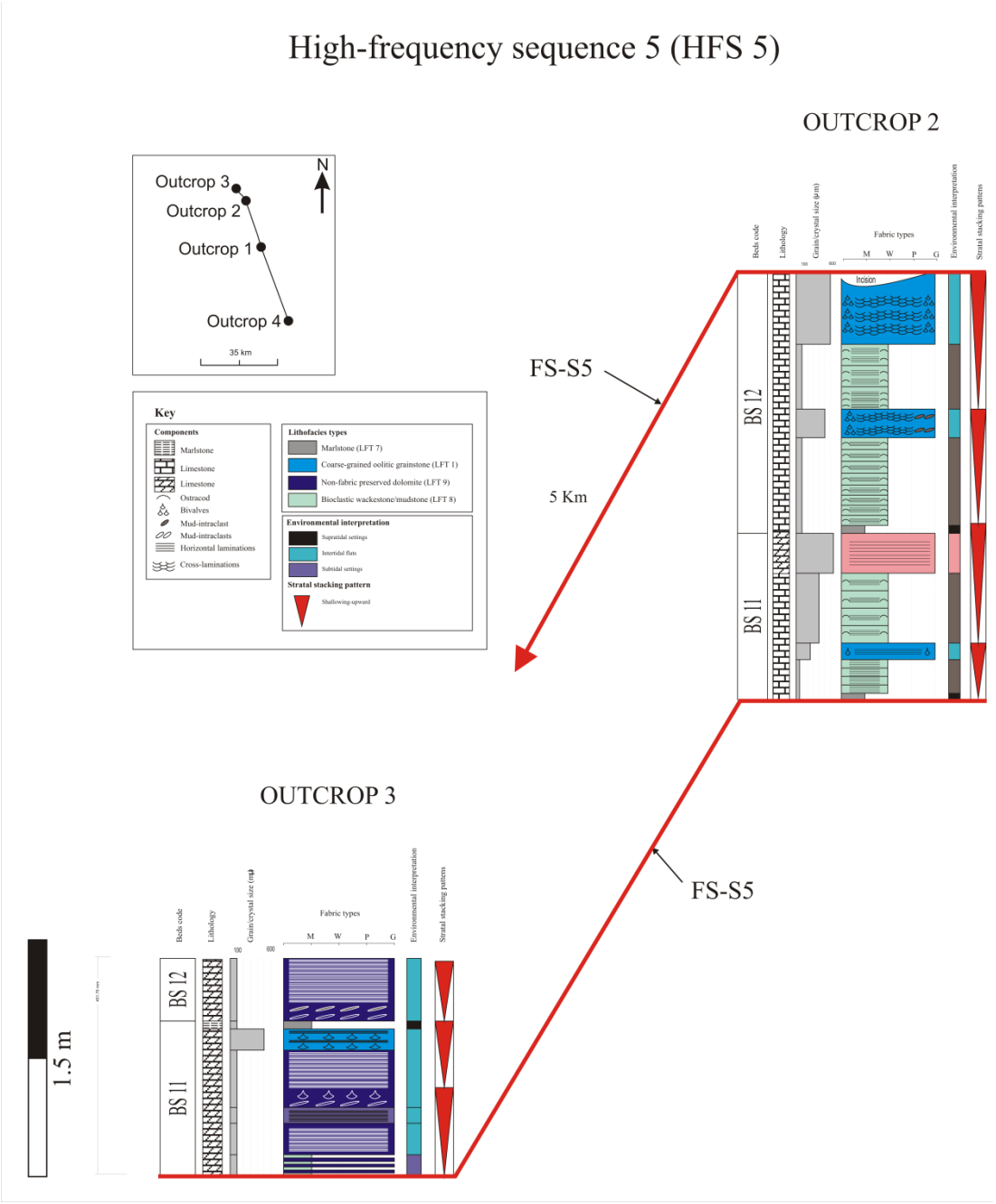

Figure 3.33. Regional correlation of the HFS 2 over the study area (outcrop 2 and 3) showing the lateral lithofacies variation in the strike direction.

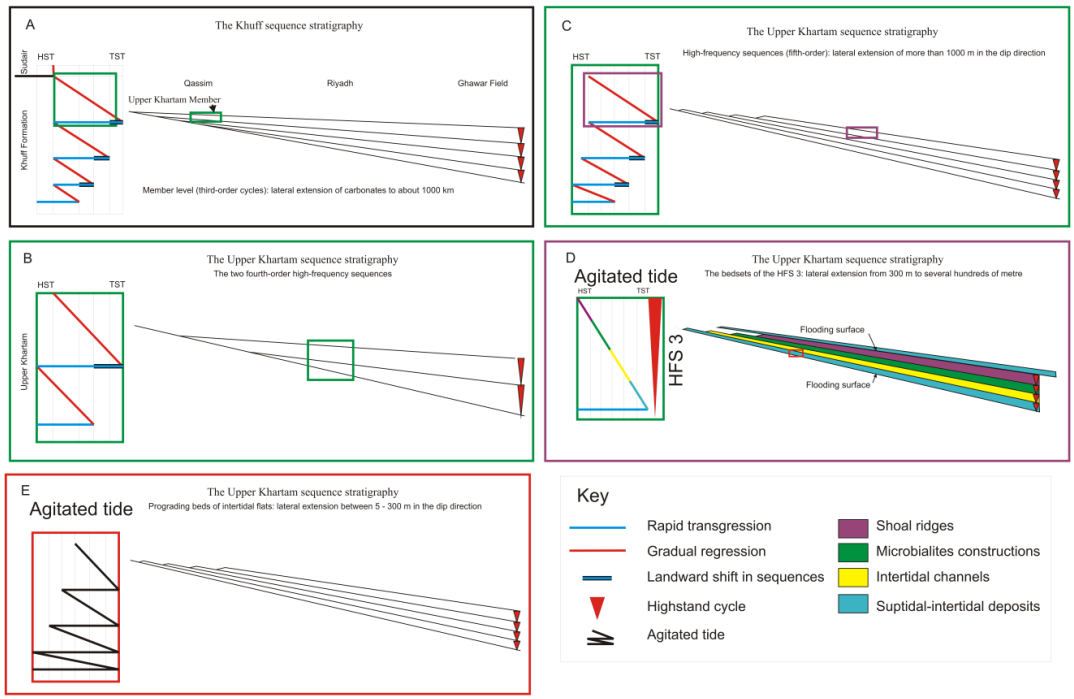

Figure 3.34. Sequence stratigraphic interpretation of the Upper Khartam Member, (A) extension of Member for great distance in the dip direction (1000 km), while fourth-order sequences, high-frequency sequences, bedsets, and beds in B, C, D, and E extend for respectively shorter distance. The mentioned lateral extension is for a single stratigraphic body. However this body possesses a genetic relationship with laterally amalgamated set of bodies. Essentially, the high-resolution stratigraphic build-ups are likely typified by regressive cycles dominated by regressive deposits followed pulses of transgressions. This nature is likely identical for the Upper Khartam (mostly third-order sequence) when compared with the Lower Khartam (mostly clayey and evaporitic deposits) and the boundary is characterized by thin (20 cm) skeletal accumulation. Note D) is the sequence stratigraphic interpretation of HFS 3, this sequence composed from bottom to top; subtidal-intertidal deposits, intertidal channels, microbialites construction, and caped by shoal ridges, indicating a shallowing-upward pattern.

CHAPTER 4

MICROPALEONTOLOGY

4.1. Overview

This work reports the first discovery of *Earlandia* foraminifera in the Early Triassic Upper Khartam Member of the Khuff Formation. The study area is located in central Saudi Arabia where four outcrop localities were logged in detail for sedimentology and micropaleontology. 300 samples were collected for detailed sedimentological and micropaleontological analysis. Of these, only six samples recovered *Earlandia*; these are dominantly observed in the interlaminated quartz-bearing recrystallized limestone lithofacies type. The *Earlandia* occur in associations with quartz grains, peloids, ooids, ostracods, bivalves, bryozoans, cephalopods, and stromatolites. The defined fossils of *Earlandia* are restricted to the lower fourth-order sequence of the Upper Khartam; where non-skeletal grains (mostly oolitic grainstones) are prevail. The skeletal grains along with the *Earlandia* occur as a thin (20 cm) transgressive lag. Furthermore, the regional occurrences of the *Earlandia* are consistent with the previously established high-frequency fifth-order sequences stratigraphic scheme, therefore, the *Earlandia* could be used as a biomarker for regional biostratigraphic correlation and enhance the high-resolution sequence stratigraphic correlations of the Upper Khartam Member. Essentially, the detailed sedimentological and micropaleontological analyse (*Earlandia*) indicates a plate-wide spread shallow epeiric sea. The latter is gently dipping and sporadically connected to the open marine system.

4.2. Introduction

The Neo-Tethys Ocean was formed as a result of a major continental rifting and crustal stretching took place in west Pangaea at the expense of the Paleo-Tethys (Al-Jallal, 1995; Alsharhan and Nairn, 1997; Sengör and Natalin, 1996; Ziegler, 2001). The opening of the Neo-Tethys Ocean was associated with the first regional marine transgression on the Arabian Plate and hence the first plate-wide development of a carbonate succession, henceforth called the Khuff Formation (1986 Alsharhan & Kendall; 1995 Al-Jallal).

The Khuff Formation crops out in central Saudi Arabia along a N-S belt that is 1200 km in length and 50 km in width (Figure **3.1**) (Powers, 1968). This formation was formally defined by Steineke et al. (1958) near Ayn Khuff. However, this formation was first described by Steineke and Bramkamp (1952). The formation unconformably overlies the Proterozoic basement of the Arabian Shield or lower Paleozoic deposits (Powers et al. 1966; Powers 1968). The upper contact is located at a sharp transition from limestone and dolomite below to red and green gypsiferous shale of the Sudair Formation. A complete stratigraphic section of the formation was described in Wadi Ar Rayn Quadrangle in Central Saudi Arabia (N: 24˚ and 23˚ and E: 46˚ 30″ and 45˚). The formation was revised and described in the Ad Dawadimi quadrangle in Central Saudi Arabia (N: 25˚ and 24˚ and E: 45˚ and 44˚30″) and was subdivided into five members: i.e. (from bottom to top) Ash Shiqqah, Huqayl, Duhaysan, Midhnab, and Khartam (Figure 1.3) (Delfour et al. 1982).

Generally, the Khuff Formation predominantly consists of low-energy carbonate and evaporite facies deposited in a relatively confined environmental setting (Vaslet et al.

2005). The latter authors subdivided the Khuff Formation into four depositional sequences (DS), i.e. (from bottom to top) Permian Khuff Huqayl (DSPKh), Permian Khuff Midhnab (DSPKm), Permian Khuff Khartam (DSPKk), and Triassic Sudair (DSTrS). Each of these sequences is characterized by a basal sequence boundary (SB), transgressive system tract (TST), maximum flooding interval (MFI), and highstand system tract (HST).

This study focuses on the Upper Khartam Member (represents the transgressive part of the DSTrS). The Upper Khartam Member is bounded at its bottom by the Permo-Triassic boundary and the thick supratidal to continental Midhnab Member (Vaslet et al. 2005), and bounded at its top by evaporites and clayey succession of the Sudair Formation. Recently, Adam et al (under review) established a detailed sedimentological and sequence stratigraphic models for the Upper Khartam Member. According to these authors, seventeen lithofacies types were defined, with oolitic grainstone, recrystallized limestone, bioclastic grainstone/packstone, and marlstone making up the bulk of the successions. These were deposited in seven depositional settings, including intertidal-subtidal flats, supratidal settings, intertidal channels and creeks, shoal ridges, reef complex, and outer ramp settings. Furthermore, four stratigraphic identities were defined, these include; beds, bedset, high-frequency fifth-order sequences, and fourth-order sequences. On the other hand, Vachard et al. (2005) systematically described the foraminifers of the Khuff Formation in Saudi Arabia. The later study recovered *Earlandia* from the Huqayl, Duhaysan, and Midhnab members, while the upper part of the Khartam Member recovered only Polarisella microfossis.

4.3. Results

Although 300 samples are collected from the studied interval, however, six samples recovered fossil *Earlandia*. These are dominantly composed of interlaminated quartz-bearing lithofacies type. The sedimentological characteristic of beds containing the *Earlandia* are illustrated in Plate 1 to 3 and described in table 1. Skeletal associations of *Earlandia* include; thin-walled ostracods, bivalves, cephalopods, bryozoans, and stromatolites. These in some place occurring as a transgressive lag deposits (Adam et al., under review). While non-skeletal associations include dominantly quartz grains and ooids and peloids.

Furthermore, the detailed sedimentological and the sequence stratigraphic analyse, Adam et al., (submitted) have defined two fourth-order sequences and six high-frequency fifth-order sequences. According to these authors, the lower fourth order sequence is dominated by non-skeletal grains (mainly oolitic grains) with sparse of skeletal fragments (bivalve and ostracods), while the upper fourth-order sequence is dominated by skeletal grains (manly bivalves and gastropods). Essentially, the fossil *Earlandia* occur predominantly in the lower fourth-order sequence. This may indicates some biochemical controls on the occurrence of the *Earlandia*. In addition to that, regional correlation of the high-frequency sequences is consistence with the regional distribution of *Earlandia*; therefore, the latter could be used as a biomarker for regional biostratigraphic correlation and enhanced high-resolution sequence stratigraphic correlations (Figure 4.1).

Essentially, the detailed sedimentological, sequences stratigraphic (Adam et al., under review), and the recent micropaleontological analysis (*Earlandia*) indicate a plate-wide spread epeiric sea. The latter is gently dipping (homoclinal platform) and

sporadically connected to the open marine system, and accordingly, agitated open marine periods are characterized by clean carbonates (thick successions dominated by oolitic and bioclastic grains), while *Earlandia*, thin-walled ostracods, and quartz grains are the characteristic of the confined giant sabkhas (Figure 4.2). Vachard et al. (2002) indicated setting similar in the sea of Taurus-Zagros-Saudi Arabia due to some barriers between the Abadeh region and Zagros in Iran.

Table 4.1. Sedimentological characteristics of the beds containing the fossils *Earlandia* foraminifera.

Bed code	**Lithofacies type**	**Sedimentological description**
COS1-B7A	Interlaminated quartz-bearing recrystallized limestone	This bed is about 12 cm and composed of interbedded pinkish skeletal packstone. Besides the quartz grains, skeletal fragments include bivalve, cephalopods, and bryozoan. Sedimentary structure is dominantly cross-laminations; the unit has variable thickness laterally.
COS1-B8E	Interlaminated quartz-bearing recrystallized limestone	this bed is 40 cm thick, light brownish in color, and composed of fine crystals of calcite, quartz grains (15%), and ostracods (<2%). Sedimentary structure includes thin-laminations.
COS2-B16A	Interlaminated quartz-bearing recrystallized limestone lithofacies type,	This bed is 26cm, reddish in color, and composed of three sets of interbedded grainstone and fissile mudstone (10, 2, and 6 cm respectively). The grainy beds are fossiliferous oolitic grainstone with quartz grain (ooids=75%, quartz=13%, bivalves=12%, and bryozoans and stromatolites), quartz grains are angular, moderately sorted, with size range from 10-50µm. Sedimentary structures include symmetrical wavy rippled and fenestral and swelling bodies.
COS3-B7B	Interlaminated quartz-bearing recrystallized limestone	The bed is 20cm thick, reddish in color, and composed of fine crystals of calcite and quart grains and few (<2) of ostracods. Quartz grains are angular, poorly-sorted, size of 25µm, scattered skeletal. Sedimentary structures include sigmoidally cross-lamination and horizontal lamination.
COS3-B9B	Interlaminated quartz-bearing recrystallized limestone	This bed is 57cm thick, pinkish in color, and dominated by fine crystals calcite, quartz grains, peloids, and ostracods. Sedimentary structures include horizontal laminations, planar cross-laminations (occasional).
COS3-B13B	Interlaminated quartz-bearing recrystallized limestone	This bed is 26cm thick, light pinkish in color, and composed of fine-crystal of calcite, quartz grains(>2%), and peloids. Sedimentary structure includes planar cross-laminations.

Plate 4.1. (Outcrop 1)

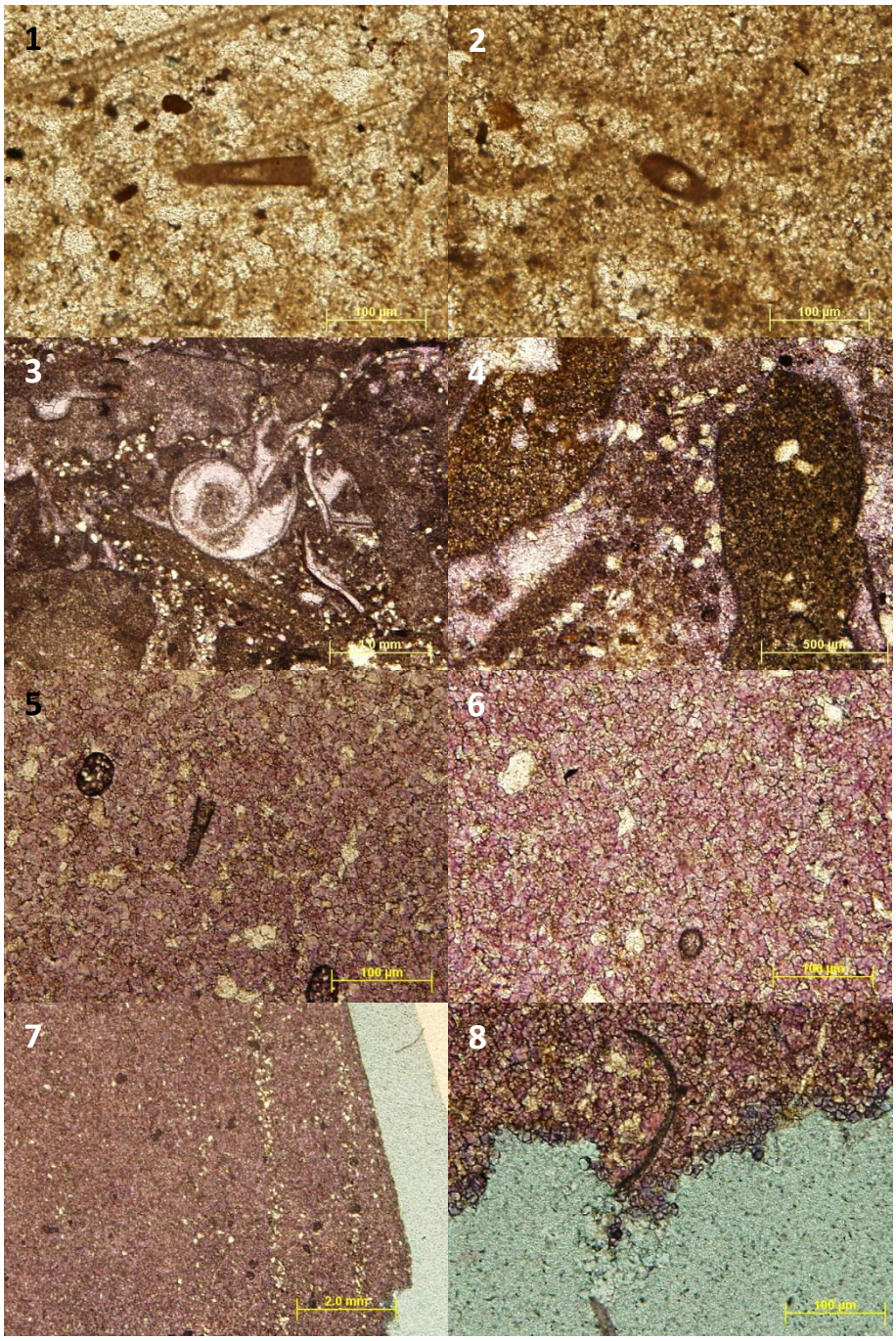

BED CODE: COS1-B7A (from 1.1 to 1.4): interlaminated quartz-bearing recrystallized limestone lithofacies type, the fossil *Earlandia* (1.1 = diagonal, 1.2 = cross section) occurring in association with quartz grains (1.3), bivalve (1.3), cephalopods (1.3), and bryozoan (1.4). BED CODE: COS1-B8E (from 1.5 to 1.8): interlaminated quartz-bearing recrystallized limestone lithofacies type, the *Earlandia* (1.5 = diagonal, 1.6 = cross section) occurring in association with quartz grains (1.7) and ostracod (1.8).

Plate 4.2. (Outcrop 2)

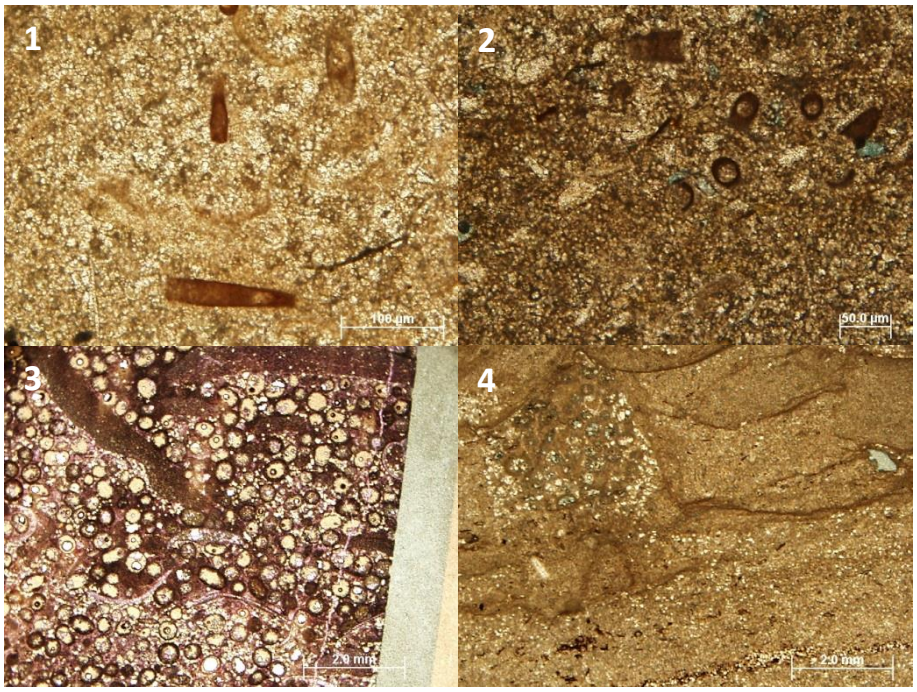

BED CODE: COS2-B16A (from 2.1 to 2.4), interlaminated quartz-bearing recrystallized limestone lithofacies type, the *Earlandia* (2.1 = diagonal, 2.2 = cross section) occurring in association with quartz grains (2.3), ooids (2.3), bivalve (2.3), bryozoan (2.3) and stromatolites (2.4).

Plate 4.3. (Outcrop 3)

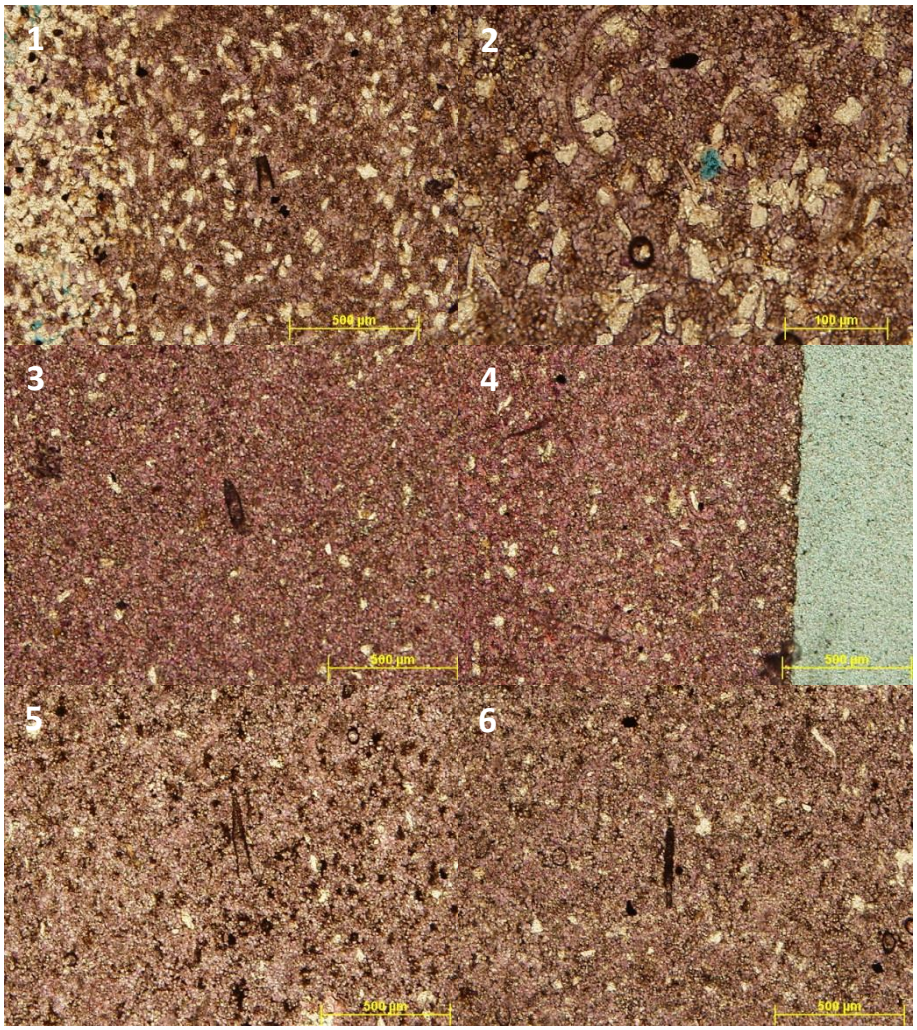

BED CODE: COS3-B7B (from 3.1 to 3.2): interlaminated quartz-bearing recrystallized limestone lithofacies type, the *Earlandia* (1 = diagonal, 2 = cross section) occurring in association with quartz grains (1 and 2), ostracod (2), BED CODE: COS3-B9B (3.3 and 3.4), interlaminated quartz-bearing recrystallized limestone lithofacies type, the *Earlandia* (3.3 = diagonal) occurring in association with quartz grains (3.4) and ostracods (3.4). BED CODE: COS3-B13B (3.5 and 3.6), interlaminated quartz-bearing recrystallized limestone lithofacies type, the *Earlandia* (3.5 = diagonal) occurring in association with quartz grains (3.6) and peloids (3.6).

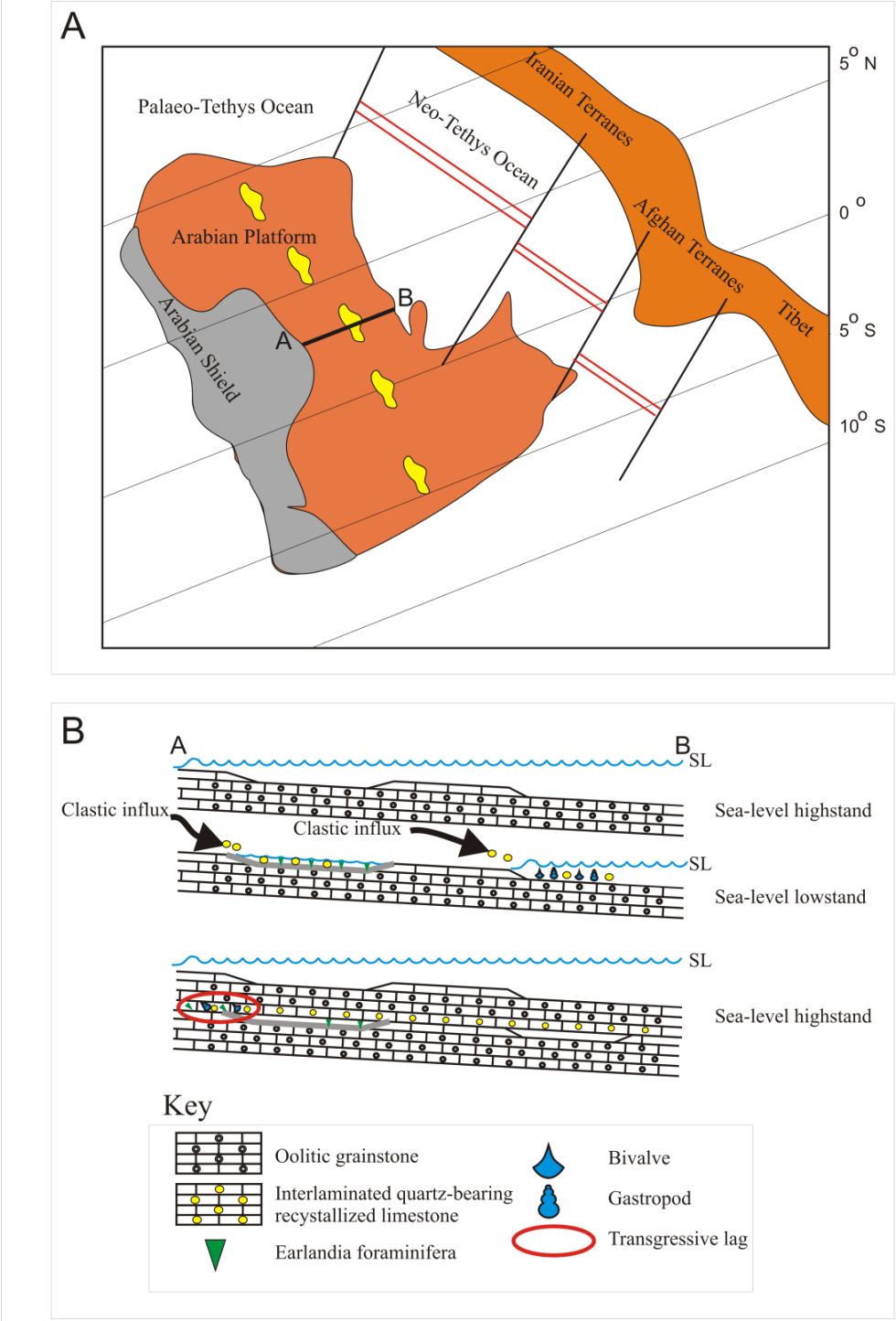

Figure 4.1. A) Palaeogeography of the later Permian (modified after Sharland et al., 2001), and B) palaeoenvironmental interpretation of the Upper Khartam Member (across A-B), oolitic grainstones are most likely prevailing during period of sea-level highstand, while, clastic influxes and *Earlandia* evolved during periods of sea-level lowstand in giant sabkhas.

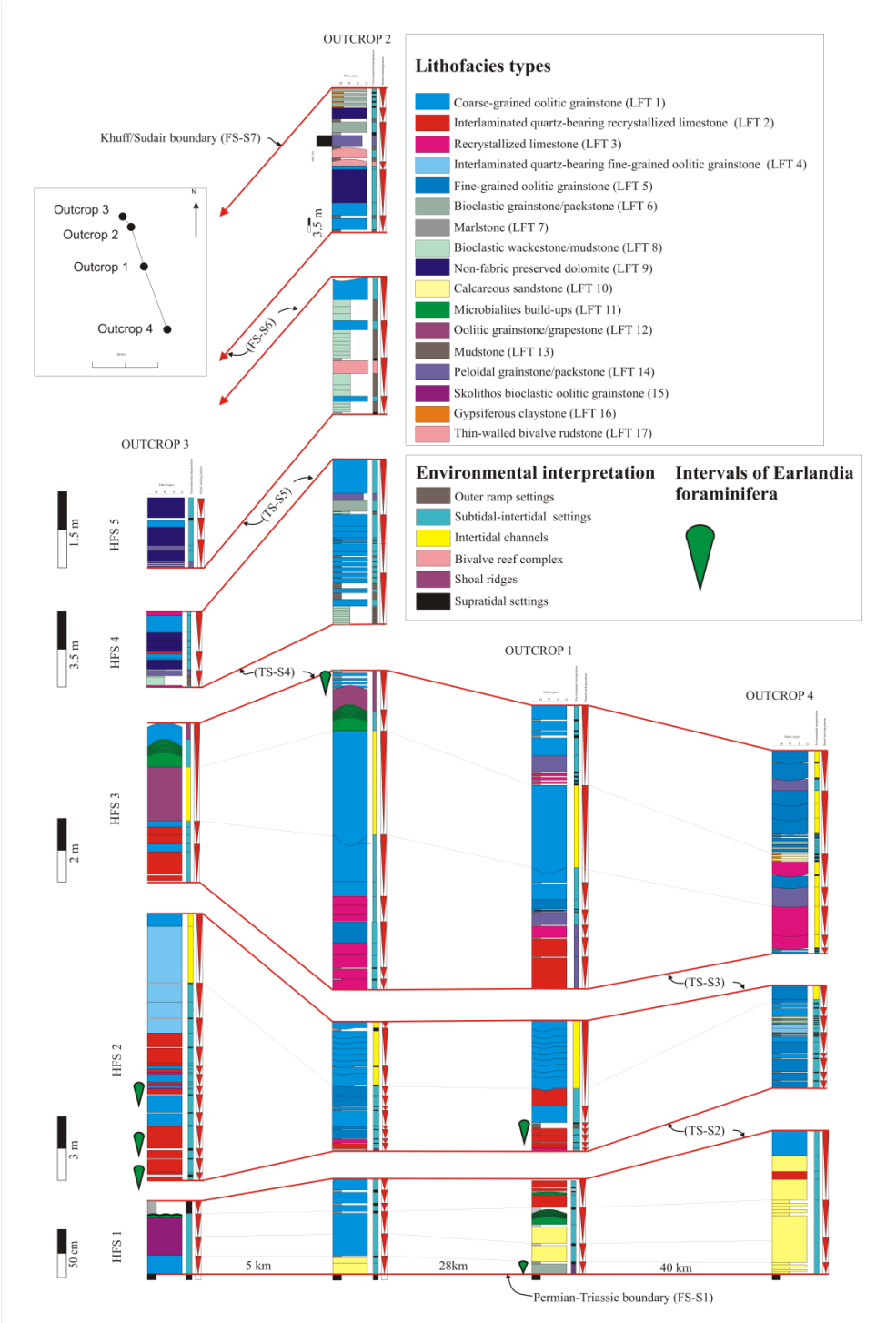

Figure 4.2. Regional correlations of the high-frequency sequences of the Upper Khartam Member (Adam et al., under review), the *Earlandia* are charactering the lower fourth-order sequence. Note the lower half of the High-frequency sequence 2 (HFS 2) yield *Earlandia* in its regional extent (over 40 km)

CHAPTER 5

RESERVOIR QUALITY AND HETEROGENEITY

5.1. Overview

The Khuff carbonates host several main gas reservoirs in the Middle East. These reservoirs are known for their complex heterogeneity, which is both of a sub-seismic scale and beyond the interwell spacing. To get a better insight in these reservoirs, the heterogeneity of the Upper Khartam Member, placed in a high-frequency sequence stratigraphic framework, was studied at a lateral resolution between logged sections of 5 m. The sedimentology and sequence stratigraphy of four outcrop localities were studied, and approximately 600 samples were collected for petrographic, porosity and permeability analyses.

The Upper Khartam Member is composed of seventeen lithofacies types, which are dominated by oolitic grainstone (40 %), recrystallized limestone (22%), bioclastic grainstone/packstone (4.4 %), and non-fabric preserved dolomite (2.4%). These lithologies occur in the form of sheet-like and channelized bodies that were deposited during periods of sea-level highstand, most probably transitioning laterally from intertidal to subtidal to reach finally deeper marine settings. Six major diagenetic processes could be differentiated in the studied outcrops, namely: dissolution, pore lining and pore blocking calcite cementation, dolomitization, fracturing, and stylolitization. Dissolution occurs in the form of partial dissolution creating molds and vugs, and is likely the result of intensive circulation of meteoric water undersaturated

with respect to calcite. Significantly, cementation has blocked most of the original intergranular porosity. Pore lining detrital clay severely impacted reservoir permeability and complicated the pore geometry. Dolomitization is associated with the upper Khuff–Sudair boundary, and is believed to be the result of an influx of water highly saturated with Mg^{+2} that developed during the deposition of the Sudair evaporites. The stylolites are controlled to a major extend by lithofacies and geobody configuration; they are relatively abundant in fine-grained oolitic grainstones occurring as sheet-like bodies when compared to coarse-grained oolitic grainstone occurring as channelized bodies. Ten porosity types could be differentiated in the studied outcrops, namely: intergranular, intragranular, shelter, dissolution-enlarged, moldic, vuggy, micro-porosity, and porosity in relation to dolomite–dedolomite, dolomite-leaching, and fracture development. The oolitic grainstones of the intertidal sheets, intertidal creeks, and intertidal channels are dominated by dissolution, moldic, and vuggy porosity, whereas intercrystalline and fracture porosity prevails in the recrystallized limestone. The interplayed diagenetic processes have impacted the ultimate reservoir quality. For example, the fine-grained oolitic grainstone have been relatively less impacted compared to coarse-grained oolitic grainstone. This was attributed to the pore-filling dolomites of the coarse-grained oolitic grainstone, while no dolomite was observed in the fine-grained oolitic grainstone. Furthermore, the intertidal creeks are characterized by a complex and heterogeneous pore geometry compared to the intertidal channels, and this can be attributed to the geobody architecture, with intertidal creeks being composed of dense and small tidal creeks (1 m in length and 20 cm in thickness), and intertidal channels composed of thick amalgamations of intertidal channels (5 m by 50 cm). Most critically, reservoir quality of the studied reservoir units along their lateral extension, as defined in their sequence

stratigraphic framework, was influenced differentially by diagenesis, which resulted in a lateral segmentation of single bodies into different, hydraulic units. XRD data show a control of certain mineralogical associations (such as SiO_2 and $SrSO_4$) on the lateral intermittence of the intra-reservoir body. SEM observations reveal a textural control on porosity and permeability. The differential mold-filling calcite cements of the oolitic grainstones of the intertidal sheets and channels have significantly reduced porosity and permeability. Generally, mineral content has little impact on the reservoir quality, although clay minerals have played a central role in lining the pore space and affecting reservoir quality. Overall, the lateral segmentation most likely was caused by a differential diagenetic evolution, and most critically, this evolution seems to have been controlled by fractures and stylolites which respectively acted as conduits to and barriers for vertical fluid flow and, hence, controlled the differential cementation and dissolution processes.

5.2. Introduction

The key question when addressing reserve estimations and propose improved productivity is to quantitatively assess reservoir heterogeneity. This includes the identification of geobody architecture and quality elements such as porosity and permeability of the reservoir building blocks at scales ranging from pore-geometry to inter-well spacing. Obviously, this range cannot be covered by subsurface data alone. Generally, outcrop analogues provide valuable insight into ancient sedimentary processes and products (Grammer et al., 2004; Pringle et al., 2006). Outcrop studies have been utilized widely to understand critical quality and reservoir geobody architecture (Smith and Read, 1999; Grammer et al., 2004; Koehrer et al., 2010, 2011,

2012; Zeller et al., 2011; Jung and Aigner, 2012; Alnazghah et al., 2013; Haase and Aigner, 2013; Walz et al., 2013). In addition to processes affecting sedimentary rock composition such as biological evolution, sea-level fluctuation, paleo-position, and tectonic overprinting, diagenetic alteration is one of the important critical factors on reservoir heterogeneity.

The Khuff reservoirs in Eastern Arabia are estimated to contain about 15%–30% of the World's gas reserves (Al-Jallal, 1995; Al-Aswad, 1997; Koehrer et al., 2010). These reservoirs are known for their complex heterogeneities at the inter-well scale that is clearly beyond the resolution of seismic data (Janson et al., 2013). Therefore, optimum exploitation of these reservoirs is highly dependent upon understanding primary internal geobody architecture and reservoir heterogeneity, which are controlled by syn-depositional processes and subsequent diagenetic overprinting. Outcrop equivalents of these reservoirs in central Saudi Arabia provide a complete stratigraphic context, where thin reservoir analogue bodies can be traced laterally over large distances, genetically related to the vertical stratal stacking patterns, and logged for porosity and permeability.

The main objective of this study is to characterize the reservoir heterogeneity of the Upper Khartam Member within a previously established primary stratigraphic framework (Adam et al., under review) at a lateral sampling spacing of about 5 m. At this scale, the existing seismic and inter-well limitations can be overcome. The Upper Khartam Member was described to be equivalent to the Khuff-A and B reservoirs in Eastern Arabia (Janson et al., 2013). Therefore the results of this study will provide essential quantitative guidance for a better understanding of the intra-reservoir heterogeneity of the Khuff reservoirs. Four outcrop sections were logged from

sedimentological and sequence stratigraphical point of view. Approximately 600 samples were collected and measured for porosity and permeability. In addition reservoir quality index (RQI), normalized porosity (Φ_z), and the flow zone indicator (FZI) were calculated and used in this study (modified after Amaefule et al., 1993).

5.3. Database and methods

Four outcrops were logged from sedimentological, sequence stratigraphical, and macro-diagenetical point of view. These outcrops are located in the Buraydah and Faydah quadrangles in central Saudi Arabia and they mostly occur along road-cuts (Figure 3.1A and C). Outcrop 1 is located in the central Buraydah quadrangle along the Qassim–Riyadh highway. Outcrop 2 is located northeast of Buraydah City along the Qassim–Hail highway about 28 km to the north of outcrop 1. Outcrop 3 occurs about 5 km to the north of outcrop 2. Outcrop 4 is located in the Al Faydah quadrangle in Jal Al Khartam, about 80 km to the south from the northernmost outcrop 3. Based on the outcrop investigation, a high-frequency sequence stratigraphic model was established (Adam et al., under review). Approximately 600 samples were collected and subsampled for porosity and permeability measurements and petrographic analysis. Porosity was measured using a helium porosimeter on core plugs 1 inch in diameter and 2 inches in length, while liquid (nitrogen) permeability was obtained from gas permeability and verification of the Klinkenberg effect using a Hassler Core Holder assembly. In addition, selective samples were prepared for XRF, XRD, SEM, and EDS analyses. Samples were collected in both vertical and lateral directions. The sampling along vertical transects was designed to investigate the vertical reservoir heterogeneity and was based on the earlier established high-frequency stratigraphic

scheme. The lateral transects sampling along bedding aimed to examine the horizontal intra-reservoir heterogeneity within inter-well space. Therefore, a single unit was followed laterally and sampled log-interval occur at intervals of 5 m. Respectively, lateral distances of 100 m and 600 m were covered in outcrop 1 and 2, and the sampled bodies include B9B, B10A, B11E, B12C, and B13C from outcrop 1, and B12B, B14C, B15B, and B20B from outcrop 2 (Figure 5.1). Plugs were always measured perpendicular to bedding.

Amaefule et al. (1993) proposed a method for the identification and characterization of hydraulic units. This method suggests that for any hydraulic unit, a log–log plot of the reservoir quality index (RQI) versus normalized porosity (Φz) should yield a straight line with a unit slope, where the RQI is equal to $0.0314\sqrt{k/\Phi}$, and Φz is equal to Φ/ (1 – Φ). The intercept of the unit slope line with Φz = 1, designated as the flow zone indicator (FZI), is a unique parameter for each hydraulic unit. A hydraulic (pore geometrical) unit is defined as the representative elementary volume (REV) (Bear, 1972) of "total reservoir rock within which geological and petrophysical properties that affect fluid flow are internally consistent and predictably different from properties of other rock volume" (Ebanks, 1987). This method has been successfully tested in both clastic and carbonate plays (Amaefule et al., 1993). Accordingly, variations in pore geometrical attributes define distinct hydraulic units with specific fluid-flow characteristics. The FZI is a unique parameter that incorporates the geological attributes of texture and mineralogy in the discrimination of distinct hydraulic units (Amaefule et al., 1993). This approach was supported by the excellent correlation between FZI and irreducible water saturation, surface area, and content of fine-grained samples, with grain size less than 30 microns (Amaefule et al., 1993).

Generally, fine-grained sediments exhibit high surface area and high tortuosity, hence low FZI. On the other hand, coarse grained and well-sorted sands exhibit lower surface areas, lower shape factor, lower tortuosity, and higher FZI values. In carbonate rocks, this could be linked to depositional environments and diagenetic processes, which control pore geometry and hence FZI. Corbett and Potter (2004) introduced the global hydraulic element (GHE) defined as intervals between specific values of FZI extracted from a wide range of possible combinations of porosity and permeability. The FZI values of the latter authors and their concept of the "GHE map" have also been adopted in this study, however, using a different visual representation. The Baker and Bloomer (1988) chart was used to estimate the original porosity and permeability of the unconsolidated sediment immediately after its deposition and hence extracting the corresponding original RQI, Φz, and FZI values.

5.4. Results

5.4.1. Lithofacies, diagenesis, and porosity analysis

The entire succession of the Upper Khartam is strongly affected by meteoric diagenesis, however, most of the lithologies preserve their original texture, except for the recrystallized lithofacies types that are composed of fine-crystalline limestone. Six diagenetic processes and ten porosity types are identified and described below within the early established lithofacies frame (Adam et al., under review). According to their properties (porosity and permeability) the lithofacies types are subdivided into two groups A and B. Group A indicates the lithofacies types representing good reservoirs while group B correspond to the non-reservoir lithofacies. Accordingly, the lithofacies

types, diagenetic processes, and porosity types are summarized in Table 5.1 and illustrated in Figure 5.2 to 4.

Group A: Reservoir lithofacies types

5.4.1.1. Coarse-grained oolitic grainstone (LFT 1; 39.5 %)

Well-sorted and well-rounded coarse-grained oolitic grainstone, with a light beige and light pinkish colour is a dominant lithology in the studied sections. Ooids range in size from 50 to 600 µm. Few (less than 5%) quartz grains are scattered. Bioclastic fragments include bivalves, gastropods, ostracods, brachiopods, and sparse of Earlandia foraminifera. Sedimentary structures include dominance of cross-laminations such as cross-herringbone, tidal bundle, planar, hummocky, and sigmoidal, trough-cross laminations, and symmetrical ripples. Rib-up mud intraclasts, localized quantities of imbrication structures, and reactivation surfaces are also observed. Units of this lithofacies occur predominantly as relatively large channel-like bodies of about 3 m width and 50 cm thick. Even though, smaller channel-like bodies of less than 1 m width and 30 cm thickness also exist. Locally the channelized bodies are associated with microbialitic build-ups. Internally fissile marlstone and stylolitic surfaces may occur, evolving one into the other. This lithofacies is recognized in three environmental settings, i.e. intertidal channels and creeks and intertidal flats.

The dominant diagenetic processes affecting this lithology include cementation, dissolution, stylolitization, fracturing, and sparse dolomitization. Cementation occurs as blocky calcites and iron-rich calcite, mosaic calcite, and sparse calcite cements rimming some particles. Dolomitization is occurring as pore-filling phases as well as cements and is limited to the upper section of the studied interval, near the Khuff-

Sudair boundary and the intertidal channels underlying microbialites build-ups. Porosity types include dominantly moldic and vuggy porosity and intergranular, intragranular, intercrystalline, and micro-fracture porosity. Molds are partially filled with calcite and dolomite.

5.4.1.2. Interlaminated quartz-bearing recrystallized limestone (LFT 2; 13.8 %)

Interlaminated quartz-bearing recrystallised limestones, possessing a light beige to dark pinkish colour and containing ostracods, Earlandia foraminifera and bird-eyes structures is a common lithology in the studied sections. Quartz grains are angular, well-sorted, and range in size from 5 to 20 µm. Their abundance ranges from 15 to 40 %. Sedimentary structures include horizontal laminations and cross-laminations (planar, sigmoidal, herringbone). This lithofacies occurs in association with marlstones. Units of this lithofacies occur predominantly as sheet-like bodies, 2 to 10 cm in thickness. A complex amalgamation of channel-like bodies is locally observed, possessing an average width and thickness of about 1 m and 20cm, respectively. This lithofacies was interpreted to reflect deposition in intertidal-subtidal flats and in intertidal creeks.

The dominant diagenetic processes include recrystallization and occurrences of stylolites and fractures. Lateral bifurcation by stylolites is common. Recrystallization gives rise to blocky and mosaic calcite textures and rare Fe-rich rimming calcite cement and replacive dolomites are also observed. The fractures are vertical, rarely oblique and are filled with calcite. Porosity types include dominance of intercrystalline porosity and occurrences of micro-fractures, vuggy, burrow, and shelter porosity.

5.4.1.3. Recrystallized limestone (LFT 3; 8.9 %)

This lithofacies is composed of fine-crystalline limestone. Bioclastic fragments mostly consist of ostracods with presence of Earlandia foraminifera and localized occurrences of mud-intraclasts with locally some vertical and horizontal bird-eye structures. Sedimentary structures consist dominantly of thin-horizontal laminations with rare cross-laminations (e.g. hummocky cross-laminations and minor reactivation surfaces). This lithofacies occurs in association with marlstone and laterally merges with carbonate mudstone. This lithofacies occurs as complex amalgamation of sheet-like bodies, with individual sheets having an average thickness of 5 to 20 cm and lengths ranging from 5 m to several hundreds of metres. Complex amalgamations of channelized bodies are also observed, with individual channelized bodies being about 1 m in width and 30 cm in thickness. This lithofacies reflects deposition in a subtidal-intertidal setting or in intertidal creeks.

The dominant diagenetic processes affecting these strata include recrystallization, fracturing and stylolitization. Recrystallization gives rise to a blocky fabric (average crystal size of 30 µm) and mosaic calcite textures with sparse dolomitization. Stylolites are horizontal while fractures are dominantly vertical or oblique. The latter are filled with calcite. Porosity types include intercrystalline, vuggy and fracture porosity.

5.4.1.4. Interlaminated quartz-bearing and fine-grained oolitic grainstone (LFT 4; 7.1 %)

The interlaminated quartz-bearing and fine-grained oolitic grainstone is light beige in colour. Quartz grains occur within laminae and ranges in contents from 1 to 10%. They are angular and well-sorted, and grain sizes vary around 50 µm. Bivalve

fragments are present as well as localized occurrence of mud-intraclasts. Ooids are well-rounded and well-sorted with average grain size of 75µm. Sedimentary structures include horizontal laminations and cross-laminations (sigmoidal to planar). Beds of this lithofacies occur as relatively uniform, flat, and continuous sheet-like bodies, ranging laterally from 50 to 150 m and having an average thickness of about 20 cm. The layers are internally crosscut by bed parallel stylolites and fissile marlstone. This lithofacies was deposited in intertidal-subtidal settings.

The diagenetic processes affecting these strata include dissolution, cementation, and stylolization. The cementation occurs as blocky and mosaic calcitic cement. Porosity types include moldic, intergranular, and vuggy porosity; molds are filled with detrital clay minerals and anhydrite.

5.4.1.5. Fine-grained oolitic grainstone (LFT 5; 5.9 %)

The fine-grained oolitic grainstones are light beige to pinkish in colour and are composed of pure and homogeneous oolitic grains which are well-sorted and well-rounded, with their size ranging from 20 to 100 µm. Sparse bivalve fragments also occur. Sedimentary structures include thin laminations and planar cross- and sigmoidal cross-laminations. This lithofacies occurs predominantly as sheet-like bodies. Units of this lithofacies are intensively affected by bed parallel stylolites and interlayered marlstone laminae. This lithofacies was deposited in intertidal-subtidal settings.

The diagenetic processes include dissolution, cementation, stylolitization, and fracturing. Cementation occurs as blocky and mosaic calcitic cements with sparse occurrences of iron-rich calcitic cement, the crystals are relatively large with average

sizes of 150 µm. Fractures are vertical and filled with calcite cements. Porosity types include moldic porosity, vuggy, intergranular, and intercrystalline porosity. Molds were partially filled with calcitic cements resulting in a relatively high porosity compared with the blocked molds of the LFT 4.

5.4.1.6. Bioclastic grainstone/packstone (LFT 6; 4.4 %)

The bioclastic grainstone/packstone is dark pinkish to light beige in colour. Bioclasts dominantly consist of bivalves with gastropods and single occurrences of Earlandia foraminifera. The bioclastic components are about 2 mm in size and they have no definite orientation. This lithology also contains oolites and quartz grains. The oolites are well-rounded and well-sorted, and range in size from 500-200µm. Sedimentary structures include abundant cross-laminations such as herringbone and trough cross-lamination and abundant mud-intraclasts displaying imbricated structures and sometimes thin laminations. The lithofacies occurs as sheet-like bodies, which ranges in length from 50 to 200 m, and their thickness varies between 20 and 40 cm. This lithofacies was deposited in intertidal-subtidal settings.

The diagenetic processes include cementation, dissolution, and dolomitization. Cementation occurs as blocky calcite cements and dolomitic cements (20-40 µm in diameter). Dolomitization is occurring near the Khuff-Sudair boundary. Porosity types include intergranular, moldic, vuggy, intragranular, and intercrystalline porosity, as well as the presence of vertical and horizontal fractures.

5.4.1.7. Bioclastic wackestone/mudstone (LFT 8; 2.8 %)

The bioclastic wackestone/mudstones are light beige in colour and contain localized mud-intraclasts. Ostracods are present. Sedimentary structure is dominated by thin

laminations. Beds of this lithofacies occur as wavy symmetrical and uniform, and continuous sheet-like as well as lenticular bodies. They can be followed from 5 m to several hundreds of metres and they range in thickness from 20 to 40 cm. This lithofacies was deposited in a outer-ramp setting.

The diagenetic processes include micro-cementation and fracturing. The fractures are vertical and filled with calcite. Porosity type includes fracture, intercrystalline, and vuggy porosity.

5.4.1.8. Non-fabric preserving dolomite (LFT 9; 2.4 %)

The non-fabric preserving dolomite is reddish, greenish, yellowish, and beige in colour. Sedimentary structures includes large imbricated structures and horizontal and planar cross-laminations. This lithofacies is restricted to the upper part of the studied interval. Units of this lithofacies occur as sheet-like bodies of uniform, flat, horizontal, and continuous geometry. Individual sheet ranges in length from 5 m to several hundreds of metres displaying thicknesses ranging between 5 and 20 cm. This lithofacies was deposited in intertidal-subtidal settings.

Obviously, the prominent diagenetic process corresponds to dolomitization, obliterating the original fabric and destructing the original grain-types. The dolomite crystals range in size from 30 to 100 µm. Fractures are also observed and they are filled with dolomite and calcite cements. Porosity type is dominantly intercrystalline porosity and dolomite-leaching (calcite and iron-rich calcite partially fills-up the leached dolomite) as well as vuggy porosity (up to 1 cm in diameter).

5.4.1.9. Calcareous sandstone (LFT 10; 2.7 %)

The calcareous sandstone is reddish in colour, and contains a quantity of spicule-like bioclasts (5%), as well as mud-intraclasts. It is intensively bioturbated. The quartz grains are angular, well-sorted, and range in size from 75 to 250 μm. Sedimentary structures dominantly consist of thin laminations with fenestral, lenticular, and crinkled laminations and rare cross-lamination. This lithofacies is associated with reddish/grayish claystone and quartz arenite within coarsening-upward sequences. They display flat and horizontal geometry. They do not so commonly occur. This lithofacies was deposited in intertidal-subtidal settings.

The diagenetic process includes calcite cementation with preserved intergranular porosity.

5.4.1.10. Microbialites build-ups (LFT 11; 2.1 %)

The microbialites are reddish to pinkish in colour and contains ooid grains (up to 20%) and scattered quartz grains as well as bioclast fragments. The microbialite build-ups have an average lateral separation distance of about 15m, and they range in size from 20 to 100 cm. This lithofacies marks intertidal settings.

Diagenetic processes include recrystallization with the development of mosaic calcitic textures possessing some intercrystalline porosity.

5.4.1.11. High-angle cross-laminated oolitic grainstone/grapestone (LFT 12; 2.1 %)

The high-angle cross-laminated oolitic grainstone/grapestone occurs in association with microbialite build-ups and mudstone lithologies. It contains a quantity of broken bioclasts. Oolitic grains are well-rounded, moderately sorted, and range in size from

500-1000 µm. Sedimentary structures includes high-angle cross-lamination and imbrication structures of mud intraclasts. Units of this lithofacies occur as convex bodies. This lithofacies was deposited in mobile shoal ridges.

The diagenetic processes include dissolution and cementation, the latter giving rise to blocky calcite cements. Porosity types include intergranular, moldic, and vuggy porosity.

5.4.1.12. Peloidal grainstone to packstone (LFT 14; 1.4 %)

The peloidal grain- to packstones are light beige to yellowish in colour. They contain a number of mud-intraclasts, ranging in size from 1 to 2 mm, and are associated with mud-lenses. Localized concentrations of bioclast fragments, mostly bivalves exist. Sedimentary structures include horizontal to lenticular and crinkled laminations with presence of bird-eye structures. Beds of this lithofacies occur as laterally uniform, horizontal, and continuous sheet-like bodies ranging in length from 5 to 200 m and thickness varying from 5 to 40 cm. This lithofacies reflects subtidal settings.

The diagenetic processes affecting these lithologies include cementation which occurs as mosaic calcitic cements. Vertical fractures filled with calcite cements also are of interest. Porosity mainly consists of micro-intercrystalline porosity.

5.4.1.13. Skolithos bioclastic oolitic grainstone (LFT 15; 0.8 %)

The Skolithos bioclastic oolitic grainstone is red in colour and is intensively bioturbated containing a quantity of skolithos, bioclastic fragments, and mud-intraclasts. Ooids are poorly-sorted. Sedimentary structures include thin laminations and cross-laminations. This lithofacies was deposited in intertidal settings.

Porosity types include dominantly moldic and vuggy porosity and intergranular, intragranular, intercrystalline, and micro-fracture porosity.

5.4.1.14. Thin-walled bivalve rudstone (LFT 17; 0.5 %)

The bivalve rudstone is pinkish to reddish in colour and it consists predominantly of *placunopsis ostracina* bivalve with sparse ostracods. This lithofacies is similar to that of the Middle Triassic Muschelkalk sequence of Central and Western Europe. The *placunopsis ostracina* is about 2 mm in size and they are horizontally oriented. This lithofacies also contains mud-intraclasts. The described sedimentary structures consist of crinkled to fenestral laminations. This lithofacies occurs as sheet-like bodies ranging in length from 5 m to several hundreds of metres and they have thickness ranging from 5 to 30 cm. They are characterised by a complex convex geometry. This lithofacies was deposited as intertidal reef complexes.

The dominant diagenetic process includes dolomitization, where the micritic envelope prevents the original fabric to be destructed. Replacive dolomite phases have average sizes of about 30µm. Porosity types include intercrystalline, intergranular, moldic and vuggy porosity.

Group A: Non-reservoir lithofacies types

5.4.1.15. Marlstone (LFT 7; 3.0 %)

Marlstones occur as thin grayish compact interbeds, and forms important stratigraphic units which form marker units in the sequence stratigraphic interpretations of the Upper Khartam Member (Adam et al., under review). Importantly, it acts as main source for clay minerals that infiltrated into underlying grainy beds, affecting reservoir quality. This lithofacies was deposited in supratidal settings. The geochemical analysis

of this lithofacies indicates high content of Si, Al, Fe, Ca, and Sr; these associations most likely reflect their fine-grained quartz and, clay mineral composition together with celestine.

5.4.1.16. Mudstone (LFT 13; 1.6 %)

The mudstones are beige to yellow in colour and sometimes contain anhydrite crystals. Sedimentary structures consist dominantly of thin lamination with localized imbrication structures. This lithofacies occurs as thin interbeds of sheet-like bodies ranging in thickness from 5 to 10 cm and they can laterally be followed over 20 to 100 m. The sheets are described to be flat, uniform, and continuous. This lithofacies was deposited in outer-ramp settings.

5.4.1.17. Gypsum and gypsiferous claystone (LFT 16; 0.5 %)

The gypsum and gypsiferous claystone possesses a clayey matrix in which clean recrystallised fibrous gypsum occur in cracks or as clayey gypsiferous interlayers. The gypsum in this lithofacies is mostly of a diagenetic origin, however, it possibly formed through recrystallization of originally deposited gypsiferous claystone. This lithofacies has deposited in supratidal flats. No porosity – permeability measurements have been analysed in this lithofacies.

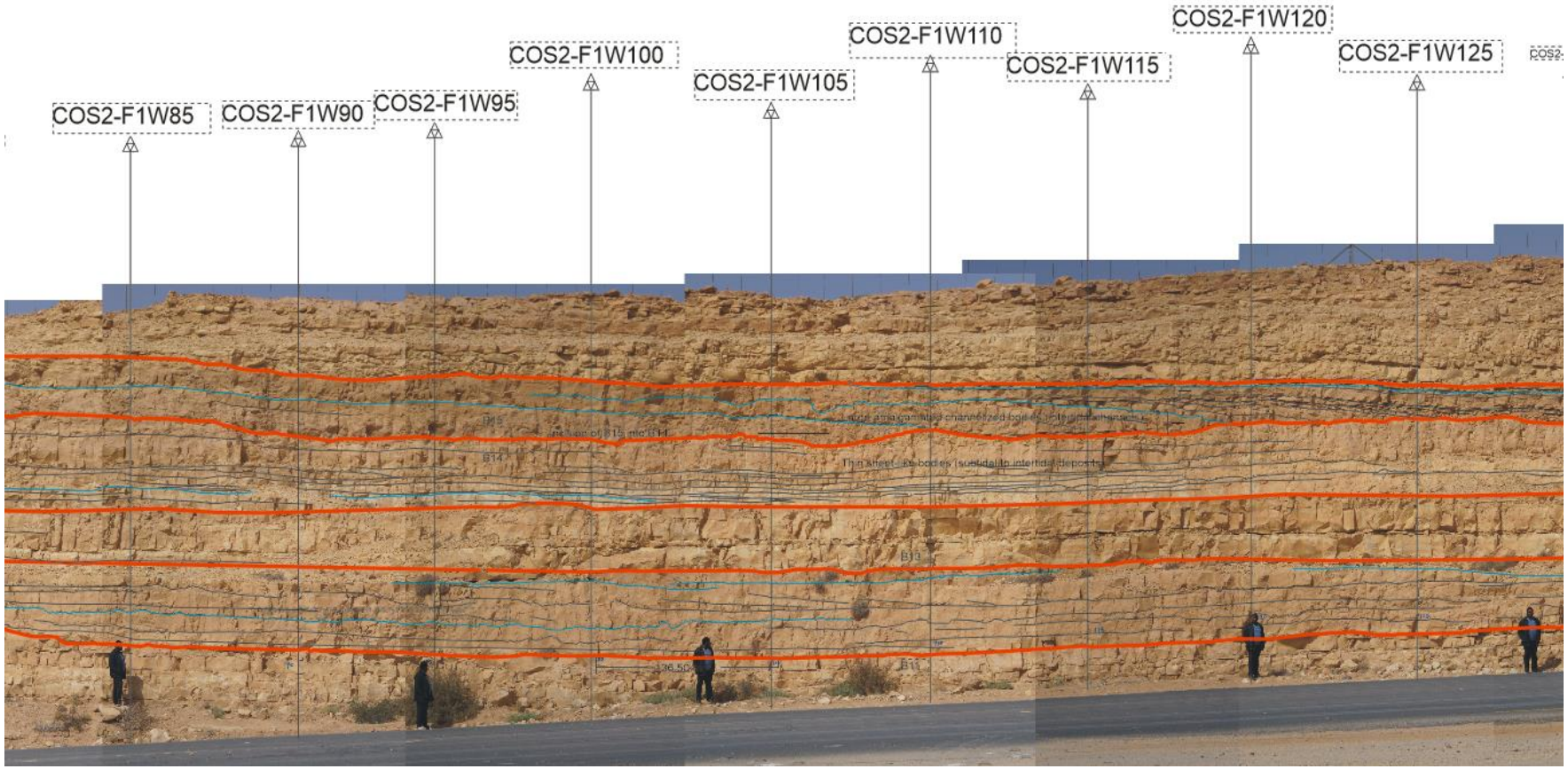

Figure 5.1. Photo-mosaic showing example of the selected intra-reservoir bodies from outcrop 2. These bodies are from bottom to top: B12B, B14B, and B15B. Note distance between vertical sections is 5 m.

Table 5.1. Summary of the Upper Khartam lithofacies and their deduced environmental settings (Adam et al., under review) and the diagenetic processes and porosity types.

Lithofacies types	Thin-section photograph	Colours and components	Sedimentary structures	Architectural description	Major diagenetic processes	Porosity types	Depositional environment
LFT 1: Coarse-grained oolitic grainstone		Light beige and light pinkish, ooids are well-sorted and well-rounded, range in size from 50 to 600 µm, few quartz grains, they are sub-angular, moderate-sorted, and about 250µm in size, bioclastic fragments include bivalves, gastropods, ostracods, brachiopods, and sparse Earlandia foraminifera	Dominance of cross-laminations such as cross-planar, hummocky, herringbone (Figure 5.6 A), sigmoidal, tidal bundle, trough-cross laminations, and symmetrical ripples (Figure 5.6B). Rib-up mud intraclasts, localized quantities of imbricating structures	Predominantly as channel-like bodies of about 3 m width and 50 cm thick Sheet-like bodies, ranges in thickness from 5 cm to 30 cm and lateral extent vary between 5 m to several hundreds of metres	Dominated by dissolution, cementation, stylolitization, fractures, and sparse dolomitization	Dominantly moldic and vuggy porosity and intergranular, intragranular, intercrystalline, and micro-fracture porosity	Intertidal channels Intertidal flats
LFT 2: Interlaminated quartz-bearing recrystallized limestone		Light beige to dark pinkish, contains ostracods and Earlandia foraminifera, quartz grains are angular, well-sorted, and range in size from 5 to 20 µm. Their abundance ranges from 15 to 40%, marlstone	Horizontal laminations (Figure 5.6C) and cross-laminations (planar, sigmoidal, herringbone), and bird-eye structures	Sheet-like bodies, thickness ranges from 2 to 10cm, length ranges from 5 to 100m Sparse of channel-like bodies, width 1m, thickness 20cm.	Dominantly include recrystallization and occurrences of stylolitization and fractures	Dominantly intercrystalline porosity and occurrences of micro-fractures and vuggy porosity	Intertidal flats Intertidal creeks
LFT 3: Recrystallized limestone		Beige colour, fine-crystals of limestone (average crystal size is 30 µm), localized occurrences of mud-intraclasts, mostly ostracods with presence of Earlandia foraminifera, marlstone and laterally merges with mudstone	Dominantly thin-horizontal laminations with rare cross-laminations and minor reactivation surfaces, some vertical and horizontal bird-eye structures	Sheet-like bodies (thickness 5-20cm, length 5-100s m), symmetrical wavy geometry. Channelized-bodies (15cm thick, 20cm width)	Dominantly include recrystallization, and fracturing and stylolitization	Include intercrystalline porosity and vuggy and fractures porosity	Subtidal flats Intertidal flats Intertidal creeks
LFT4 : Interlaminated quartz-bearing and fine-grained oolitic grainstone		Light beige in colour, quartz grains occur as lamination and ranges in contents from 1 to 10%, they are angular and well-sorted, and their grain sizes varies around 50 µm, bivalve fragments, localized occurrence of mud-intraclasts, ooids are well-rounded and well-sorted with average grain size of 75µm	Horizontal laminations and cross-laminations (sigmoidal to planar)	Relatively uniform, flat, horizontal, and continuous sheet-like bodies, range in their extent from 50 m to 150 m and have average thickness of about 20 cm.	Recrystallization, fractures, and stylolitization, recrystallization occurs as blocky calcite cements (average crystal size of 30 µm) and mosaic calcites and sparse of dolomites	Include intercrystalline porosity and vugy and fractures porosity	Intertidal to subtidal flats
LFT 5: Fine-grained oolitic grainstone		Light beige to pinkish in colour, pure and homogeneous oolitic grains which are well-	Thin laminations and planar cross-laminations	Laterally uniform, horizontal, and	Include dissolution, cementation, and	Include moldic, intergranular, and vugy	Intertidal to subtidal flats

		sorted and well-rounded, and range in size from 20 to 100 µm, sparse bivalve fragments	(Figure 5.6D) and sigmoidal cross-laminations (Figure 5.6E).	continuous sheet-like bodies, local swelling and pinching geometry, lateral amalgamation distance of about 100 m	stylolitization, cementation occurs as blocky and mosaic calcitic cement	porosity; molds are filled with micritic clay minerals and anhydrites	
LFT6: Bioclastic grainstone/packstone		Dark pinkish to light beige in colour, bioclasts dominantly bivalves with gastropods (2 mm in size) and single presences of Earlandia foraminifera and they have no defined orientation, contains oolitic and quartz grains, ooids are well-rounded and well-sorted, and range in size from 500-200µm, occurs in association with gypsiferous claystone	Abundant of cross-laminations such as herringbone and trough cross-lamination and abundant of mud-intraclast and imbricates and sparse of thin laminations	Sheet-like bodies, ranges in length from 50 m to 200 m, and thickness varies between 20 cm and 40cm	Include cementation, dissolution, and dolomitization, cementation occurs as blocky calcite cements and dolomitic cements (20-40 µm)	Include intergranular, moldic, vuggy, intragranular, and intercrystalline porosity, presence of vertical and horizontal fractures	Intertidal to subtidal flats
LFT 7: Marlstone		Thin grayish interbeds, important stratigraphic units and has significances in the sequence stratigraphic interpretations since it interbeds with the carbonates of the Upper Khartam Member	Thin-laminations	Thin-sheets interbeds with the carbonates all-over the studied interval	Important stratigraphic unit act as main source for pore-lining claystone and destructed the reservoir quality parameters		Outer-ramp
LFT8: Bioclastic wackestone/mudstone		Light beige in colour, localized mud-intraclasts, and bioclastic grains are ostracods	Dominated by thin laminations, symmetrical wavy rippled.	Wavy symmetrical geometry and uniform, horizontal, and continuous sheet-like and lenticular bodies, range in their extent from 5 m to several hundreds of metre and they range in thickness from 20 cm to 40 cm	Include micro-cementation and fracturing, fractures are vertical and filled with calcite	Includes fracture, intercrystalline, and vuggy porosity	Outer-ramp
LFT 9: Non-fabric preserved dolomite		Reddish, greenish, yellowish, and beige in colour, dolomite crystals range in their size from 30 to 100 µm	Large imbricated structures (Figure 5.6F) and horizontal and planar cross-laminations.	Sheet-like bodies of uniform, flat, horizontal, and continuous geometry, ranges in length from 5 m to several hundreds of metres and has thickness range between 5 cm and 20 cm	Obviously, is dominated by dolomitization, the dolomite crystals range in their size from 30 to 100 µm, fractures are also observed and they are filled with dolomite and calcite cements	Dominantly intercrystalline porosity and dolomite-leaching (calcite and iron-rich calcite partially filled the leached dolomite) and vuggy porosity (1cm)	Intertidal to subtidal setting
LFT 10: Calcareous sandstone		Reddish to grayish and yellowish, quartz grains are angular, moderately sorted, and range in size from 75 to 250 µm, locally contains mud-intraclasts, undefined bioclasts (up to 10%), reddish/grayish claystone, quartzwacke, and quartz arenite	Dominantly thin laminations to fenestral, lenticular, and crinkled laminations with rare cross-lamination, Intensive bioturbation.	Sheet-like bodies	Includes calcitic cementation	Include intergranular porosity	Intertidal to subtidal settings
LFT 11: Microbialites build-ups		Reddish to pinkish in colour, contains ooids grains (up to 20%) and scattered quartz grains and bioclastic fragments, occurs in association with thickening- and coarsening-upward strata of marlstone and bioclastic and oolitic grainstone	Crinkled laminations (microbialites films)	The microbialitic heads have a lateral separation distance of 15m, and they range in size from 100 to 20 cm	Includes recrystallization which occurs as mosaic calcitic cements	Intercrystalline porosity	Intertidal flats
LFT 12: High-angle cross-laminated oolitic grainstone/grapestone		Beige colour, oolitic grains are well-rounded, moderately sorted, and range in size from 500-1000µm, quantity of bioclasts grains, occurs in association with the microbialite build-ups and mudstone and channel-like bodies	High-angle cross-lamination and imbricates of mud intraclasts, s. It is contains a quantity of bioclasts grains	Convex geometry	Include dissolution and cementation, cementation occurs as blocky calcitic cements	Include intergranular, moldic, and vuggy porosity	Mobile shoal ridges

LFT 13: Mudstone		Beige to yellow in colour and sometimes contains anhydrite crystals	Dominantly thin lamination and localized imbricates	Flat, uniform, and continuous sheet-like bodies range in thickness from 5cm to 10 cm and they have lateral extent ranges from 20 m to 100 m	Micro-recrystallization	Micro-intercrystalline porosity	Outer-ramp
LFT 14: Peloidal grainstone to packstone		Light beige to yellowish in colour, quantity of mud-intraclasts, range in size from 1 to 2 mm, localized concentrations of bioclast fragments, mostly bivalves	horizontal to lenticular laminations with presence of bird-eyes structures	Uniform, horizontal, and continuous sheet-like bodies range in length from 5 to 200 m and thickness varies from 5 to 40 cm	Includes cementation and recrystallization which occurs as mosaic calcitic cements, vertical fractures filled with calcite cements	Intercrystalline	Subtidal settings
LFT 15: Skolithos bioclastic oolitic grainstone		Red in colour, bioclastic fragments, and mud-intraclasts, ooids are poorly-sorted, domal stromatolites	Intensively bioturbated and contains a quantity of skolithos, thin laminations and cross-laminations	Limited lateral exposure, horizontal sheet-like bodies			Intertidal flats
LFT 16: Gypsiferous claystone		Clean white fibrous gypsum, occurs in associations with the marlstone		Thin-seems			Supratidal flats
LFT 17: Thin-walled bivalval rudstone		Pinkish to reddish in colour, consists predominantly of thin-walled bivalves with ostracods (2 mm size), these are horizontally oriented indicating in-place deposition, mud-intraclasts	Crinkled to fenestrally laminations.	Occurs as sheet-like bodies range in length from 5 m to several hundreds of metres and they have thickness ranges from 5 to 30 cm.	Include dolomitization, the micritic envelope prevent the destruction of the original fabric, dolomite cements have average size of about 30μm	Includes intercrystalline, intergranular, moldic, and vugy porosity	Intertidal reef complex

Figure 5.2. Thin-section photomicrographs of lithofacies types, most of them taken under plane polarizing light (PPL) except D which was taken under cross-polarizing light (XPL). (A) coarse-grained oolitic grainstone (LFT 1), (B) dolomitized coarse-grained oolitic grainstone (LFT 1), (C) interlaminated quartz-bearing recrystallized limestone (LFT 2) - red colour is alizarin stain, (D) recrystallized limestone (LFT 3), (E) interlaminated quartz bearing fine-grained oolitic grainstone (LFT 4), (F) fine-grained oolitic grainstone (LFT 5) - red colour is alizarin stain.

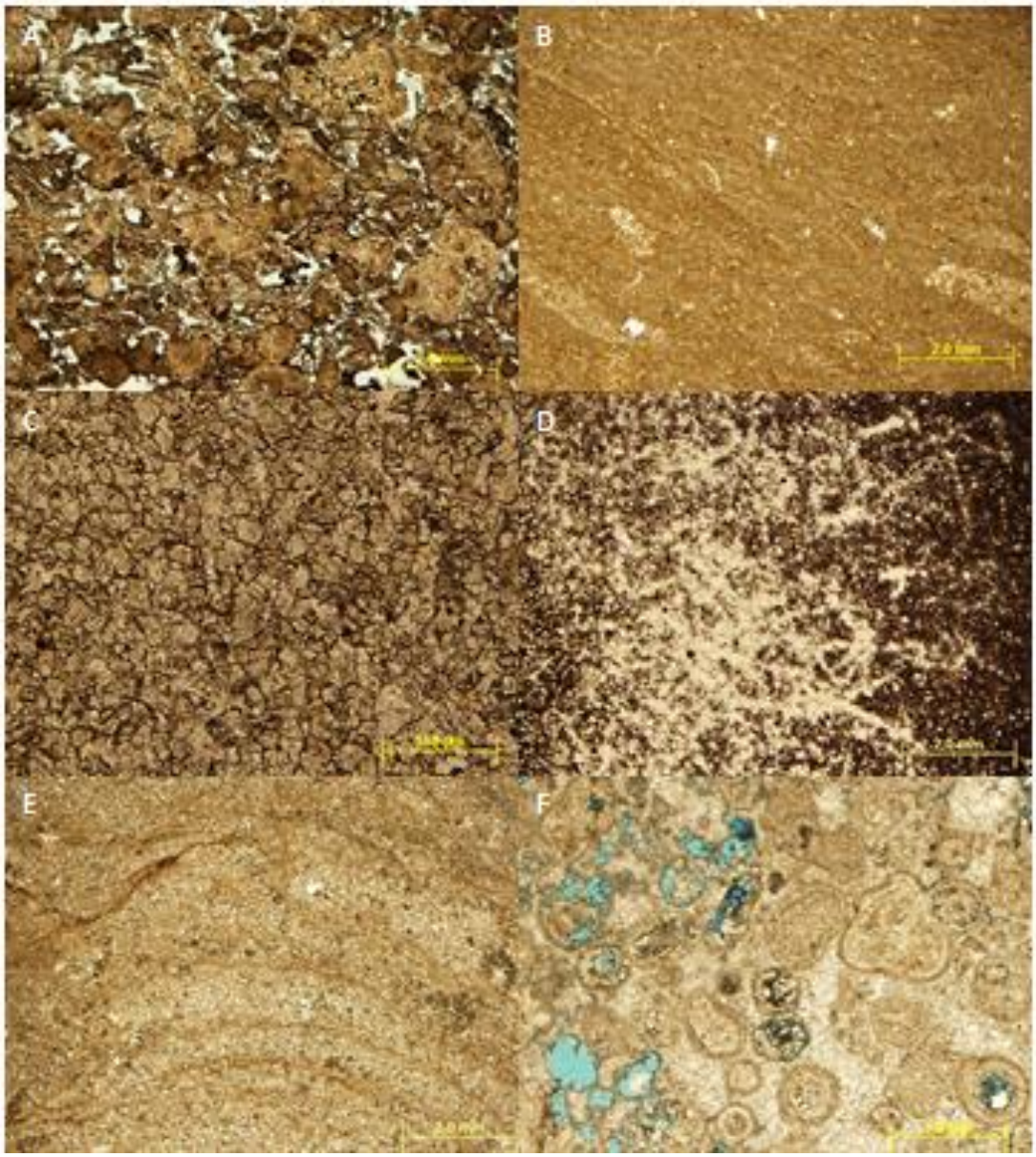

Figure 5.3. Thin-section photomicrographs of lithofacies types, most of them taken under plane polarizing light (PPL). (A) bioclastic grainstone/packstone (LFT 6), (B) bioclastic wackestone/mudstone (LFT 8), (C) non-fabric preserving dolomite (LFT 9), (D) intensively bioturbated calcareous sandstone (LFT 10), (E) microbialites bindstone (LFT 11), (F) oolitic grainstone/grapestone (LFT 12).

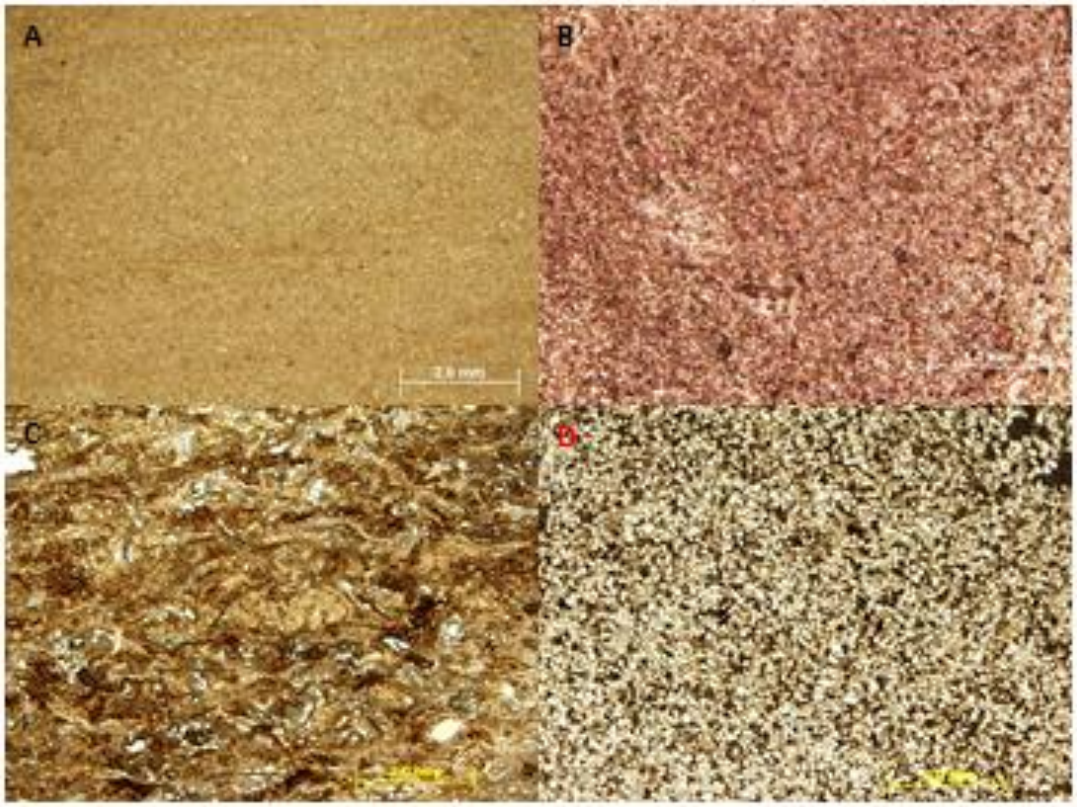

Figure 5.4. Thin-section photomicrographs of lithofacies types, most of them taken under plane polarizing light (PPL). (A) horizontally thin-laminated mudstone (LFT 13), (B) peloidal grainstone/packstone (LFT 14) - red colour is alizarin stain, (C) thin-walled bivalve grainstone (LFT 17), (D) calcareous sandstone (LFT 10).

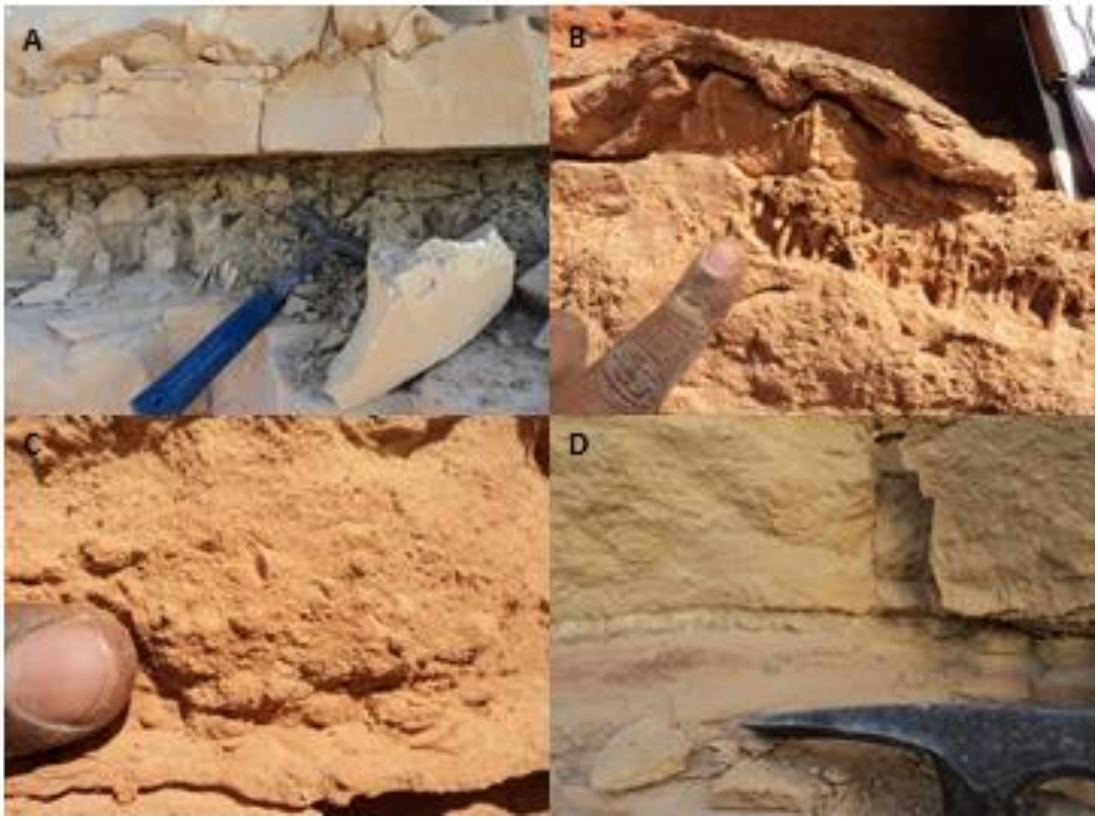

Figure 5.5. Field photographs of the lithofacies types. (A) fissile marlstone (LFT 7), (B) gypsiferous claystone (LFT 16), and (C and D) skolithos bioclastic oolitic grainstone (LFT 15), note the bivalve bioclasts and ooids grains in C and skolithos in D.

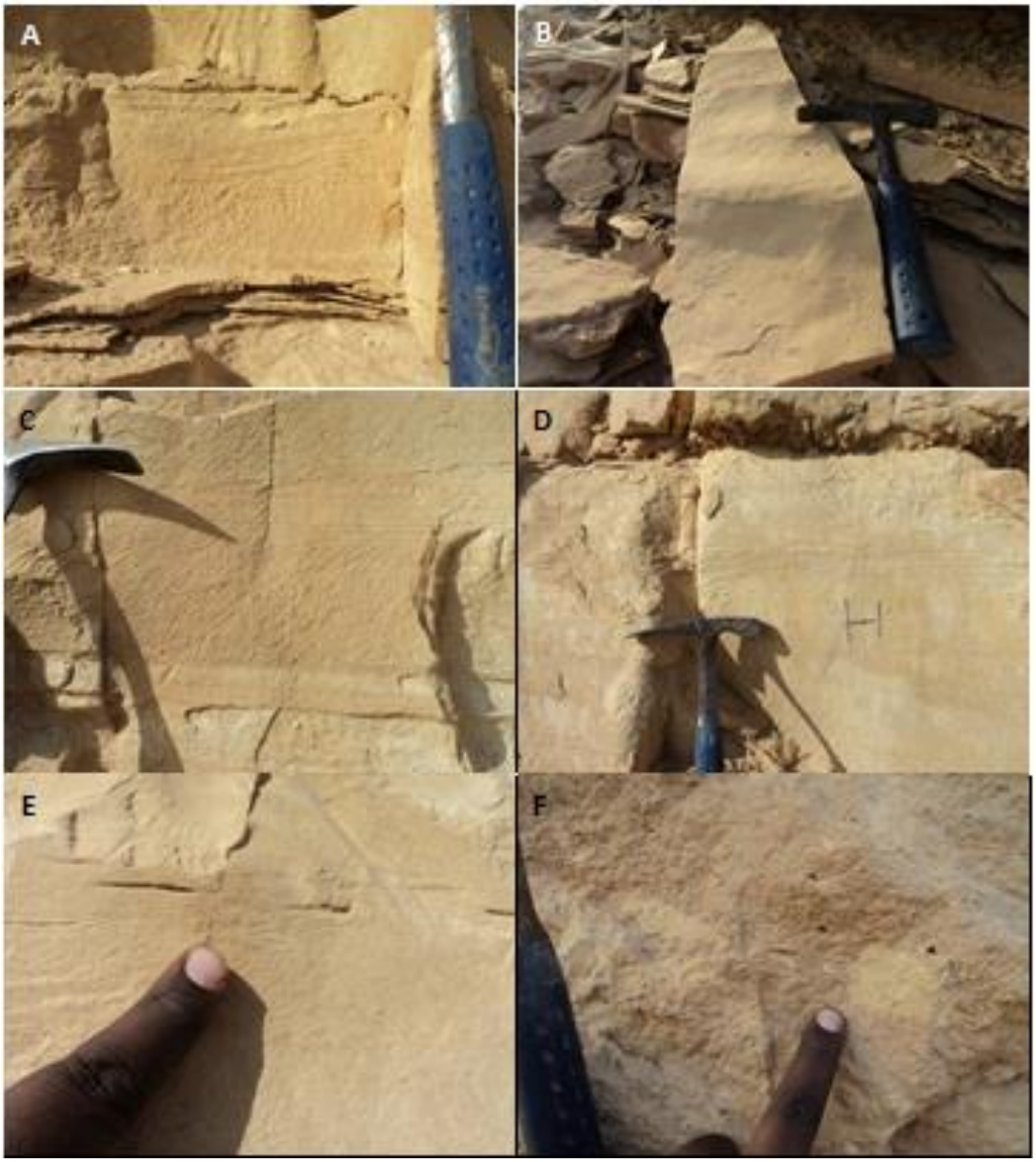

Figure 5.6. Photographs of the sedimentary structures observed in the field. (A) herringbone cross-laminations in the coarse-grained oolitic grainstone (LFT 1), (B) asymmetrical wavy ripples (LFT 1), (C) horizontal thin laminations in the interlaminated quartz and fine-grained oolitic grainstone (LFT 4), (D) planar cross-lamination in the coarse-grained oolitic grainstone with stylolite in fine-grained oolitic grainstone (LFT 5), (E) hummocky cross-laminations in the interlaminated quartz and recrystallized limestone (LFT 3), (C) imbrication structures in the non-fabric preserved dolomite (LFT 9).

Table 5.2. Elemental composition (from XRF) for selected samples of the marlstone lithofacies type (LFT 7). Abbreviation: ms% mass percentage.

Elements	COS1-B11D (ms%)	COS1-B8E-9A (ms%)	COS2-B9A-B9B (ms%)	COS2-B15A (ms%)
Mg*	0.3	0.4	0.5	0.2
Al	4.8	7	7.8	2.6
Si	14.9	18.2	23.2	8.4
S	2.7	0.2	0.4	0.8
K	13.5	11.2	13.7	6.3
Ca	32.5	22. 4	23.5	37.4
Ti	3.1	6.2	5.4	1.3
Fe	22.7	29	22.3	12.1
Sr	4.0	0.7	1.2	30.3

5.4.2. Vertical reservoir heterogeneity and quality (at sub-seismic scale)

The recalculated original, unconsolidated, depositional texture of the Upper Khartam Member reflects a high average primary porosity and permeability of about 42% and 12 D, respectively. These porosity and permeability values were derived from an analysis of grain size and sorting using the graphical chart of Baker and Bloomer (1988). The primary porosity and permeability was subsequently partially obliterated by diagenetic processes (Table 5.3). The overprinted porosity and permeability are proportional with each other (figure 67). The oolitic grainstone lithofacies (LFT 1 and 4) are characterized by a wide range of overprinted porosities (ranging between 0.05 and 0.4), while most of the other lithofacies are characterized by a relatively narrow range with low overprinted porosities (Figure 5.7). The coarse-grained oolitic grainstone extends through a wide range of grain sizes, porosities, and permeabilities. Importantly, the original grain size has subtle control on porosity and permeability values (Figure 5.8) Overall, six major diagenetic processes were observed in the studied outcrops: dissolution, cementation, pore lining cementation, dolomitization, fracturing, and stylolitization (Figure 5.9). Cements develop equant, mosaic, micro, and rimming calcite cements with two different mineralogies: ferroan calcite and more frequently non-ferroan calcite. Significantly, cementation has blocked most of the original intergranular porosity (Figure 5.9A). Dissolution occurs in the form of partial dissolution, molds, and vugs, and is likely the result of intensive circulation of meteoric water undersaturated with respect to aragonite and/or calcite. The coarse-grained oolitic grainstone (LFT 1; making about 40% of bulk stratigraphy) is

characterized by prominent ooid dissolution and blocky calcite cementation; these processes most likely occurred simultaneously with the ooids possessing an original aragonitic mineralogy. The undersaturated meteoric water infiltrated into the oolitic beds and dissolved the grains and became saturated with respect to low Mg-calcite. This meteoric water infiltrated downward and caused the precipitation of blocky calcite cements (Figure 5.10). Critically, the permeability was reduced by several orders of magnitude, which was mainly the result of diagenesis in function of stratigraphic position. Indeed, the Upper Khartam Member is composed of interbeds of carbonates and fissile marlstone. The marlstone contains detrital clay, which infiltrated into the underlying highly porous rocks together with meteoric water and caused the deposition of pore lining detrital clay, which severely affected the reservoir permeability and complicated the pore geometry (Figure 5.12). The elemental analysis of the pore lining minerals is similar to that of the marlstone (Table 2). This similarity along with their stratigraphic position supports the interpretation of the origin of the pore lining clay minerals and its relationship to the marlstone.

Based on their vertical extent and lateral spacing, three types of fractures and fracture sets can be differentiated: (i) major fracture corridors, cross-cutting the entire succession vertically with a lateral spacing of 50 m, (ii) vertical, bed-controlled fractures with an average lateral spacing of less than 1 m, which are associated with the major fracture corridors, and (iii) vertical or oblique (60°), open fractures and veins with partial calcite fillings, which can best be observed in thin-sections and slabs. The first two types are open fractures which likely acted as major conduits for the diagenetic fluids. Stylolites are dominantly horizontal with varying amplitudes and shapes. Quantitatively, their abundance is likely controlled by lithofacies and geobody

architecture, as they are relatively abundant in the fine-grained oolitic grainstone (LFT 5; occurring as sheet-like bodies) if compared to the coarse-grained oolitic grainstone (LFT 1; occurring as channelized bodies) (Figure 5.13). Dolomitization is associated with the Khuff–Sudair boundary and the microbialite build-ups in the studied sections, and is believed to be the result of an influx of highly Mg^{2+}-saturated water concomitant to the deposition of the Sudair evaporites (Figure 5.14). Accordingly, ten porosity types are described in the studied outcrops, namely intergranular, intragranular, shelter, dissolution enlarged, moldic, vuggy, micro-porosity, dolomite–dedolomite porosity, dolomite-leaching, and fracture porosity (Figure 5.15). The oolitic grainstones of the intertidal sheets, intertidal creeks, and the intertidal channels are dominated by dissolution enlarged, moldic, and vuggy porosity, whereas intercrystalline and fracture porosities are prevailing in the recrystallized lithofacies types. The dolomite and dolomite-leaching porosities are stratigraphically controlled and localized near the boundary between the Upper Khartam and Sudair Formations and the oolitic grainstone of the intertidal channels underlying the microbialite build-ups.

The present-day succession is composed of nine hydraulic units (HUs). The capacity and productivity (linked to pore attributes) of these units was mainly obliterated by diagenetic processes and shifted toward poorer quality (mid-center FZI = 0.75–1.5; with an occurrence of 50%; Figure 5.16). Importantly, these units do not occur as connected bodies, however, they follow the stratigraphic patterns of the Upper Khartam Member, and therefore, they occur as complex amalgamation of sheet-like and channelized bodies marked by different architectural parameters and lithofacies types (Figure 5.17 to 23). Diagenetic processes played a major role in modifying the

pore attributes, while the original depositional textures (grain size) exerted little control on these modifications. This is inferred from the interferences of the lithofacies qualities and the absence of any correlation between FZI values and grain size (Figure 5.21). Diagenetic processes clearly impacted the ultimate reservoir quality. For example, the reservoir quality of the fine-grained oolitic grainstone (occurring as sheet-like bodies) have been relatively less impacted compared to the coarse-grained oolitic grainstone (occurring as sheet-like bodies). This is attributed to the pore-filling dolomites occurring in the coarse-grained oolitic grainstone, while no dolomite was observed in the fine-grained oolitic grainstone. Furthermore, the intertidal creek deposits are characterized by a complex and heterogeneous porosity networks compared to the intertidal channels, which can be attributed to the architectural parameter, where intertidal creeks are composed of dense and small tidal creeks (1 m in length and 20 cm in thickness), while intertidal channels are composed of thick amalgamations of intertidal channels (5 m by 50 cm). In addition, pore-types have critical control on the ultimate reservoir quality. For example, the vuggy coarse-grained oolitic grainstone are of better quality compared to the moldic coarse-grained oolitic grainstone. Vugs enhanced the connectivity between the pores, while molds are often disconnected by blocky calcite cement (Figure 5.22). To summarize, the vertical reservoir quality heterogeneity of the Upper Khartam Member is mainly controlled by cementation, dissolution, dolomitization, and pore-lining clay.

Table 5.3. Summary of reservoir quality data for the defined lithofacies types. Depositional parameters refer to estimated measurements from grain-size analysis and present day core measurements respectively. Abbreviations: Φ and K, respectively porosity and permeability, and Max, Min, Average, and STD are respectively maximum, minimum, average and standard deviations.

Lithofacies Type	Statistical analysis	Core plug measurements				
		Φ	K (mD)	RQI	Φ	FZI
LFT 1	Max	0.40	88.36	0.70	0.68	15.01
	Min	0.01	0.02	0.02	0.01	0.06
	Average	0.13	5.67	0.13	0.17	1.55
	STD	0.09	12.21	0.11	0.15	2.15
LFT 2	Max	0.23	47.07	0.45	0.30	4.57
	Min	0.01	0.02	0.04	0.01	0.36
	Average	0.07	3.40	0.10	0.08	1.50
	STD	0.04	8.43	0.08	0.05	0.95
LFT 3	Max	0.09	1.87	0.14	0.10	3.41
	Min	0.04	0.11	0.05	0.04	0.66
	Average	0.06	0.63	0.09	0.07	1.43
	STD	0.01	0.55	0.03	0.02	0.66
LFT 4	Max	0.13	3.22	0.18	0.15	1.75
	Min	0.07	0.37	0.07	0.07	0.78
	Average	0.10	1.77	0.12	0.11	1.17
	STD	0.02	1.44	0.05	0.03	0.43
LFT 5	Max	0.15	5.46	0.25	0.17	2.63
	Min	0.06	0.05	0.02	0.06	0.23
	Average	0.10	1.44	0.10	0.11	1.01
	STD	0.03	1.48	0.06	0.03	0.62
LFT 6	Max	0.30	104.10	0.70	0.44	2.67
	Min	0.06	0.04	0.02	0.07	0.23
	Average	0.16	30.28	0.24	0.21	1.06
	STD	0.10	46.16	0.29	0.16	1.02
LFT 8	Max	0.06	0.27	0.09	0.07	3.02
	Min	0.03	0.01	0.02	0.03	0.48
	Average	0.04	0.11	0.05	0.05	1.31
	STD	0.01	0.09	0.03	0.01	0.98
LFT 9	Max	0.20	31.75	0.44	0.25	4.66
	Min	0.03	0.17	0.03	0.03	0.19
	Average	0.12	6.87	0.16	0.14	1.55
	STD	0.05	10.25	0.13	0.07	1.43
LFT 10	Max	0.15	7.52	0.31	0.18	3.60
	Min	0.08	0.76	0.08	0.09	0.44
	Average	0.11	3.50	0.17	0.12	1.83
	STD	0.04	3.86	0.13	0.05	1.68
LFT 11	Max	0.08	1.04	0.15	0.09	3.77
	Min	0.03	0.05	0.03	0.03	0.44
	Average	0.06	0.48	0.08	0.06	1.79
	STD	0.02	0.44	0.05	0.03	1.44
LFT 14	Max	0.04	0.55	0.15	0.04	6.37
	Min	0.02	0.09	0.05	0.02	1.39
	Average	0.03	0.34	0.11	0.03	3.94
	STD	0.01	0.23	0.05	0.01	2.49
LFT 17	Max	0.30	40.52	0.41	0.42	1.36
	Min	0.19	6.73	0.19	0.24	0.70
	Average	0.24	24.06	0.30	0.32	0.98
	STD	0.05	16.94	0.11	0.09	0.36

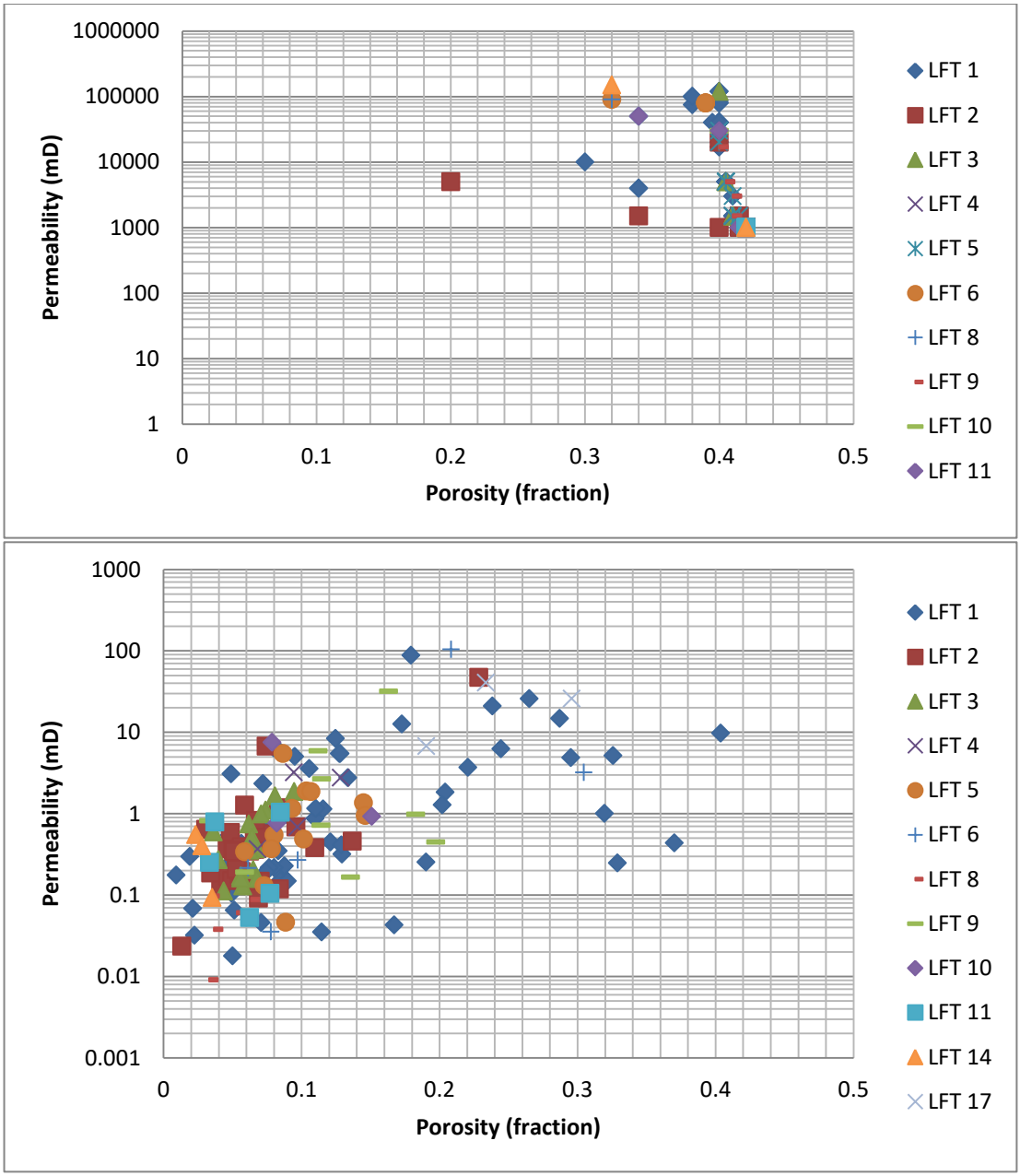

Figure 5.7. Porosity-permeability relationship. (A) original recalculated depositional relationship based-estimations from thin-section (B) and present-day measurements from core-plugs. Generally the depositional cross-plot shows no definite relationship while the overprinted texture displays a well-developed proportional relationship. Most of the lithofacies types define narrow ranges and are superimposed while the coarse-grained oolitic grainstone (LFT 1) displays a wide range of porosity.

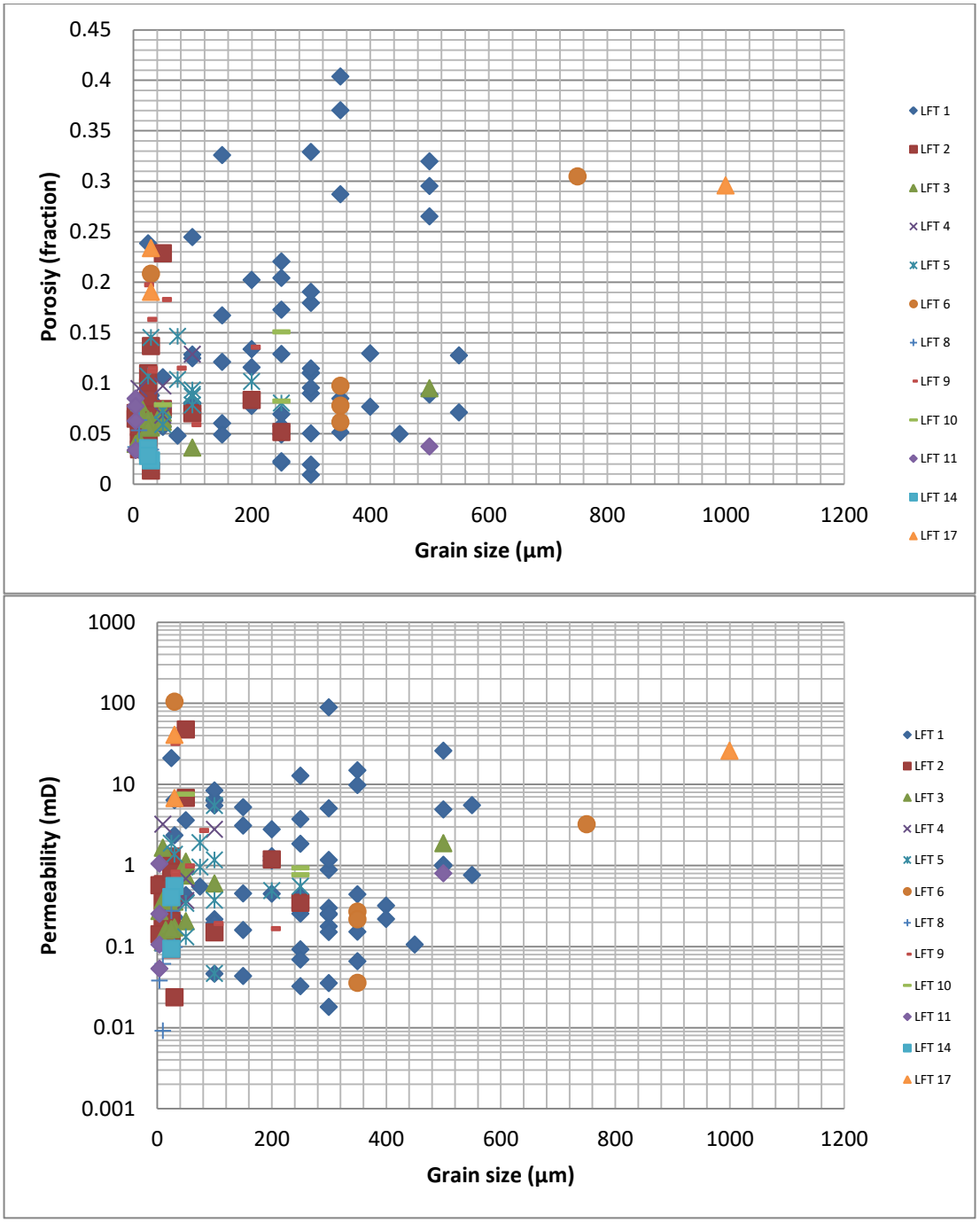

Figure 5.8. Cross-plots showing the subtle relationship between the grain size and porosity or permeability (A and B respectively). Overall, grain size has a relative better correlation with porosity than permeability. Only data from vertical and horizontal sections were used.

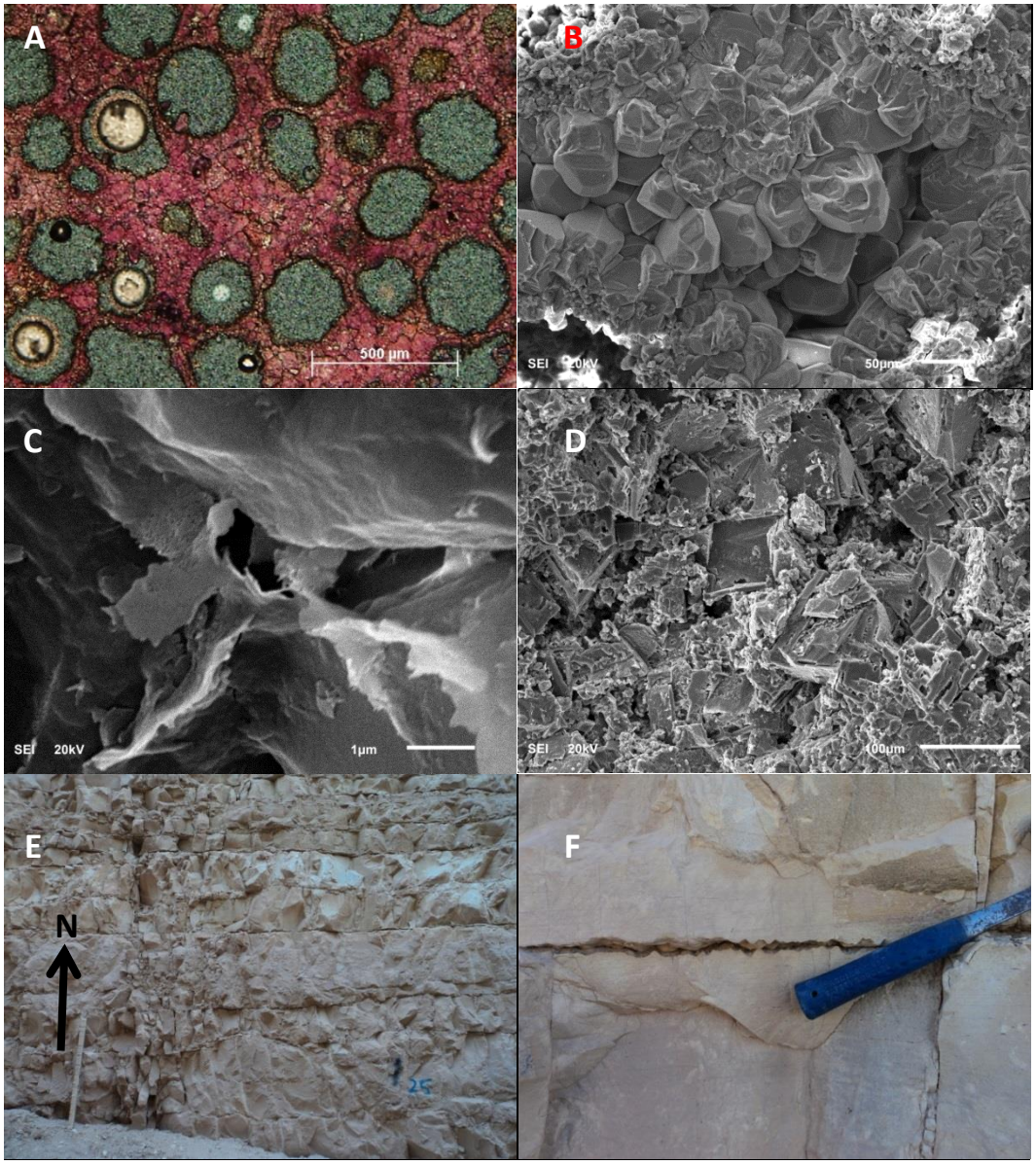

Figure 5.9. Illustrations of major diagenetic features. A) thin-section showing dissolved ooids with equant calcite cementation (stained red, alizarin), B) SEM photo showing pore-filling blocky calcite cement. C) SEM photo showing pore-filling and pore-lining clay phases. D) SEM photo showing pore-filling dolomitization in coarse-grained oolitic grainstone (LFT 1), E) field-photo showing vertical fracture corridor (with fractures extending in N-S direction), F) field-photo showing horizontal stylolite associated with fissile marlstone.

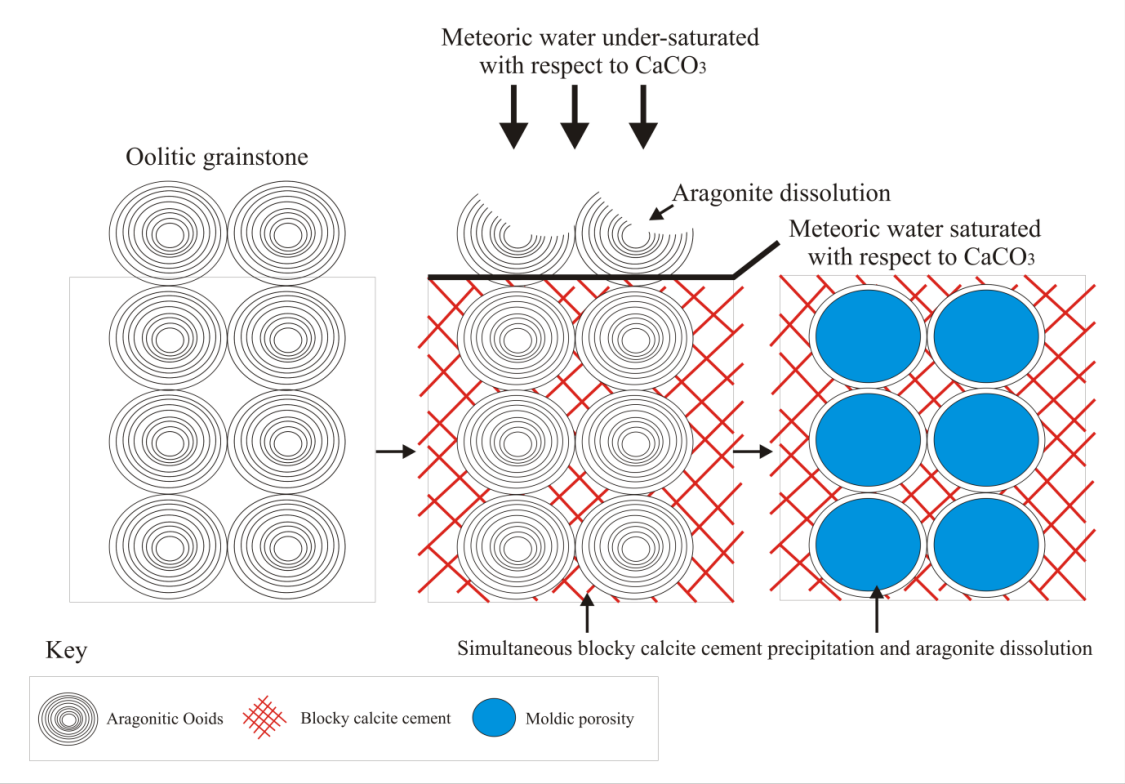

Figure 5.10. Schematic illustration showing simultaneous dissolution of aragonite (grains) and precipitation of blocky calcite (cement). Initially, the meteoric water was undersaturated with respect to CaCO3. This water infiltrated into the oolitic bed causing extensive dissolution, and then became saturated with low-Mg calcite. The latter gave rise to blocky calcite cementation around the aragonitic grains which became differentially dissolved latter.

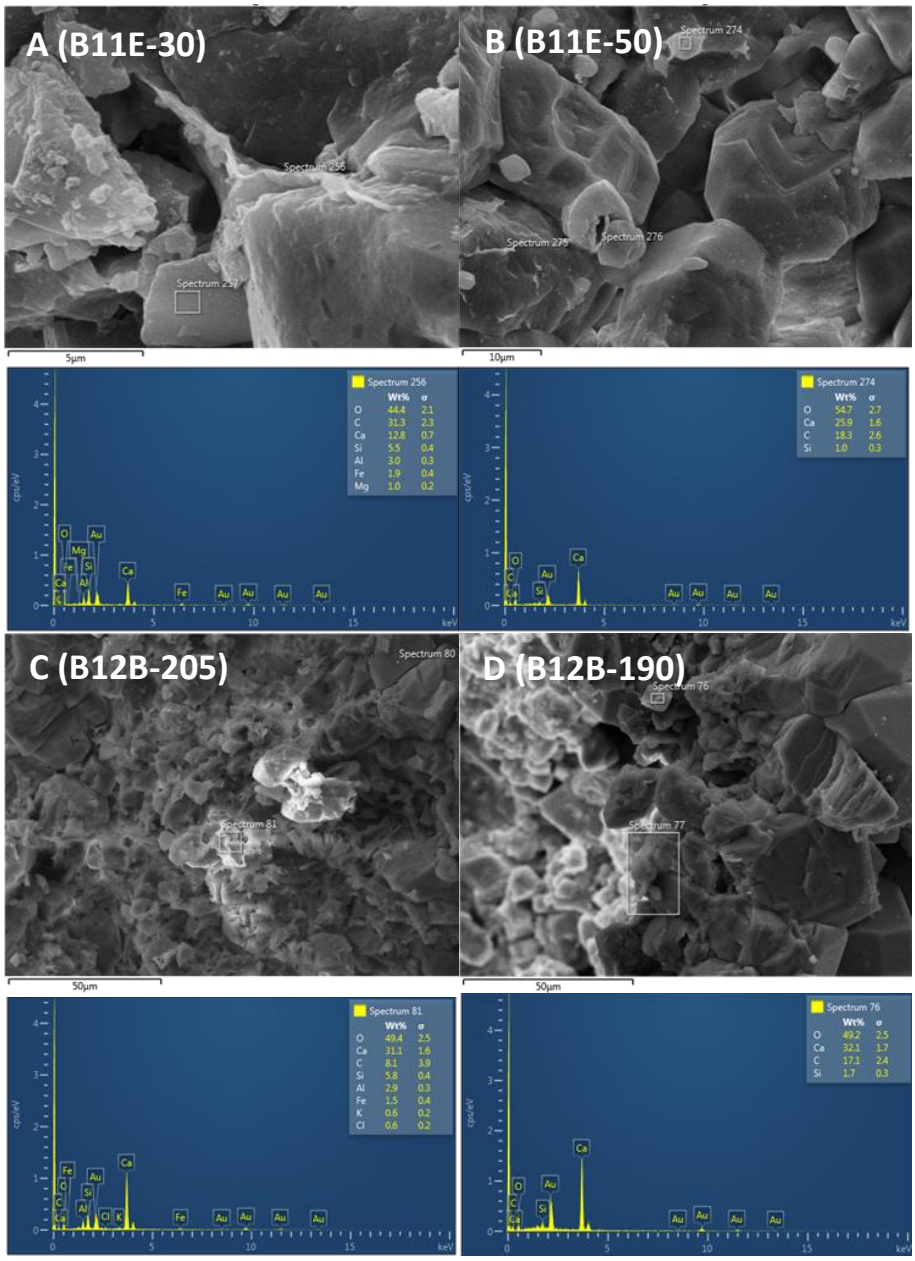

Samples	Φ (fraction)	K (md)	Samples	Φ (fraction)	K (md)
A (B11E-30)	0.13	0.04	C (B12B-190)	0.30	52.9
B (B11E-50)	0.15	23.6	D (B12B-205)	0.78	0.04

Figure 5.11. SEM photographs of pore-lining clay minerals and their EDS spectra below the photographs as well as porosity and permeability. A and B are from the same geobody but taken at a different horizontal distance of about 20m (coarse-grained oolitic grainstone; intertidal channels) A contains notable amount of pore-lining clay minerals, while B is relatively clean. The presence of clay minerals caused a reduction in the permeability values (see the table). Similarly C and D are from the same geobody but were collected at a distance in between the samples of about 15 m (coarse-grained oolitic grainstone; intertidal creeks) C contains notable amount of pore-lining clay minerals, while D is relatively clean. The presence of clay minerals again affects permeability (see the table).

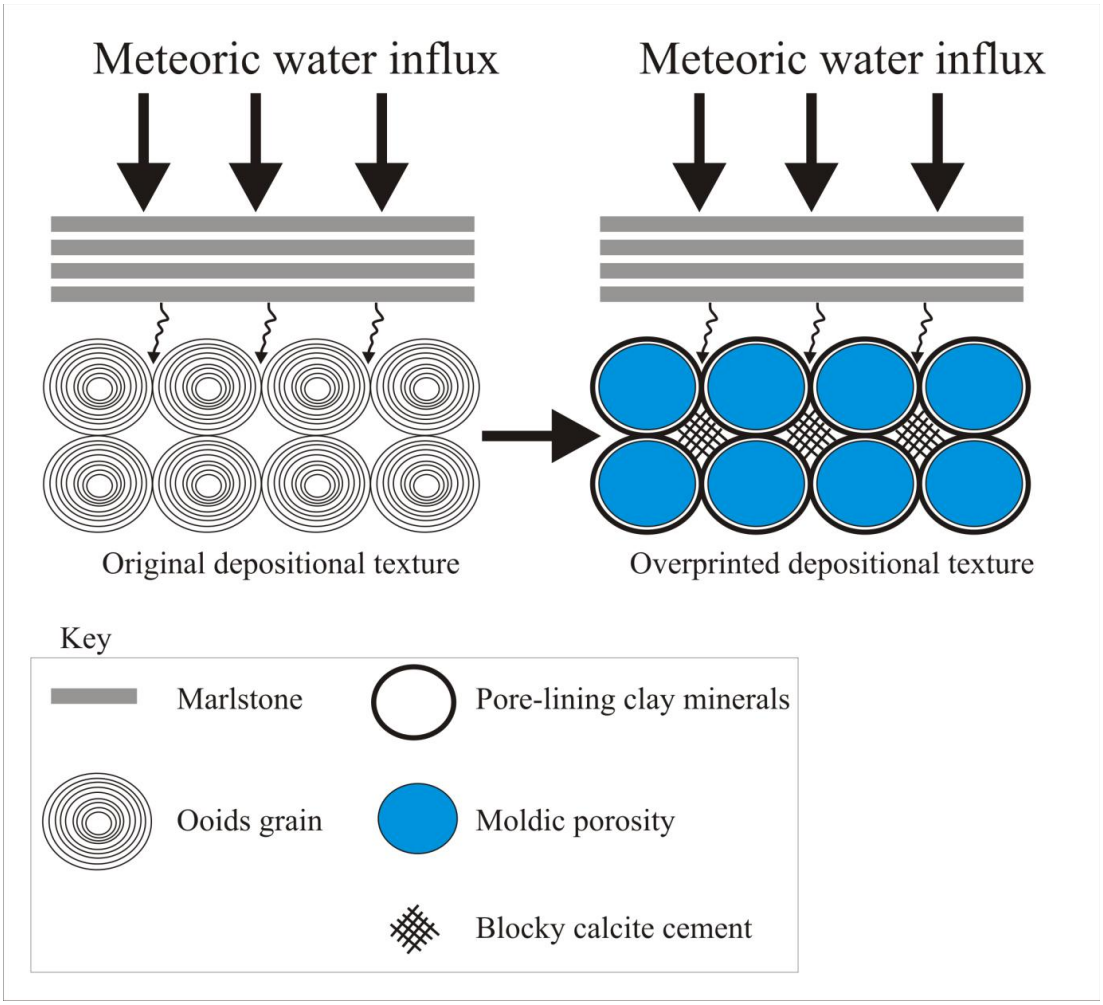

Figure 5.12. Schematic illustration of the interplay of diagenesis and stratigraphic position on the vertical reservoir heterogeneity of the Upper Khartam Member. The overlying fissile marlstone (containing clay minerals) infiltrates into the underlying highly porous media with meteoric water. Hereby clay minerals line up along the pores space affecting the quality of the reservoir.

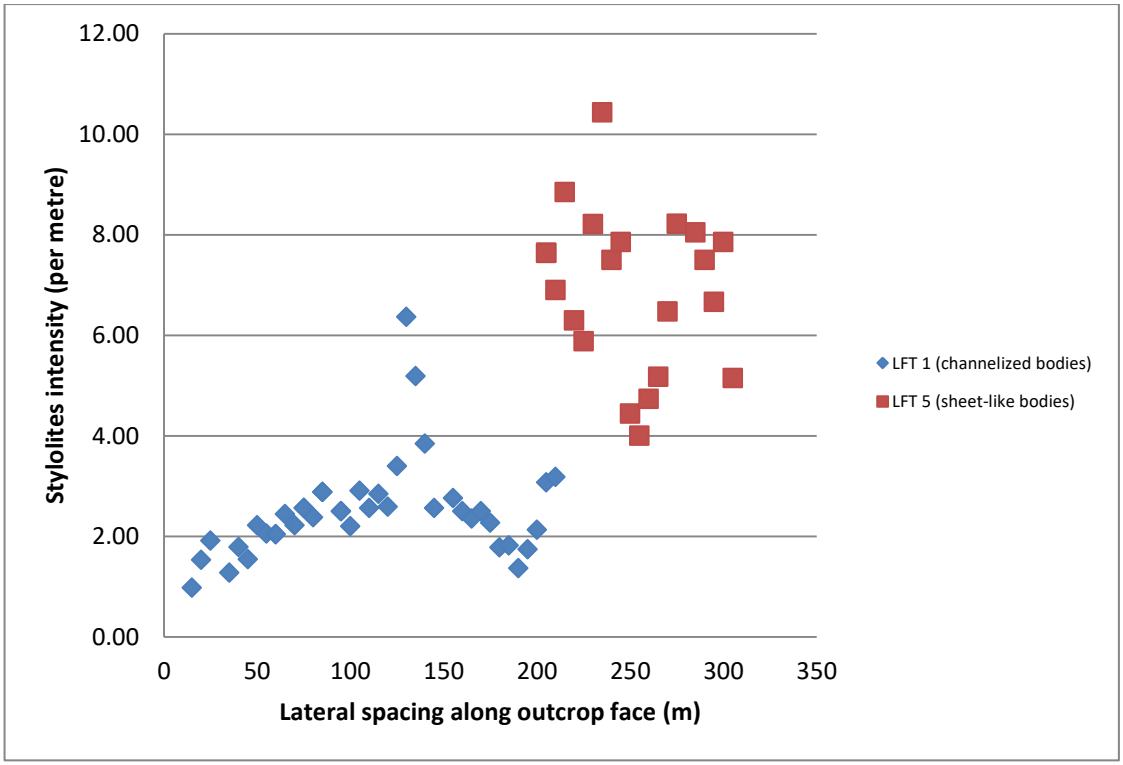

Figure 5.13. Cross-plot showing the control of the lithofacies and geobody architecture on the amount of stylolites. Stylolites are relatively abundant in the fine-grained oolitic grainstone (LFT 5 occurring as sheet-like bodies) when compared to coarse-grained oolitic grainstone (LFT 1 occurring as channelized bodies).

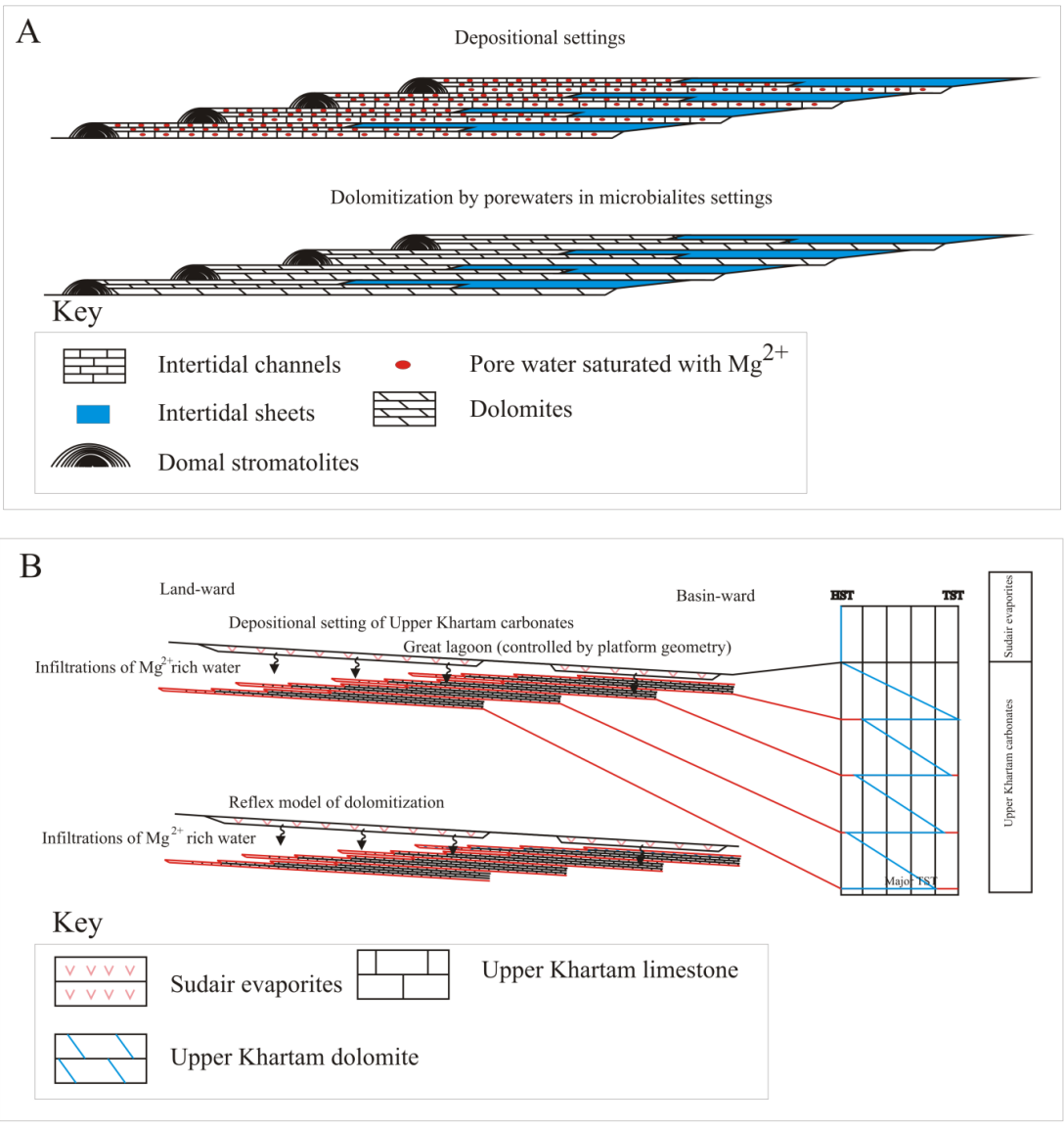

Figure 5.14. Dolomitization models of the Upper Khartam dolomites. A) Dolomitization by pore-water in the microbialite build-ups, B) Dolomitization by the influx of Mg2+ saturated water after deposition of Sudair evaporites (reflux model). These mechanisms were described by Adams and Rhodes (1960) from the Permian reef complex of West Texas.

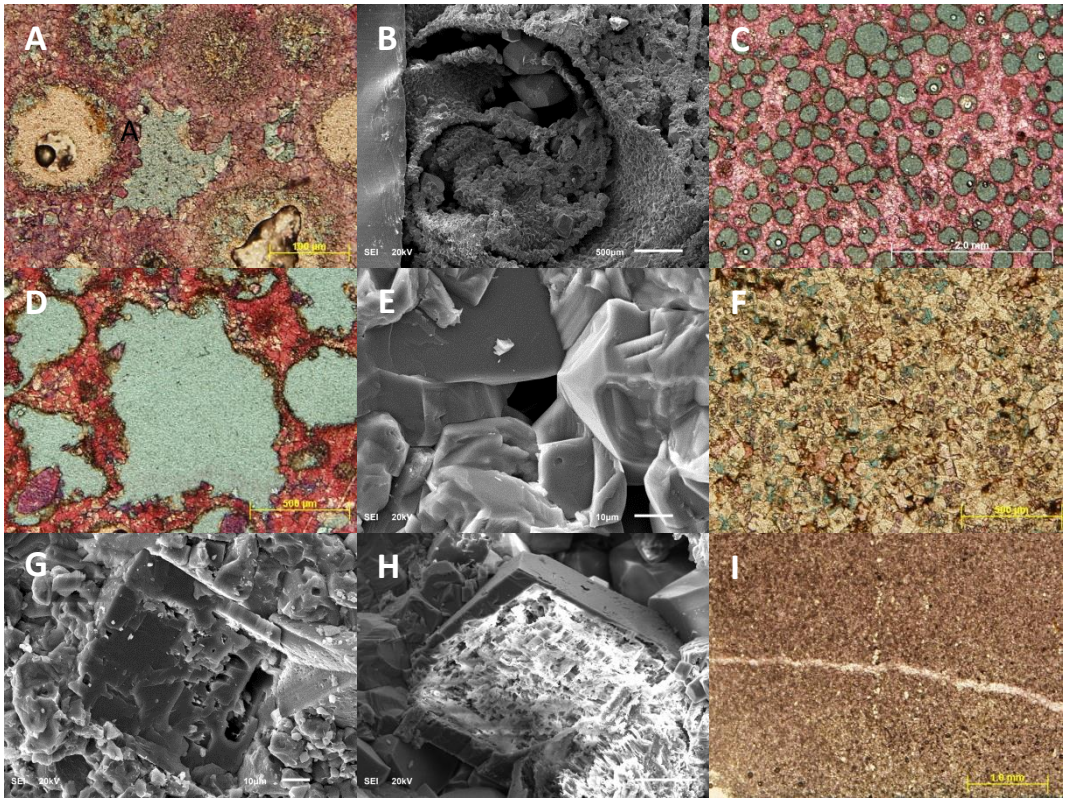

Figure 5.15. Porosity types. A) intergranular porosity of oolitic grainstone, B) shelter porosity in the bioclastic oolitic grainstone, C) moldic porosity in oolitic grainstone of the intertidal sheets, D) Vuggy porosity in oolitic grainstone of the intertidal flats, E) micro-intercrystalline porosity in the interlaminated quartz-bearing recrystallized limestone reflecting intertidal flats, F) intercrystalline dolomite porosity in non-fabric preserving dolomite, G) dolomite porosity in oolitic grainstone of intertidal channels, H) dolomite-leaching porosity in bioclastic grainstone of the intertidal flats, I) fracture porosity in the interlaminated quartz-bearing recrystallized.

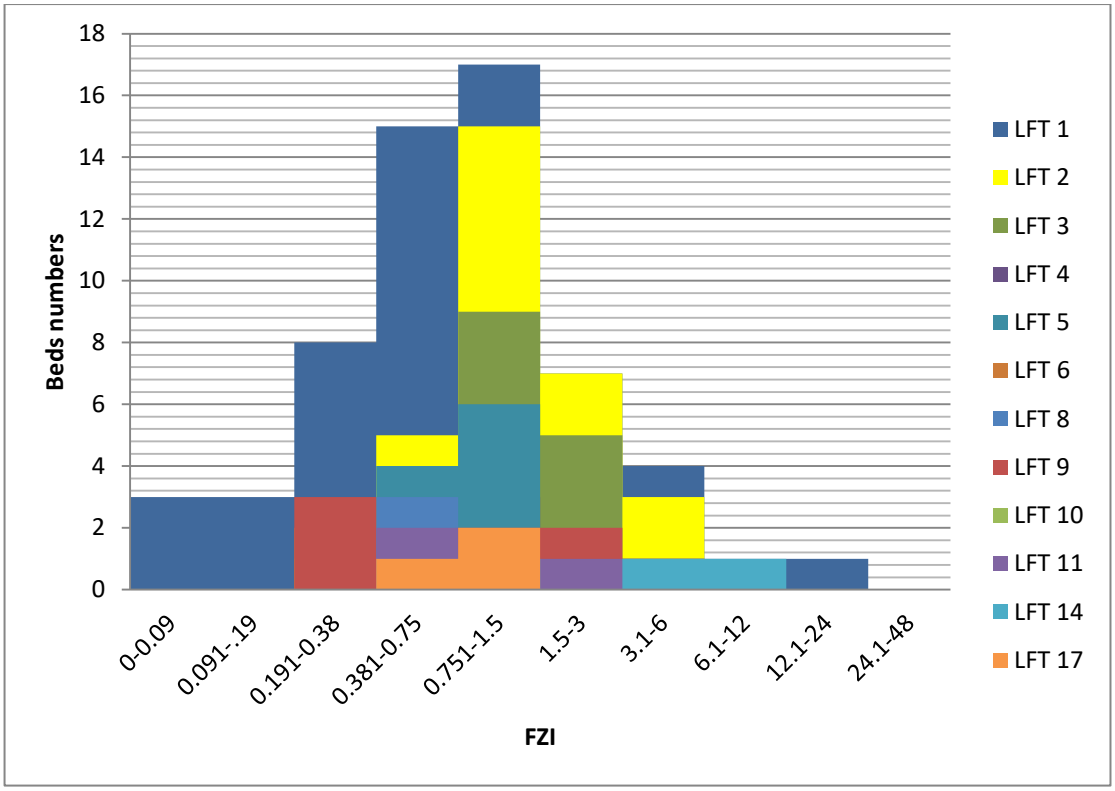

Figure 5.16. Histograms showing the segmentation of vertical stratigraphy into different hydraulic units. The overprinted reservoir qualities have been segmented into wide classes of hydraulic units ranging from poor to good qualities.

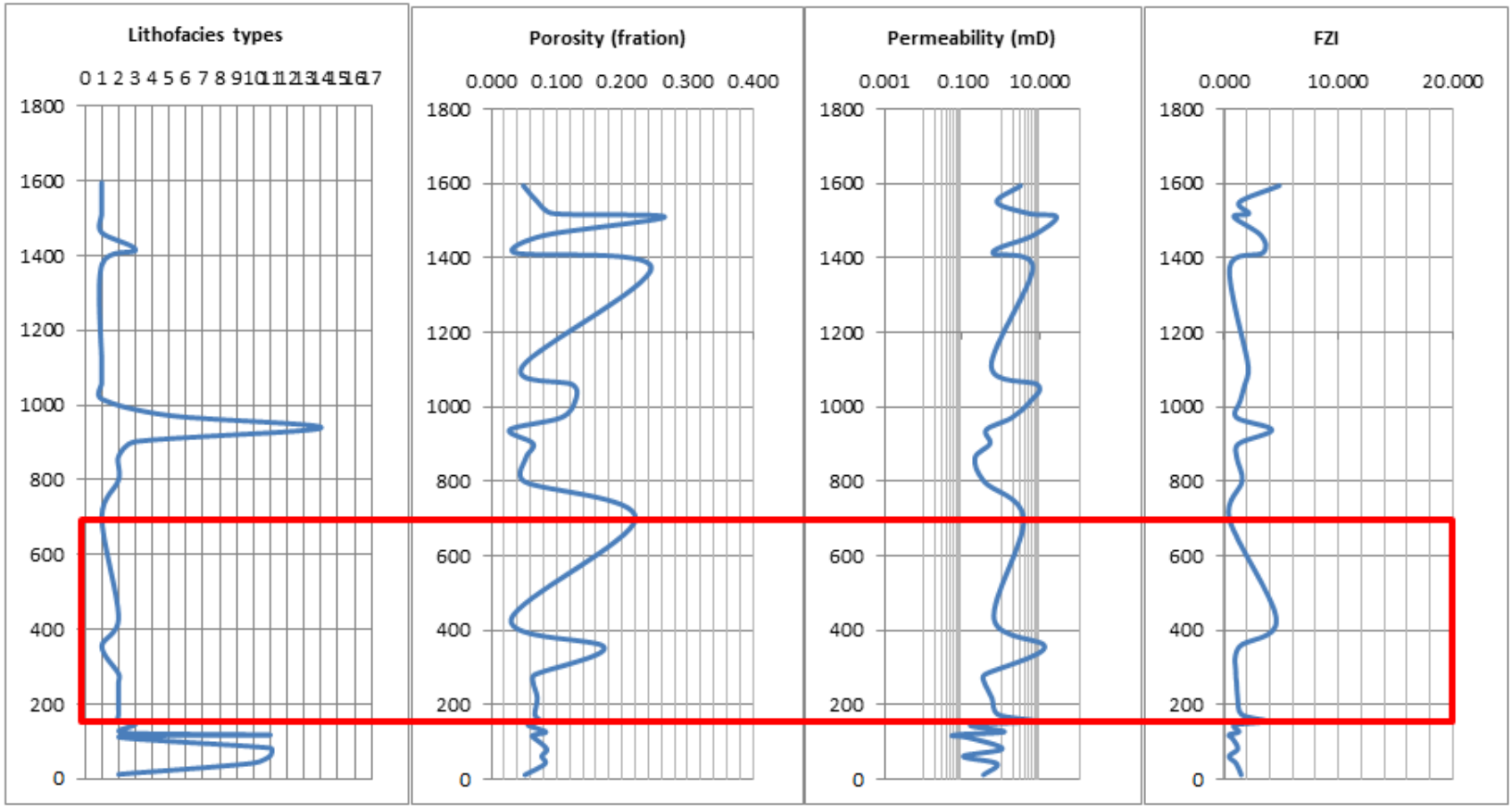

Figure 5.17. Vertical stack of the intra-reservoir bodies shown in function of their lithofacies types, porosity, permeability, and quality indices. Data from outcrop 1.

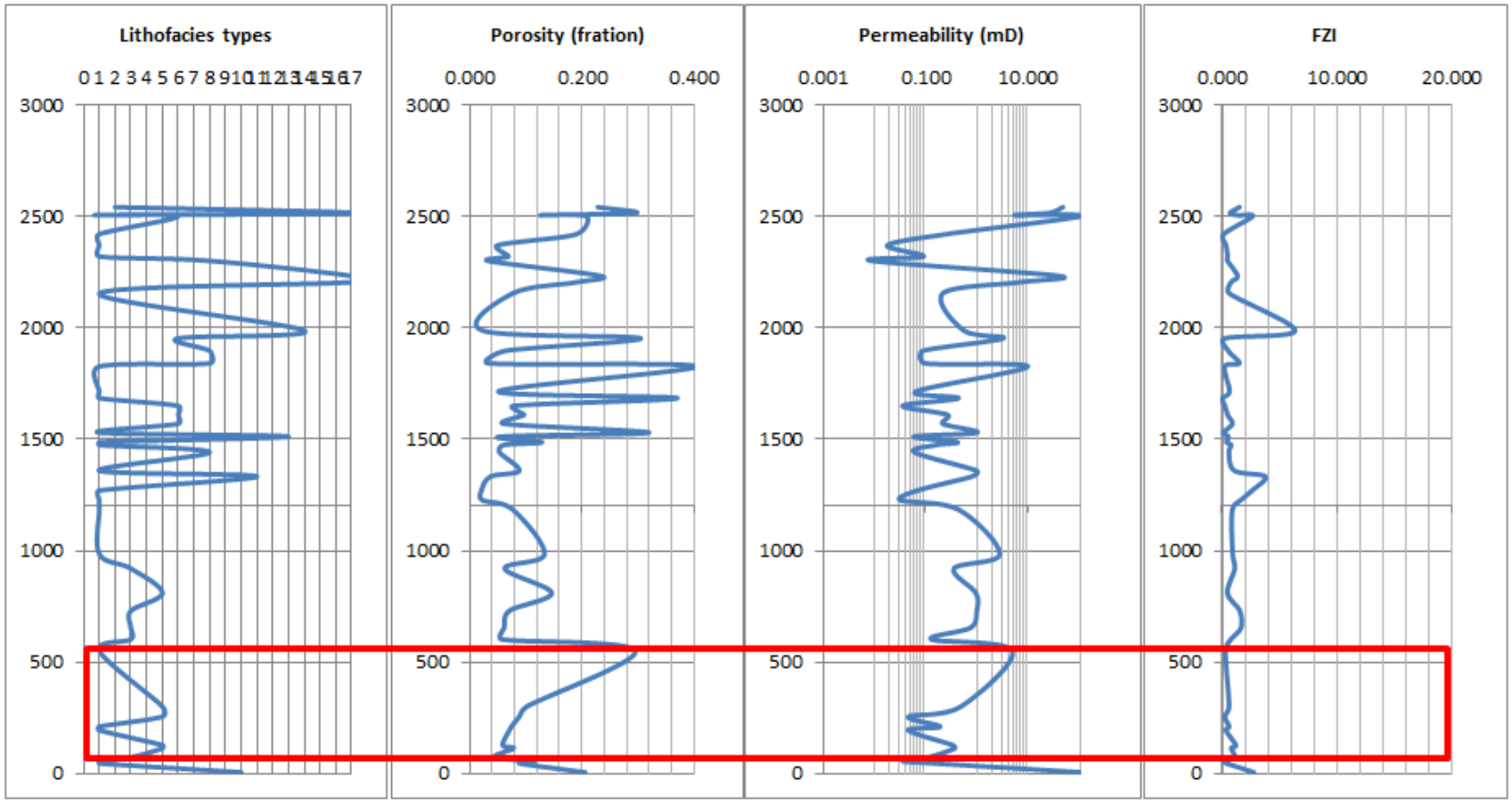

Figure 5.18. Vertical stack of the intra-reservoir bodies shown in function of their lithofacies types, porosity, permeability, and quality indices. Data from outcrop 2.

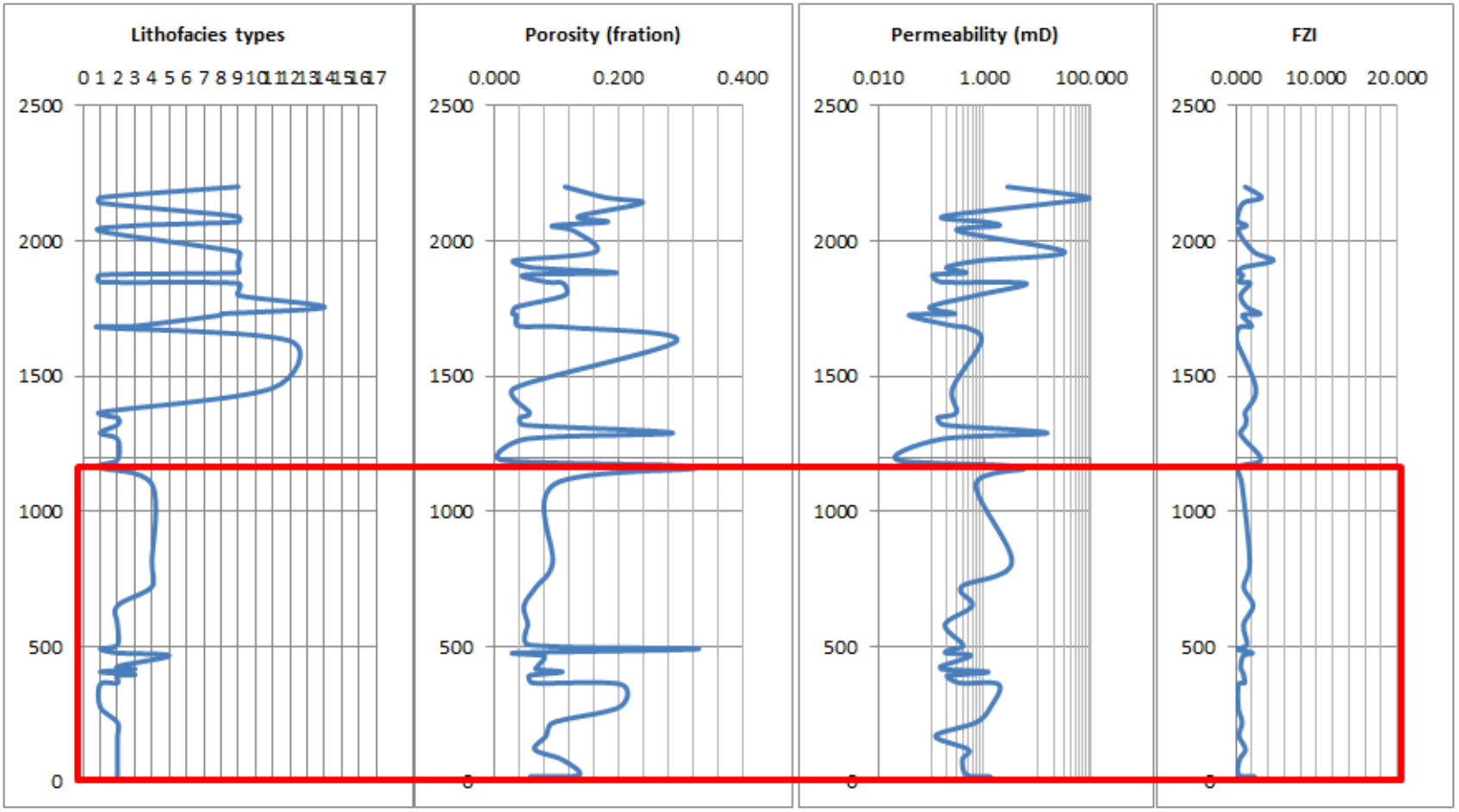

Figure 5.19. Vertical stack of the intra-reservoir bodies shown in function of their lithofacies types, porosity, permeability, and quality indices. Data from outcrop 3.

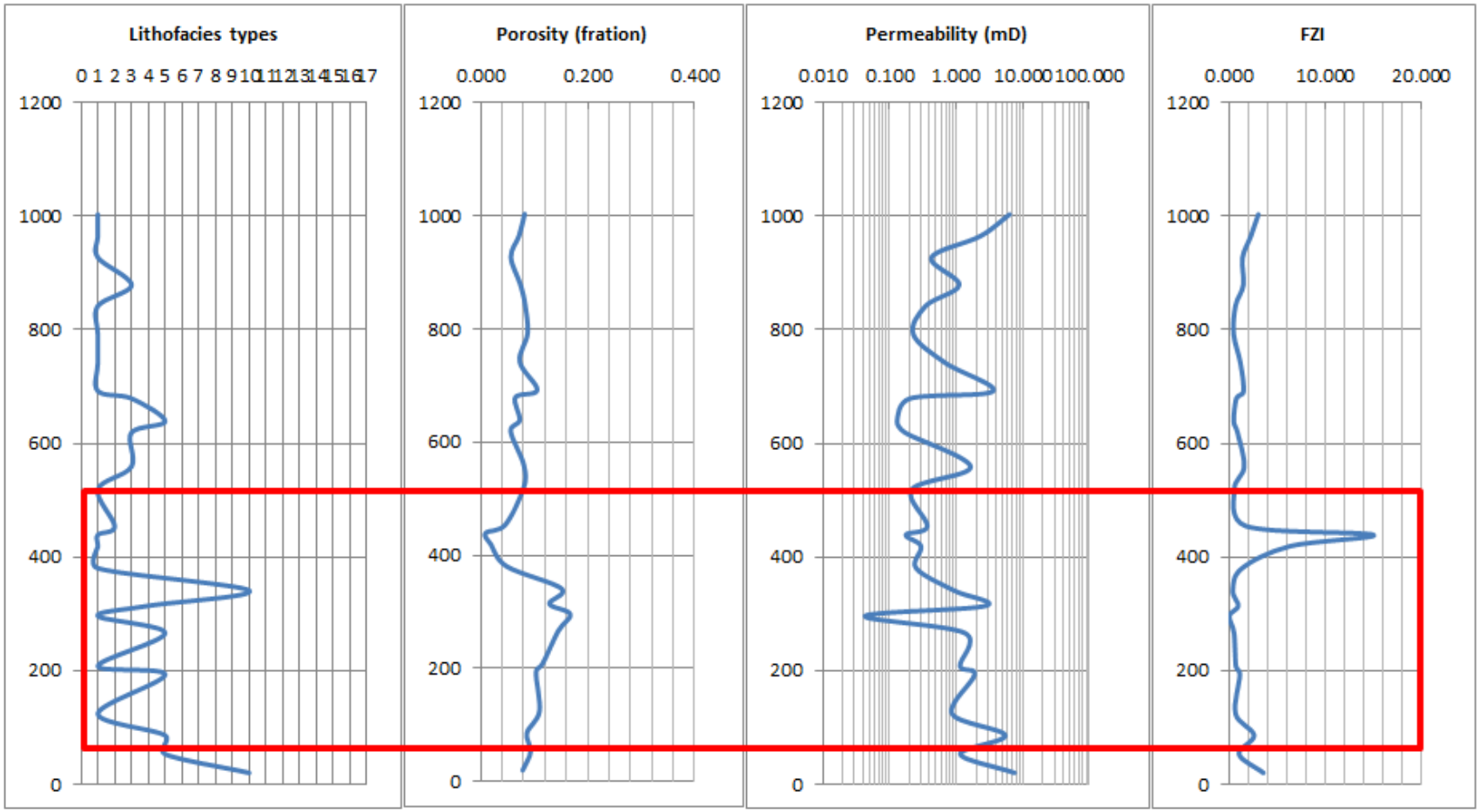

Figure 5.20. Vertical stack of the intra-reservoir bodies shown in function of their lithofacies types, porosity, permeability, and quality indices. Data from outcrop 4.

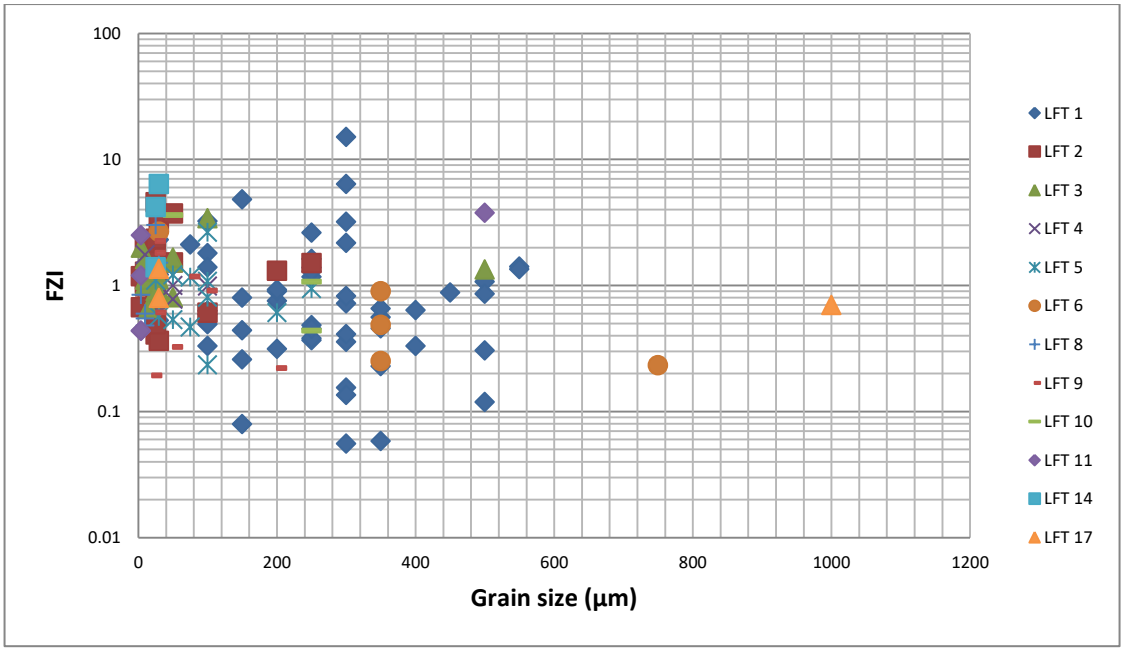

Figure 5.21. Cross-plot showing the absence of any correlation between grain size and FZI.

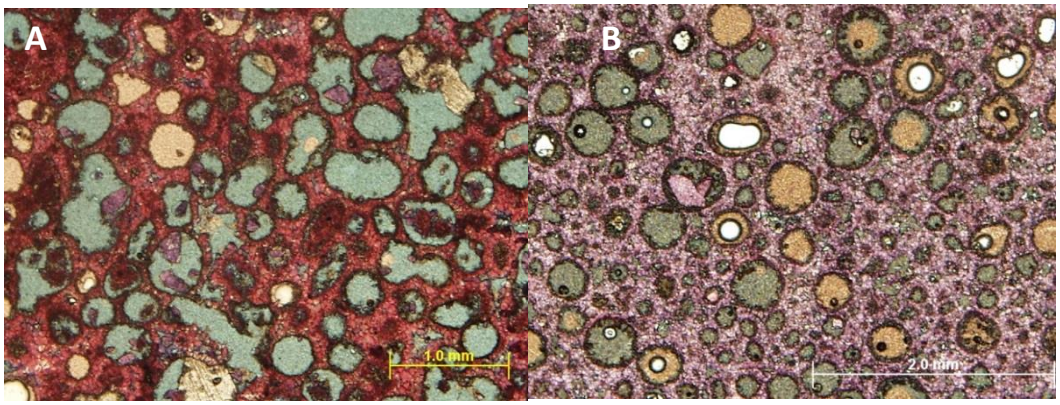

Lithofacies type		Coarse-grained oolitic grainstone (A)	Coarse-grained oolitic grainstone (B)
Grain size		500	500
Depositional texture	Porosity (fraction)	0.4	0.4
	Permeability (mD)	120000	120000
	RQI	17.2	17.2
	ΦZ	0.67	0.67
	FZI	25.8	25.8
Overprinted texture	Porosity (fraction)	0.27	0.305
	Permeability mD	25.8	4.9
	RQI	0.3	0.1
	ΦZ	0.36	0.42
	FZI	0.9	0.3

Figure 5.22. Thin-section microphotographs and reservoir quality data illustrating the control of pore-type on reservoir quality. (A) vugs are most likely enhancing the connectivity (B) illustration of isolated molds of dissolution enhanced oomoldic porosity. Lower table given some reservoir characteristics.

5.4.3. Horizontal reservoir heterogeneity and quality (at inter-well scale)

The geobody architecture of the Upper Khartam Member is composed of a complex amalgamation of intertidal-subtidal sheet-like and channelized bodies (Adam et al., under review). Even though, the depositional reservoir quality is expected to have great lateral continuity and a high degree of homogeneity at least at inter-well spacing (5 km). This is mainly controlled by the syn-depositional processes favored during deposition of the Upper Khartam sediments.

To study the lateral reservoir connectivity nine reservoir bodies (five bodies from outcrop 1, i.e. bodies B9B, B10A, B12C and B13C that occur as sheet-like bodies and B11E occurring as intertidal channels) and four from outcrop 2 (including B12B occurring as tidal creeks, B14C and B20B occurring as sheet-like bodies, and B15B occurring as intertidal channels). Geobodies are defined based on macroscopic uniform lithological characteristics that are different from over- and underlying lithologies. The studied geobodies are composed of four dominant lithofacies types (LFT 1, 2, 5, and 6) and sampled transect occur over a lateral spacing of 5 m (Figure 3). The samples were analyzed for porosity and permeability to calculate RQI, Φz, and FZI (Table 5.4). The depositional quality of the selected reservoir bodies show, as expected, homogeneous and unique quality indices over their lateral extend. Essentially, the overprinted reservoir qualities of the studied lithofacies types in their lateral extension were obliterated by diagenesis, which resulted in a segmentation of a single unit into ranges of qualities and hence several hydraulic units (4–7 HUs; Figure 5.23), which range in quality from extremely poor to moderate. For example in

outcrop 1 (geobody B9B), the interlaminated quartz-bearing recrystallized limestone lithofacies type (LFT2), occurring as sheet-like bodies was segmented into six hydraulic classes (with FZI values ranging between 0 and 3; Figure 23A and C). Similarly, the coarse-grained oolitic grainstone (LFT1) occurring as channelized bodies (geobody B11E) was segmented into three hydraulic classes (with FZI values ranging between 0.19 and 6; Figure 23A and C). Furthermore, in outcrop 2, the coarse-grained oolitic grainstone occurring as intertidal creeks (geobody B12B) was segmented into five hydraulic classes (with FZI values ranging between 0 and 3; Figure 23A and C). Similarly, the coarse-grained oolitic grainstone occurring as channelized bodies (geobody B15B) has been segmented into four HUs classes (with FZI values ranging between 0 and 0.75; Figure 23A and C). Certainly, these compartmentalisations have critically influenced pore attributes and eventually affected lateral intra-reservoir body connectivity. On the other hand, XRD data confirm the proportional relationship between FZI and calcite content (Figure 5.25) Additionally, quartz (likely of detrital origin, since authigenic quartz is scarese) and (diagenetic) celestine show a proportional relationship with the FZI (Figure 5.25). In addition, clay minerals and iron-oxides are occurring as dispersive pore lining phases as evidenced by SEM and EDS (Figure 5.26), and differentially affected reservoir quality (Figure 5.11), while quartz and celestine (from XRD) occur as partial pore-filling minerals and hence will have relatively less impact on the pore geometry compared to the damage that can be caused by the pore-lining clay minerals. Celestine most probably formed during the transformation of the aragonite to calcite and preferentially developed in the coarse-grained oolitic grainstone of the intertidal channels that underly the microbialite build-ups (Baker and Bloomer, 1988). In general, accessory mineral content has little impact on the quality indices of the

studied units, except clay minerals that can block the pore space causing a conspicuous reduction of the permeability values.

The SEM observations revealed a prominent control of cementation and dissolution on porosity and permeability, which are related to pore and pore-throat attributes (e.g., geometry, type, and size). The differential mold-filling calcite cement of the oolitic grainstone of the intertidal sheets and intertidal channels significantly reduced porosity and permeability and hence affected the lateral connectivity of a single intra-reservoir layer at the inter-well spacing. This caused a lateral compartmentalization (Figure 87 and 88 and Table 5.4.). Therefore, the observed lateral compartmentalization was caused by this differential cementation. Most critically, the diagenetic evolution was also controlled by stylolites and fractures, which form both barriers (stylolites) to and conduits (fractures) for vertical fluid flow and most likely control differential cementation and dissolution processes. This is inferred from a cross-plot showing the proportional relationship between FZI ranges and stylolites intensity (Figure 5.29). The B12B body (intertidal creeks) is characterized by relatively less stylolite intensity compared to the B14C body (intertidal flats). In addition, B14C has wide ranges of FZI along its lateral extension, while B12B has a narrow range of FZI. This indicates that stylolites exert some influence on the lateral reservoir quality over short inter-well distances. In addition, the lateral connectivity of the intra-reservoir bodies in their regional extend (high-frequency sequences; field-scale) is also heterogeneous and this is attributed to the regional variations in the lithofacies and geobody architecture. For example, in one of the high-frequency sequences described by Adam et al. (under review; i.e.HFS 2), the lithofacies changes laterally from fine-grained oolitic grainstone to coarse-grained oolitic grainstone and from interlaminated quartz-bearing recrystallized limestone to fine-grained oolitic

grainstone (Figure 5.30) These variations are associated with changes in reservoir properties (Figure 5.17 to 23). Furthermore, regional high-resolution stratigraphy (at fifth-order level; Adam et al., under review) indicated a regional change in the architectural types, which further complicates regional field scale reservoir connectivity that eventually will impact fluid flow.

In summary, the detailed diagenetic analysis allowed the establishment of the diagenetic paragenesis. The Upper Khartam carbonates were subjected to three major diagenetic settings, i.e. eogenesis, mesogenesis, and tellogenesis. These settings differentially affected the quality and the heterogeneity of the studied reservoir interval (Figure 5.31). Eogenesis is characterized by fibrous shallow marine cementation and partial and moldic dissolution with prominent dolomitization preferentially taking place in two stratigraphic positions, i.e. in association with microbialites and near the contact with the Sudair evaporites. Ooids seem not to suffer from physical compaction since neither plastic nor brittle deformation features have been observed. This is attributed to framework stabelisation due to early cementation. In a recent study on the Upper Dalan reservoir in Kish Gas field, Iran (equivalent to Khuff reservoir of KSA, Bahrain, Oman, Qatar, and UAE) prominent moldic and vuggy porosity was recognised (Amel et al., 2015). This may point to a period of intense meteoric diagenesis prior to burial diagenesis. Therefore eogenesis positively affected reservoir quality and most likely enhanced the porosity and permeability. The mesogenesis is mainly characterized by stylolitization and fracturing. These act as very important barriers and conduits for the diagenetic fluids respectively. Accordingly they played a central role in the differential cementation and hence compartmentalization of the intra-reservoir bodies at the inter-well spacing.

Tellogenesis overprinted the earlier diagenetic products. This setting is characterized by consecutive orders of equant cementation, dissolution, and development of pore lining clay minerals. These have been oriented by the mesogenesis stylolites and fractures and they cause a severe raise in the level of the reservoir heterogeneity.

Table 5.4. Selection of reservoir quality data for the studied intra-reservoir bodies. Abbreviations: Φ and K correspond to porosity and permeability respectively, and Max, Min, Average, and STD (maximum, minimum, average and standard deviations).

Reservoir bodies	Lithofacies types	Architectural type	Statistical analysis	Present-day measurements				
				Φ (f)	K (mD)	RQI	Φz	FZI
B9B	LFT 2	Sheet-like	Max	0.24	6.69	0.23	0.32	1.64
			Min	0.08	0.03	0.01	0.09	0.06
			Average	0.15	1.19	0.07	0.18	0.46
			STD	0.05	1.62	0.06	0.07	0.43
B10A	LFT 2	Sheet-like	Max	0.08	3.06	0.19	0.09	2.03
			Min	0.04	0.01	0.02	0.04	0.24
			Average	0.06	0.53	0.06	0.06	0.91
			STD	0.01	0.82	0.05	0.02	0.54
B11E	LFT 1	Channelized	Max	0.25	23.58	0.39	0.34	4.64
			Min	0.01	0.04	0.04	0.01	0.35
			Average	0.11	3.99	0.13	0.13	1.55
			STD	0.07	5.49	0.09	0.09	1.18
B12C	LFT 1	Sheet-like	Max	0.29	18.08	0.27	0.40	2.11
			Min	0.29	18.08	0.27	0.40	2.11
			Average	0.11	0.19	0.03	0.13	0.10
			STD	0.06	4.87	0.08	0.09	0.57
B13C	LFT 5	Sheet-like	Max	0.15	0.75	0.09	0.18	0.89
			Min	0.06	0.11	0.03	0.07	0.18
			Average	0.11	0.29	0.05	0.12	0.45
			STD	0.03	0.22	0.02	0.03	0.27
B12B	LFT 1	Small creeks	Max	0.32	52.91	0.42	0.46	1.62
			Min	0.06	0.04	0.02	0.07	0.07
			Average	0.21	4.11	0.09	0.28	0.37
			STD	0.07	8.29	0.07	0.10	0.31
B14B	LFT 5	Sheet-like	Max	0.13	12.22	0.34	0.15	3.80
			Min	0.02	0.05	0.04	0.02	0.36
			Average	0.08	2.39	0.13	0.09	1.59
			STD	0.03	2.92	0.08	0.03	0.84
B15B	LFT 1	Channelized	Max	0.30	26.93	0.30	0.42	1.28
			Min	0.06	0.04	0.01	0.07	0.05
			Average	0.16	1.83	0.06	0.20	0.33
			STD	0.06	4.39	0.05	0.08	0.23
B20B	LFT 6	Sheet-like	Max	0.36	14.42	0.27	0.56	1.28
			Min	0.07	0.03	0.02	0.08	0.08
			Average	0.20	3.06	0.10	0.26	0.45
			STD	0.08	3.98	0.07	0.13	0.33

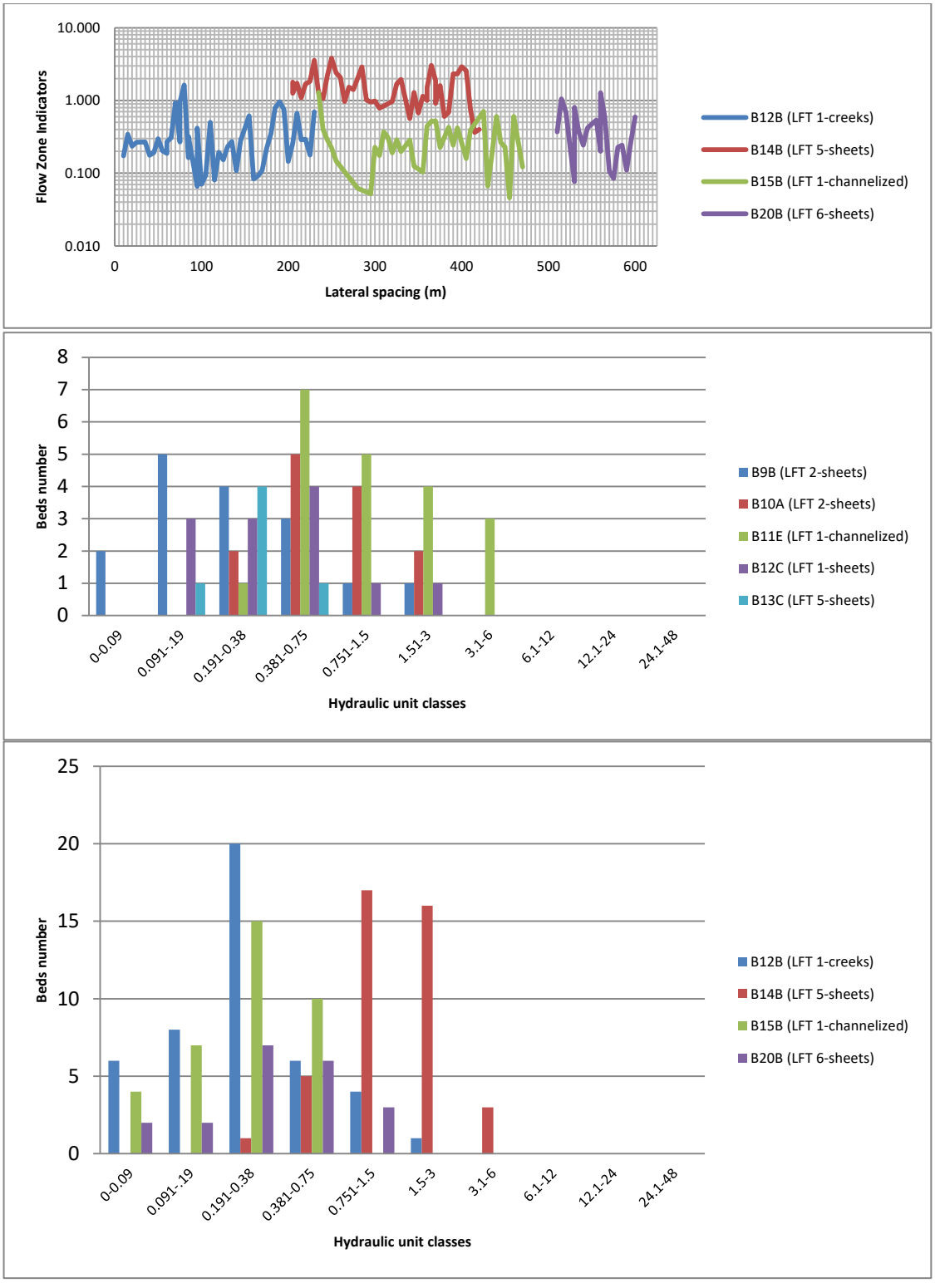

Figure 5.23. Present-day qualities of the studied intra-reservoir bodies. A) illustration of the intensive lateral variations in the FZI (compare with Figure 12-A). B) and C) show the segmentation of the studied bodies in function of their lateral extension of the outcrop 1 and 2 respectively (see the text).

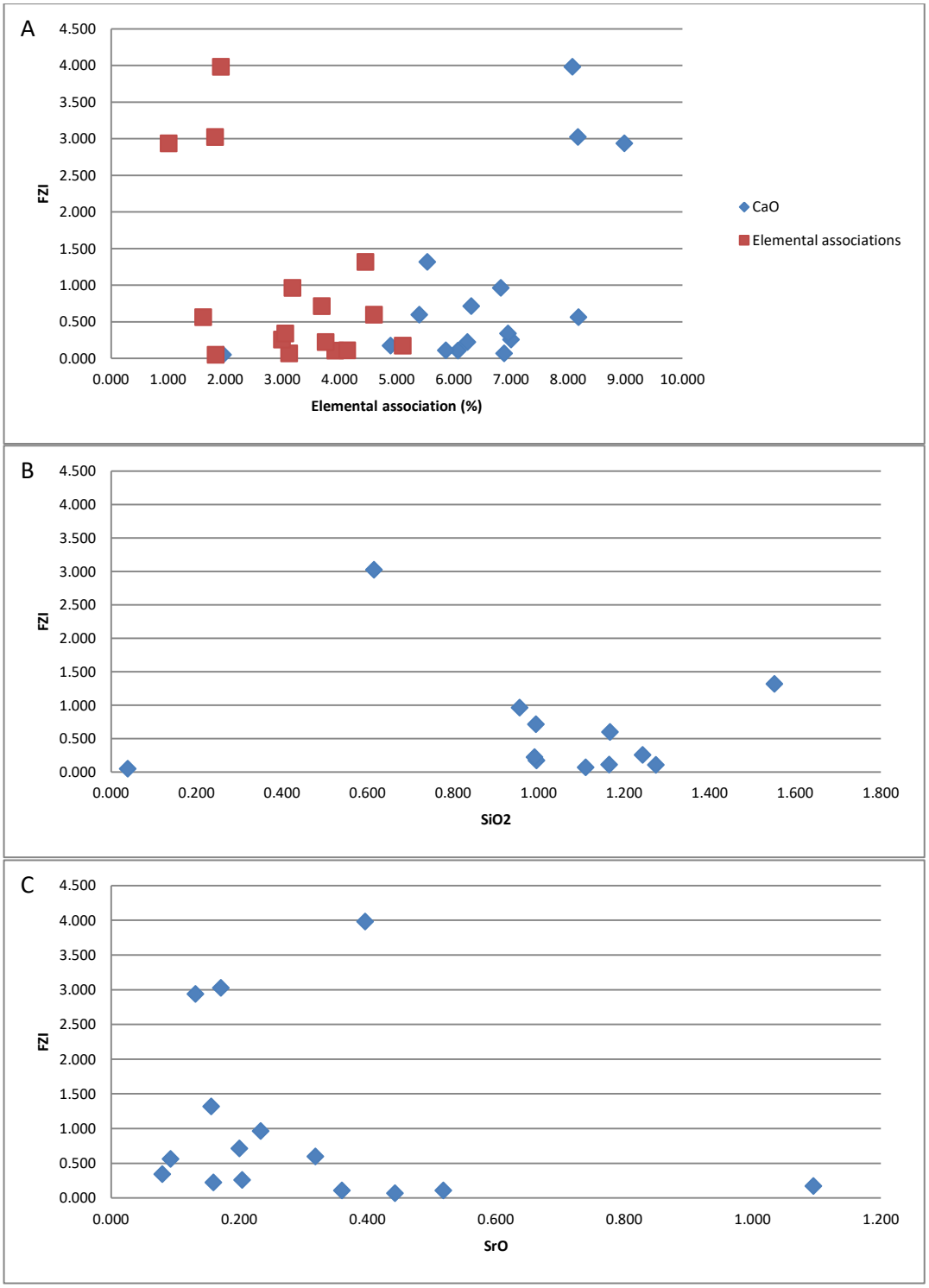

Figure 5.24. Crossplots between the FZI values and certain geochemical associations (from XRF). A) Showing the proportional relationship between the FZI and CaO content and the inverse relationship between the FZI and the other geochemical associations such as Si, Sr, Fe, SO content, B) and C) show the clear inverse relationship between FZI and Si and Sr respectively.

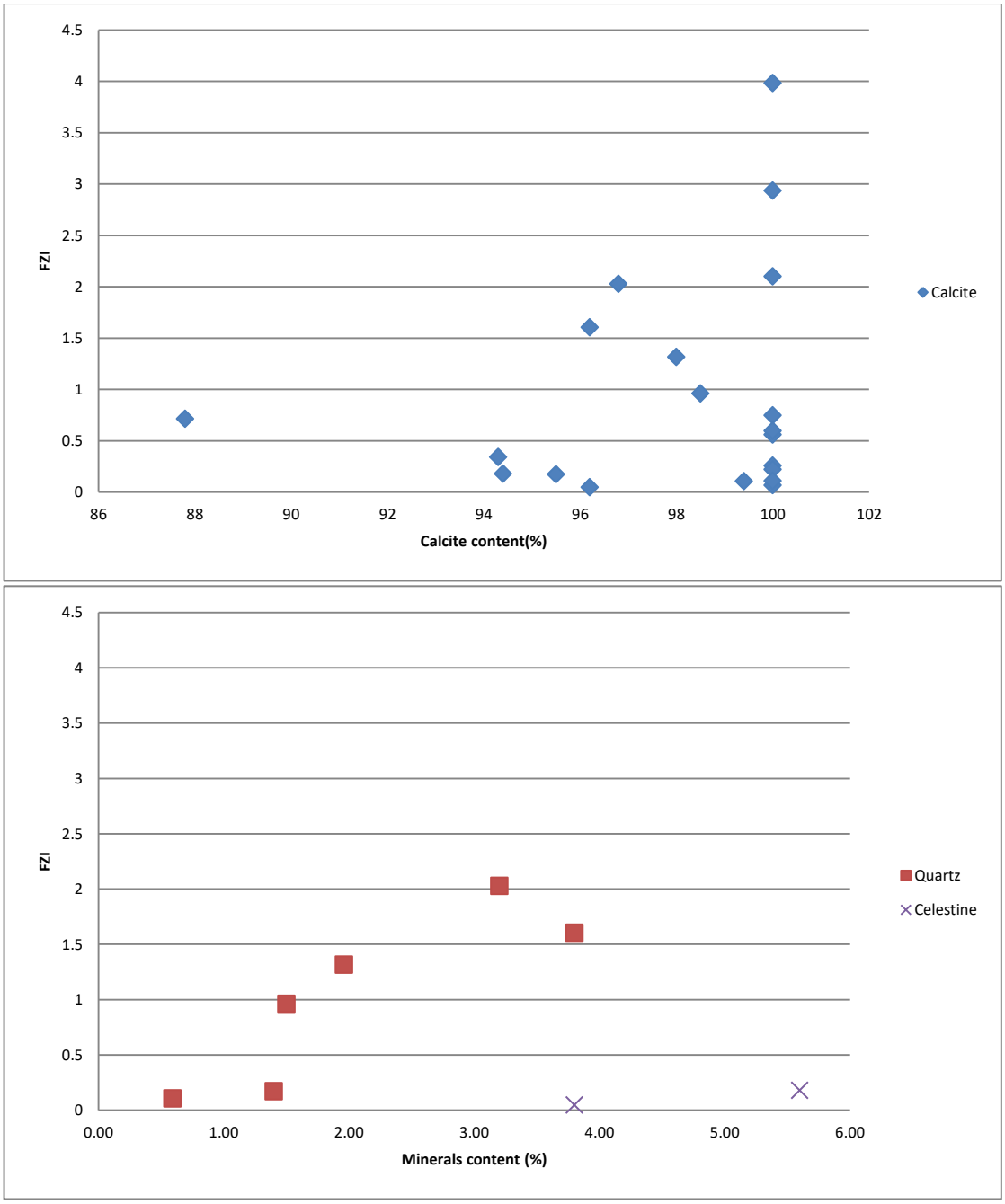

Figure 5.25. Crossplots between FZI and the mineralogical associations (from XRD). A) and B) illustration of the proportional relationship between FZI and the calcite ($CaCO_3$), quartz (SiO_2), and celestine ($SrSO_4$).

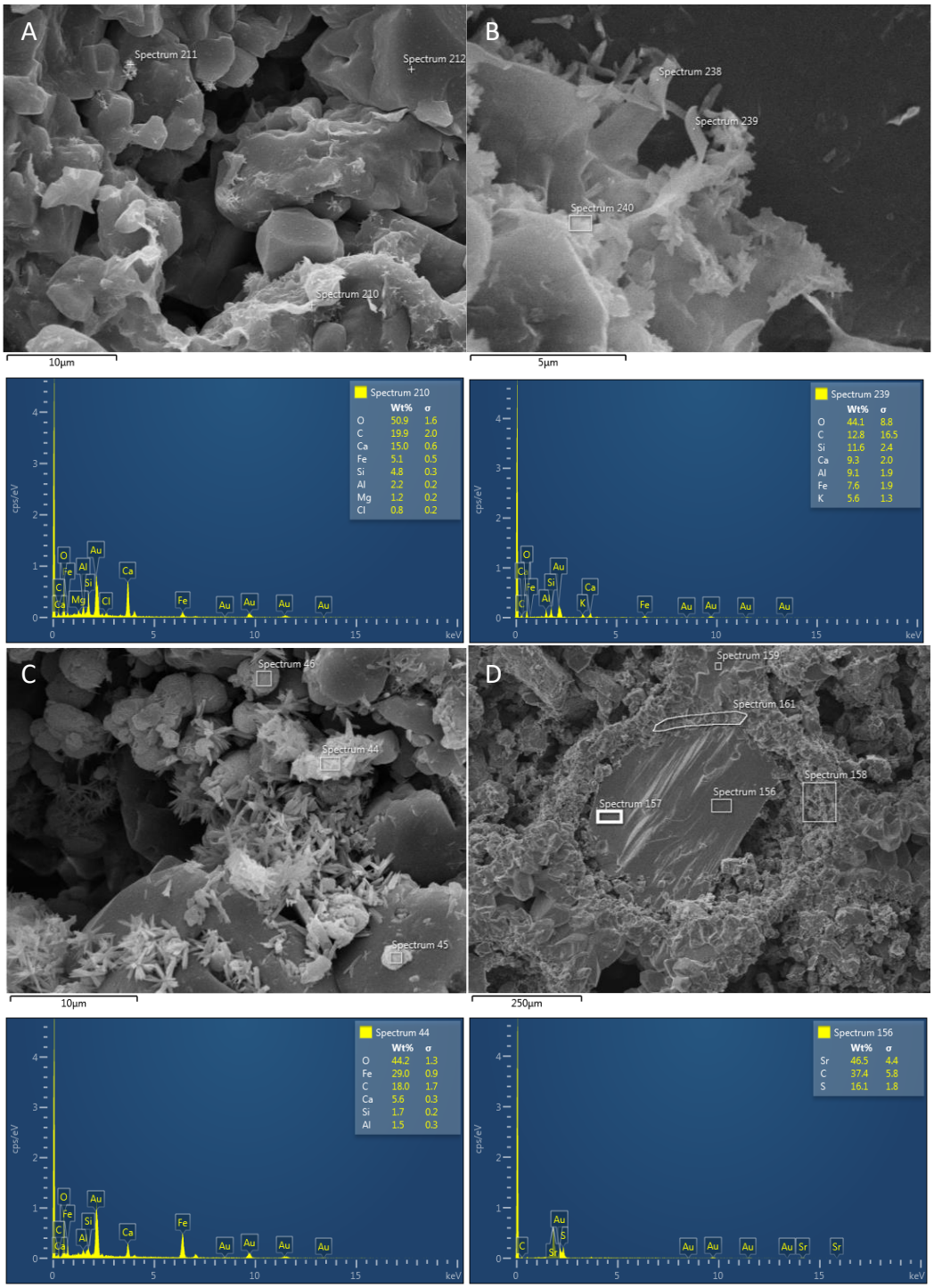

Figure 5.26. SEM photographs of pore-lining and pore-filling minerals and their EDS spectra below the photographs. A and B) Illustration of clay minerals lining the pores and destroying reservoir quality (samples are from B9B and B14B respectively), C) Iron oxides lining the pore walls and decreasing the FZI values (sample from B14B), D) Celestine crystal filling a pore. This has a relatively limited negative impact on reservoir quality (sample from B12C).

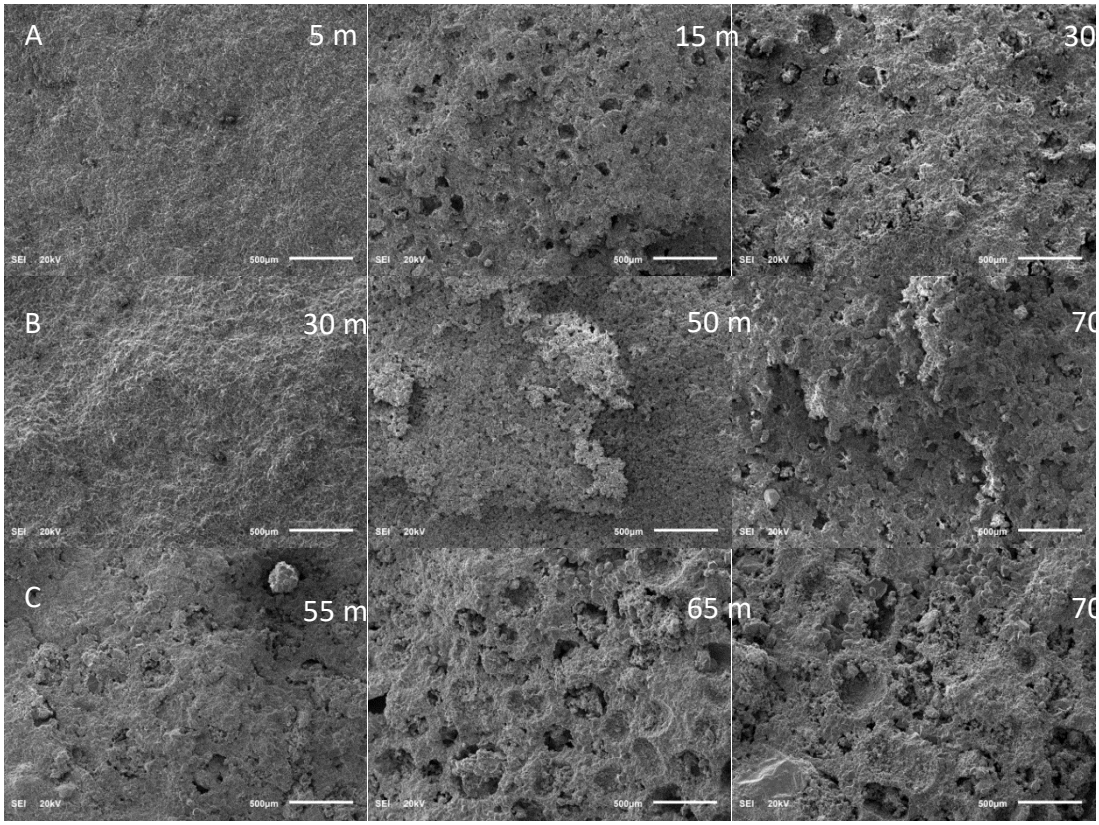

Figure 5.27. SEM images showing the cementation and variations in moldic porosity in the studied reservoir lithologies (outcrop 1). A) Illustration of reservoir lithology B9B at lateral distances of 5, 15, and 30m respectively, B) Illustration of reservoir lithology B11E at lateral distances of 30, 50, 70 m respectively, C) Illustration of reservoir body B12C at lateral distances of 55, 65, 70 m respectively. These variations in the degree of cementation and dissolution causes the lateral heterogeneities in reservoir quality in a single reservoir segment (see Table 5.5).

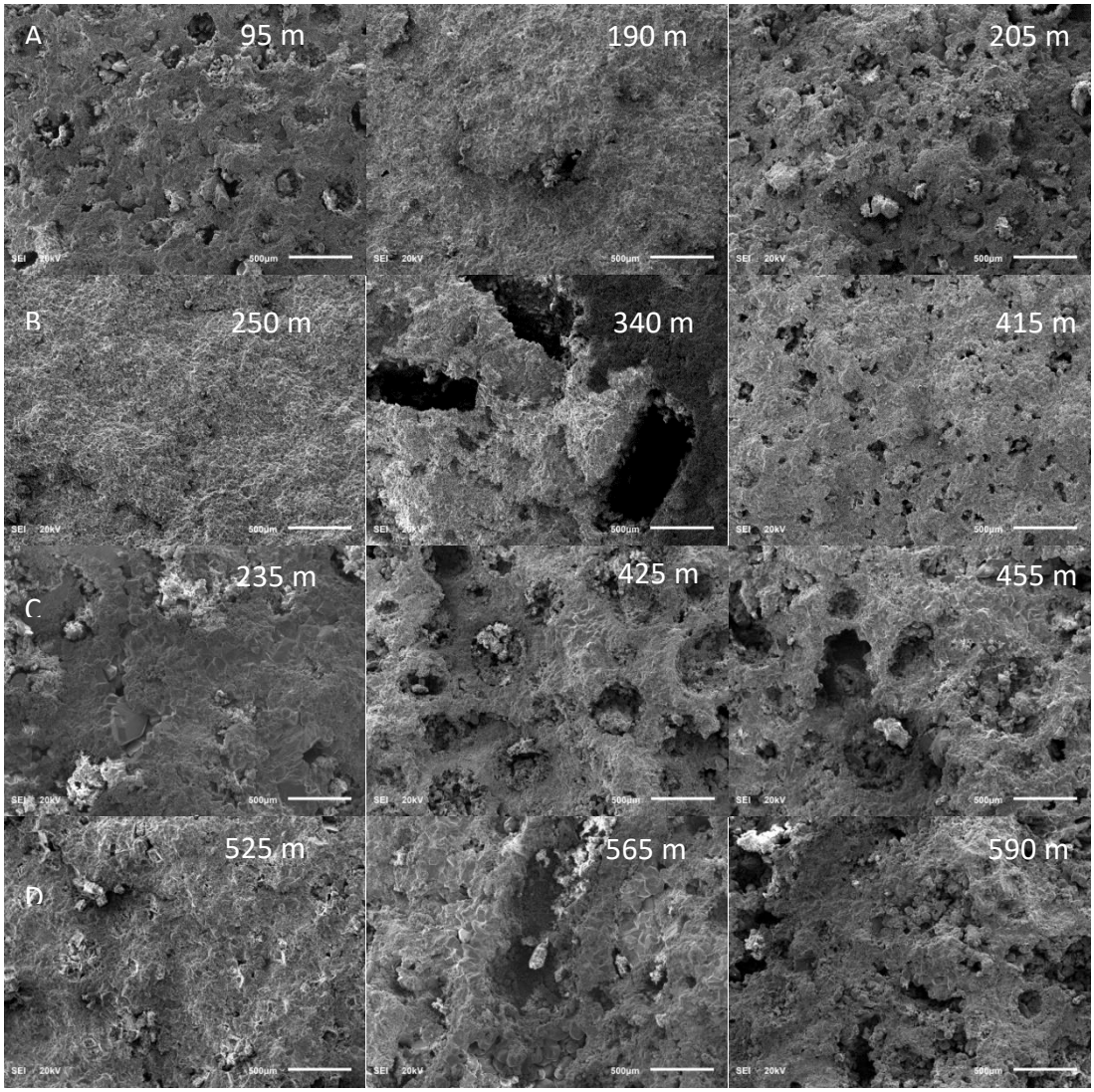

Figure 5.28. SEM images showing the cementation and variations in porosity types in the studied reservoir lithologies (outcrop 2). A) Illustration of reservoir body B12B at lateral distances of 95, 190, 205m respectively. B) Illustration of reservoir body B14B at lateral distances of 250, 340, 415m respectively. C) Illustration of reservoir body B15B at lateral distances of 235, 425, 455m respectively. D) Illustration of reservoir body B20B at lateral distances of 525, 565, 590 m respectively. These variations illustrate the lateral heterogeneities in reservoir quality in a single body (see Table 5.5).

Table 5.5. Data on heterogeneities of the presented samples in figure 87 and 88. Abbreviations; Φ, K, RQI, Φz, and FZI are core porosity, permeability, reservoir quality index, normalized porosity, and flow zone indicator.

Outcrop code	Sample ID	Φ (fraction)	K (mD)	RQI	Φz	FZI
Outcrop 1	B9B-5	0.081	0.270	0.057	0.088	0.650
	B9B-15	0.167	0.140	0.029	0.200	0.144
	B9B-30	0.218	0.080	0.019	0.279	0.068
	B11E-30N	0.013	0.040	0.056	0.013	4.332
	B11E-70N	0.253	8.600	0.183	0.339	0.541
	B11E-50	0.153	23.600	0.390	0.181	2.159
	B12C-55N	0.113	8.200	0.267	0.127	2.100
	B12-65N	0.260	18.100	0.262	0.351	0.746
	B12C-70	0.287	1.500	0.072	0.403	0.178
Outcrop 2	B12-95	0.305	0.260	0.029	0.439	0.066
	B12-140	0.181	0.100	0.023	0.221	0.106
	B12-190	0.302	52.900	0.416	0.433	0.961
	B12-205	0.078	0.037	0.022	0.085	0.256
	B14-250	0.016	0.068	0.065	0.016	3.981
	B14-365	0.102	12.200	0.343	0.114	3.023
	B14-340	0.114	0.600	0.072	0.129	0.560
	B14-400	0.102	11.500	0.333	0.114	2.935
	B14-415	0.125	0.300	0.049	0.143	0.341
	B15-230	0.063	0.500	0.088	0.067	1.316
	B15-305	0.147	0.130	0.030	0.172	0.171
	B15-425	0.296	26.900	0.299	0.420	0.712
	B15-455	0.276	0.090	0.018	0.381	0.047
	B20-525	0.137	0.170	0.035	0.158	0.221
	B20-565	0.264	12.200	0.213	0.359	0.595
	B20-590	0.358	1.300	0.060	0.558	0.107

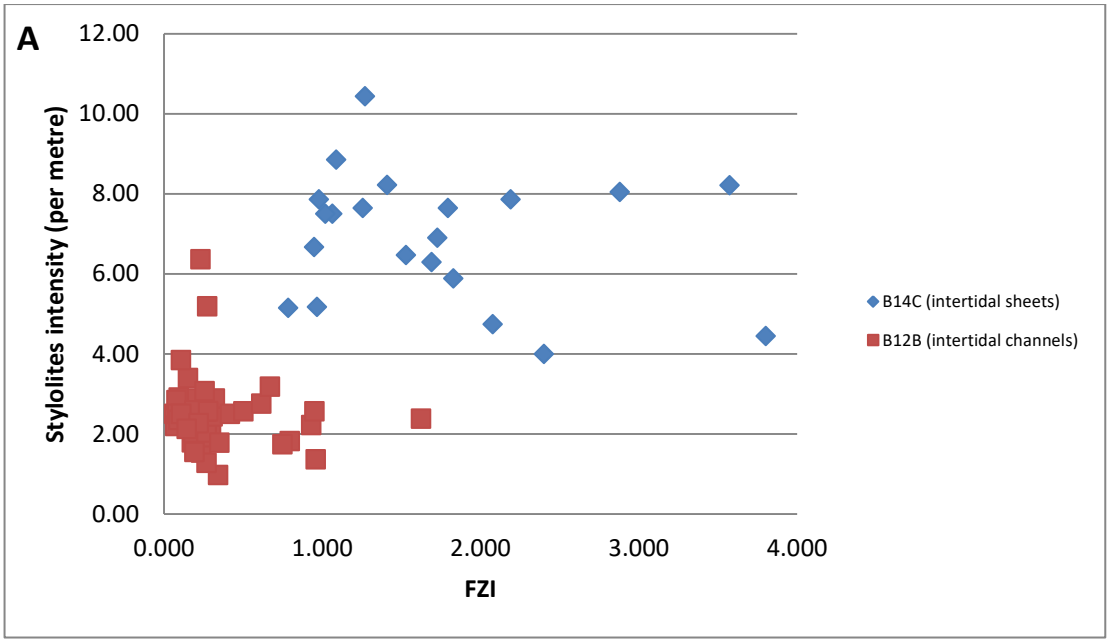

Figure 5.29. A) Field-photos showing stylolite frequency in B12B and B14B, with higher frequency in B12B compared B14B, B) Correlation between stylolite frequency (per metre) and lateral reservoir quality heterogeneity (FZI). This cross-plot indicates that the intertidal creeks (B12B; grain sizes of 500µm) display a lower stylolite frequency compared with the intertidal flats (B14C; grain sizes 200 µm). In addition, the intertidal sheet-like bodies of B14C has wide ranges of FZI along its lateral extension, while B12B has a narrow range of FZI. This indicates that stylolites exert a clear influence on the lateral reservoir quality over short inter-well distances. Note; red is the geobody boundaries, blue and black are the stylolites.

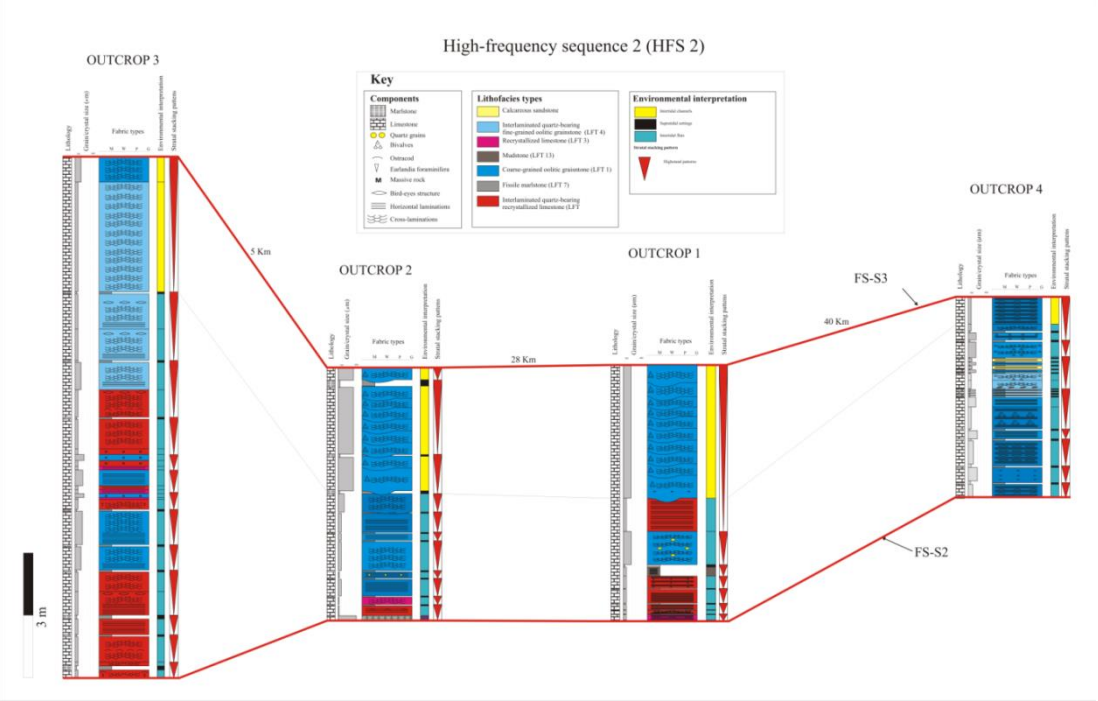

Figure 5.30. Regional correlation of the HFS 1 over the study area (70 km) showing the lateral lithofacies variation in the strike direction (Adam et al., under review).

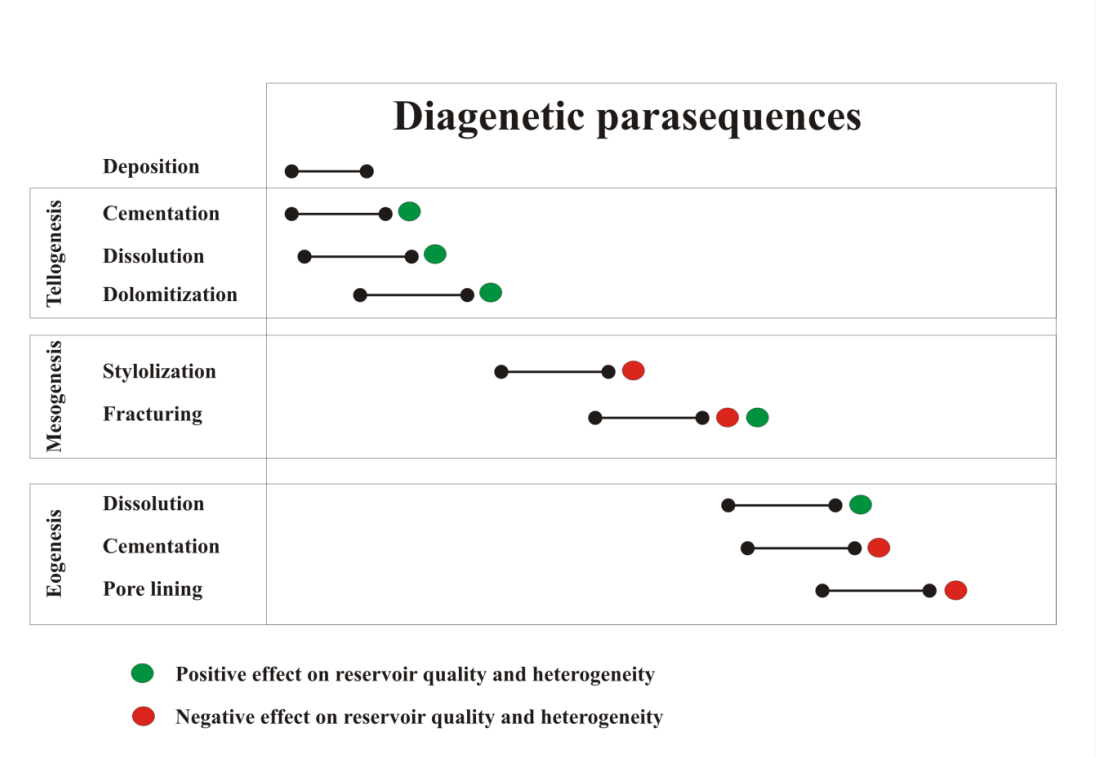

Figure 5.31. Schematic illustration of the diagenetic parasequences and their subsequent positive and negative effect on reservoir quality and heterogeneity.

CHAPTER 6

GEOSTATISTICAL MODELLING

6.1. Overview

The Khuff reservoirs are known for having heterogeneities properties and these were described to occur at inter-well and sub-seismic scale. Unrealistic geological modeling of these properties will impact optimal development and assessment of the Khuff reservoirs. The main objective is to build outcrop-based and valid geological models and deduce the implications of these models on fluid flow simulations. In this study we build multi-realization models based on three stratigraphic levels. The models are based on the high-resolution sequence stratigraphy framework and lateral resolution of 5 m. A total of 120 well sections were logged from sedimentological and petrophysical point of view. The wells are systematically arranged with 5 metre interwell spacing and coverage area of 750m (north-east) by 450m (south-west). This area was designed to cover the interwell spacing.

The Upper Khartam carbonates composed of seventeen lithofacies with the oolitic grainstone (40 %), recrystallized limestone (22%), bioclastic grainstone/packstone (4.4 %), and non-fabric preserved dolomite (2.4%) making up the bulk of the stratigraphy. At the bedset and fifth-order sequence stratigraphic levels, these lithofacies show lateral continuity with slight changes in the architectural parameter. Therefore, The Assign Value method of geostatistical modeling is used for building the lithofacies models at these levels. Although the data was drastically distorted at the high-frequency sequences, however, bedset level to some extent preserved the original

data. The Upper Khartam carbonates are composed of complexly amalgamated beds of different architectural elements and lithofacies types. Critically, these will impact reservoir heterogeneity and continuity and eventually fluid flow and productivity. Therefore, the detailed bed-level informations are used to model the Upper Khartam carbonates. Sequential Indicator Simulation method is used and the detailed variogram parameters are deterministically edited. Most critically, models are valid and consistent with the detailed sedimentological and sequence stratigraphic data.

Sequential Gaussian Simulation is used to model the petrophysical properties. Detailed matching process indicates major and minor directions of petrophysical properties of 70 and 330 degree respectively. These are obviously following the depositional trend. However, the porosity of intertidal sheets is of great horizontal ranges compared with the intertidal channels and creeks. They have average ranges of about 300 m, while intertidal channels and creeks have average ranges of about 150m. Even though, the minor porosity ranges of the different architectural types have the same values of about 50 m. Permeability variograms show no control of architectural types on ranges and continuities. Generally, the permeability has major ranges of 200 m wile minor continuity is about 60 m.

6.2. Introduction

Optimal exploitation of hydrocarbon reservoirs depends on the qualitative as well as quantitative geological characterization of these reservoirs. This includes the identification of architectural and quality elements from core plug to inter-well scale. This up-scaling addresses vertical (often at cm-scale) to lateral (regularly at metre-decametre-scale) correlations. Ultimately, this information should be represented in a 3D geocellular models with all geostatistical parameters (i.e., variograms parameters).

Small scale heterogeneities are believed to be beyond subsurface data. Outcrop analogues provide valuable insight into understanding ancient sedimentation processes and products (Grammer et al., 2004; Pringle et al., 2006; Catuneanu and Zecchin, 2013; Zecchin and Catuneanu, 2013). Outcrop studies have been utilized widely to understand critical quality and architectural elements within reservoir bodies (Zecchin and Catuneanu 2013; Alnazghah et al., 2013; Grammer et al., 2004; Haase and Aigner, 2013; Smith and Read, 1999; Zeller et al., 2011). Outcrops provide unique opportunity to characterize small scale heterogeneities at the interwell spacing and beyond seismic resolution. Time- and depositional-equivalent outcrops are key in characterizing sub-surface carbonate reservoirs. Consequently, integrating outcrop-based geocellular modeling will enhance development and production of subsurface hydrocarbon bearing reservoirs. For examples, variograms parameter from outcrop equivalence will critically provide quantitative data on small scale heterogeneities near boreholes.

The Khuff reservoirs in Eastern Arabia are estimated to contain about 15 to 30% of the world's gas reserves (Al-Jallal, 1995; Al-Aswad, 1997; Koehrer et al., 2010). These reservoirs are known for having complex heterogeneities at the inter-well scale that is beyond seismic resolution (Janson et al., 2013). Therefore, optimum exploitation of these reservoirs is highly dependent upon understanding internal architectural structure that are controlled by syn-depositional processes and diagenetic overprinting. Outcrop equivalents of these reservoirs in central Saudi Arabia provide an interesting stratigraphic context, where thin bodies can be traced laterally over large distances. The latter can genetically be related to vertical stratal stacking patterns.

The main objective of this paper is to build multi-realization 3D geocellular models and eventually extracting geostatistical parameter for small scale intra-reservoir interwell heterogeneities of the Upper Khartam Member of the Khuff Formation. Eventually examine the impact of these models on fluid flow simulations. This member was described to be equivalent to Khuff A and B reservoirs in Eastern Arabian (Al-Dukhayyil and Al Tawil, 2006). The applied workflow allows for the better understanding of the intra-reservoir heterogeneities and provides a new quantitative analysis of quality heterogeneity of Khuff reservoirs. For this purpose, 120 outcrop sections were logged in detail from sedimentological and petrophysical point of view. The studied sections are covering an area of 750m by 450m and they have lateral spacing of 5m. Along bedding, beds were logged and a detailed composite section was established and about 500 samples were collected for petrographic and petrophysical analysis.

6.3. Database and methods

A total 120 outcrop sections were logged in detail from sedimentological and petrophysical point of view. A composite section was established and four intra-reservoir bodies were logged laterally at the well sections. The outcrop sections are located in the Buraydah quadrangle in central Saudi Arabia (Figure 6.1). The sections have a lateral spacing of 5m and they cover an area of 750m by 450m. The logs are based on a bed-by-bed field description and approximately 500 samples were collected for detailed petrographic and petrophysical analysis. Core plugs are mostly horizontal and 2 inch by 1 inch in length and diameter respectively. Porosity was measured using a helium porosimeter, while liquid (nitrogen) permeability was

obtained from gas permeability and verification of the Klinkenberg effect using a Hassler Core Holder assembly.

Three stratigraphic levels were modelled; these include the early established fifth-order high-frequency sequences, bedsets, and beds levels; these have cells number of 75336 (146X86X7), 213452 (146X86X18), and 2837656 (146X86X226) respectively (Figure 6.2). The measured sections were digitised and the lithofacies types were numerically coded using Microsoft Excel. The outcrop section, stratigraphic horizons, and the lithofacies, porosity, and permeability data were imported into Petrel 2016 for facies and petrophysical modeling and fluid flow simulations.

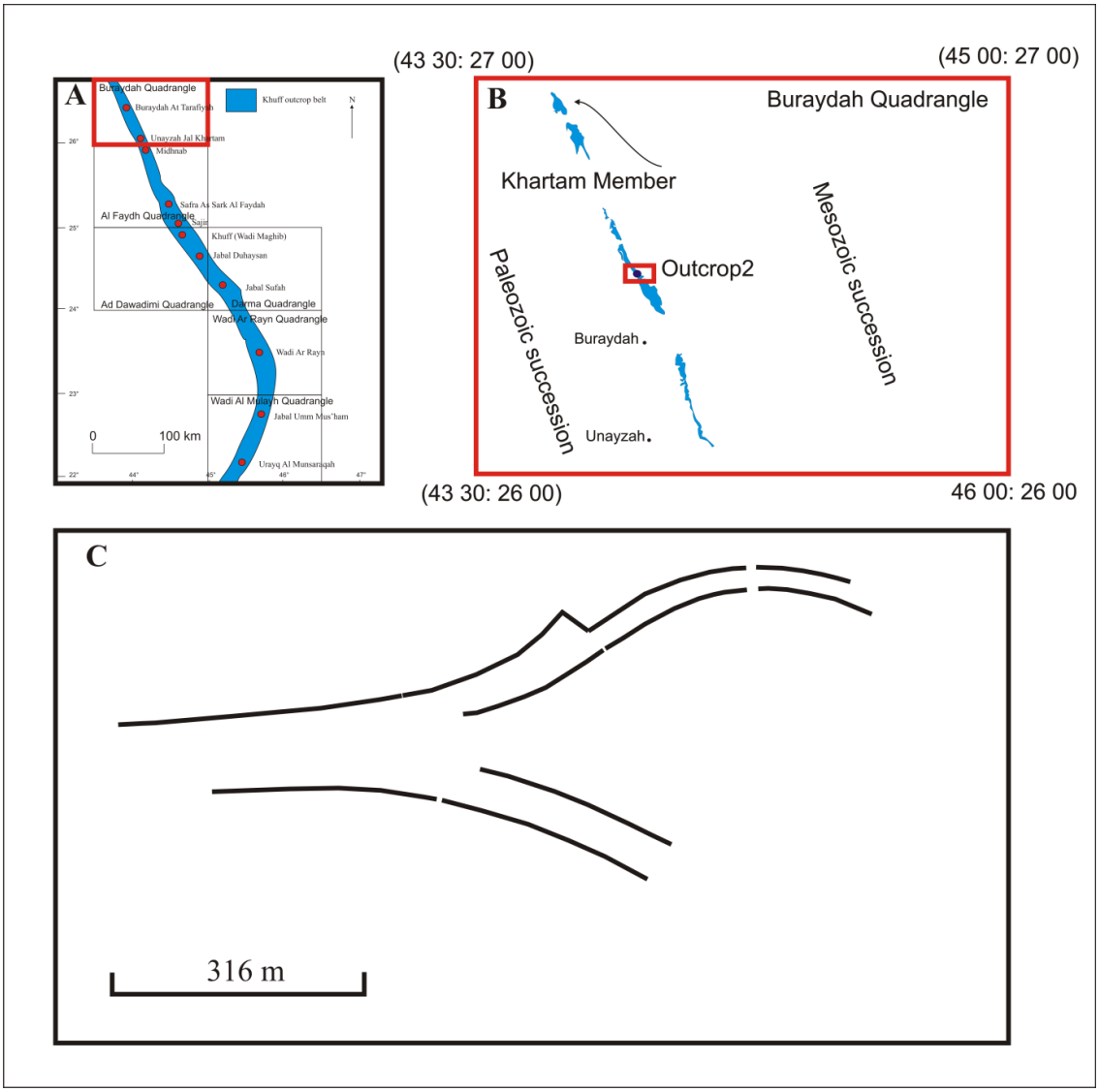

Figure 6.1. A) The Khuff Formation outcrop in central Saudi Arabia, B) the Khartam Member belt in the Buraydah quadrangle (red rectangular), C) the studied outcrop located in the Buraydah quadrangle (modified after Manivit et al., 1985b; Vaslet et al., 1985, 2005).

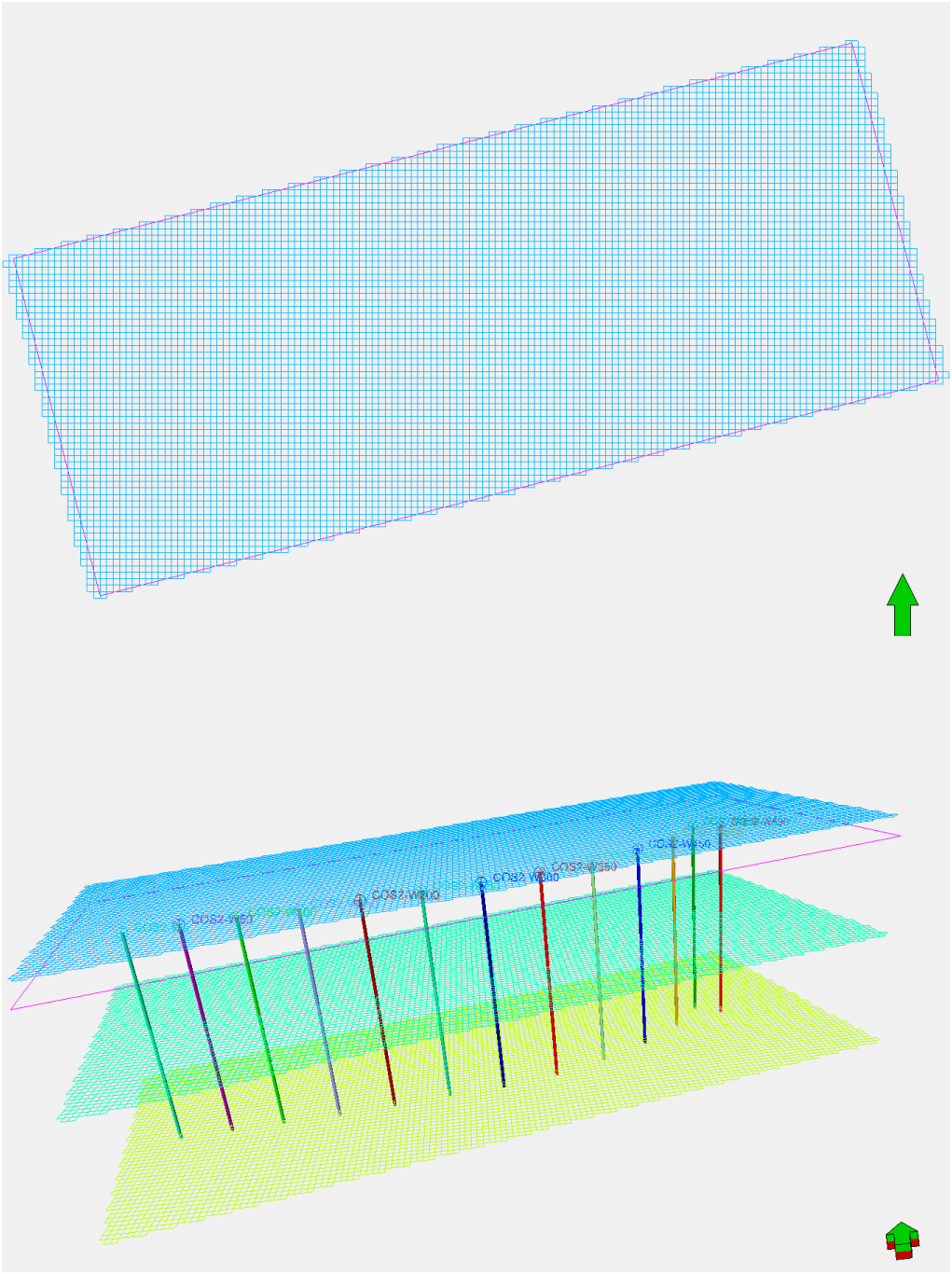

Figure 6.2. Pilar gridding of the studied area, the modelled rectangular is oriented in the north-east direction with symmetrical cells size in the horizontal direction (5m by 5m; spacing of the vertical outcrop sections), while vertical resolution designed to cover the on the modelled stratigraphic levels (7, 18, and 226 layers for HFS, BS, and bed level modeling respectively).

6.4. Results

6.4.1. Geological modeling

6.4.1.1. Zones and layering

Three stratigraphic levels were modelled; these include the previously established stratigraphic levels of Adam et al (under review), and they include the high-frequency sequences (HFS), bedsets (BS), and beds. The boundaries of the HFS and BS are used for zonation processes, while layering processes was based on the architectural characteristic of the beds within the bedsets. The detailed modeling parameters of the defined zones (bedsets) are summarized in Table 6.1 and 2. For example, the BS4 is about 300 cm thick and composed of sheet-like bodies of intertidal flats. Beds of this bedset are of 10 cm thickness, and accordingly, a layer thickness of 10 cm was chosen to subdivide the BS4 into thin layers (Figure 6.3). The above mentioned information was used to subdivide the Upper Khartam Member into zones and layers according to the modelled stratigraphic level (Figure 6.4).

6.4.1.2. Lithofacies modeling

The lithofacies models at the HFS and BS levels were established directly by assigning values from the upscaled lithofacies types (Figure 6.5 and 7). Although the method is very simple, however, it to some extent represents the nature since the detailed lateral sedimentological log shows no change in the lithofacies types at a lateral extent of 1000 m in dip direction. Furthermore, the upscaled lithofacies data at the bedset level shows good correlation with the logged lithofacies types, while prominent distortion in the upscaled lithofacies data is observed in the HFS level (Figure 6.7). Even though, beds are complexly amalgamated and stacked. Therefore,

Sequential Indicator Simulation (SIS) method is used to model the lithofacies types and the architectural elements at the bed level. The beds of the Upper Khartam Member are dominantly stacked in complex patterns of back-stepping geometry, this linked to the nature of the high-frequency sea-level changes (Adam et al. under review). These are occurring in the form of sheet-like and channelized geometry and they been genetically grouped into fourteen bedsets. Each bedset has characteristic beds geometry; therefore, the bedsets boundaries were chosen to subdivide the succession into zones within which lithofacies and beds geometries have been modelled. Generally, the sheet-like beds of the Upper Khartam Member range in thicknesses from 5 to 40 cm and possess a lateral extension varying between 5 and 300 m, while channelized bodies have two anatomies, i.e. small tidal creeks (1m in width by 30cm in height) and large tidal channels (3m in width by 50cm in height). The vertical stacks of the lithofacies types and the architectural elements of each bedset were used to build the lithofacies models. For example, the BS 4 is composed of complex amalgamations of back-stepping beds. The latter have an average thickness of 10cm and extend for about 50 m in the dip direction. Regional setting and correlation of this bedset indicates a lateral extent of 1000 m in the strike direction (Adam et al. under review). Accordingly, vertical layering thickness of 10 cm and horizontal variograms with ranges of 50 m and 1000 m are deterministically defined along dip and strike directions respectively. Depositional setting indicates a homoclinal platform with strike direction extended from north-west to south-east directions (around 150˚) (Adam et al. (under review) and Janson et al., 2013). The above mentioned parameters were deterministically edited and used to model the BS4 (Figure 6.8). Most critically, the build 3D models is in excellent correlation with the detailed sedimentological and sequences stratigraphic setting of the Upper Khartam

Member, a clear shallowing-upward trends and back-stepping geometry were observed (Figure 6.9).

Table 6.1. Summary of the modeling parameters of the high-frequency sequences and the bedset levels.

Stratigraphic level	Zone	Top surface	Lithofacies types	Code	Petrophysical parameters				Modeling method
					Phi (meas)	K (meas)	Phi (core)	K (core)	
HFS modeling	HFS6	FS-S7	Bioclastic grainstone/packstone	LFT6	0.33	20125	0.12	31.74	Assign value
	HFS5	FS-S6	Bioclastic grainstone/packstone	LFT6	0.36	31667	0.09	4.40	Assign value
	HFS4	FS-S5	Coarse-grained oolitic grainstone	LFT1	0.36	49125	0.13	3.47	Assign value
	HFS3	FS-S4	Recrystallized limestone	LFT3	0.40	51275	0.08	0.66	Assign value
	HFS2	FS-S3	Coarse-grained oolitic grainstone	LFT1	0.19	18781	0.12	0.33	Assign value
	HFS1	RS-S2	Coarse-grained oolitic grainstone	LFT1	0.20	16100	0.06	10.80	Assign value
Bedset modeling	BS14	FS-S7	Bioclastic grainstone/packstone	LFT6	0.23	21292	0.12	35.20	Assign value
	BS13	BS13/BS14	Bioclastic grainstone/packstone	LFT6	0.41	15500	0.14	52.10	Assign value
	BS12	FS-S6	Coarse-grained oolitic grainstone	LFT1	0.34	23583	0.10	7.91	Assign value
	BS11	BS11/BS12	Thin-walled bivalve rudstone	LFT17	0.33	25333	0.14	8.42	Assign value
	BS10(2)	FS-S5	Coarse-grained oolitic grainstone	LFT1	0.40	38000	0.05	0.38	Assign value
	FZ-B20B	Top B20B	Bioclastic grainstone/packstone	LFT6	0.32	90000	0.26	4.74	Assign value/SGS
	BS10(1)	Bottom B20B	Coarse-grained oolitic grainstone	LFT1	0.38	62750	0.14	2.50	Assign value
	BS9	BS9/BS10	Bioclastic grainstone/packstone	LFT6	0.40	47000	0.12	0.34	Assign value
	BS8(2)	FS-S4	Oolitic grainstone/grapestone	LFT12	0.37	175000	0.17	0.83	Assign value
	FZ-B15B	Top B15B	Coarse-grained oolitic grainstone	LFT1	0.40	30000	0.02	0.07	Assign value/SGS
	FZ-B14C	BS7/BS8	Coarse-grained oolitic grainstone	LFT1	0.40	30000	0.02	0.03	Assign value/SGS
	BS7(1)	Bottom B14C	Recrystallized limestone	LFT3	0.40	20000	0.11	1.61	Assign value
	BS6	BS6/BS7	Recrystallized limestone	LFT3	0.41	1375	0.09	0.76	Assign value
	FZ-B12B	FS-S3	Coarse-grained oolitic grainstone	LFT1	0.34	50000	0.31	0.57	Assign value/SGS
	BS5(1)	Bottom B12B	marlstone	LFT7	0.00	0	0.00	0.00	Assign value
	BS4	BS4/BS5	Fine-grained oolitic grainstone	LFT5	0.22	6344	0.05	0.41	Assign value
	HFS1	RS-S2	Coarse-grained oolitic grainstone	LFT1	0.20	16100	0.06	10.80	Assign value

Table 6.2. Summary of the modeling parameters of the bed level.

High-frequency sequences	Bedsets	Lithofacies types	Total thickness (cm)	Architectural characteristics	Dimensions (m)	Layers thickness (cm)	Layers number	Modeling method
HFS1	BS1	LFT10	20	Sheet-like bodies	50 by 1000	10	2	SIS
	BS2	LFT1, LFT7	50	Sheet-like bodies	50 by 1000	10	5	SIS
	BS3	LFT1, LFT7	50	Sheet-like bodies	50 by 1000	10	5	SIS
HFS2	BS4	LFT6, LFT2, LFT3, LFT5, LFT1	300	Sheet-like bodies	50 by 1000	10	30	SIS
	BS5	LFT1, LFT7	250	Small tidal creeks	250	30	10	SIS
HFS3	BS6	LFT3, LFT5, LFT7	213	Sheet-like bodies	50 by 1000	10	10	SIS
	BS7	LFT3, LFT5, LFT7	370	Sheet-like bodies	75 by 1500	15	12	SIS
	BS8	LFT1, FT11, LFT7, LFT12	450	Large tidal channels	500	50	9	SIS
HFS4	BS9	LFT6, LFT8, LFT1	356	Sheet-like bodies	50 by 10000	10	35	SIS
	BS10	LFT1, LFT13, LFT8, LFT6, LFT14	414	Sheet-like bodies	250 by 5000	50	8	SIS
HFS5	BS11	LFT8, LFT1, LFT17, LFT7	114	Sheet-like bodies	50 by 1000	10	10	SIS
	BS12	LFT8, LFT1	187	Sheet-like bodies	100 by 2000	20	9	SIS
HFS6	BS13	LFT1, LFT9	150	Sheet-like bodies	50 by 1000	10	15	SIS
	BS14	LFT17, LFT14, LFT6, LFT9, LFT7, LFT16	169	Sheet-like bodies	100 by 2000	20	8	SIS

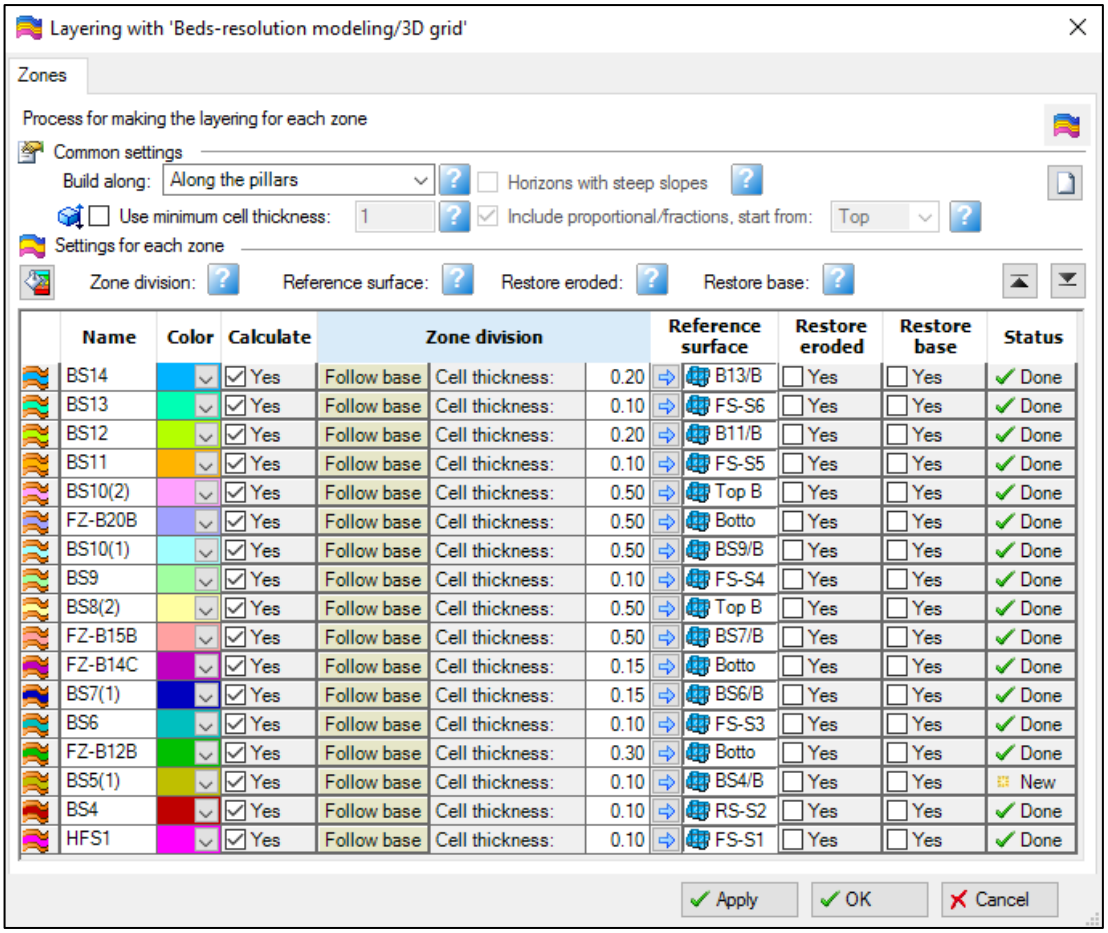

Figure 6.3. The layering process used to model the bed level stratigraphy. Follow base type was used as a reference surfaces, this represents the back-stepping nature of internal stratigraphy of the studied section, cells thicknesses were deterministically edited and they best described beds thicknesses of each zone, for example, zone BS4 is composed of complexly amalgamated beds of 10cm thickness, and accordingly, 0.1 m thickness is used to establish layers of this bedset.

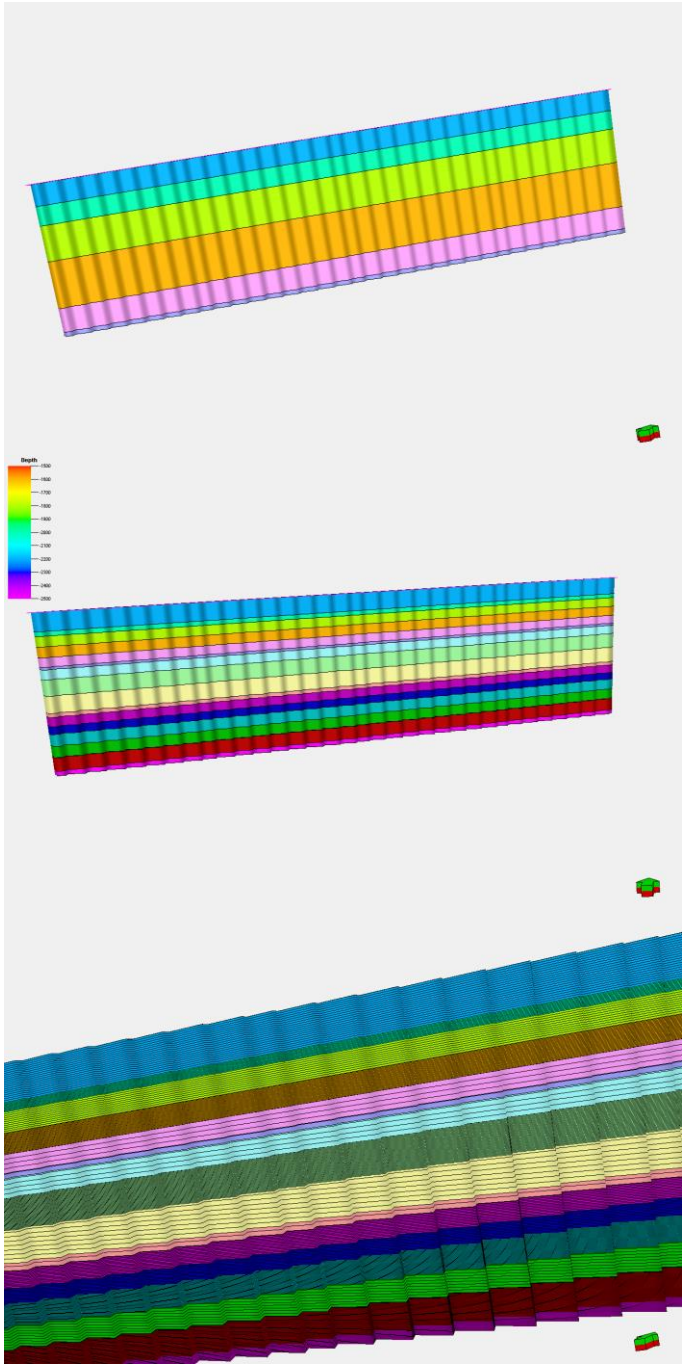

Figure 6.4. A, B, and C) Zones and layers of the HFS, BS, and bed level models respectively.

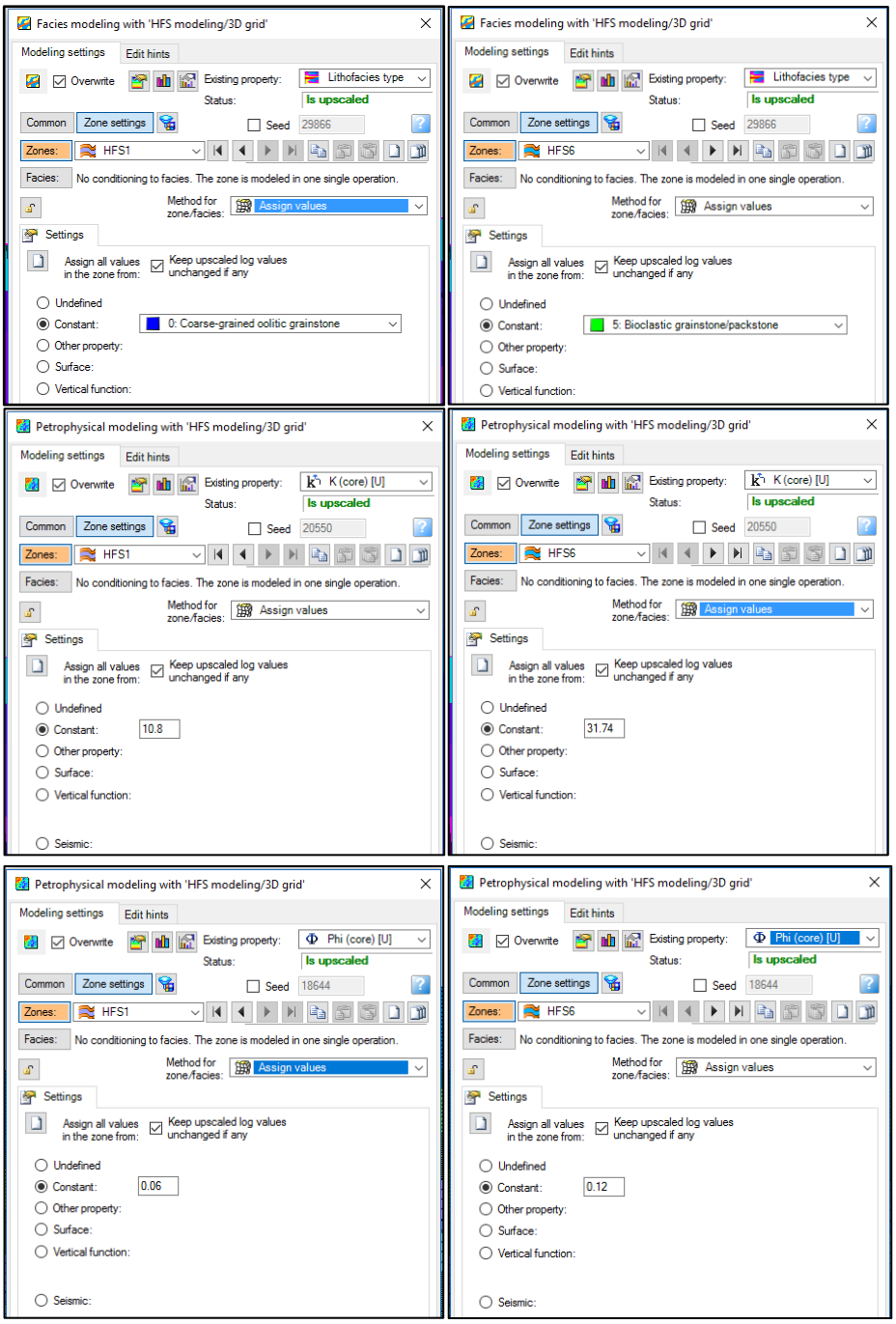

Figure 6.5. Examples for facies and petrophysical modeling at HFS level using Assigning Value method, for comparison see table 1.

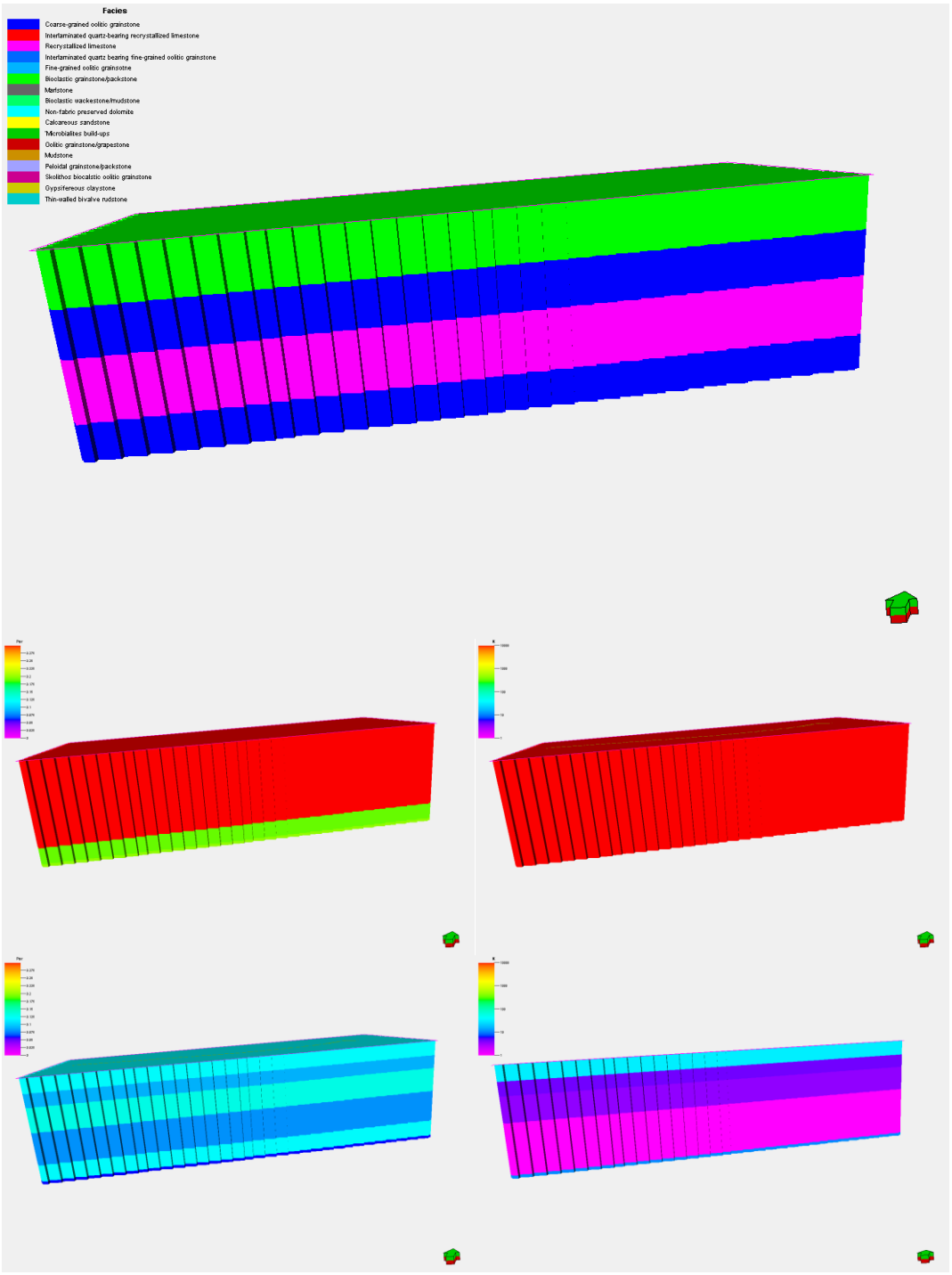

Figure 6.6. 3D geocellular models at the HFS level using Assigning Value method, A) lithofacies model, B and C) measured porosity and permeability models, D and E) core porosity and permeability models.

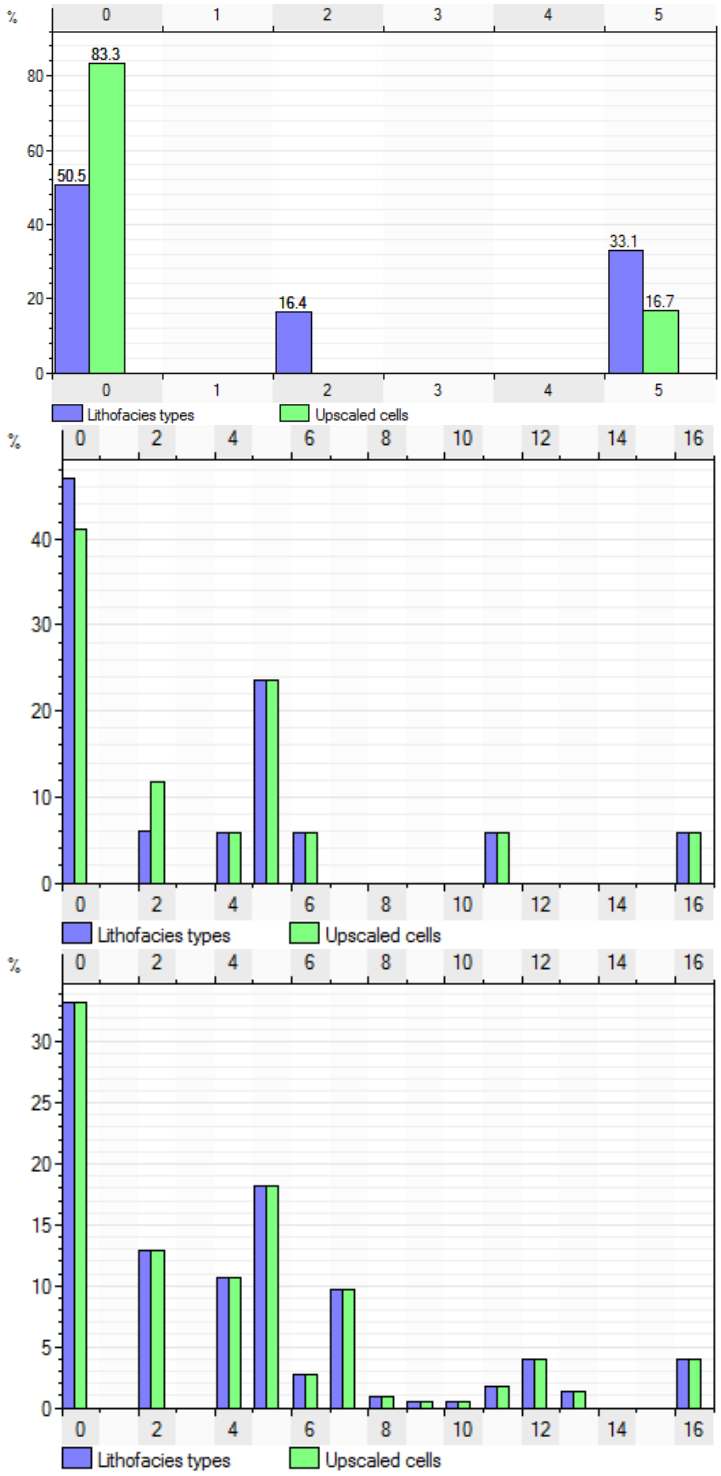

Figure 6.7. The upscaled lithofacies data for the differed stratigraphic levels HFS, BS, and bed level respectively, prominent distortion in the HFS level is observed (in A) , while upscaled cells in the bedset level (in B) is relatively close to original data set in C.

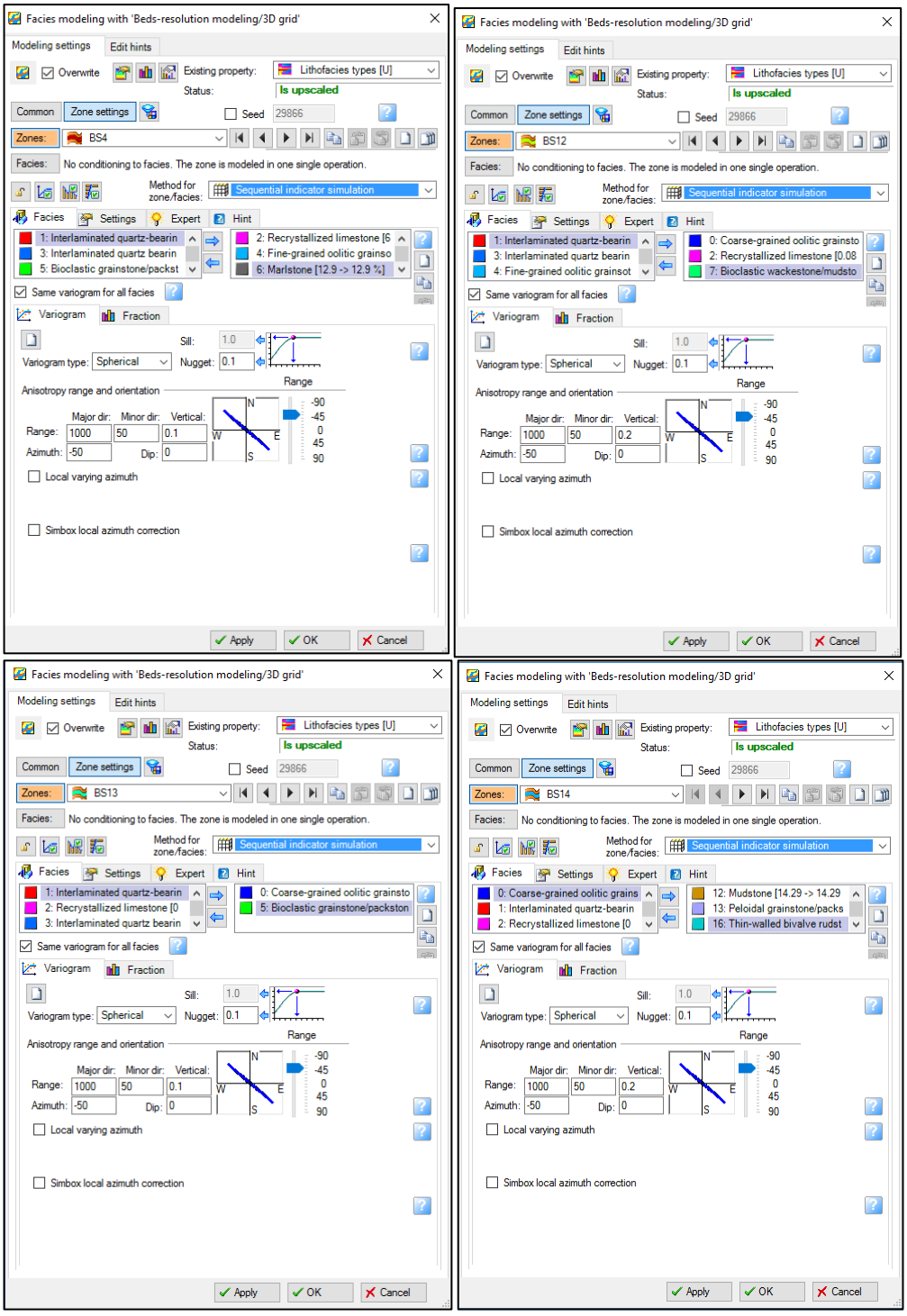

Figure 6.8. Modeling parameter of BS4, BS12, BS13, and BS14, lithofacies types, ranges, and azimuth are deterministically edited and they are consistent with sedimentological and depositional setting of this bedset.

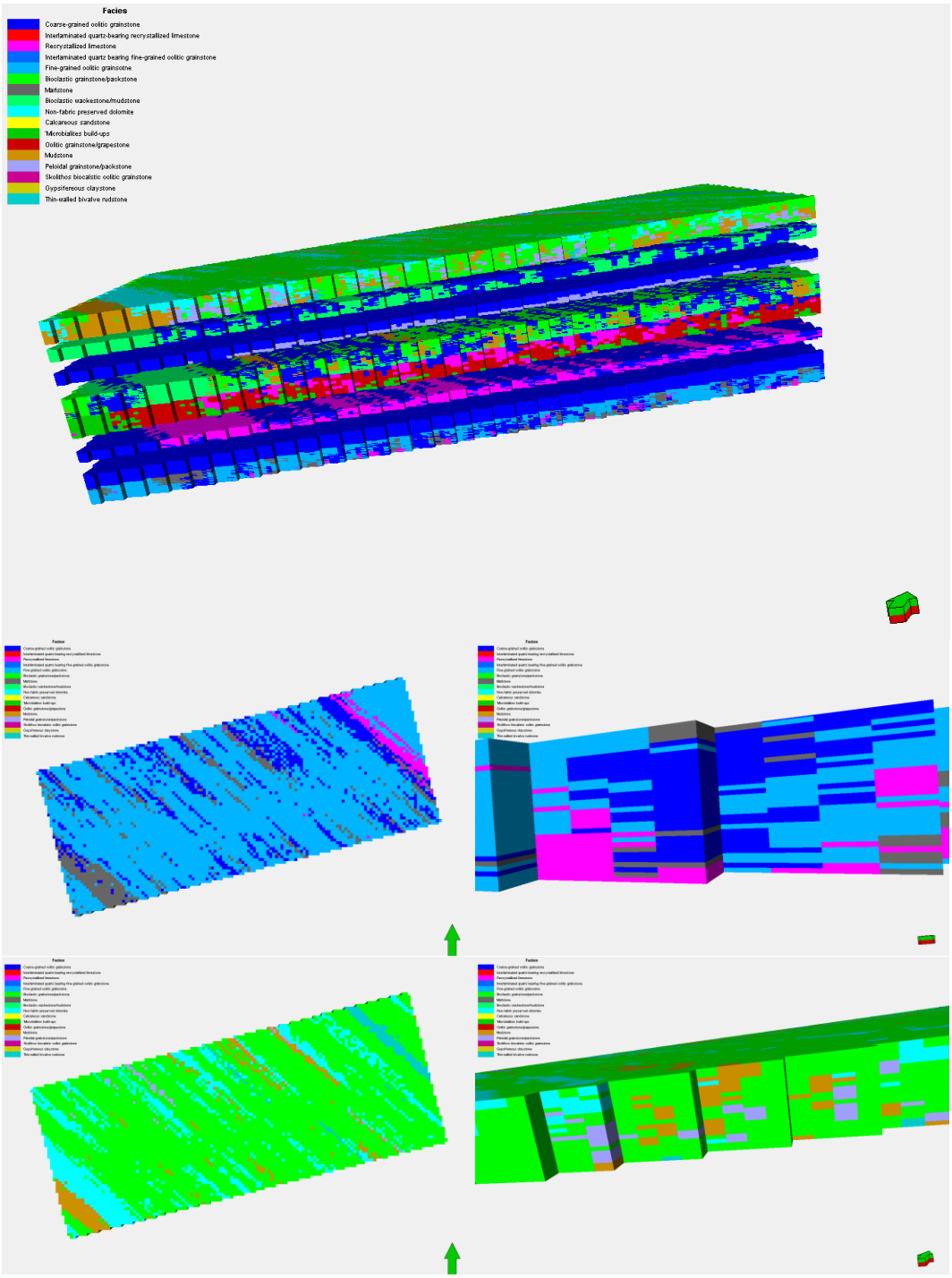

Figure 6.9. 3D geocellular model of the Upper Khartam Member (A), importantly, the model is in consistent with the detailed geological settings, for example in B and C, the back-stepping nature of the lithofacies types is clear, in B, marlstone, coarse-grained oolitic grainstone, and fine-grained oolitic grainstone of BS 4 are associated in a shallowing-upward trend, this nature also clear in C (cross-section of the same bedset), similarly, the bioclastic grainstone/packstone, peloidal grainstone/packstone, and the mudstone show similar character.

6.4.2. Petrophysical modeling

The main objective of this section is to extract critical geostatistical parameter for short scale heterogeneities at interwell spacing. Additionally, multi-realization models also built to examine the impact the different stratigraphic levels on fluid flow simulation. Four intra-reservoir bodies were logged laterally from petrophysical point of view along the vertical outcrop sections (120 vertical sections with 5m spacing). These include FZ-B12B, FZ-B14C, FZ-B15B, and FZ-B20B. Similar to lithofacies, upscaled porosity and permeability at the bedset level show preserved data, while clear distortion was observed at the high-frequency sequence level (Figure 6.10 and 12). Two methods were used to model the petrophysical properties; these include Assigning Value (AV) and Sequential Gaussian Simulation (SGS). The AV method was used to model the porosity and the permeability at the HFS and BS level while SGS was used to model porosity and permeability of the laterally logged intra-reservoir bodies. Spherical model types were used and the best fitted variograms models and maps indicated major direction in north-east direction (around 70˚). The porosity models of the intertidal sheets have relatively great lateral continuity in the north-east direction (about 250m) when compared with the porosity models of the intertidal creek and intertidal channels (about 150m). This was inferred from values of major ranges of the variogram models (Figure 6.12). While permeability models show all most the same range for the different reservoir architecture and geometry (Figure 6.13). Small scale heterogeneities in the petrophysical properties are oriented in the north-west direction (minor range of about 330 degree); these are defined to have ranges values around 60m (Figure 6.12 and 14). The numerical data of the variogram models for the studied intra-reservoir bodies is summarized in Table 6.3**.**

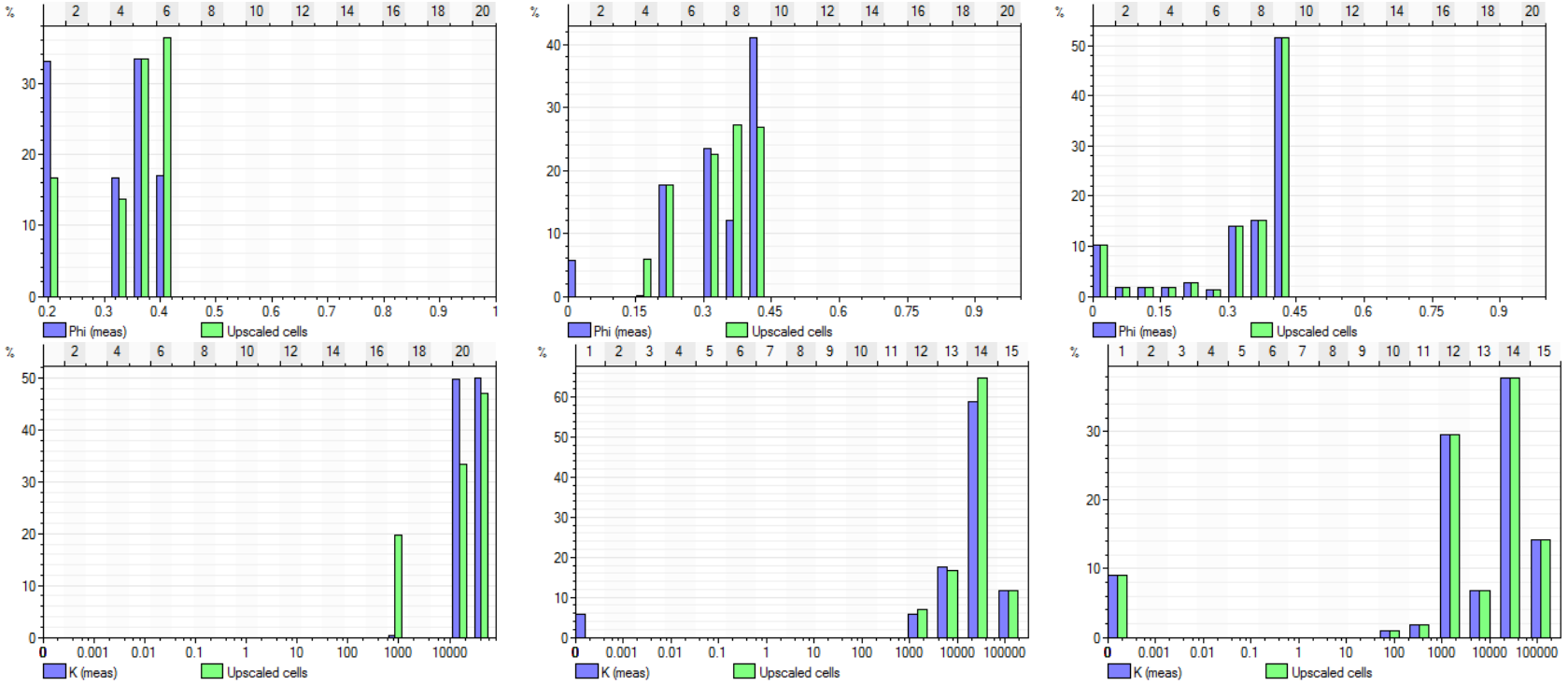

Figure 6.10. Histograms show comparison between measured and upscaled porosities. A1, A2, and A3) measured porosity at HFS, BS, and bed levels respectively, while B1, B2, and B3 core porosities at HFS, BS, and bed levels respectively. a clear distortion is observed in the original data was observed in the porosity data at the HFS level (A1 and B1), while upscaled porosity at the BS level (A2 and B2) is to some extend similar to original data (A3 and B3).

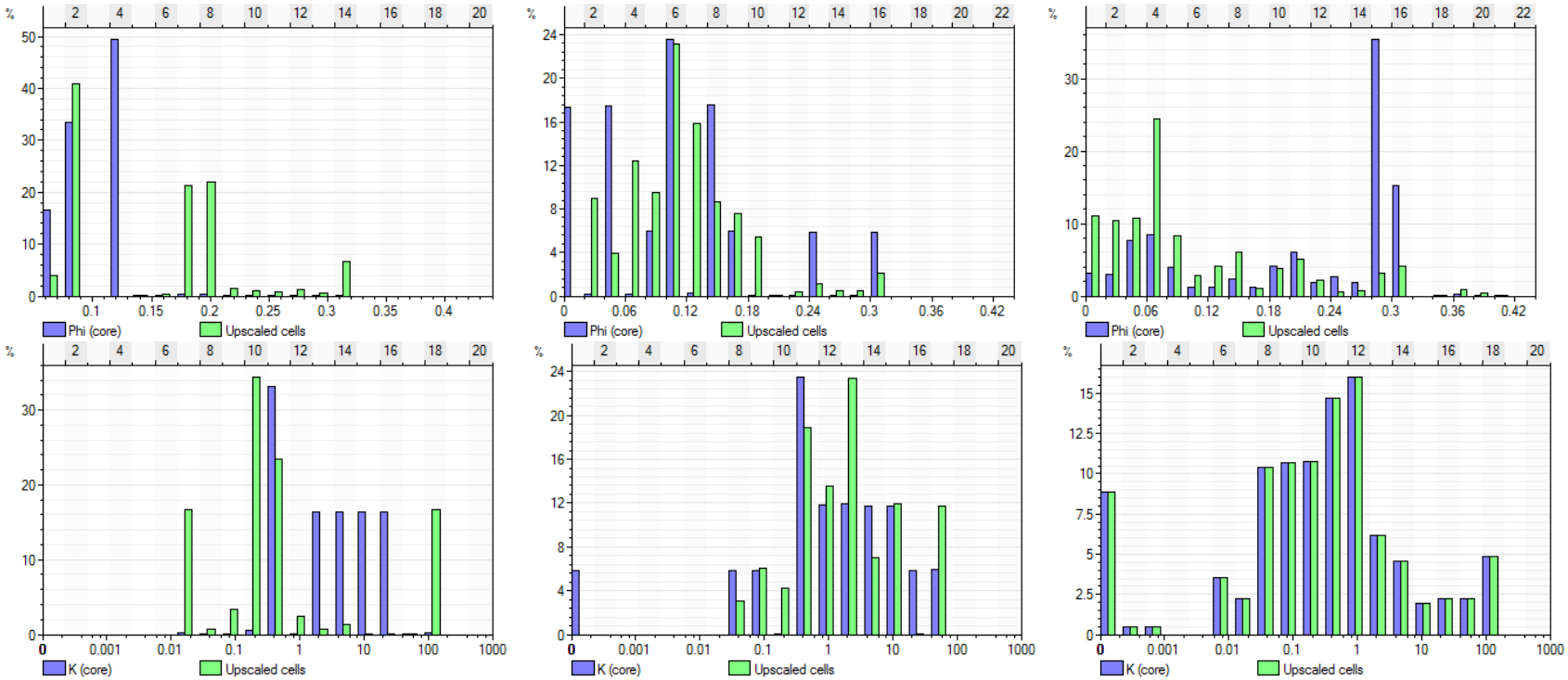

Figure 6.11. Histograms show comparison between measured and upscaled permeabilities. A1, A2, and A3) measured permeabilities at HFS, BS, and bed levels respectively, while B1, B2, and B3 core permeabilities at HFS, BS, and bed levels respectively. A clear distortion is observed in the original permeability data at the HFS level (A1 and B1), while upscaled permeability data at the BS level (A2 and B2) is to some extend similar to original data (A3 and B3).

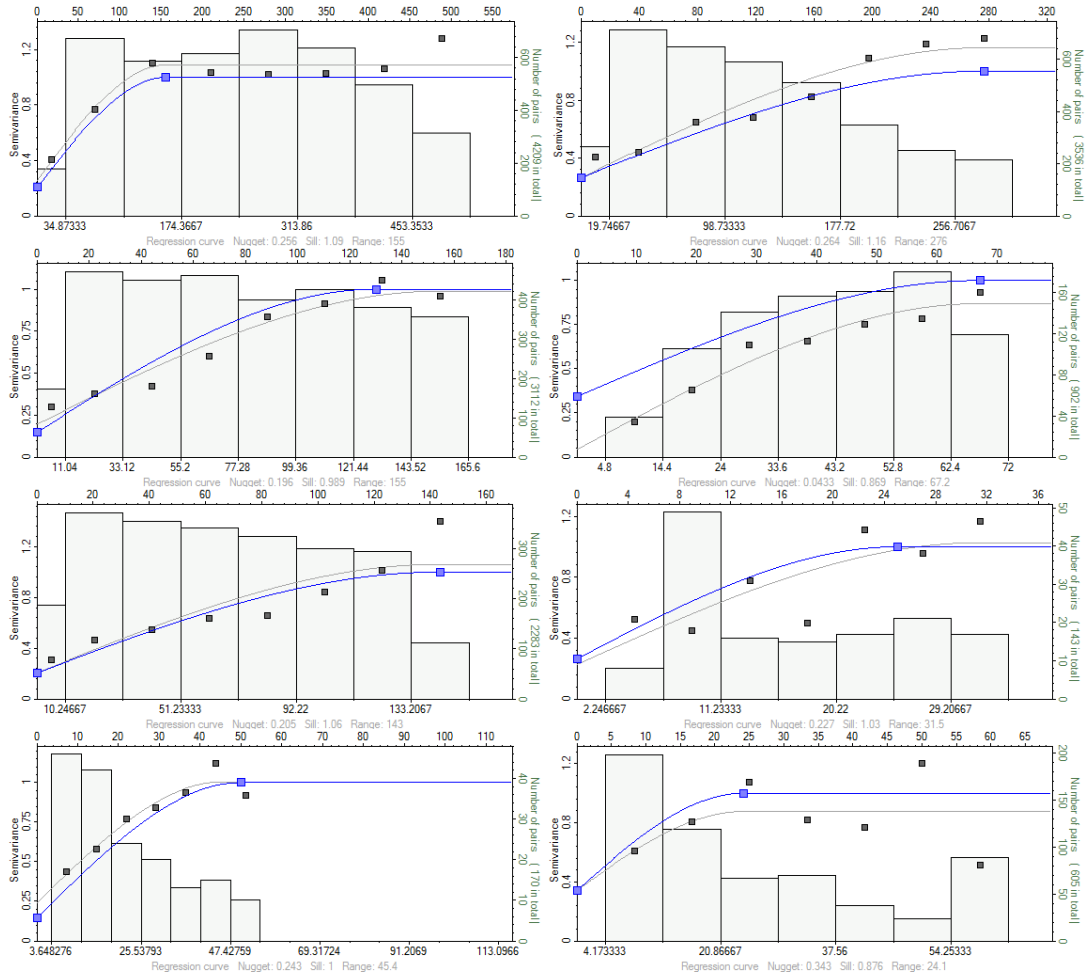

Figure 6.12. Variogram models of porosity in the studied area. A, B, C, and D) major direction of studied intra-reservoir units FZ-B12B, FZ-B14C, FZ-B15B, and FZ-B20B respectively, E, F, G, and H) minor direction of studied intra-reservoir units FZ-B12B, FZ-B14C, FZ-B15B, and FZ-B20B respectively. The porosity models of the intertidal sheets (B) have relatively great lateral continuity in the north-east direction (about 250m) when compared with the porosity models of the intertidal creek and intertidal channels (A and C; about 150m), minor range are of same values around 50m.

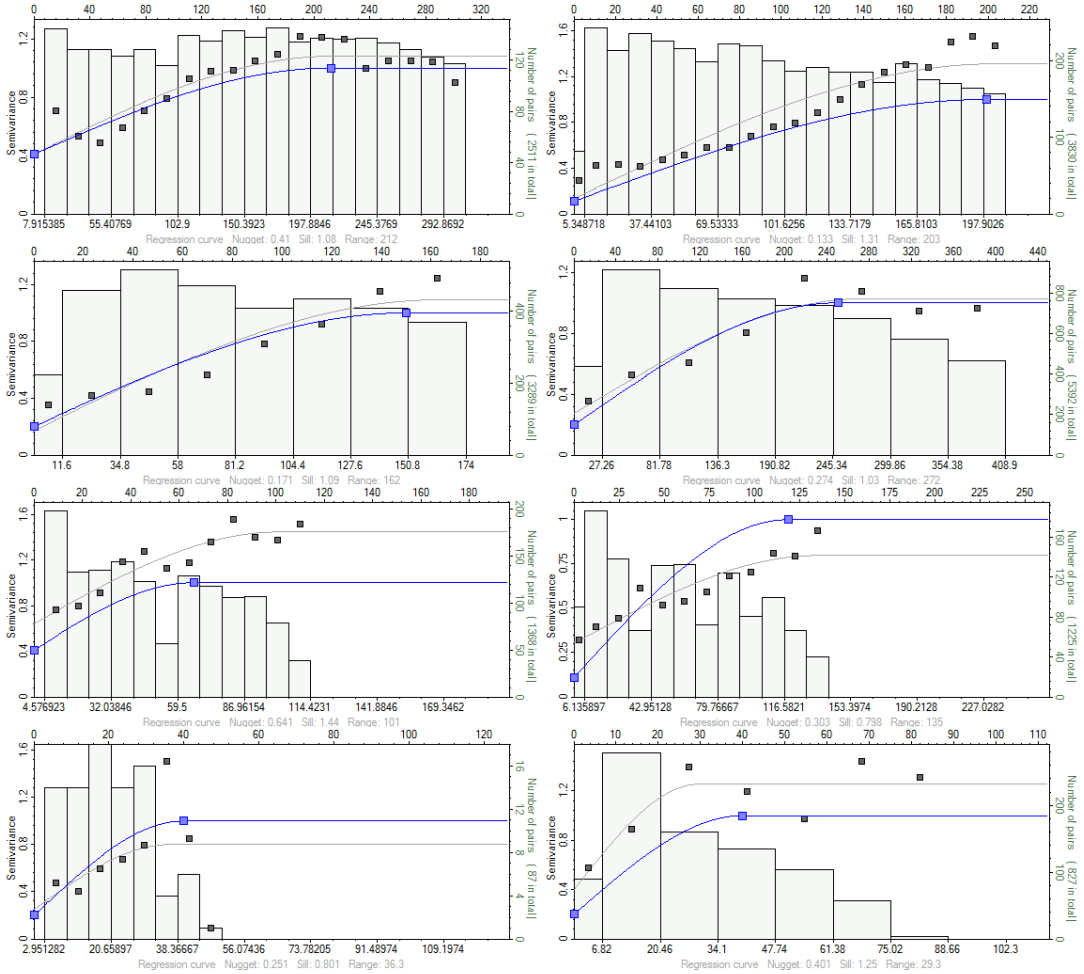

Figure 6.13. Variogram models of permeability in the studied area. A, B, C, and D) major direction of studied intra-reservoir units FZ-B12B, FZ-B14C, FZ-B15B, and FZ-B20B respectively, E, F, G, and H) minor direction of studied intra-reservoir units FZ-B12B, FZ-B14C, FZ-B15B, and FZ-B20B respectively.

Table 6.3. Variograms parameters of the studied flow units.

Property	Parameter	FZ-B12B	FZ-B14C	FZ-B15B	FZ-B20B
Porosity	Major direction	74	75	76	66
	Minor direction	344	345	346	336
	Dip	0	0	0	0
	Type	Spherical	Spherical	Spherical	Spherical
	Sill	1	1	1	1
	Nugget	0.205	0.264	0.147	0.343
	Major range	155	276.5	130	67.2
	Minor range	143.5	25	50	24.1
	Vertical range	100	100	100	100
Permeability	Major direction	66	66	68	77
	Minor direction	336	336	338	347
	Dip	0	0	0	0
	Type	Spherical	Spherical	Spherical	Spherical
	Sill:	1	1	1	1
	Nugget	0.41	0.11	0.2	0.2
	Major range	212.1	199.4	150	250
	Minor range	66.1	119	40	40
	Vertical range	100	100	100	100

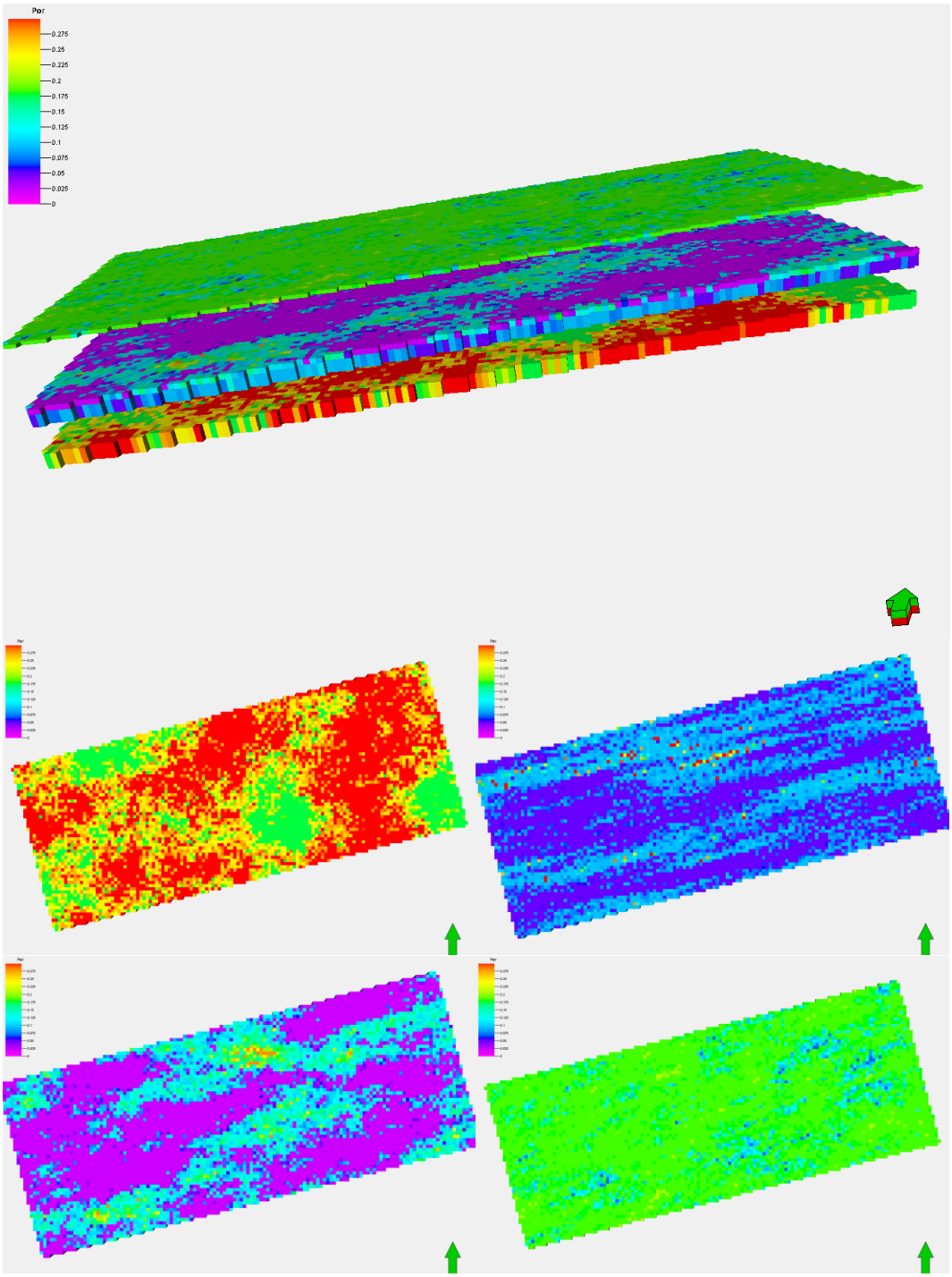

Figure 6.14. 3D geocellular model of porosity.

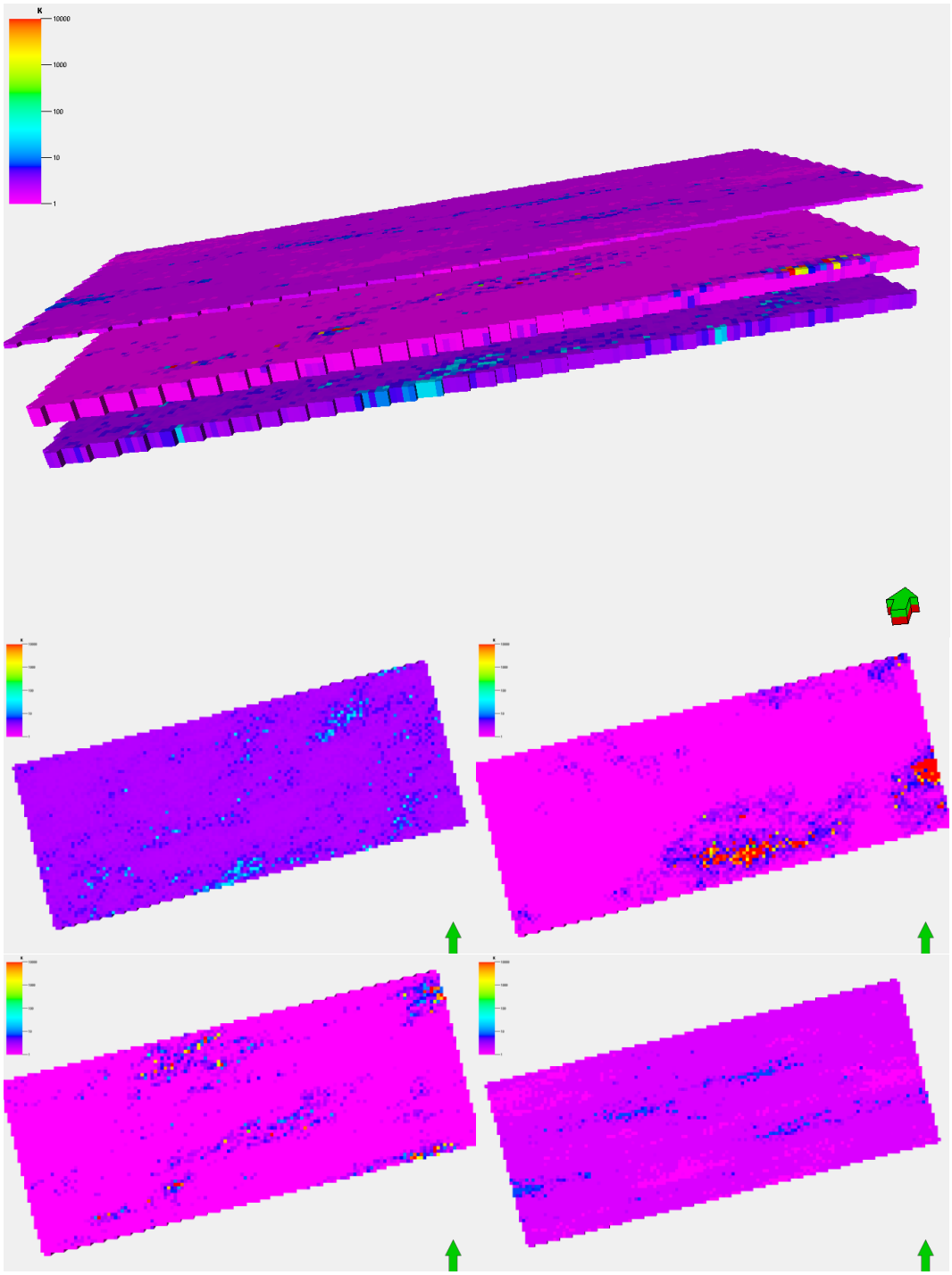

Figure 6.15. 3D geocellular model of permeability.

CHAPTER 7

CONCLUSION

- The Khuff carbonates were deposited on homoclinal ramp platform sloping gently to the east. The studied Upper Khartam Member is composed of seventeen lithofacies types, with coarse-grained oolitic grainstone, interlaminated quartz-bearing recrystallized limestone, recrystallized limestone, interlaminated quartz-bearing fine-grained oolitic grainstone, and bioclastic grainstone/packstone making up the bulk of the successions.
- The defined lithofacies types occurring in two different architectures; sheet-like and channelized bodies. The sheet-like bodies range in thicknesses from 5 to 40 cm and have lateral extend varying between 5 and 300 m, whereas the channelized bodies have two anatomies, small tidal creeks (1 m in width and 30 cm thick) and large tidal channels (3 m in width and 50 cm thick).
- According to the detailed lithofacies and architectural analysis, seven depositional settings are inferred, i.e.: supratidal settings, shoal ridges, reef complex, intertidal channels, intertidal-subtidal flats, and outer ramp settings.
- Four stratigraphic levels are defined, these includes beds, bedset, high-frequency fifth-order sequences, and fourth-order sequences. About 20,000 beds are followed laterally and described; these range in length from 5 to 300 m and in thickness from 5 to 40 cm. The beds are grouped into fourteen bedsets range in extend from 300 to few thousand of metre in the dip-direction, and their thickness ranges from 1 to 5 m. The deposition of the beds and bedsets is most likely controlled by slight shift in sea-level (may be linked to

tide actions), accommodation space, and sediment supply. The bedsets are grouped to form six high-frequency sequences with the prominent shift in the shoreline trajectories. The HFSs are traceable in the dip direction along 1000 m exposure (rare pinching) and correlatable over the studied outcrop (strike-direction; 70 km). The fifth-order sequences are similar to the Middle Triassic Muschelkalk small-scale cycles of Aigner et al., 1999; Koehrer et al., 2009, and they are most likely related to Milankovitch cycles (eccentricity = 100,000 year). Furthermore, and based on the sedimentological characters and nature of stacking patterns, the HFSs could be grouped into two fourth-order sequences, these are separated by major sequences boundary associated with large intertidal channels, microbialites constructions, and dolomitization.

- Essentially, the high-resolution stratigraphic build-ups of the Upper Khartam Member are likely typified by regressive cycles dominated by regressive deposits. This nature is likely identical for the entire Upper Khartam (mostly third-order sequence) where the nature of the rapid transgression characterized by thin (20 cm) lag deposits overlying the clayey evaporitic succession of the Lower Khartam Member.
- A high degree of similarity is expected between the studied outcrops and the Khuff reservoirs, as inferred from the nature of high-resolution sequence stratigraphy. Therefore, the studied succession of the Upper Khartam Member in central Saudi Arabia is possibly represents an excellent analogue for the Khuff reservoirs in Eastern Arabia, and thus, our results could enhance the quantitative and the qualitative assessment of the Khuff reservoirs heterogeneities. For example, these results should be used as an input data for

enhanced geological modelling and fluid simulation as well as inversed stratigraphic analysis.

- From reservoir assessment point of view, the variation in lithofacies types and architectural complexity will influenced reservoir properties and eventually the capacity and productivity and vertical reservoir continuity at interwell spacing. Additionally, regional correlation has shown lateral facies changes, this in turn will elevate level of heterogeneity at field-scale.
- This research reports the first discovery of *Earlandia* foraminifera in the Upper Khartam Member of the Khuff Formation. 300 samples were collected for detailed sedimentological and micropaleontological analysis. Of these, only six samples recovered fossil Earlandia foraminifera; these are dominantly observed in the interlaminated quartz-bearing recrystallized limestone lithofacies type.
- The *Earlandia* occur in associations with quartz grains, peloids, ooids, ostracods, bivalves, bryozoans, cephalopods, and stromatolites. The defined fossils of the Earlandia are restricted to the lower fourth-order sequence of the Upper Khartam, where non-skeletal grains (mostly oolitic grainstones) are prevailing. The skeletal grains along with the *Earlandia* occur as a thin (20 cm) transgressive lag.
- Furthermore, the regional occurrences of the *Earlandia* are consistent with the previously established high-frequency sequences stratigraphic scheme, therefore, the *Earlandia* could be used as a biomarker for regional biostratigraphic correlation and enhance the high-resolution sequence stratigraphic correlations of the Upper Khartam Member.

- Essentially, the detailed sedimentological and micropaleontological analyse (*Earlandia*) indicates a plate-wide spread shallow epeiric sea. The latter is gently dipping and sporadically connected to the open marine system.
- The calculated original, unconsolidated, depositional texture of the Upper Khartam Member had a high average primary porosity and permeability of about 42% and 12 D, respectively. These porosity and permeability characteristics were subsequently altered by diagenetic processes. Overall, six major diagenetic processes were observed in the studied outcrops: dissolution, cementation, pore lining cementation, dolomitization, fracturing, and stylolitization. Cements develop as blocky, mosaic, micro, and rimming calcite cements with two different mineralogies: ferroan calcite and more frequently non-ferroan calcite. Significantly, cementation has blocked most of the original intergranular porosity. Dissolution occurs in the form of partial dissolution, molds, and vugs, and is likely the result of intensive circulation of meteoric water undersaturated with respect to aragonite and/or calcite. Pore lining detrital clays severely impacted the reservoir permeability and complicated the pore geometry. Stylolite development is controlled by lithofacies and geobody architecture, with for example a relatively higher abundance in fine-grained oolitic grainstone (LFT 5 occurring as sheet-like bodies) when compared to coarse-grained oolitic grainstone (LFT 1 occurring as channelized bodies). Dolomitization is associated with the Khuff–Sudair boundary and the microbialite build-ups in the studied sections, and is believed to be the result of an influx of highly Mg^{2+}-saturated water during the deposition of the Sudair evaporites.

- Ten porosity types are differentiated in the studied outcrops, namely intergranular, intragranular, shelter, dissolution enlarged, moldic, vuggy, micro-porosity, dolomite–dedolomite porosity, dolomite-leaching, and fracture porosity. The oolitic grainstones of the intertidal sheets, intertidal creeks, and the intertidal channels are dominated by dissolution enlarged, moldic, and vuggy porosity, whereas intercrystalline and fracture porosities are prevailing in the recrystallized lithofacies types.
- The capacity and productivity of the Upper Khartam carbonates was mainly obliterated by diagenetic processes and shifted toward poorer quality (mid-center FZI = 0.75–1.5; with an frequency of 50 %). The interplayed diagenetic processes have impacted the ultimate reservoir quality. For example, the quality of the fine-grained oolitic grainstone (occurring as sheet-like bodies with grain sizes varying around 200 μm) have been relatively less impacted compared to the coarse-grained oolitic grainstone (occurring as sheet-like bodies with grain size varying around 500 μm). This was attributed to the pore-filling dolomites of the coarse-grained oolitic grainstone, while no dolomite was observed in the fine-grained oolitic grainstone. Furthermore, the intertidal creeks (with average grain size of 500 μm) are characterized by an overall complex and heterogeneous pore geometry compared to the intertidal channels (with average grain size of 500μm), which can be attributed to the architectural parameter, where intertidal creeks are composed of dense and small tidal creeks (1 m in length and 20 cm in thickness) while the intertidal channels are composed of thick amalgamations of larger intertidal channels (5 m by 50 cm). In addition, the vuggy coarse-grained oolitic grainstone has better reservoir quality compared to the moldic coarse-grained oolitic

grainstone. This indicates a control of pore-types on the ultimate reservoir quality. Vugs enhanced the connectivity between the pores, while molds are often disconnected, often due to blocky calcite cement infill.

- Overprinted reservoir qualities of the studied bodies in function of their lateral extension were differentially obliterated by diagenesis. This resulted in a segmentation of individual reservoir units into segments with ranges of qualities and hence several hydraulic subunits. XRD data indicated a proportional relationship between FZI and calcite, quartz and celestine compared. Also the damage caused by the pore-lining clay minerals is noteworthy. The SEM observations revealed a prominent control of cementation and dissolution on porosity and permeability, which are related to pore and pore-throat attributes (e.g., geometry, type, and size). The differential mold-filling calcite cement of the oolitic grainstone of the intertidal sheets and intertidal channels has significantly reduced the porosity and permeability. It hence affected the lateral connectivity of a single intra-reservoir unit at the inter-well spacing and caused the lateral segmentation. Therefore, the observed lateral compartmentalization especially relates to differential cementation. Furthermore, the diagenetic control on reservoir characteristics is also controlled by stylolites and fractures, which form both barriers (stylolites) to and conduits (fractures) for vertical fluid flow and most likely control differential cementation and dissolution processes. Hence, they also exerted an influence on the lateral reservoir quality over short inter-well distances. In addition, the regional variations in the lithofacies and geobody architecture (high-frequency sequence stratigraphic scheme; field-scale; Adam et al., under

review) further complicates field-scale connectivity and eventually will impact fluid flow.

- The Assign Value method of geostatistical modeling is used for building the lithofacies models at the defined stratigraphic levels. Although the data was drastically distorted at the high-frequency sequences, however, bedset level to some extent preserved the original data.
- The Upper Khartam carbonates are composed of complexly amalgamated beds of different architectural elements and lithofacies types. Critically, these will impact reservoir heterogeneity and continuity and eventually fluid flow and productivity. Therefore, the detailed bed-level information are used to model the Upper Khartam carbonates. The Sequential Indicator Simulation method is used and the detailed variogram parameters are deterministically edited. Most critically, models are valid and consistent with the detailed sedimentological and sequence stratigraphic data.
- Sequential Gaussian Simulation is used to model the petrophysical properties. Detailed matching process indicates major and minor directions of petrophysical properties of 70 and 330 degree respectively. These are obviously following the depositional trend.
- Porosity of intertidal sheets is of great horizontal ranges compared with the intertidal channels and creeks. They have average range of about 300 m, while intertidal channels and creeks have average ranges of about 150m. Even though, the minor porosity ranges of the different architectural types have the same values of about 50 m.

- Permeability variograms show no control of architectural types on ranges and continuities. Generally, the permeability has major ranges of 200 m while the minor continuity is about 60 m.

REFERENCES

Adam, A., and O. Abdullatif, 2013, Diagenetic Evolution and Subsequent Implications on Reservoir Qualities, Khartam Member, Permo-Triassic Khuff Formation, Central Saudi Arabia: EGU General Assembly, Geophysical Research Abstracts, v. 15.

Adam, A., O. Abdullatif, H. Eltom, A. A. Babaloa, Lameed Mohamed Abdelgadir, M. Osman, and M. Bashiri, 2013, High resolution stratigraphy and implications on critical reservoir architecture, lithofacies, and petrophysical properties of Khartam Member of the Permo-Triassic Khuff Carbonate: Outcrop reservoir analog approach from Central Saudi Arabia: International Association of Sedimentologists, Abstract.

Adam, A., H. Eltom, O. Abdullatif, L. Babaloa, A. Mohamed, Abdelgadir Asaad, M. Osman, and M. Bashiri, 2014, High Resolution Stratigraphy of the Khartam Member of the Permo-Triassic Khuff Carbonate: Outcrop Reservoir Analog from Central Saudi Arabia: 11th Middle East Geosciences Conference and Exhibition.

Adams, J. E., and M. L. Rhodes, 1960, Dolomitization by seepage refluxion: Am. Ass. petrol. Geol., v. 44, p. 1912–1920.

Agar, R. ., 1985, The Najd fault system revisited; a two-way strike-slip orogen.: Journal of Structural Geology 9, ., p. 41–48.

Aigner, T., M. Schauer, W.-D. Junghans, and L. Reinhardt, 1995, Outcrop gamma-ray logging and its applications: examples from the German Triassic: Sedimentary Geology, v. 100, no. 1-4, p. 47–61, doi:10.1016/0037-0738(95)00102-6.

Al-Aswad, A. A., 1997, Stratigraphy, sedimentary environment and depositional

evolution of the Khuff Formation in south-central Saudi Arabia: Journal of Petroleum Geolog, v. 20, no. July, p. 307–326.

Al-Dukhayyil, R. K., and A. A. Al Tawil, 2006, Reservoir Architecture of the Triassic Khartam Carbonate Sequence, Khuff Outcrop Analogue in Al-Qassim, central Saudi Arabia: Abstract in: GEO 2006 Middle East Conference and Exhibition.

Al-fares, A. A., M. Bouman, and P. Jeans, 1998, A New Look at the Middle to Lower Cretaceous Stratigraphy , Offshore Kuwait: v. 3, no. 4, p. 543–560.

Al-Husseini, M. I., 1997, Jurassic Sequence Stratigraphy of the Western and Southern Arabian Gulf: GeoArabia, v. 2, no. 4, p. 361–382.

Al-Husseini, M. I., 2000, Origin of the Arabian Plate Structures: Amar Collision and Najd Rift: GeoArabia, v. 5, no. 4, p. 527–542.

Al-Husseini, M., J. Amthor, J. Grotzinger, and J. Mattner, 2003, Arabian Plate Precambrian-Cambrian Boundary interpreted in Oman ' s Ara Group: v. 8, no. 4, p. 578–580.

Al-Jallal, I. J., 1987, Diagenetic effects on reservoir properties of the Permian Khuff Formation in eastern Saudi Arabia, *in* Society of Petroleum Engineers, 6th Middle East Oil Show, Bahrain: p. 465–476.

Al-Jallal, I. ., 1995, The Khuff Formation: its regional reservoir potential in Saudi Arabia and other Gulf countries; depositional and stratigraphic approach: In, M.I. Al-Husseini (Ed.), Middle East Petroleum Geosciences Conference, GEO'94. Gulf PetroLink, Bahrain, v. 1, p. 103–119.

Al-Laboun, A. A., 1986, Stratigraphy and hydrocarbon potential of the Paleozoic succession in both Tabuk and Widyan basins, Arabia. In, M.T. Halbouty (Ed.), Future Petroleum Provinces of the World: American Association of Petroleum

Geologists, v. Memoir 40, p. 373–397.

Al-Laboun, A. A., 1982, The subsurface stratigraphy of the pre-Khuff formations in central and northwestern Arabia: Unpublished PhD thesis, Faculty of Earth Sciences, King Abdulaziz University, Jiddah, Saudi Arabia, p. 102.

Al-Laboun, A. A., 1987, Unayzah Formation: a new Permian-Carboniferous unit in Saudi Arabia: American Association of Petroleum Geologists Bulletin, v. 71, no. 1, p. 29–38.

Alnazghah, M. H., B. Bádenas, L. Pomar, M. Aurell, and M. Morsilli, 2013, Facies heterogeneity at interwell-scale in a carbonate ramp, Upper Jurassic, NE Spain: Marine and Petroleum Geology, v. 44, p. 140–163, doi:10.1016/j.marpetgeo.2013.03.004.

Alsharhan, A. S., 2006, Sedimentological character and hydrocarbon parameters of the Middle Permian to Early Triassic Khuff Formation , United Arab Emirates: v. 11, no. 3.

Alsharhan, A. S., and C. G. Kendall, 1986, Precambrian to Jurassic rocks of the Arabian Gulf and adjacent areas: their facies, depositional setting and hydrocarbon habitat: American Association of petroleum Geologist, v. 70, p. 977–1002.

Alsharhan, A. S., and A. E. . Nairn, 1997, Sedimentary Basins and Petroleum Geology of the Middle East: Amsterdam, Elsevier Science, p. 942 pp.

Amaefule, J., M. Altunbay, D. . Kersey, and D. . Keelan, 1993, Enhanced Reservoir Description: Using Core and Log Data to Identify Hydraulic (Flow) Units and Predict Permeability in Uncored Intervals/Wells,: Paper SPE-26436, presented at the SPE Annual Technical Conference and Exhibition, Houston, Texas, USA, 3-6

October.

Amel, H., A. Jafarian, A. Husinec, A. Koeshidayatullah, and R. Swennen, 2015, Microfacies, depositional environment and diagenetic evolution controls on the reservoir quality of the Permian Upper Dalan Formation, Kish Gas Field, Zagros Basin: Marine and Petroleum Geology, v. 67, p. 57–71, doi:10.1016/j.marpetgeo.2015.04.012.

Angiolini, L., D. Vaslet, Y. Le Nindre, and M. Zarbo, 2006, New records and new taxa of Permian brachiopods from the Khuff Formation , Midhnab Member , central Saudi Arabia: v. 11, no. 4, p. 45–58.

Baker, P. A., and S. H. Bloomer, 1988, The origin of celestite in deep-sea carbonate sediments: Geochimica et Cosmochimica Acta, v. 52, no. 2, p. 335–339, doi:10.1016/0016-7037(88)90088-9.

Bear, J., 1972, Dynamics of fluids in porous media: American Elsevier Pub. Co, 764 p.

Bell, A., 2004, The creation of late Proterozoic basement highs and their subsequent influence on sedimentation patterns of the Arabian Peninsula, abstract: GeoArabia, v. 9 (1), 50.

Bendias, D., B. Koehrer, M. Obermaier, and T. Aigner, 2013, Mid-Permian Khuff Sequence KS6 : Paleorelief-influenced facies and sequence patterns in the Lower Khuff time-equivalent strata , Oman Mountains , Sultanate of Oman: GeoArabia, v. 18, no. 3, p. 135–178.

Bramkamp, R.A. and Steineke, M., 1952, Stratigraphical introduction: In W.J. Arkell, (Ed.), Jurassic ammonites from Jebel Tuwaiq, central Arabia: Royal Society London Philosophical Transactions, v. Series B, , p. 241–313.

Brew, G., and M. Barazangi, 2001, Tectonic and Geologic Evolution of Syria: v. 6, no. 4.

Bruna, P.-O., Y. Guglielmi, J. Lamarche, M. Floquet, F. Fournier, J.-P. Sizun, A. Gallois, L. Marié, C. Bertrand, and F. Hollender, 2013, Porosity gain and loss in unconventional reservoirs: Example of rock typing in Lower Cretaceous hemipelagic limestones, SE France (Provence): Marine and Petroleum Geology, v. 48, p. 186–205, doi:10.1016/j.marpetgeo.2013.08.008.

Calvo, R. M., E. Garcia-Rodeja, and F. Macias, 1983, Mineralogical variability in weathering microsystems of a granitic outcrop of Galicia (Spain): CATENA, v. 10, no. 3, p. 225–236, doi:10.1016/0341-8162(83)90033-4.

Catuneanu, O. et al., 2009, Towards the standardization of sequence stratigraphy: Earth-Science Reviews, v. 92, no. 1-2, p. 1–33, doi:10.1016/j.earscirev.2008.10.003.

Catuneanu, O., and M. Zecchin, 2013, High-resolution sequence stratigraphy of clastic shelves II: Controls on sequence development: Marine and Petroleum Geology, v. 39, no. 1, p. 26–38, doi:10.1016/j.marpetgeo.2012.08.010.

Chirat, R., D. Vaslet, and Y. Le Nindre, 2006, Nautiloids of the Permian-Triassic Khuff Formation , central Saudi Arabia: v. 11, no. 1, p. 81–92.

Cogné, N., P. R. Cobbold, C. Riccomini, and K. Gallagher, 2013, Tectonic setting of the Taubaté Basin (Southeastern Brazil): Insights from regional seismic profiles and outcrop data: Journal of South American Earth Sciences, v. 42, p. 194–204, doi:10.1016/j.jsames.2012.09.011.

Corbett, P. W. M., and D. Potter, 2004, Petrotyping: A base map and atlas for navigating through permeability and porosity data for reservoir comparison and

permeability prediction: International Symposium of the Society of Core Analysts held in Abu Dhabi, UAE.

Crasquin-Soleau, S., D. Vaslet, and Y.-M. Le Nindre, 2005, Ostracods as markers of the Permian-Triassic boundary in Saudi Arabia (Khuff Formation): Palaeontology, v. 48 part 4, p. 853–868.

Crasquin-soleau, S., D. Vaslet, and Y. Le Nindre, 2006, Ostracods of the Permian-Triassic Khuff Formation , Saudi Arabia : palaeoecology and palaeobiogeography: v. 11, no. 1, p. 55–76.

Dasgupta, S. N., M. Hong, and I. A. Al-jallal, 2002, Accurate reservoir characterization to reduce drilling risk in Khuff-C carbonate , Ghawar field , Saudi Arabia: v. 7, no. 1, p. 81–100.

Delfour, J., R. Dhellemmes, P. Elsass, D. Vaslet, J.-M. Brosse, Y.-M. Le Nindre, and O. Dottin, 1982, Explanatory notes to the geologic map of the Ad Dawadimi Quadrangle, Kingdom of Saudi Arabia. Geoscience Map GM-60C, scale 1:250,000, sheet 24G. Deputy Ministry for Mineral Resources, Ministry of Petroleum and Mineral Resources, Kingdom of Saudi Arabia: p. 36.

Ebanks, W. J. J., 1987, Flow Unit Concept--Integrated Approach to Reservoir Description for Engineering Projects: AAPG Annual Convention, Los Angeles, California.

Edgell, S., 1992, Basement tectonics of Saudi Arabia as related to oil field structures: Kluwer Academic Publishers, p. p. 169–193.

El-Khayal, A. A., and R. H. Wagner, 1983, Upper Permian stratigraphy and megafloras of Saudi Arabia: palaeogeographic and climatic implications., *in* 10 Congreso Internacional de estratigrafía y geología del Carbonífero. Instituto

Geologico y Minero de España, Madrid: p. 158.

Eltom, H., O. Abdullatif, M. Makkawi, and A. Abdulraziq, 2013, MICROPOROSITY IN THE UPPER JURASSIC ARAB-D CARBONATE RESERVOIR, CENTRAL SAUDI ARABIA: AN OUTCROP ANALOGUE STUDY: Journal of Petroleum Geology, v. 36, no. 3, p. 281–297, doi:10.1111/jpg.12556.

Embry, B. A., 2009, Practical Sequence Stratigraphy: Canadian Society of Petroleum Geologists, p. 81.

Enay, R., Y.-M. Le Nindre, C. Mangold, J. Manivit, and D. Vaslet, 1987, Le Jurassique d‟Arabie Saoudite Centrale: nouvelles donnees sur la lithostratigraphie, les paleoenvironnements, les faunes d‟ammonites, les ages et les correlations: In R. Enay (Ed.), Geobios, Lyons, v. Memoir Spe, p. 13–65.

Eschard, R., E. Albouy, R. Deschamps, T. Euzen, and A. Ayub, 2003, Downstream evolution of turbiditic channel complexes in the Pab Range outcrops (Maastrichtian, Pakistan): Marine and Petroleum Geology, v. 20, no. 6-8, p. 691–710, doi:10.1016/j.marpetgeo.2003.02.004.

Fischer, J., Y. Le Nindre, J. Manivit, and D. Vaslet, 2001, Jurassic Gastropod Faunas of Central Saudi Arabia: v. 6, no. 1.

Frykman, P., 2001, Spatial variability in petrophysical properties in Upper Maastrichtian chalk outcrops at Stevns Klint, Denmark: Marine and Petroleum Geology, v. 18, no. 10, p. 1041–1062, doi:10.1016/S0264-8172(01)00043-5.

Gardner, M. H., J. M. Borer, J. J. Melick, N. Mavilla, M. Dechesne, and R. N. Wagerle, 2003, Stratigraphic process-response model for submarine channels and related features from studies of Permian Brushy Canyon outcrops, West Texas: Marine and Petroleum Geology, v. 20, no. 6-8, p. 757–787,

doi:10.1016/j.marpetgeo.2003.07.004.

Gorin, G. E., L. G. Racz, and M. . Walter, 1982, Late Precambrian-Cambrian sediments of Huqf Group, Sultanate of Oman: American Association of Petroleum Geologists Bulletin, v. 66 (12), p. 2609–2627.

Grammer, G. ., P. . Harris, and G. . Eberli, 2004, Integration of outcrop and modern analogs in reservoir modeling: Overview and examples from the Bahamas, in Integration of outcrop and modern analogs in reservoir modeling: AAPG Memoir, v. 80, p. 1–22.

Haase, M. M., and T. Aigner, 2013, High-resolution anatomy of a grainstone package in Khuff Sequence KS4 , Oman Mountains , Sultanate of Oman: no. 4, p. 17–44.

Haq, B. U., and A. M. Al-qahtani, 2005, Phanerozoic cycles of sea-level change on the Arabian Platform Rationale for an Arabian Platform Cycle Chart: v. 10, no. 2, p. 127–160.

Homewood, P., P. Razin, C. Grélaud, H. Droste, V. Vahrenkamp, M. Mettraux, and J. Mattner, 2008, Outcrop sedimentology of the Natih Formation , northern Oman : A field guide to selected outcrops in the Adam Foothills and Al Jabal al Akhdar areas: v. 13, no. 3.

Hughes, G. W., 2005, Jurassic Carbonates of Saudi Arabia: Field Trip Guide Book, v. 31, no. Technical Memorandum, p. 99.

Hughes, G. ., 2004, Middle to Upper Jurassic Saudi Arabian carbonate petroleum reservoirs: biostratigraphy, micropalaeontology and palaeoenvironments: GeoArabia, v. 9 (3), p. 79–114.

Hughes Clarke, M. ., 1988, Stratigraphy and Rock-Unit Nomenclature in the Oil Producing Area of Interior Oman: Journal of Petroleum Geology, v. 11, p. 5–60.

Hughes, G. W., O. Varol, and M. Al-khalid, 2008, Late Oxfordian micropalaeontology , nannopalaeontology and palaeoenvironments of Saudi Arabia: GeoArabia, v. 13, no. 2, p. 15–46.

Hunt, D., and M. E. Tucker, 1992, Stranded parasequences and the forced regressive wedge systems tract: deposition during base-level'fall: Sedimentary Geology, v. 81, no. 1-2, p. 1–9, doi:10.1016/0037-0738(92)90052-S.

Husseini, M. I., 1988, The Arabian Infracambrian extensional system: Tectonophysics, v. 148, p. 93–103.

Imlay, R., 1970, Some Jurassic ammonites from central Saudi Arabia: United States Geological Survey, Professional Paper, p. 644–D, 19 pp.

Iñigo, J. F., S. E. Laubach, and J. N. Hooker, 2012, Fracture abundance and patterns in the Subandean fold and thrust belt, Devonian Huamampampa Formation petroleum reservoirs and outcrops, Argentina and Bolivia: Marine and Petroleum Geology, v. 35, no. 1, p. 201–218, doi:10.1016/j.marpetgeo.2012.01.010.

Janson, X., F. J. Lucia, J. W. Jennings, J. A. Bellian, A. A. AbuBshait, R. K. Al-Dukhayyil, H. W. Mueller, and D. Cantrell, 2013, Outcrop-based 3D Geological and Reservoir Model of the Uppermost Khuff Formaiton in Central Saudi Arabia: EAGE Book chapter12, no. January2014, p. 269–301.

Jennings, J., S. . Ruppel, and W. . Ward, 2000, Geostatistical Analysis of Permeability Data and Modeling of Fluid-Flow Effect in Carbonate Outcrop: Engineering, SPE Reservoir Evaluation and, v. 3, p. 292–303.

Jung, A., and T. Aigner, 2012, Carbonate geobodies: hierarchical classification and database – a new workflow for 3D reservoir modelling: Journal of Petroleum Geology, v. 35, no. 1, p. 49–65, doi:10.1111/j.1747-5457.2012.00518.x.

Kidwell, S. M., 1991, Condensed deposits in siliciclastic sequences: expected and observed features. In: Einsele, G., Ricken, W., Seilacher, A. (Eds.), Cycles and Events in Stratigraphy.: Springer-Verlag, Berlin, p. 682–695.

Koehrer, B., T. Aigner, H. Forke, and M. Pöppelreiter, 2012, Middle to Upper Khuff (Sequences KS1 to KS4) outcrop-equivalents in the Oman Mountains : Grainstone architecture on a subregional scale: GeoArabia, v. 17, no. 4, p. 59–104.

Koehrer, B., T. Aigner, and M. Pöppelreiter, 2011, Field-scale geometries of Upper Khuff reservoir geobodies in an outcrop analogue (Oman Mountains, Sultanate of Oman): Petroleum Geoscience, v. 17, no. 1, p. 3–16, doi:10.1144/1354-079310-009.

Koehrer, B., M. Zeller, T. Aigner, M. Pöppelreiter, P. Milroy, H. Forke, and S. Al-kindi, 2010, Facies and stratigraphic framework of a Khuff outcrop equivalent : Saiq and Mahil formations , Al Jabal al-Akhdar , Sultanate of Oman: GeoArabia, v. 15, no. 2, p. 91–156.

Konert, G., A. M. Afifi, and and H. J. D. Al-hajri, 2001, Paleozoic Stratigraphy and Hydrocarbon Habitat of the Arabian Plate: GeoArabia, v. 6, no. 3, p. 407–442.

Konyuhov, A. I., and B. Maleki, 2000, The Persian Gulf Basin: Geological History, Sedimentary Formations, and Petroleum Potential: GeoArabi, v. 5 (4), p. 344–361.

Lindsay, R. ., and G. Hughes, 2010, Saudi Arabian Jurassic outcrop Reservoir equivalents. A pictorial Review: The oil Drop, v. 22, no. 02, p. 6–11.

Lüning, S., S. Kolonic, D. K. Loydell, and J. Craig, 2003, Reconstruction of the original organic richness in weathered Silurian shale outcrops (Murzuq and

Kufra basins , southern Libya): v. 8, no. 2, p. 299–308.

Manivit, J., C. Pellaton, D. Vaslet, Y.-M. Le Nindre, J.-M. Brosse, J.-P. Breton, J. Fourniguet, and J.-C. Prevot, 1985, Explanatory notes to the geologic map of the Darma' Quadrangle, Kingdom of Saudi Arabia. Geoscience map GM-101C, scale 1:250,000, sheet 24H: Deputy Ministry for Mineral Resources, Ministry of Petroleum and Mineral Resources, Kingdom of Saudi Arabia, p. 33.

Manivit, J., C. Pellaton, D. Vaslet, Y.-M. Le Nindre, J.-M. Brosse, and F. J, 1985, Geologic map of the Wadi al Mulayh quadrangle sheet 22H, Kingdom of Saudi Arabia (with text): Saudi Arabian Deputy Ministry Mineral Resources, Geoscience Map GM-92, scale 1/250000.

Manivit, J., D. Vaslet, A. Berthiaux, P. Le Strat, and J. Fourniguet, 1985, Geological map of the Buraydah quadrangle, sheet 26 G, Kingdom of Saudi Arabia: Saudi Arabia Deputy Ministry of Mineral Resources, Geoscience Map GM-114, Scale 1:250,000, with text, p. 32.

Manivit, J., D. Vaslet, Y.-M. Le Nindre, and F. X. Vaillant, 1983, Stratigraphic drill hole SHD-1 through the lower part of the Jilh Formation, Sudair Shale and Khuff Formation in the Durma quadrangle (sheet 24H): Saudi Arabian Directorate General of Mineral Resources, open file report 0F-03-50, p. 1–34.

Mattner, J., and M. Al-husseini, 2002, Essay : applied cyclo-stratigraphy for the Middle East E & P industry Hanifa sedimentary cycles : a typical outcrop example: v. 7, no. 4, p. 734–744.

Maurer, F., R. Martini, R. Rettori, and H. Hillgärtner, 2009, The geology of Khuff outcrop analogues in the Musandam Peninsula , United Arab Emirates and Oman: no. 3, p. 125–158.

Meyer, F. O., R. C. Price, I. A. Al-ghamdi, I. M. Al-goba, S. M. Al-raimi, and J. C. Cole, 1996, Sequential Stratigraphy of Outcropping Strata Equivalent to Arab-D Reservoir , Wadi Nisah , Saudi Arabia: v. 1, no. 3.

Montenat, C., P. Barrier, and H. J. Soudet, 2003, Aptian faulting in the Haushi-Huqf (Oman) and the tectonic evolution of the southeast Arabian platform-margin: v. 8, no. 4.

Mukti, M. M., and M. Ito, 2010, Discovery of outcrop-scale fine-grained sediment waves in the lower Halang Formation, an upper Miocene submarine-fan succession in West Java: Sedimentary Geology, v. 231, no. 3-4, p. 55–62, doi:10.1016/j.sedgeo.2010.09.005.

Mulder, T. et al., 2010, High-resolution analysis of submarine lobes deposits: Seismic-scale outcrops of the Lauzanier area (SE Alps, France): Sedimentary Geology, v. 229, no. 3, p. 160–191, doi:10.1016/j.sedgeo.2009.11.005.

Le Nindre, Y.-M., J. Manivit, and D. Vaslet, 1990a, Histoire géologique de la bordure occidentale de la plate-forme Arabe, v. 3: Le Permo-Trias d'Arabie centrale. Bureau de Recherches Géologiques et Minières, Document no. 193, 262 p., 51 figures, 4 tables, 11 plates, 3 appendices.

Le Nindre, Y.-M., J. Manivit, and D. Vaslet, 1990b, Stratigraphie séquentielle du Jurassique et du Crétacé en ;pol Arabie Saoudite: Bulletin, Société géologique de France, Paris, v. 8 (6), p. 1025–1034.

Nindre, Y. Le, D. Vaslet, S. S. Maddah, and M. I. Al-husseini, 2008, Stratigraphy of the Valanginian ? to Early Paleocene succession in central Saudi Arabia outcrops : Implications for regional Arabian sequence stratigraphy: v. 13, no. 2, p. 51–86.

Nindre, Y. Le, J. M. Y.-M., and D. Vaslet, 1990, Histoire géologique de la bordure occidentale de la plate-forme Arabe, v. 2: Géodynamique et paléogéographie de la plate-forme Arabe du Permien au Jurassique: Bureau de Recherches Géologiques et Minières, Document no. 192, 278 p., 54 figures, 4 tables, 4 appendices.

Olsen, T., 1995, Sequence Stratigraphy on the Northwest European Margin, Proceedings of the Norwegian Petroleum Society Conference: Elsevier, Norwegian Petroleum Society Special Publications, 75-96 p., doi:10.1016/S0928-8937(06)80064-0.

Philip, J. M., U. De Provence, J. Roger, D. Vaslet, B. De Recherches, F. Cecca, S. Gardin, and U. D. P. Vi, 2002, Sequence stratigraphy , biostratigraphy and paleontology of the Maastrichtian-Paleocene Aruma Formation in outcrop in Saudi Arabia: v. 7, no. 4, p. 699–718.

Pöppelreiter, M. C., C. J. Schneider, M. Obermaier, H. C. Forke, B. Koehrer, and T. Aigner, 2011, Seal turns into reservoir : Sudair equivalents in outcrops , Al Jabal al-Akhdar , Sultanate of Oman: no. 1, p. 69–108.

Posamentier, H. W., and W. R. Morris, 2000, Aspects of the stratal architecture of forced regressive deposits: Geological Society of London, Special Publication, v. 172, no. 0305-8719, p. 19–46.

Powers, R. ., 1962, Arabian Upper Jurassic carbonate reservoir rocks: American Association of Petroleum Geologists, Memoir, v. 1, p. 122–192.

Powers, R. ., 1968, Saudi Arabia: Lexique Stratigraphique International, 3, Centre National de la Recherche Scientifique, Paris, p. 171pp.

Powers, R. W., L. F. Ramirez, C. D. Redmond, and E. . Elberg, 1966, Geology of the

Arabian Peninsula, Sedimentary geology of Saudi Arabia: Geological Survey Professional Paper 560-D, United States Government Printing Office, Washington, p. 147.

Pringle, J. ., J. . Howell, D. Hodgetts, A. . Westerman, and D. . Hodgson, 2006, Virtual outcrop models of petroleum reservoir analogues: a review of the current state-of-the-art: First break, v. 24, p. 33–42.

Pyles, D. R., J. P. M. Syvitski, and R. M. Slatt, 2011, Defining the concept of stratigraphic grade and applying it to stratal (reservoir) architecture and evolution of the slope-to-basin profile: An outcrop perspective: Marine and Petroleum Geology, v. 28, no. 3, p. 675–697, doi:10.1016/j.marpetgeo.2010.07.006.

Retallack, G. J., and D. L. Dilcher, 2012, Outcrop versus core and geophysical log interpretation of mid-Cretaceous paleosols from the Dakota Formation of Kansas: Palaeogeography, Palaeoclimatology, Palaeoecology, v. 329-330, p. 47–63, doi:10.1016/j.palaeo.2012.02.017.

Schwab, A. M., P. W. Homewood, F. S. P. Van Buchem, and P. Razin, 2005, Seismic forward model of a Natih Formation outcrop : the Adam Foothills Transect (northern Oman): v. 10, no. 1.

Senalp, M., and A. Al-Duaiji, 1995, Stratigraphy and sedimentation of the “Unayzah Reservoir” central Saudi Arabia: In, M.I. Al-Husseini (Ed.), Middle East Petroleum Geosciences Conference, GEO’94. Gulf PetroLink, Bahrain, v. 2, p. 837–847.

Sengör, A. M. C., and B. . Natalin, 1996, Paleotectonics of Asia: fragment of a synthesis: In: An, Yin, Harrison, T.M. (Eds.), The Tectonic Evolution of Asia: Cambridge University Press, Cambridge, p. 486–640.

Sharland, P. R., R. Archer, D. M. Casey, R. B. Davies, S. H. Hall, A. . Heward, A. D. Horbury, and M. D. Simmons, 2001, Arabian Plate Sequence Stratigraphy: Gulf PetroLink, Bahrain, GeoArabia Special Publication, v. 2, p. 371 pp., 3 charts.

Sharland, P. R., D. M. Casey, R. B. Davies, M. D. Simmons, and O. E. Sutcliffe, 2004, Arabian Plate Sequence Stratigraphy – revisions to SP2: v. 9, no. 1, p. 199–214.

Smith, L. B., and J. F. Read, 1999, Application of high-resolution sequence stratigraphy to tidally influenced Upper Mississippian carbonates, Illinois Basin: SEPM (Society for Sedimentary Geology) Special Publication, v. 63, p. 107–126.

Steineke, M., and R. A. Bramkamp, 1952, Mesozoic rocks of eastern Saudi Arabia: American Association of Petroleum Geologists Bulletin. Abstract, v. 36, no. 5, p. 909.

Steineke, M. R., R. A. Bramkamp, and N. J. Sander, 1958, Stratigraphic relations of Arabian Jurassic oil. In, L.G. Weeks (Ed.), Habitat of Oil: American Association of Petroleum Geologists Symposium, p. 1294–1329.

Stephenson, M. H., P. L. Osterloff, and J. Filatoff, 2003, Palynological biozonation of the Permian of Oman and Saudi Arabia : progress and challenges: v. 8, no. 3, p. 467–496.

Tiab, D., and E. Donaldson, 2012, Petrophysics: Theory and Practice of Measuring Reservoir Rock and Fluid Properties: Gulf Publishing Company.

Tuuling, I., and T. Flodén, 2011, Seismic stratigraphy, architecture and outcrop pattern of the Wenlock–Přidoli sequence offshore Saaremaa, Baltic Sea: Marine Geology, v. 281, no. 1-4, p. 14–26, doi:10.1016/j.margeo.2011.01.003.

Vachard, D., J. Gaillot, D. Vaslet, and Y. Le Nindre, 2005, Foraminifers and algae

from the Khuff Formation (late Middle Permian-Early Triassic) of central Saudi Arabia: GeoArabia, v. 10, no. 4, p. 137–186.

Vachard, D., M. Hauser, R. Martini, L. Zaninetti, A. Matter, and T. Peters, 2002, Middle Permian (Midian) foraminiferal assemblages from the Batain Plain (Eastern Oman): their significance to Neotethyan paleogeography: Journal of Foraminiferal Research, v. 32, no. 2, p. 155–172.

Vaslet, D., M. Beurrier, M. Villey, J. Manivit, P. Le Strat, Y.-M. Le Nindre, Berthiaux, A. Brosse, and J.-M. J. Fourniguet, 1985, Explanatory notes to the geologic map of the Al Faydah Quadrangle, Kingdom of Saudi Arabia. Geoscience Map GM-102C, scale 1:250,000, sheet 25G.: Deputy Ministry for Mineral Resources, Ministry of Petroleum and Mineral Resources, Kingdom of Saudi Arabia, p. 28.

Vaslet, D., J. Manivit, Y.-M. Le Nindre, J.-M. Brosse, J. Fourniguet, and J. Delfour, 1983, Explanatory notes to the geologic map of the Ar Riyad Quadrangle, Sheet, sheet 23H, Kingdom of Saudi Arabia.: Saudi Arabian Deputy Ministry for Mineral Resources Geoscience Map GM-63, scale 1:250,000, with text, p. 46 pp.

Vaslet, D., Y. Le Nindre, D. Vachard, J. Broutin, S. Crasquin-soleau, M. Berthelin, J. Gaillot, M. Halawani, and M. Al-Husseini, 2005, The Permian-Triassic Khuff Formation of central Saudi Arabia: GeoArabia, v. 10, no. 4, p. 77–134.

Vaslet, D., C. Pellaton, J. Manivit, Y.-M. Le Nindre, J.-M. Brosse, and J. Fourniguet, 1985, Geologic map of the Sulayyimah quadrangle, sheet 21H, Kingdom of Saudi Arabia: Saudi Arabian Deputy Ministry for Mineral Resources Geoscience Map GM-100 A, scale 1:250,000, with text, p. 32 pp.

Van Wagoner, J. C., R. M. Mitchum, K. M. Campion, and V. D. Rahmanian, 1990,

Siliciclastic sequence stratigraphy in well logs, cores, and outcrops: AAPG Methods in Exploration, v. 7, p. 55.

Walz, L., T. Aigner, and B. Koehrer, 2013, Khuff Sequence KS5 outcrop-equivalents in the Oman Mountains , Sultanate of Oman : Variations to the simple " layer-cake " stratigraphy: no. 4, p. 179–218.

Warren, C. A., and H. S. Price, 1961, Flow in heterogeneous porous media: Soc. Petrol Eng., v. I, p. 153–169.

Weidlich, O., and M. Bernecker, 2004, Quantification of depositional changes and paleo-seismic activities from laminated sediments using outcrop data: Sedimentary Geology, v. 166, no. 1-2, p. 11–20, doi:10.1016/j.sedgeo.2003.12.004.

Wender, L. E., J. W. Bryant, M. F. Dickens, A. S. Neville, and A. M. Al-moqbel, 1998, Paleozoic (Pre-Khuff) Hydrocarbon Geology of the Ghawar Area , Eastern Saudi Arabia: v. 3, no. 2.

Wilson, P., D. Hodgetts, F. Rarity, R. L. Gawthorpe, and I. R. Sharp, 2009, Structural geology and 4D evolution of a half-graben: New digital outcrop modelling techniques applied to the Nukhul half-graben, Suez rift, Egypt: Journal of Structural Geology, v. 31, no. 3, p. 328–345, doi:10.1016/j.jsg.2008.11.013.

Zecchin, M., 2007, The architectural variability of small-scale cycles in shelf and ramp clastic systems: The controlling factors: Earth-Science Reviews, v. 84, no. 1-2, p. 21–55, doi:10.1016/j.earscirev.2007.05.003.

Zecchin, M., and O. Catuneanu, 2013, High-resolution sequence stratigraphy of clastic shelves I: Units and bounding surfaces: Marine and Petroleum Geology, v. 39, no. 1, p. 1–25, doi:10.1016/j.marpetgeo.2012.08.015.

Zeller, M., B. Koehrer, E. W. Adams, M. Pöppelreiter, and T. Aigner, 2011, Near well-scale heterogeneities in a Khuff outcrop equivalent (Saiq plateau, al Jabal al Akhdar, Sultanate of Oman): Journal of Petroleum Geology, v. 34, no. 3, p. 241–260, doi:10.1111/j.1747-5457.2011.00504.x.

Ziegler, M. A., 2001, Late Permian to Holocene Paleofacies Evolution of the Arabian Plate and its Hydrocarbon Occurrences: GeoArabia, v. 6, no. 3, p. 445–504.

VITAE

Personal Particulars

Name	:Ammar Mohammed Adam Mohammed
Nationality	:Sudanese
Date of Birth	:8/24/1982
Email	:ammarmohammed65@yahoo.com
Address	:Red Sea University, Portsudan, Red Sea State, Sudan
Academic Background	:Geology

Education

PhD. Geology **Graduation Date: January 2017**

- Thesis: High-resolution Sedimentology, Sequence Stratigraphy, and Diagenesis of the Upper Khartam Member Khuff Formation. Implication on Reservoir Architecture and Quality. Outcrop Analog from Central Saudi Arabia
- King Fahd University of Petroleum and Minerals, Geosciences Department, Dhahran, Saudi Arabia
- CGPA: 3.53

M.Sc. Petroleum Geosciences **Graduation Date: October 2010**

- Thesis: Development of a stratigraphic scheme for the southern Malay Basin using sequence stratigraphic concept
- University Technology Petronas, Geosciences Department, Perak, Malaysia
- CGPA: 3.79

Graduate Diploma, Petroleum Geoscience **Graduation Date: October 2010**

- France Institute of Petroleum Geosciences (IFP). This Programme is conducted jointly with UTP in Malaysia, and leads to the award of the UTP M.Sc degree.

B.Sc. Geophysics **Graduation Date: December 2006**

- Delineation of Groundwater Aquifers using an Electrical Resistivity Survey in the Akwat Region, Red Sea State, Eastern Sudan
- Red Sea University, Portsudan, Sudan
- CGPA: 3.23 (honors)

Professional Experience

Sept 2011 – Present Lecturer B, King Fahd University, Petroleum Department

- Teaching the following labs: Physical Geology, Optical mineralogy, Petrology, and Field Geology, and assisting in Petroleum Geology

Jan 2011-Sept 2011 Graduate Assistant, University Technology Petronas, Perak, Malaysia

- Assisting and teaching physical geology, petrology, and geochemistry

Sept 2010-Present Lecturer, Faculty of Earth Sciences, Red Sea University, Sudan

- Teaching physical geology, petrology, igneous rocks, metamorphic rocks, sedimentary rocks, structural geology, geological maps, and general geophysics
- Supervising final year projects

Nov 2007-Jan 2009 Groundwater Exploration geophysicist, East Sudan Development Project, Portsudan, Sudan

- Geological and geophysical investigation for Aquifers Delineation using an Electrical Resistivity Survey, Red Sea State, Sudan

Nov 2007- Oct 2010 Teaching Assistant, Faculty of Earth Sciences, Red Sea University, Sudan

- Teaching the following labs: Physical Geology, Optical mineralogy, Petrology, and Field Geology.

Projects

I participated in the following projects as a PhD student

1. NSTIP Project # 09-OIL767-04, funded by Kacst NSTIP. Dr. Osman Abdullatif (PI). High Resolution Geological and geostatistical model of Arab D Reservoir, outcrop Analog, Central Saudi Arabia.
2. NSTIP Project # 10-OIL 1379-04, funded internally by Kacst, NSTIP. Dr. Osman Abdullatif (PI) (2011). High Resolution Outcrop Analog for Khuff Carbonate Reservoir: Integrated Approach using Terrestrial Lidar Technology, Geological and Geostatistical Models from central Saudi Arabia.
3. Fast Track Project # 100032. Dr. Osman Abdullatif (PI) Geological and geostatistical modeling of rock properties, porosity and permeability of shallow marine sediments. SW Saudi Arabia, completed, funded internally by KFUPM.

Journal Papers under review:

1. **Adam, A.,** Swennen, R., Abdullatif, O., Hariri, M., Abdulghani, W, 2017. The Khuff carbonates, central Saudi Arabia I: High-resolution stratigraphy and sedimentology. **Under review, Journal of Petroleum Geology**
2. **Adam, A.,** Swennen, R., Abdullatif, O., Hariri, M., Abdulraheem, A., Mahmoud, M., Abdulghani, W, 2017. The Khuff carbonates, central Saudi Arabia II: Reservoir quality and heterogeneity. **Under review, Marine and Petroleum Geology**
3. **Adam, A.,** Abdulraheem, A., Swennen, R., Abdullatif, O., Hariri, M., Mahmoud, M., Abdulghani, W, **2017**. Multi-realization geological modeling: implications on fluid flow simulation, Upper Khartam carbonates, reservoir analog from Central Saudi Arabia. **In progress, Journal of Petroleum Geosciences**

4. **Adam, A.,** Kaminski, Abdullatif, O., Hariri, M., Abdulghani, W, 2017 . Sedimentological and stratigraphic associations of *Earlandia foraminifera*; from the barren Khuff carbonates; central Saudi Arabia. **In progress, Journal of Micropaleontology.**

Conference Papers

1. **Ammar M. Adam**, Rudy Swennen, and Osman Abdullatif. 2017. Reservoir Heterogeneity and Quality of Khuff Carbonates (Central Saudi Arabia). AAPG Annual Convention & Exhibition (ACE), 2-5 April 2017 at the George R. Brown Convention Center in Houston, Texas.
2. **Ammar M. Adam**, Mike Kaminski, Osman Abdullatif. 2017. Sedimentological and Stratigraphic Associations of Earlandia Foraminifera; in the Early Triassic Succession of Khuff Carbonates; Central Saudi Arabia. European Geosciences Union General Assembly.
3. **Ammar M. Adam**, Osman Abdullatif, Ammar J. Abdlmutalib, Mohammed Elhibir1, Mazin Bashari, Moaz Mohammed, Mohammed Jabir, Abdallah Abdelkarim. 2014. High-Resolution Stratigraphy and Sedimentology of Upper Khartam Member of the Permo-Triassic Khuff Formation; Outcrop Reservoir Analog Approach from Central Saudi Arabia. September 15, 2015 Tuesday 1:45 P.M. International Conference & Exhibition, Melbourne, Australia.
4. **Ammar M. Adam**, Osman Abdullatif, Mohamed A. Yassin, Hassan A. Eltom, Lamidi O. Babalola, Asaad Abdelraziq, Mutasim S. Osman1 and Mazin A. Bashri. 2014. Enhanced Reservoir Heterogeneity Description; Khartam Member of the Permo-Triassic Khuff Carbonate: Outcrop Reservoir Analog Approach from Central Saudi Arabia. AAPG International Conference & Exhibition. September 14-17, 2014, Istanbul, Turkey
5. **Ammar M. Adam**, Hassan Eltom, Osman Abdullatif, Lameed Babaloa, Mohamed Abdelgadir, Asaad Abdelraziq, Mutasim Osman and Mazin Bashiri. 2014. High Resolution Stratigraphy of the Khartam Member of the Permo-Triassic Khuff Carbonate: Outcrop Reservoir Analog from Central Saudi Arabia. Abstract (accepted) to GEO 2014 Conference, Manama, Bahrain.
6. **Ammar M. Adam**, Osman Abdullatif. 2013. Diagenetic Evolution and Subsequent Implications on Reservoir Qualities, Khartam Member, Permo-Triassic Khuff Formation, Central Saudi Arabia. Vol. 15, EGU2013-9416, 2013 EGU.
7. Osman Abdullatif and **Ammar M. Adam**. 2013. High Resolution Chemostratigraphy of Khartam Member of the Permo-Triassic Khuff Carbonate: Outcrop Reservoir Analog Approach from Central Saudi Arabia. 2013EGU GA.15.9295A.
8. **Ammar M. Adam**, Osman Abdullatif, Hassan A. Eltom, Mohamed A. Yassin, , Lamidi O. Babalola, Asaad Abdelraziq, Mutasim S. Osman, and Mazin A. Bashri. 2013. High-resolution stratigraphy and implication on critical reservoir architecture, lithofacies and petrophysical properties of Khartam member of

the Permo-Triassic Khuff carbonate: Outcrop reservoir analog approach from central Saudi Arabia. Abstract. IAS meeting, Manchester, U.K.

9. **Ammar M. Adam**; Kaka, SanLinn. 2013. Delineation of Groundwater Aquifers using an Electrical Resistivity Survey in the Dordab Region, Red Sea State, Eastern Sudan. AAPG 2013 Annual Convention and Exhibition, Pittsburgh, Pennsylvania.
10. **Adam et al**., 2017. Multi-realizations geostatistical modeling: Implication on reservoir quality and heterogeneity. Outcrop analog of Khuff carbonates. AAPG ACE 2017
11. **Adam et al**., 2017. High-resolution stratigraphy and sedimentology of Khuff carbonates (central Saudi Arabia). Submitted to AAPG ACE 2017

Skills

- **Lab Equipment:** Thin-section preparations, Portable Gamma Ray, coring machines, poro-perm equipments, X-ray fluorescence (XRF), Scanning Electron Microscopy (SEM), X-ray diffraction (XRD)
- **Industry Related Software**: Resix (electrical resistivity data processing and interpretation), IP (electrical resistivity data processing and interpretation), Petrel (seismic interpretation and reservoir modelling), Landmark (seismic interpretation and well log correlation), Fracaflow (fracture reservoir modelling), Geologs (formation evolution), Eclipse (basin simulation), EasyCore (software for acquiring and archiving core descriptions), CorelDRAW (graphics design application; lithofacies and stratigraphic analysis)
- **Personal Skills:** Excellent Communication Skills, Self-motivated team player, Problem Solving Ability, Ability to work under pressure, open minded to new ideas and new technologies